ELECTROFABRICATION OF Ni-BASED ALLOY COATINGS FOR ANTICORROSION AND WATER SPLITTING APPLICATIONS

Thesis

Submitted in partial fulfillment of the requirements for the degree of

DOCTOR OF PHILOSOPHY

by

CINDRELLA NISHMITHA GONSALVES

DEPARTMENT OF CHEMISTRY

NATIONAL INSTITUTE OF TECHNOLOGY, KARNATAKA

SURATHKAL, MANGALURU-575025

JULY, 2022

DECLARATION

By the Ph.D. Research Scholar

I hereby declare that the Research Thesis entitled **"Electrofabrication of Ni-based alloy coatings for anticorrosion and water splitting applications"** which is being submitted to the **National Institute of Technology Karnataka, Surathkal** in partial fulfillment of the requirements for the award of the degree of **Doctor of Philosophy in Chemistry** is a *bonafide report of the research work carried out by me.* The material contained in this Research Thesis has not been submitted to any University or Institution for the award of any degree.

CINDRELLA NISHMITHA GONSALVES

Reg. No.: 177126CY001

Department of Chemistry

Place: NITK, Surathkal

Date: 19/07/2022

CERTIFICATE

This is to certify that the Research Thesis entitled **"Electrofabrication of Ni-based alloy coatings for anticorrosion and water splitting applications"** submitted by **Cindrella Nishmitha Gonsalves (Register No.: 177126CY001)** as the record of research work carried out by her is *accepted as the Research Thesis submission* in partial fulfillment of the requirements for the award of the degree of Doctor of Philosophy.

Prof. A. Chitharanjan Hegde

Research Guide

Date: 19.7.2022

Dr. A. CHITHARANJAN HEGDE
Professor and Former Head
Department of Chemistry
NITK, Surathkal, Srinivasnagar
MANGALORE - 575 025, D.K.

Chairman-DRPC

Date: 19/07/2022

HEAD, DEPARTMENT OF CHEMISTRY
National Institute of Technology Karnataka
Surathkal, Srinivasnagar
MANGALORE- 575 025, D.K.

DEDICATED TO
MY BELOVED FAMILY

ACKNOWLEDGEMENT

CINDRELLA N. GONSALVES

ABSTRACT

This thesis titled '***Electrofabrication of Ni-based alloy coatings for anticorrosion and water splitting applications***' presents a comprehensive study on development and characterization of two Ni-based alloy coatings from newly formulated baths, namely (Ni-Mo) and (Ni-Fe). Standard Hull cell method was used to optimize bath constituents and operating conditions for best performance of alloy coatings against corrosion, as well as for good electro-catalytic activity for water electro-splitting applications. The corrosion protection efficacy of monolayer Ni-based alloy coatings were improved further by modern methods of electroplating, namely magneto-electrodeposition (MED) and composition modulated multilayer electrodeposition (CMM-ED) approach. Poor corrosion resistance of (Ni-Mo) alloy coatings, limited by the low concentration of metal ions was successfully alleviated by taking the advent of magnetic field (B) effect, applied simultaneously to the process of deposition. Experimental investigation revealed that corrosion protection efficacy of monolayer (Ni-Mo) alloy coatings can be improved about 5 times and 8 times better, through MED technique by superimposing the B, parallel and perpendicular (to the direction of movement of metal ions), respectively. The attractiveness of electroplating linked to the cathode current density has been explored effectively for the development of multilayer (Ni-Fe) alloy coatings of better corrosion resistance, compared to their monolayer counterpart. The multilayer (Ni-Fe) alloy coatings of much higher corrosion resistance were developed by proper manipulation of composition and thickness of alternate layers of alloys by proper modulation of amplitude and duration of current pulse, respectively. In addition, the electro-catalytic activity of (Ni-Mo) and (Ni-Fe) alloy coatings have been tested for their efficacy for both HER and OER in water splitting applications in 1.0 M KOH. The effect of composition, surface morphology and phase structure of alloy coatings on their electro-catalytic efficacies have been studied, using CV and CP methods. The effect of addition of redox-active polyoxometalates (POM), and Ag-nanoparticles into electrolytic baths of (Ni-Mo) and (Ni-Fe) on electro-catalytic activities of their coatings were studied, and reasons responsible for improved activities were discussed. Corrosion performance of all coatings were studied by electrochemical AC and DC methods in 3.5 % NaCl, and results were compared. The process and product of electrodeposition were characterized using SEM, EDS, AFM and XRD techniques. The performance of alloy coatings developed under different conditions of current density are compared, and results are discussed with Tables and Figures.

Keywords: *Electrodeposition, (Ni-Mo) and (Ni-Fe) alloy coatings, multilayer coating, magneto-electrodeposition, corrosion study, alkaline water electrolysis*

CONTENTS

LIST OF FIGURES

x

LIST OF TABLES

NOMENCLATURE

A. LIST OF ABBREVIATIONS:

AC	Alternate current
AFM	Atomic Force Microscopy
CCCD	Cyclic cathode current density
c.d.	Current density
CMM-ED	Composition Modulated Multilayer Electrodeposition
CP	Chronopotentiometry
CR	Corrosion rate
CV	Cyclic Voltammetry
DC	Direct current
ED	Electrodeposition
EDL	Electrical double layer
EDS	Energy Dispersive X-ray Spectroscopy
EIS	Electrochemical Impedance Spectroscopy
FESEM	Field Emission Scanning Electron Microscopy
HER	Hydrogen evolution reaction
JCPDS	Joint Committee on Powder Diffraction standards
MED	Magneto-electrodeposition
MHD	Magneto hydrodynamic
OCP	Open circuit potential
OER	Oxygen evolution reaction
PDP	Potentiodynamic polarization
RE	Reference electrode
SCE	Saturated calomel electrode
SEM	Scanning Electron Microscopy
TE	Test electrode
Wt. %	Weight percentage
XRD	X-ray diffraction

B. LIST OF SYMBOLS:

i_{pa}	Anodic peak current density
A dm^{-2}	Ampere per decimeter square
β_a	Anodic Tafel slope
R_a	Average roughness
C_B	Bulk concentration of metal ions
i_{pc}	Cathodic peak current density
β_c	Cathodic Tafel slope
R_{ct}	Charge transfer resistance
i_{corr}	Corrosion current density
E_{corr}	Corrosion potential
δ	Diffusion layer thickness
kHz	Kilo Hertz
i_L	Limiting current density
F_L	Lorentz force
B	Magnetic field
mm y^{-1}	Millimeter per year
mV	Millivolt
M	Molarity
nm	Nanometer
R_P	Polarization resistance
R_q	Root mean square roughness
R_s	Solution resistance

CHAPTER 1

INTRODUCTION

CHAPTER 1

INTRODUCTION

This chapter gives introductory aspects of electrodeposition with a special emphasis on basic principles of alloy plating. Different methods of modern electroplating to achieve better performances of alloy coatings are outlined here. The principles of electrochemical methods of corrosion study and electrocatalytic study of alloy coatings for alkaline water electrolysis are overviewed.

1.1 ELECTRODEPOSITION TECHNIQUE

Metallic materials have been used widely for ages in various household, medical, transportation, electronics, and engineering applications. However, they have a limited lifetime as they are susceptible to their contact environment which leads to various chemical and electrochemical changes on their surfaces. Such 'unwanted' changes are technically termed as 'corrosion'. By definition, corrosion is a process of destruction and deterioration, and consequent loss of metal/alloy due to chemical and electrochemical attack by its environment (Kanani 2004). Hence, corrosion is the combined effect of both metal and the medium. As per recent studies, it is found that about 5-7% loss of Indian Gross Domestic Product (GDP) is inflicted solely due to metal corrosion. This is because, corrosion not only weakens the functionality of base metals, but also leads to loss of energy, water, and the human effort used in its production and fabrication (Revie and Uhlig 2008). In this direction, electroplating is the most promising approach to combat the corrosion of metallic structures. Today electroplating technology is growing in both revolutionary and evolutionary ways to control corrosion by imparting better surface properties to base metal. Electroplating is considered to be the most promising approach in the area of Metal Finishing. Thus, *electroplating or electrodeposition* may be defined as the process of depositing a thin and uniform layer of another metal/alloy, having better properties than the base metal by passing direct current (DC) through its electrolyte solution. Electrodeposition is basically an atomistic deposition process in which the metal ions from the electrolyte solution are getting deposited as metal atoms on the surface of a substrate in a controlled way. Thus, electro-crystallization of solid metallic films is going to take place onto the surface of a conductive substrate.

Even though the exact date of the first electroplating is debatable, most agree that Luigi V. Brugnatelli, an Italian chemist and a friend of Alessandro Volta, was the first to explain the basics of electroplating in the early 19th century by successfully plating gold on silver, using voltaic pile. Since then, electroplating process with so many improvements has grown as technology to serve many purposes, right from improving the aesthetics of the base metals to protecting them from harsh environments, keeping their economic viability in mind (Parthasaradhy 1988).

1.2 CHEMISTRY OF ELECTROPLATING

Electroplating, or alternatively electrodeposition is a good old surface finishing technique, whose fundamentals are governed by universally accepted *Faraday's laws of electrolysis* (postulated by Michael Faraday in 1833). Basically, electrodeposition is carried out in an electrochemical cell made of three components- the electrodes (anode and cathode), the electrolyte, and the electric current. The schematic set of electroplating process is shown in Figure 1.1. During the process, the anode is made either as metal to be deposited, or an inert material, like graphite, platinum etc., and cathode, the substrate to be coated is placed parallel to the anode, and they act as sites for electrochemical redox reactions to take place. Both anode and cathode are immersed in ionic solution (electrolyte), containing metal ions to be deposited, and are kept in contact through an external power source. On applying direct current (DC), the anode undergoes oxidation leading to the spontaneous dissolution of metal atoms from its lattice into the electrolyte; and positively charged metal ions in the vicinity of cathode undergoes reduction, and get adsorbed as metal atoms on the cathodic surface, *via* electrolysis (Kanani 2004).
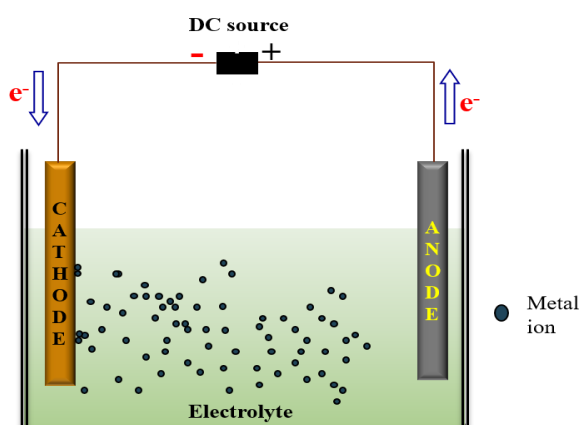
Figure 1.1- Basic components of conventional electroplating unit

The redox reactions taking place for an electrolyte MA can be given as follows:

i) Ionization of electrolyte in aqueous solution

$$MA_{(aq)} \rightleftharpoons M^+_{(aq)} + A^-_{(aq)}\text{...} (1.1)$$

ii) Depletion of the anode to give metal ions (oxidation)

$$M \rightarrow M^+_{(aq)} + e^- \quad \text{...} (1.2)$$

iii) Deposition of metal atoms on the cathode surface (reduction)

$$M^+_{(aq)} + e^- \rightarrow M_{(lattice)}\text{...} (1.3)$$

However, in the case of insoluble anodes such as graphite or platinum, oxidation of water takes the lead.

$$2H_2O \rightarrow 4H^+ + O_2 + 4e^-\text{.......................................} (1.4)$$

Thus, during electroplating, free metal ions from electrolyte solution are getting deposited on the surface of the substrate as metal atoms, and the process of deposition is driven by the current from the power source.

1.3 MECHANISM OF ELECTRODEPOSITION

Since metals have well-defined crystal structures, the electrodeposition of metal is similar to that of crystal growth, where the metal ions are discharged as metal atoms on cathode in the region of Electrical double layer (EDL), and get deposited as a thin film. This overall process is termed as *electro-crystallization,* and it occurs sequentially through the following stages (Paunovic and Schlesinger 2006):

i) *Ionic migration:* It is the electric field-assisted movement of hydrated metal ion(s) in the electrolyte into the diffuse double layer or EDL, formed at the cathode surface.

ii) *Electron transfer:* At the diffuse layer, the hydrated metal ions are loosely held by a weak electric field present in this layer. Subsequently, these metal ions enter into the compact layer of cathode surface where due to a higher field present, the hydration sheath is lost giving rise to adatoms.

iii) *Surface diffusion:* It is the spontaneous movement of adatoms due to concentration gradient. As a result, diffusion of adatoms occurs across the cathode surface and gets incorporated into the most favourable kink sites.

iv) **Nucleation:** It is the primitive stage where the substrate (cathode) gets covered with a few atomic layers of the metal. It requires high overvoltage and is thermodynamically stable.

v) **Growth of the deposit**: Once the nuclei have attained a critical size, it undergoes fusion and grows rapidly in one, two or three dimensions, at a relatively low overvoltage to form a metallic layer at the cathode surface. The atoms (*adatoms*) that are formed during the plating process on the crystal plane, quickly move and occupy favourable sites such as the *kink site (*where an atom interacts with three neighbours) or *edge site* (two neighbours) or remain as adatoms (one neighbour).

Thus, during actual deposition, there exists a dynamic equilibrium between the metal cations (in the electrolyte) and metal atoms (on the surface of substrate), due to external power source. On attainment of equilibrium, fully solvated (hydrated) metal ions get attracted towards the oppositely charged electrode surface by coulombic forces. Thus electrons furnished by the power source bring about the reduction of metal ions, and consequently, metal atoms are deposited on the cathode, and this process is called electro-crystallization. The actual structure of electrode-electrolyte (E-E) interface responsible for the reduction of metal ions (from the bulk electrolyte into metal atoms) as metal atoms (onto the surface of cathode) is shown schematically in Figure 1.2.
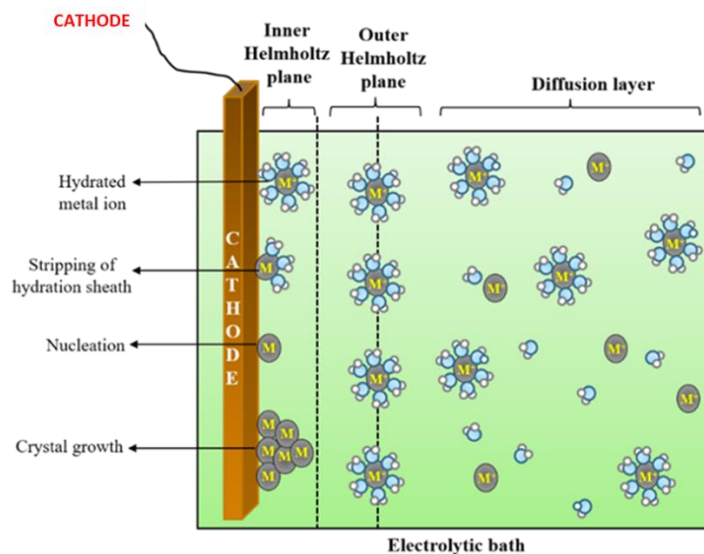
Figure 1.2- *Schematic representation showing different stages of electro-crystallization during electrodeposition of a metal on cathode (Adopted and modified from Ray 2015)*

6

In EDL, the inner layer closest to the electrode is known as the *inner Helmholtz plane*, composed largely of oriented water dipoles interposed by some preferentially adsorbed ions. The outer layer, known as the *outer Helmholtz plane*, reflects the array of ions having a charge opposite to that of the electrode. These cations are adsorbed onto the cathode surface by displacing the attached water molecules as shown in Figure 1.2. On continuous depletion of depositing ions from EDL, fresh ions are supplied from the bulk of electrolytes (Ray 2015). When the overall reaction is controlled solely by the rate at which the electroactive species gets from the bulk electrolyte to the electrode, it is said to be *mass transport limited*. However, the structure of the deposit is largely determined by steps (ii) and (iii). Hence, during plating, the operating parameters are adjusted in such a way that these steps predominate.

1.4 ALLOY ELECTROPLATING

Though metals have always had a significant role in the past civilizations, today's complex world is in constant search of simple and subtle alternatives to produce coatings with multifunctional properties, with a prime focus on the protection of commercially important base materials, like mild steel, copper, aluminium etc., from the effect of corrosion. In this aspect, *alloy electroplating* becomes a useful, economically viable, easy-to-perform surface coating technique, and can be accomplished by electro-codeposition of alloy constituents from the electrolyte containing the respective ions. By definition, an *alloy* is a mixture of a metal with a second metal or other non-metal material (additives) which are known to exhibit desirable properties such as increased hardness and lower melting points. As deposited alloys possess the combination of properties of pure metals, they are found to be a way better than the individual metal deposits (Brenner 1963). Hence, they can effectively serve many purposes such as improved corrosion resistance, wear resistance, abrasion tolerance, mechanical strength, thermal resistance, optical reflectivity, magnetic properties etc. in addition to improve the attractive appearance of base material, and thereby to increase their market value. Another key advantage of alloy plating is that certain metals such as Mo, Ge, W, etc. which by themselves are incapable of forming a deposit, can be codeposited as an alloy from the electrolytes containing Fe-group elements such as Fe, Co or Ni (Brenner 1963). In this way, alloy plating provides an

easy route for developing the material of specific properties and is considered to be a *boon* in the coating industry to meet many of the recent technological demands, which is otherwise unattainable by conventional metal electroplating.

1.4.1 Factors affecting alloy plating

Similar to conventional electrodeposition (ED), alloy plating is also an art of coating a thin layer of an alloy of the desired composition on the surface of a conductive substrate from various possible electrolytes (aqueous, non-aqueous, ionic liquids, molten salts etc.). However, in terms of theoretical and technical perspective, alloy plating needs an in-depth understanding as it requires stringent control over the electrolyte composition, additives and other dependent variables such as plating current density (c.d.), pH, temperature, agitation, mass transport process etc. A good electrodeposit is characterized by good adhesion, fine-grained structure, uniform thickness, good throwing power, and brightness. A poor deposit is characterized by an outward growth (whisker or dendritic) along with a powdery, burnt texture due to macroscale features such as steps, ridges, and polycrystalline block growth. In other words, the deposit obtained is coarsely crystalline, non-uniform, and dull in appearance. Following are a few critical elementary factors, out of many which can influence the nature of electrodeposits, during electroplating of any metal/alloy.

1.4.1.1 Bath composition

The plating bath consists of electroactive species, supporting electrolytes, complexing agents, and organic additives (Prakash et al. 2011).

i) Electroactive species: These are the ones that can participate in electrode reactions. During electroplating, exceeding higher concentrations of metal ions increase the mass transfer leading to poor deposit. When metal salt concentration is kept high, the high current density is employed for the deposition to occur increasing the grain size. A decrease in metal ion concentration decreases the grain size and results in fine adherent coating films. Thus, under optimal metal ion concentration, a smooth and uniform coatings are formed.

ii) Supporting electrolytes: These are the inorganic salts that are added to increase the conductivity of the plating bath. Actually, they do not participate in the electrode reactions but facilitate the uniform distribution of the current in the bath, and thereby control the pH changes. NaCl, NH_4Cl, Na_2SO_4, etc. are a few commonly used conducting salts, generally used in electroplating.

iii) Complexing agents: The metal ions are converted into a metal complex by the inclusion of a suitable complexing agent in the plating bath, where metal ions are available as metal complex ions. These complex ions furnish the metal ions in a controlled way to get a fine-grained and more adherent deposit, by avoiding bulk deposition. Complexing agents are generally used for: a) To make the deposition potential more negative so that the plating takes place at a lower potential, b) To prevent the passivation of anodes so that anode dissolves easily and improve the current efficiency, c) To improve the throwing power (a measure of relative thickness of coatings on different parts of cathode) of the plating bath, and d) To inhibit the reactivity of plating metal ion with the cathode metal, to avoid immersion coating. Few examples of complexing agents are cyanides, citrates, gluconates, sulphamates, etc.

d) Organic additives: Organic additives are basically organic compounds that are added deliberately into the electrolytic bath to bring structural and morphological modification to the electrodeposited coatings. A variety of organic additives are used in electroplating to meet various applications. It includes *brighteners* (e.g., thiourea, gelatin, coumarin), *levellers* (e.g., sodium allyl sulphonate), *structure modifiers* (e.g., saccharin), and *wetting agents* (sodium lauryl sulphate). These additives are used either individually or in combination. However, they should give a synergistic effect on the properties and performance of electrodeposits.

1.4.1.2 Current density

Current is the driving force required for a non-spontaneous process (electrodeposition) to become spontaneous. Current density (c.d.) is the amount of current flowing per unit cross-sectional area of the substrate to be coated and is expressed in mA cm^{-2}, A dm^{-2}, or A m^{-2}. It strongly influences the plating quality and the deposition rate. At low c.d., diffusion of metal ions is fast compared to the electron transfer (discharge of metal

ions), and the adatoms find the most favourable positions (kink sites) resulting in a well-formed deposit. But as the current density is increased, the rate of deposition increases, and the adatoms do not reach the most favourable positions. At high current density, mass transport of ions, due to migration of ions and evolution of hydrogen predominate, causing fast depletion of metal ions and H^+ ions in the close vicinity of cathode. Consequently, the number of nuclei increases on the surface of cathode, leading to less ordered deposits with macroscale features. In other words, bulk deposition occurs.

1.4.1.3 Temperature

Operating temperature of a bath is a vital parameter for consistent performance of any electroplating bath. Even though the quality of electrodeposits do improve with increase of bath temperature, elevated temperature may throw some adverse effects on the nature of electrodeposits, like increased hydrogen evolution at the cathode, corrosion of plating equipment, and decomposition of organic additives. At moderate temperatures, depletion of metal ions at cathode film do take place very easily, due to decreased viscosity of bath solution, good deposition does take place on cathode. Deviations of more than $5^{\circ}C$ from its optimum temperature value can throw adverse effect on the quality of deposits, like deposition rate, nature of coatings etc. Hence, an optimal temperature range is preferred for good deposition to take place, ideally in the range of $28^{\circ}C$ - $60^{\circ}C$.

1.4.1.4 pH

Generally, at low pH, excessive hydrogen evolution occurs at the cathode resulting in a burnt deposit. At a very high pH, metal ions do undergo hydrolysis, causing to form insoluble metal hydroxide on cathode surface. Therefore, an optimum pH range of 4-8 is generally recommended, depending on the nature of electrolytic bath. The pH of the plating bath needs to be maintained constant during deposition, using a suitable buffer.

1.4.1.5 Agitation

Agitation has the same effect as that of the temperature. It brings more metal ions to the cathode film and decreases the thickness of the cathode diffusion layer, thus leading to an increase in the proportion of more noble metal in the deposit. However, on increasing further, the effective thickness of the diffusion layer diminishes; hence the

diffusion rate increases. Agitation not only helps in decreasing the thickness of the cathode diffusion layer, but also causes the metal ratio of the diffusion layer to approach more closely to that of the solution in the body of the bath (Brenner 1963). The most important aspect of steady agitation of bath is to overcome the concentration polarization by avoiding the concentration gradient of metal ions near cathode.

1.4.1.6 Polarization

Polarization is defined as a process in which there is a variation in electrode potential due to the slow supply of ions from the bulk solution to the electrode. When there is a passage of current, the metal ion concentration in the vicinity of the electrode surface decreases owing to the reduction of metal ions. Due to this, there is a shift in the equilibrium and a change in the electrode potential. The concentration gradient between the bulk solution and the area surrounding the electrode surface leads to diffusion of ions and thus, equilibrium is re-established.

1.4.1.7 Hydrogen overvoltage

When the applied voltage is slightly more than the standard decomposition potential, electrolysis occurs uninterruptedly. This excess voltage that needs to be applied above the theoretical potential for continuous electrolysis to occur, and is known as *overvoltage or overpotential* (η). Electrochemically, metal deposition is always accompanied by hydrogen evolution due to presence of H^+ ions in the electrolyte. The potential at which hydrogen gas is formed from H^+ ions, due to the potential difference that exists between a reversible hydrogen electrode and an electrode when they are in the same solution is termed as *hydrogen overvoltage*. The H_2 gas liberated during electro-codeposition of metal/alloy often has a dominant effect on the polarization as well as on the composition of alloy formed. If the overpotential for hydrogen evolution is high, then the current corresponding to the individual metals will be close to the limiting values, and deposition takes place smoothly. Contrary to this, if the overpotential for hydrogen evolution is low, there will be an excess liberation of H_2 gas on the cathode surface, thereby leading to a poor deposition with a change in the alloy composition, or no deposition takes place. Thanks to hydrogen overvoltage, due to which electrodeposition of metals, having negative E° values from their aqueous

solutions are possible. For example, Zn with $E^° = -0.76V$, being having a very high hydrogen overvoltage (0.70 V), its deposition from its solution is possible.

1.4.2 Different types of alloy deposition

In alloy deposition, the choice of parent metals is made in such a way that the two have their deposition potentials closer. However, this concept need not be true always, and this condition is not considered as a basic principle as well. Therefore, based on the preference for co-deposition of parent metals, alloy deposition is broadly classified into five types (i) Regular, (ii) Irregular, (iii) Equilibrium, (iv) Anomalous, and (v) Induced deposition. The types (i)-(iii) are categorized as *normal co-deposition*, which involves preferential co-deposition of more noble metal and the types (iv) and (v) are collectively referred to as *abnormal co-deposition*, where the more noble metal does not necessarily deposit preferentially (Brenner 1963).

i) Regular co-deposition

This type of alloy deposition is characterized by the plating process that is in control of the diffusion phenomenon. In this case, the amount of more noble metal in the alloy increases with an increase in total metal ion concentration in the electrolytic bath, decrease in current density, raise in temperature and agitation. It is most likely to occur in baths in which the static potentials of the metals are far apart, and with metals that do not form solid solutions. Regular co-deposition probably occurs in a bath containing simple metal ions, but may sometimes occur in complex ion-containing baths as well. (Mn-Ni) and (Cd-Zn) systems are a few representatives of this type.

ii) Irregular co-deposition

This refers to as a process that is controlled by the cathode potentials and occurs in metals that form a solid solution. Irregular co-deposition is most likely to happen with solutions of complex ions, specifically with systems in which the static potentials of the parent metal are distinctively affected by the concentration of the complexing agent. Since deposition in these systems are controlled by irregularities of the potentials of metal ions in the solution, the plating variables are comparatively less effective on the composition of the deposit, compared to regular alloy plating systems. (Cu-Zn), (Sn-Zn), (Cd-Cu) systems are typical examples.

12

iii) Equilibrium co-deposition

Equilibrium co-deposition is characterized by the deposition of an alloy from a solution that is in chemical equilibrium with the constituent metals. A distinct feature of this type is that the ratio of metal content in the deposit is the same as that in the bath solution. (Cu-Bi) and (Pb-Sn) systems fall into this category.

iv) Anomalous co-deposition

This type of co-deposition is a rare and peculiar process characterized by an irregularity, where the less noble metal deposits preferentially. It occurs only in few types of alloy coatings, under explicit conditions of concentrations and operating variables. It is frequently associated with the electrodeposition of alloys containing one or more of the three metals of the Fe-group, *i.e.,* Fe, Co, and Ni, and in alloys of mutual metals of Fe-group. In case of (Zn-Fe) alloy system, Ni (E°_{Ni} = -0.25 V) being nobler than that of Zn (E°_{Zn} = -0.76 V), it could be assumed that the former would preferentially deposit. But it is not the case in reality, instead less noble Zn deposit preferentially than more noble (Ni). Consequently, the ratio of wt.% Zn to wt.% Ni in the deposit is more than that in the bath.

v) Induced co-deposition

In this type of co-deposition, one of the metals does not deposit on its own from its aqueous solution. However, they can readily be co-deposited with iron group metals, and thereby give enhanced properties to alloy coatings. The metals which trigger or induce the deposition are termed *inducing metals,* and metals that do not deposit on their own are termed as *reluctant metals.* Mo, W, V, and Ti are a few examples. The induced type of co-deposition has its distinction from other types of alloy deposition from the fact that effects of plating variables (like, current density and temperature) on deposit characters (like, composition and surface morphology) are quite vagarious and unpredictable. For example, in (Ni-Mo), (Ni-W), (W-Co) alloy coatings.

1.5 MODERN TRENDS IN ELECTROPLATING

Today, electrodeposits with new properties, better performances and modern methods of synthesis are capable to influence the crystal structure and atomic configurations to a great extent to cater to the needs of recent technological demands. One of the common

methods is to incorporate additives in the growth medium that can preferentially adsorb on specific crystallographic planes and substantially alter the deposit characteristics by increasing the surface area of alloy coatings (Prioteasa 2010, Shetty et al. 2018). However, in electroplating, the mass transport resistance resulting from the depletion of the electroactive species at the cathode surface, due to mass transport limitation is considered as the most important factor responsible for the composition and phase structure of coatings. In this regard, alloy coatings of better performance can be synthesized through other modern methods using mass transport process of metal ions as tool. The electrodeposition of alloys, having better material properties can be accomplished by the periodic modulation of mass transport process near EDL, during deposition using sophisticated power sources. The performance of monolayer (monolithic) alloy coatings can be improved several-fold better by relying on the modulation of mass transport of metal ions towards EDL, through any of the following methods.

- Composition Modulated Multilayer electrodeposition (CMM - ED)
- Magneto-electrodeposition (MED)
- Sono-electrodeposition (SED)

1.5.1 Composition Modulated Multilayer Electrodeposition

Composition modulated multilayer electrodeposition (CMM-ED), or simply multilayer electrodeposition is a method of developing coatings in a layered fashion, having alternate layers of two different metals or alloys (having two or more metals). It can be developed by periodic modulation of cathode current density, during deposition The composition modulated alloy (CMA) coatings show better performance compared to its monolayer counterpart, which is not possible through any other metallurgical methods. There are several methods for obtaining CMA coatings, they are physical vapour deposition (PVD), chemical vapour deposition (CVD), molecular beam epitaxy (MBE) and sputtering techniques. These techniques are categorized under the *Dry process* and are known to possess several advantages, and are used for specific applications. But due to certain limitations, like high capital and energy costs, other alternative methods are used. In this direction, production of multilayer alloy coatings through *Wet process*, or electrodeposition method is considered to be more reliable, and economically viable.

Multi-layered alloy coatings developed by electrodeposition method basically consists of layers of alloys of two (or more) metals, having alternatively different composition. They are deposited as thin layers, stacked one over the other by periodic modulation of mass transport towards cathode, during deposition. This periodic modulation of mass transport of metal ions towards cathode can be affected by pulsing either the current or convection (through either agitation, or by pulsing the magnetic field effect). There are plenty of reports in the literature on the development of multilayer alloy coatings, developed by periodic pulsing of cathode current density (CCD) (Bhat and Hegde 2012). Since individual layer thickness is in the limit of nano-meter scale, these layered coatings can bring a marked effect overall performance of alloy coatings, which is not possible by any conventional method.

Today, multilayer alloy coatings are considered as the most protective coatings as their benefits exceed that of their monolayer alloy coatings, deposited from the same bath for same duration. The unusually different properties of CMM coatings are due to layers of alternatively different phase structures and compositions. In addition, the performances of multilayer alloy coatings, like corrosion resistance, micro-hardness, tensile strength and other electronic properties were found to be increased with the degree of layering, or with decrease of individual layer thickness.

1.5.2 Magneto-electrodeposition

Magneto-electrodeposition refers to electrodeposition under the effect of induced magnetic field. Magneto-electrodeposition is another effective approach to improve the properties of metal/alloy coatings by impacting the mass transport phenomenon through forced convection, called *magneto-convection, i.e.,* by superimposing an external magnetic field, applied simultaneously to the process of electrodeposition. Magneto-electrodeposition works on the principle that development of alloy coatings on the cathode surface occurs under the influence of magnetoconvection. Similar to conventional electrodeposition, magneto-electrodeposition is a simple, cost-effective and room-temperature technology, which can be easily scaled up for use in large-size areas as well. Magneto-electrodeposition is inherently interdisciplinary subject, bringing concepts from electrochemistry, hydrodynamics and magnetism, with results which are sometimes surprising (Monzon and Coey 2014). The elucidation of results of magneto-electrodeposition can lead to unexpected insights into fundamental

electrochemical processes, as well as new practical applications. Today, magneto-electrodeposition is of great scientific interest, due to *magnetoconvection effect,* which is responsible for altering the flow patterns of ions at E-E interface, which in turn increase the rate of deposition and modify the microstructure of electrodeposits (Fahidy 2001). Though the benefits of large-scale convection can be effectively achieved by means of mechanical agitation, the magnetic field (*B*) induced convection has its own merits in terms of the electrochemical changes taking place at EDL. Thus, magneto-electrodeposition can be used as a tool to manipulate the flow pattern of the electrolyte near EDL, by changing its both direction and intensity, and can be a better option to develop alloy coatings of better performance, compared to conventional electrodeposited (ED) alloy coatings.

During magneto-electrodeposition, the electrolytic cell connected to the external power source is held in between the two poles of electromagnet as shown in Figure 1.3. When electric current is made to flow through the electrolytic solution, the ions with fixed magnetic moments present within the electrolyte, start spinning in the presence of magnetic field. This, in turn, generates turbulence within the electrolytic solution due to the combined effect of magnetic field along with electric field and therefore ions behave as tiny individual magnets and align themselves in the vicinity of E-E interface, as shown schematically in Figure. 1.3.
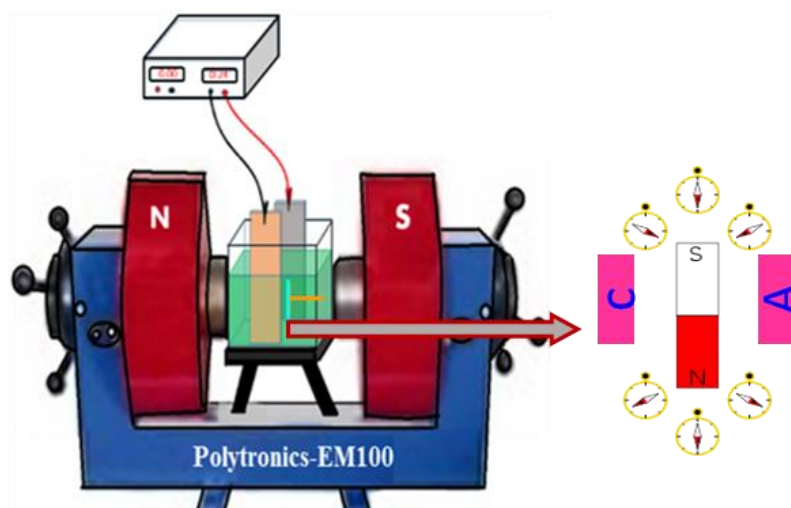
Figure 1.3 - *Schematic experimental set-up used for magneto-electrodeposition of alloy coatings, under the combined effect of magnetic field (B) and electric field, using proper electrolytic bath*

1.5.2.1 Theoretical aspect of magneto-electrodeposition

The convective forces that a magnetic field creates on the solutions during electrochemical deposition of metal ions are responsible for changed physico-mechanical properties of magneto-electrodeposited (MED) coatings. Generally, during electroplating, the mass transport resistance resulting from the depletion of the electroactive species at the cathode surface (due to mass transport limitation) is basically considered as the most important factor responsible for change of composition and phase structure of coatings. In a mass transport-controlled electrolytic process the effect of imposed magnetic field strength on properties of the diffusion boundary layer is explained by the phenomenon, called *magneto-hydrodynamic* (MHD) effect (Fahidy 2002). MHD effect is essentially about the additional convection effect, derived from magnetic energy origin that acts inside the diffusion layer, leading to the so-called magnetoconvection.

For simple linear diffusion, under limiting conditions the rate of mass transport is governed by the limiting current density(i_L), given by the Equation (1.5) (Kanani 2004),

$$i_L = (nFDC_B)/\delta \dots\dots\dots\dots\dots\dots\dots\dots\dots\dots\dots\dots(1.5)$$

where n is the number of electrons transferred during the electrochemical process, F is the Faraday constant (96500 C), D is the diffusion coefficient, C_B is the bulk concentration of the reactant species, and δ is the thickness of EDL. The limiting current density (i_L) actually stands for the current density at which the rate of deposition is maximum, under given experimental conditions. Therefore, from Equation (1.5), it may be concluded that for a given electrolytic bath, i_L of particular metal ions can be increased by decreasing the thickness (δ), which can be accomplished by imparting MHD effect inside the bath, during deposition.

When an external magnetic field, B is superimposed on the electrolytic deposition process, an additional convection is created in the electrochemical cell, which increases the i_L in the diffusion-controlled regime due to the localized magnetic stirring of the electrolyte (Monzon and Coey 2014). The net force exerted on a moving charged particle (such as ion or electron) in an electromagnetic field, termed as Lorentz force is given by the Equation (1.6)

$$F_L = qE + qvBSin\theta \ldots\ldots\ldots\ldots\ldots\ldots\ldots\ldots\ldots\ldots\ldots\ldots(1.6)$$

where 'q' is the charge of the ion moving with the velocity v, in an electric field E and magnetic field B. The Equation 1.6, consists of two parts, the first part is contributed by the electric field, and the second part is due to magnetic force which is proportional to q and to the magnitude of the induced B, *i.e.* the vector cross product $v \times BSin\theta$. Here, θ is the angle between B and electric field. Since Lorentz force (F_L) is the vector product of q and B, it is zero when B and q are parallel, and it is the largest when they are perpendicular. Representative diagram showing the effect of magnetic field (B) on the movement of metal ions towards cathode, when B is applied parallel and perpendicular to the direction of electric field (j) is given in Figure 1.4. The hydrodynamic flow of metal ions towards cathode in a uniform magnetic field (B), when it is applied parallel to the direction of j is shown in Figure 1.4(a), where primary MHD flow is parallel to the direction of j. When applied B is perpendicular to the direction of j, the primary MHD flow is a vortex around the rim, due to Lorentz force (F_L), as shown in Figure 1.4(b). Consequently, the secondary micro-MHD vortices arise around protuberances on the surface of cathode as shown in Figure 1.4 (c).
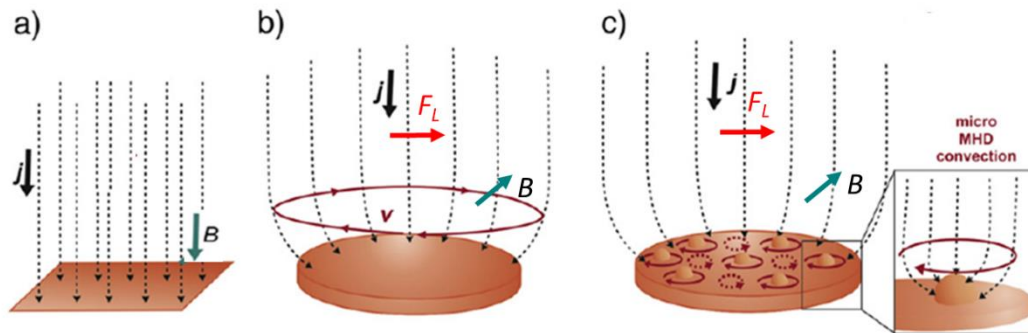
Figure 1.4 - *Hydrodynamic flow at an electrode in a uniform magnetic field. a) Magnetic field (B) is applied parallel to the direction of electric field (j), where primary MHD flow is perpendicular to the surface. b) B is applied perpendicular to j, where primary MHD flow is a vortex around the rim, due to Lorentz force, and c) secondary micro-MHD vortices arise around protuberances on the surface (Adopted and modified from Monzon and Coey 2014).*

As current density is invariably non-uniform at the edge of electrodes, there is normally an MHD flow around the rim when a magnetic field is perpendicular to the electrode surface. Furthermore, uneven growth at the cathode during electrodeposition produces a locally non-uniform current distribution giving rise to secondary micro MHD vortices that protrude into the diffusion layer (Figure 1.4 c). Consequently, there is thinning of EDL at electrode surface; thereby affecting the optimum mass transport process at the EDL. In other words, *B*-induced Lorentz force, coupled with local current density allows to induce the flow patterns magnetically, on a scale that would be otherwise unattainable. There are numerous studies concerning possible effects of static magnetic fields on the process of electrodeposition, and several potential interaction mechanisms have also been proposed. Based on the inventions, several authors have reviewed the influence of superimposed magnetic field on the properties of electrolyte, electrode kinetics, mass transport, and changes in electrodeposited metal properties (Fahidy 1983), their practical applications in electrochemistry (Tacken and Janssen 1995), influence of constant magnetic field effects on metal surfaces (Fahidy 2001) and the effect of Lorentz force on the electrodeposition process (Monzon and Coey 2014). As a result, experimental research relating the process of electrodeposition with applied magnetic field has gained the interest of many, and has been thus used in the production of various materials such as paramagnetic metals, alloys and metal-non-metallic composites. In addition, the application of constant magnetic field has also been diversified in electropolymerization and many other organic reactions (Kolodziejczyk et al. 2018).

1.6 CORROSION

Most of the metals except noble metals occur in nature in their combined state as their oxides, sulphates, carbonates etc. They are extracted from their ores by reduction which is an endothermic process and thus have a strong tendency to revert back to their combined state. Corrosion is a gradually occurring destructive phenomenon where the pure or refined metal is naturally converted to its undesirable metallic form due to a chemical or electrochemical reaction, with its environment. In reality, corrosion is the transformation of pure metal into its more stable oxide, hydroxide or sulphide state, depending on the environment in which they are to perform. Everyday examples of corrosion include rusting of steel utensils, water pipes, metallic statues, bluish-green

patina formation on copper, or brass structures, silver tarnishing etc. (Gadag and Shetty 2006). As a whole, corrosion gives rise to various socio-economic consequences such as poor appearance, product contamination, loss of efficiency, depletion of natural resources, effect on safety and reliability in handling hazardous materials and loss of valuable products.

1.6.1 Electrochemical theory of corrosion

Electrochemical corrosion of metals occur by the formation of anodic and cathodic sites on the same metal surface, or when two different metals are in contact with each other in the presence of a conducting medium (Fontana 2005). These redox sites at metal-electrolyte interface together make up a *corrosion cell*, which is shown schematically in Figure 1.5 (Stansbury and Buchanan 2000). It may be observed that the electrons from atoms at the surface of the metal (anode) migrate to a suitable electron acceptor (cathode), or depolarizers (oxygen, acids or cations of less active metals) *via* a moist medium.
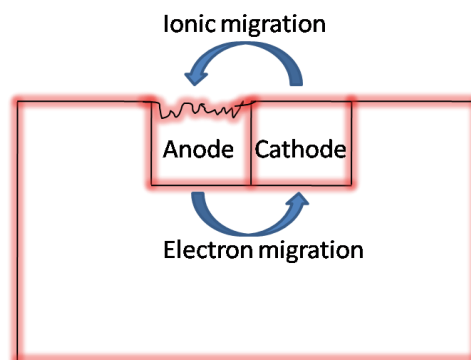
Figure 1.5 - Schematic representation of a corrosion cell with anode, cathode and conducting medium

To begin with, dissolution of metal takes place at anode, and may be shown as follows:

$$M \rightarrow M^{n+} + ne^- \ \text{..(1.7)}$$

Actually, the complexity of corrosion lies in the type of cathodic reaction, depending on the nature of the corrosion environment. Hence, the cathodic reaction may be classified as below:

a) **Hydrogen evolution type:** It involves the liberation of hydrogen in absence of oxygen, and cathodic reactions may take place as follows:

i) In acidic medium,

$$2H^+ + 2e^- \rightarrow H_{2\,(g)} \quad\text{...} (1.8)$$

ii) In neutral or alkaline medium,

$$2H_2O + 2e^- \rightarrow 2OH^- + H_{2(g)} \quad\text{.............................} (1.9)$$

  b) **Oxygen absorption type:** If cathodic reaction involves absorption of oxygen, it may be shown as follows, depending on the constituents of the medium.

  i) In acidic medium,

$$4H^+ + O_2 + 4e^- \rightarrow 2H_2O_{(l)} \quad\text{...........................} (1.10)$$

  ii) In neutral or alkaline medium,

$$2H_2O_{(l)} + O_{2(g)} + 4e^- \rightarrow 4OH^- \quad\text{.......................} (1.11)$$

Here, Fe^{+2} ions formed at the anodic site, and OH^- ions formed at cathodic sites show tendency to diffuse towards each other to form $Fe(OH)_2$, which eventually turns into $Fe_2O_3.3H_2O$ (haematite) and $Fe_3O_4.3H_2O$ (magnetite), depending on availability of air and moisture. Thus, all metals during corrosion get transformed into their stable compound form, due to the effect of environment.

1.6.2 Electrochemical methods for corrosion evaluation

Since metallic corrosion occurs *via* redox reaction at the metal-electrolyte interface, it is possible to evaluate the corrosion behaviour using electrochemical measurements. Unlike traditional weight-loss method, electrochemical methods are quick, accurate and provide lot of mechanistic information, which helps to design and implement corrosion protection strategies. The weight-loss method is beneficial to study those metals/alloys which are highly corrosive by nature. In electrochemical methods of corrosion study, a test sample of a known surface area of a few dimensions is immersed in the corrosion medium and used as working electrode in a three-electrodes cell. Additional two electrodes (counter and reference) are used to measure the current-potential response of the working electrode by connecting it to an electrochemical workstation called a potentiostat/galvanostat. A representative three-electrode set up used for the corrosion study is shown in Figure 1.6 (Souza et al. 2019).
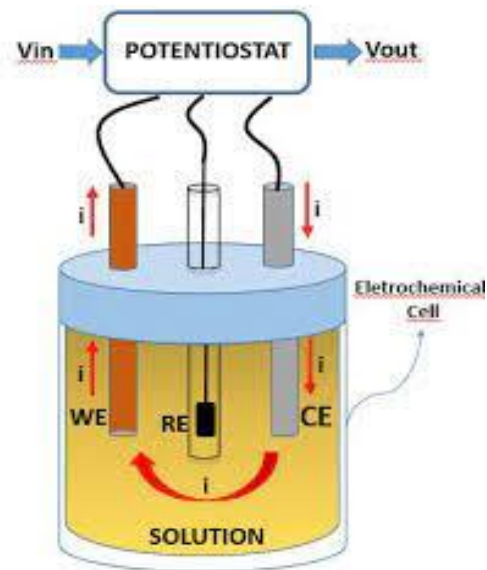
Figure 1.6- *Three-electrode set-up for corrosion characterization through electrochemical AC and DC methods. The working electrode (Test specimen), reference electrode, counter electrode and test solution may be seen (Adopted from Souza et al. 2019)*

Depending on the type of current used, corrosion measurement techniques may be broadly classified as:

i)   Potentiodynamic polarization (PDP), or Tafel extrapolation method (DC method)
ii) Electrochemical impedance spectroscopy (EIS), or AC technique

Based on the quantitative kinetic parameters of both anodic and cathodic reactions, the corrosion behaviour, and corrosion rates of test sample is evaluated using computer-operated softwares, using the principles of Butler-Volmer equation, and Faraday's first law of electrolysis, respectively. The nature of anodic and cathodic polarization curves, corrosion current (i_{corr}) and corrosion potnetial (E_{corr}) values give valuable information with regard to the mechanistic aspects of corrosion.

1.6.2.1 Potentiodynamic polarization method

Potentiodynamic polarization (PDP), or Tafel extrapolation method is one of the widely accepted methods for monitoring or evaluating the corrosion rate (*CR*) of the metal sample, under test in a given medium. The technique employs a three-electrode assembly comprising of working electrode (metal test sample), counter electrode and a reference electrode (Figure 1.6). The working electrode taken in the corrosion medium

is subjected to oxidation (metal dissolution) and reduction (hydrogen evolution) reactions by sweeping the potential across ±250 mV at a constant scan rate of 1.0 mV s^{-1}, starting from -ve potential. The resulting current response will be recorded in the form of a logarithmic graphical plot, commonly called as Tafel plot. Figure 1.7 shows a typical Tafel plot, a plot of electrode potential vs. log of current density (i) of the test specimen.
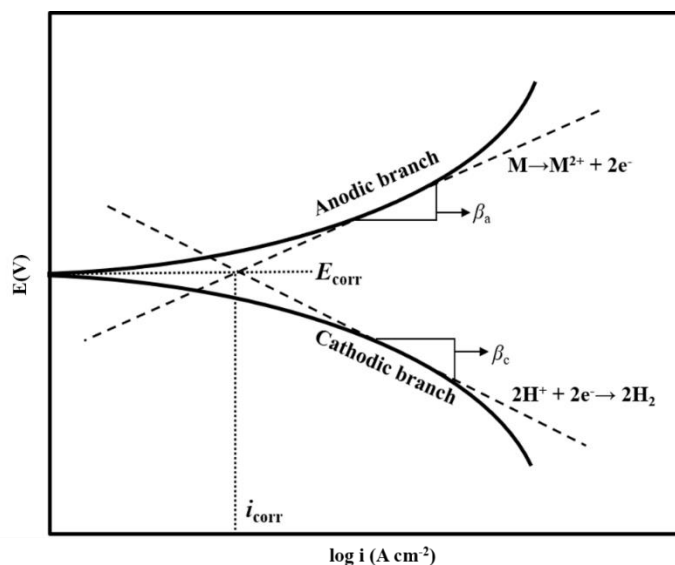
Figure 1.7- A typical Tafel plot showing anodic and cathodic polarization curves. Corrosion current (i_{corr}) and corrosion potential (E_{corr}) values can be obtained on extrapolation of anodic and cathodic curves

Usually, potentiodynamic polarization experiments are carried out by scanning the working electrode in a potential window starting from -250 mV from open circuit potential (OCP), till +250 mV from OCP, through the potential of zero net current, called corrosion potential (E_{corr}) which might be different from the OCP of the E-E interface, under test. Thus two diverging polarization curves, corresponding to anodic and cathodic currents are obtained as shown by solid lines in Figure 1.7. The linear portion of polarization curves are extrapolated to meet at a particular point to get the value of corrosion current (i_{corr}), as shown in Figure 1.7. The value of this corrosion current (i_{corr}), obtained for a particular test specimen can be used to calculate its corrosion rate (CR), using the principle of Faraday's law. The slopes of oxidation and reduction reactions (where applied potential are, respectively positive and negative with respect to OCP) are called Tafel slopes (expressed in mV decade^{-1}), and their values

can be determined from the plot. The value of anodic Tafel slope, represented by β_a is a measure of the tendency of test electrode to undergo oxidation (dissolution), whereas cathodic Tafel slope, represented by β_c is a measure of its tendency to undergo reduction. As the applied potential is made more negative, the rate of reduction also increases (Bard and Faulkner 2004, Yang 2008). Thus the values of β_a *and* β_c gives mechanistic information with regard to anodic and cathodic reactions of corrosion process.

Accordingly, the linear portions of both anodic and cathodic branches of the polarization curve are extrapolated to get $E_{corr,}$ and the value of current corresponding to that point of intersection will give corrosion current density (i_{corr}), as shown in Figure 1.7. This approach of determining the value of i_{corr}, allows one to determine the corrosion rate (CR) of a test specimen, using the relation given in Equation 1.12. This method of determining the value of CR from polarization curves is called Tafel extrapolation method.

$$CR = \frac{K \times EW \times i_{corr}}{D}$$………………………………………………..(1.12)

where,

        CR = corrosion rate of corroding test specimen

        EW = equivalent weight of corroding material

        i_{corr} = corrosion current density, expressed in $\mu A\ cm^{-2}$

        D =density of the corroding material

        K= conversion factor = 0.00327, when CR is expressed in $mm\ y^{-1}$

Thus, this potentiodynamic polarization method or Tafel method allows the determination of CR of a test sample, quickly and with a great degree of accuracy. Thus, it is possible to determine the Tafel slopes β_a and β_c as well as the corrosion potential (E_{corr}) and corrosion current density (i_{corr}) from PDP curves. Despite of many advantages of this method, it has some shortcomings, like:

i) While doing PDP measurements, the sample specimens are undergoing dissolution (during cathodic polarization). Hence, they can be polarized only once. In other words, this method is destructive.

ii) It is difficult to obtain in-depth information about the passivity and pitting vulnerability of specific materials to corrosion in designated environments,

because much larger anodic polarizations (higher cathodic polarization) are required to obtain these types of information. (Fontana 2005, Yang 2008).

1.6.2.2 Electrochemical Impedance Spectroscopy (EIS)

Electrochemical Impedance Spectroscopy (EIS) is a versatile, highly sensitive, non-destructive technique that enables the study of electrochemical processes occurring at an electrode interface (Cesiulis et al. 2016). The basis of EIS is the analysis of the impedance (resistance of alternating current) of the observed system with respect to the applied frequency and exciting signal. In EIS, a small amplitude of AC perturbation (typically a sine wave of amplitude ± 10 mV) is applied to the system under investigation, in a wide range of frequencies ranging from 10^5 to 10^{-3} Hz and the response of the current at each frequency(ω) is measured, and corresponding electrical impedance (resistance of alternate current) is obtained. The value of impedance is determined by $Z(\omega)= V(\omega)/i(\omega)$ (Yuan et al. 2009). Various processes taking place on the surface of test specimen are responsible for current output, for a given voltage input at discrete frequencies, causing a time lag and a measurable angle θ, between the time-dependent excitation and response signals. These processes have been simulated by resistive-capacitive electrical networks. The impedance, Z (ω) is a combination of real $Z'(\omega)$ and imaginary $Z''(\omega)$ components and may be expressed in terms of Nyquist plots as shown in Figure 1.8.
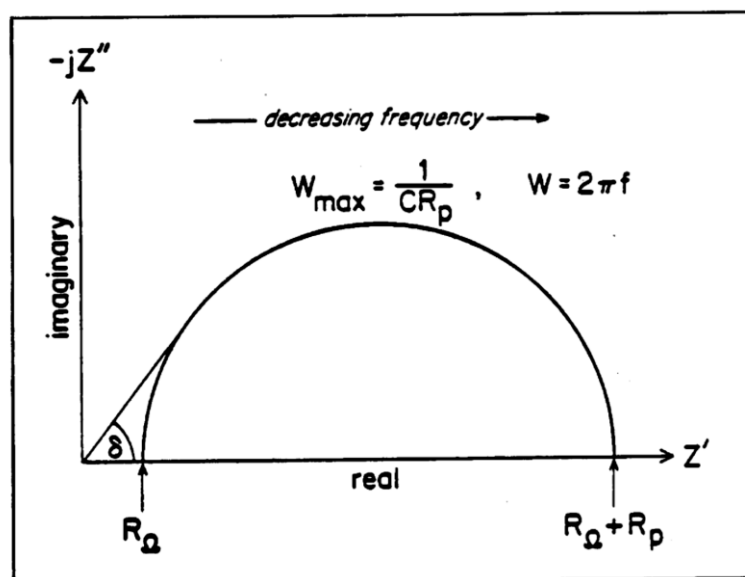
Figure 1.8 *- Representative Nyquist Plot showing real (Z') and imaginary(Z") components of impedance (Z) over range of frequency (f)*

25

The Nyquist plot shows a semicircle, with increasing frequency in a counter-clockwise direction as shown in Figure 1.8. At very high frequency, the imaginary component Z'' disappears leaving only the solution resistance, R_S. At very low frequency, Z'' disappears, leaving a sum of R_S and the Faradaic reaction resistance or polarization resistance, R_P. Polarization resistance, R_P is inversely proportional to the corrosion rate (CR). R_S measured at high frequency can be subtracted from the sum of R_S and R_P at low frequency to give the compensated value of R_P free of ohmic interferences. Since the amplitude of excitation signal is small enough for the system to be in the equilibrium state, EIS measurements can be effectively used to evaluate the system properties without significantly disturbing them. Frequency sweeping in a wide range from high to low frequency enables the reaction steps with different rate constants, such as mass transport, charge transfer, and chemical reaction, to be separated.

Another important advantage of EIS analyses is to create an "*equivalent circuit*" of the system using resistors and capacitors in series and parallel. The physical behaviour of the corrosion system can be simulated and quantified with this circuit to gain insight into the important process in the corrosion system (Ribeiro and Abrantes 2016). The impedance spectra are modelled by assuming a circuit made up of resistors, capacitors, and inductors and then fitting that circuit to the spectra to extract values of circuit elements. The values may then be related to the physical phenomena taking place on the surface of test specimen, to understand the corrosion process with better insight. Thus the distinct advantages of EIS method, made it find its applications in the following areas of corrosion measurement:

- Rapid estimation of corrosion rates.
- Estimation of extremely low corrosion rate and metal contamination rate.
- Estimation of corrosion rates in low conductivity media.
- Rapid assessment of corrosion inhibitor performance in aqueous and non-aqueous media.
- Rapid evaluation of coatings.

Apart from corrosion study, EIS technique is also used in many other electrochemical studies in electrode kinetics, photovoltaics, batteries, solid-state electrochemistry, and bio-electrochemistry etc.

Advantages of AC technique over DC technique

i) As AC impedance technique uses very small excitation amplitudes (usually in the range of 5-10 mV), damage to the electrochemical test system is very minimal. Hence, this method is non-destructive in nature.

ii) Since AC impedance measurements provide data on both electrode capacitance and charge transfer kinetics, the technique can provide valuable mechanistic information.

iii) AC impedance technique does not involve a potential scan, and hence it can be applied even to low conductivity solutions, but DC techniques are subject to serious potential control errors.

1.7 WATER ELECTROLYSIS

Hydrogen, a clean burning fuel is considered as one of the advantageous alternatives for unsustainable fossil fuels due to its high electrochemical reactivity, energy density and widespread availability. Hydrogen plays a vital role in ammonia production, petroleum refining, metal refining, and electronics fabrication, with average worldwide consumption of about 40 million tons, and thus can finds its place as a promising fuel in the future energy market. Globally, most of the hydrogen production is contributed by the reformation of natural gas, heavy oil, gasification of coal and petroleum coke etc. However, in return, an enormous amount of energy and CO_2 gets emitted (Santos and Sequeira 2013). To realize a hydrogen-based economy, hydrogen must be efficiently and sustainably produced. In order to attain this, many other alternative routes like the thermochemical method (steam reforming), biochemical method (anaerobic decomposition), and electrochemical method (water electrolysis) have been tried. Although steam reforming is a less expensive method, it is not suggested due to the usage of methane, which being a greenhouse emitter can indirectly contribute towards global warming. Therefore, from all these aspects, the production of hydrogen *via water electrolysis* is considered to be the most economically viable and promising one.

Water electrolysis or water splitting is a process of breaking down water into its basic elements *i.e.*, H_2 and O_2, using electric current. Despite the fact that this method is not the cheapest one, it is preferred due to high degree of purity of the gases, obtained therefrom. Room-temperature water electrolysis can take place under acidic or alkaline conditions. In case of acidic conditions, an electrolyzer with Proton exchange membrane (*PEM*) is used to perform water electrolysis and is commonly known as *PEM water electrolysis*. Although PEM water electrolysis systems offer several advantages (such as high energy efficiency, good hydrogen production rate and a compact design), their extensive use is prevented by the prohibitive cost of catalysts and short durability of membranes. Therefore, alkaline electrolyzers are commonly preferred. The major set back of this method is its high HER (hydrogen evolution reaction) overpotential, which is the main hindrance for large-scale production of hydrogen, and this could be overcome only by using a suitable electrocatalyst. An electrocatalyst is an electrode material that participates in an electrochemical reaction to speed up the process, but still remains unaltered at the end of the reaction. As adsorption/desorption processes are taking place steps on the surface of electrocatalysts, electro-catalytic reactions of electrodes are essentially heterogeneous in nature.

1.7.1 Pre-requisites of a good electrocatalyst

For efficient electrolysis to take place, the electrode material need to be stable, abundant and active in its all working conditions. The fundamental requirements of an ideal electrocatalyst are as follows (Sapountzi et al. 2017):

i) Low intrinsic overpotential for the desired electrochemical reaction (for both hydrogen, or oxygen evolution reaction).

ii) High active surface area which facilitates both good accessibility to the reactants and sufficiently fast removal of products.

iii) High electrical conductivity (by providing easy pathways for electrons)

iv) Proper chemical stability (its compatibility with electrolyte)

v) Electrochemical stability (not being corroded at working condition)

vi) Good mechanical stability (especially for high-temperature electrolysis)

1.7.2 Volcano plot

The well-known 'Sabatier Principle', proposed by Paul Sabatier (a French Nobel laureate) is a qualitative way to predict the activity of heterogeneous catalysts. The principle states that to have high catalytic activity, the interaction between reactants and catalysts should neither be too strong, nor be too weak (Ooka et al. 2021). If the interaction is too weak, then there will be no reaction on the surface, because it is difficult for the catalyst surface to bind with reactants. Suppose the interaction is too strong, then the reactant or product is difficult to get desorbed from the catalyst surface, and this also lowers the activity. This phenomenon has been cast into an intuitive tool, termed as 'volcano plots', as shown in Figure 1.9. This picture characterizes catalytic activity with respect to catalyst/intermediate interactions. Volcano plots are first introduced by Balandin (Milan and Nedeljko 1998). The basic idea is that, if the plotting rate of a chemical reaction on a heterogeneous catalyst with some adsorption property, say adsorption enthalpy, then according to Sabatier's principle, the plot will have a maximum, showing the shape like a volcano. Volcano plots contain a minimum of two slopes, meeting at the top. The volcano shape aids the comparison of the thermodynamics between different catalysts, thereby facilitating the identification of *good* candidates. Thermodynamically optimal candidates are those fulfilling Sabatier's principle, which appear near the highest point of the volcano. The volcano slopes delineate situations in which the catalyst/substrate interaction is either too strong (left slope) or too weak (right slope) (Busch et. al. 2015).
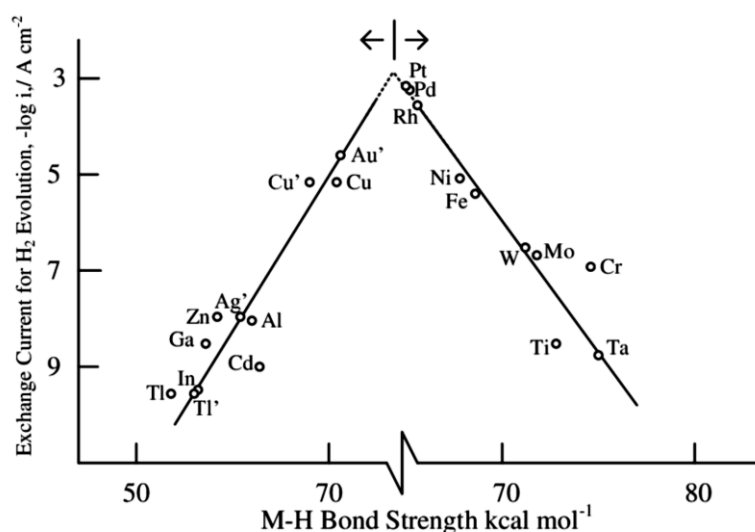
Figure 1.9- *Typical volcano plot for HER (Adopted from Bockris et. al. 2002)*

29

1.8 ALLOY COATINGS AS ELECTROCATALYSTS

Platinum is known to exhibit best HER activity. But due to its high cost, there is a need to replace the noble metals with low-cost novel materials that can exhibit high activity for HER. In this regard, three categories of non-noble metal electrocatalysts are extensively studied: Transition metal alloys, transition metal compounds, and carbonaceous nanomaterials. However, the most practical option based on both electrocatalytic activity and stability seems to be the transition metal alloys, among which the most significant are considered to be nickel-based binary/ternary codeposits. The high activity, good corrosion resistance and low cost of Ni-based electrode materials made them as efficient catalysts for HER. In oxygen evolution reaction (*OER*), the main energy loss is due to high overpotentials occurring at the anode. IrO_2, RuO_2 though considered as the most active materials for OER, they are least abundant. In this direction, research is ever-growing to get new materials, which are abundantly available at a lower cost. This has been achieved in alkaline electrolysis by the use of transition metal catalysts. Non-platinum metals like Fe, Ni, Co are considerably cheaper but they tend to corrode and passivate under reaction conditions. In this direction, mutual alloys of Fe-group metals (Fe, Ni, Co, Mn), binary alloy transition metals (W, Sn, Mo), with Fe-group metals are good alternatives for better electrocatalytic activity. In addition, their properties can be tuned to the requirement, by proper manipulation of their composition, surface morphology and corrosion stability, if they are synthesized through electrodeposition method.

1.8. Electro-catalytic behaviour of alloy coatings in alkaline water splitting

There are plenty of reports in the literature pertaining to the use of binary alloy coatings, as electrode materials for alkaline water electrolysis, as both cathode and anode (Gong and Dai 2015, Li et al. 2019, Raj 1993, Subramania et al. 2007, Ullal and Hegde 2014). In alkaline medium, the hydrated hydroxyl ions behave as charge carriers and the overall electrolysis involves the following half-reactions. The schematic representation of overall HER and OER mechanism on the surface of alloy coated electrode material is shown in the following steps, and the overall mechanism for HER and OER is given in Figure 1.10.

Cathodic half reaction: $2H_2O_{(l)} + 2e^- \rightarrow H_{2\,(g)} + 2OH^-$ ....(1.13)

Anodic half reaction: $2OH^- \rightarrow {}^1\!/_2\,O_{2(g)} + H_2O_{(l)} + 2e^-$ ....(1.14)

Overall water splitting reaction: $H_2O_{(l)} \rightarrow H_{2\,(g)} + {}^1\!/_2\,O_{2\,(g)}$ ....(1.15)
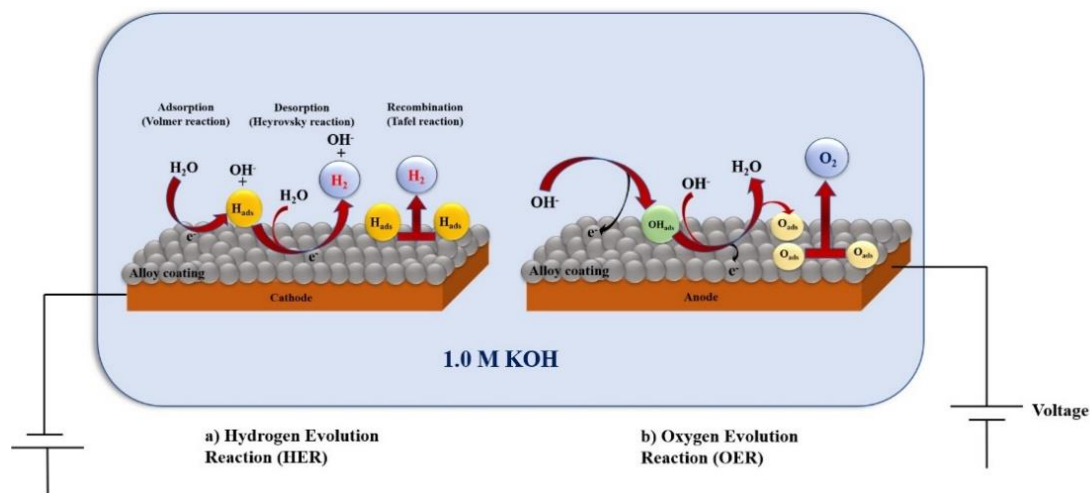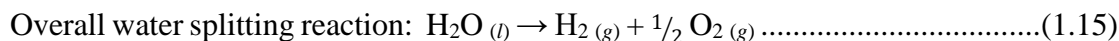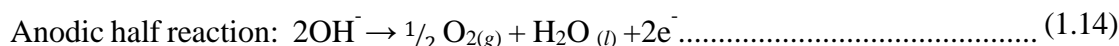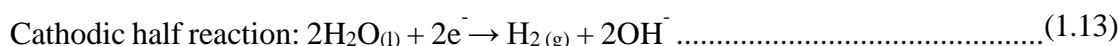
Figure 1.10- *Mechanism of HER and OER on the surface of electrodeposited alloy coatings in alkaline KOH medium*

In heterogeneous electrocatalysis, the mechanistic pathway in the presence of the electrocatalyst (M) could be given as follows:

*a) Hydrogen evolution reaction (HER)***:**

It involves the reduction of water molecules to hydrogen and is considered to be the amalgamation of three basic steps (Manazoğlu et al. 2016).

i) Electroreduction of water molecules with hydrogen adsorption on the catalyst surface (Volmer reaction)

$$M + H_2O_{(l)} + e^- \rightarrow M\text{-}H_{ads} + OH^-$$ ....(1.16)

ii) Electrochemical hydrogen desorption (Heyrovsky reaction)

$$M\text{-}H_{ads} + H_2O_{(l)} + e^- \rightarrow M + H_{2(g)} + OH^-$$ ....(1.17)
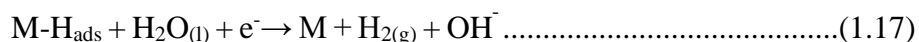
iii) Chemical recombination (Tafel reaction)

$$M\text{-}H_{ads} + M\text{-}H_{ads} \rightarrow 2M + H_{2(g)}$$ ....(1.18)
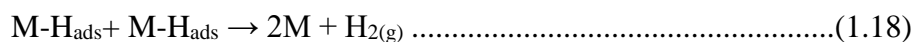
b) Oxygen evolution reaction (OER):

It involves the oxidation of hydroxyl ions to give oxygen. The reaction takes place on the oxide surface and proceeds with the formation of highly energetic surface adsorbed intermediates (Matsumoto and Sato 1986).

i) Electrochemical adsorption of hydroxyl ion on the surface of catalyst

$$M + OH^- \rightarrow M\text{-}OH_{ads} + e^- \quad \text{.. (1.19)}$$

ii) Electrochemical oxidation to form M-O$_{ads}$ and water

$$M\text{-}OH + OH^- \rightarrow M\text{-}O_{ads} + H_2O_{(l)} + e^- \quad \text{.. (1.20)}$$

iii) Chemical recombination

$$M\text{-}O_{ads} + M\text{-}O_{ads} \rightarrow 2M + O_{2(g)}^- \quad \text{.. (1.21)}$$
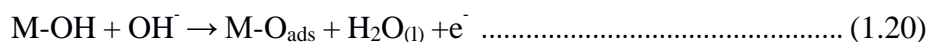
Since water electrolysis is kinetically a sluggish process, leading to low energy efficiencies (Khan et al. 2018), efficient electrode materials are an essential requirement for the electrolysis of water. Therefore, to speed up the overall water-splitting reaction, ideal heterogeneous electrocatalysts are required to effectively split nature abundant water into its elemental form, *i.e.*, hydrogen (H$_2$) and oxygen (O$_2$) by spending small amount of electric current (Sapountzi et al. 2017). From this count, electroplated Ni-based binary/ternary alloy codeposits are being used as substitutes for precious Pt-based, Ru-based electrode materials for water electrolysis due to their large availability, low-cost, long-term durability, and environment benign nature (Platatorres et al. 2007).

CHAPTER 2

LITERATURE REVIEW,

SCOPE AND OBJECTIVES

CHAPTER 2

LITERATURE REVIEW, RESEARCH SCOPE AND OBJECTIVES

This chapter outlines the literature review on electrodeposition and characterization of Ni-based alloy coatings in general, and both (Ni-Mo) and (Ni-Fe) alloy coatings in particular. The effect of different additives into electrolytic bath on corrosion and electro-catalytic activities of (Ni-Mo) and (Ni-Fe) alloy coatings have been surveyed. Based on the literature, scope and objectives intended to be achieved in this project have been stated at the end.

2.1 REVIEW OF LITERATURE

Nickel is a highly versatile metal known for its good corrosion resistance, wear resistance and temperature endurance properties. Even though monolithic Ni-electrodeposits have their own advantages, compared to many other non-noble metals, electrodeposited Ni-based alloy coatings were found to exhibit much better properties, compared to its single metal coatings. This is because Ni being highly ductile in nature, it serves as an excellent base for developing specialized alloy coatings with superior corrosion resistance properties. Another attractive property of Ni is that, it can trigger or induce the electrolytic reduction of the reluctant metal ions, like Mo or W which can otherwise not be deposited in its elemental form from an aqueous solution. Such kind of peculiar co-deposition behaviour was identified, and termed as '*induced co-deposition*', by Brenner (1963). Till date, a wide range of Ni-based alloy coatings have been practically utilized in chemical plants, like (Ni-Mo), nuclear power reactors (Ni-Mo-Cr), marine environments (Ni-Cu), medical and aerospace applications (Zn-Ni, Ni-P), petrochemical industries, electronic and communication devices (Ni-Fe, Ni-Co) etc. In addition, Ni-based alloy coatings are well known to exhibit good electro-catalytic activity of water electrolysis for hydrogen evolution reactions (HER) and oxygen evolution reactions (OER). Hence, they are extensively studied as efficient electrode materials in alkaline water splitting applications at lesser cost, compared to the use of noble metals (Raj 1993). Keeping this reason in mind, in this project it is planned to formulate two new Ni-based alloy baths for better corrosion protection and effective electro-catalytic response for alkaline water splitting applications, using proper additives.

2.1.1 (Ni-Mo) alloy coatings

Electrodeposited (Ni-Mo) alloy coatings are regarded as possible candidates to replace electroplated hard chromium owing to its less toxicity in marine environment, high corrosion, wear-resistant properties (Brooman 2004, Chassaing et al. 2004, Lima-Neto et al. 2010, Melo et al. 2012). Due to this, they have been widely investigated for good corrosion protection ability, and found wide-range of applications in aerospace industry, predominantly in the production of high temperature structural parts of missiles; oil and gas industry, electrical and electronic devices, nuclear and coal-fired power stations (Eliaz and Gileadi 2008, Lima-Neto et al. 2010, Mousavi et al. 2016). In addition, electrodeposited (Ni-Mo) are found to be efficient cathode material for HER activity (Alemu and Jüttner 1988, Eliaz and Gileadi 2008, Kubisztal et al. 2007, Manazoğlu et al. 2016, Raj 1993, Shetty et al. 2018, Wang et al. 2018), and to some extent for OER activity (Kubisztal and Budniok 2008, Shetty et al. 2017) in alkaline water electrolysis. However, co-deposition of Mo with iron group metals (Fe, Co or Ni) from its bimetallic electrolytic bath is considered to be highly unpredictable and vagarious owing to its inherent induced co-deposition behaviour (Brenner 1963), and several hypotheses have been put forth to elucidate its electroreduction mechanism (Fukushima et al. 1979). Moreover, the presence of complexing agents such as glycinate (Ahmad et al. 2014), acetate, citrates, (Prioteasa 2010, Beltowska-Lehman and Indyka 2012, Hasan et al. 2019) have been found to play a vital role in stabilizing the metal ions involved in induced co-deposition and the most preferably accepted combination is sodium citrate together with ammonia (Chassaing et al.1995, Sanches et al. 2003, Prioteasa 2010). In this context, Podlaha and Landolt (1997) designed a mathematical model to explain the induced co-deposition behaviour using (Ni-Mo), (Co-Mo), and (Fe-Mo) alloy deposits developed from citrate-ammoniacal bath. According to this model, Ni (II) reduction follows an independent pathway whereas molybdenum reduction eventuated by the formation of a mixed adsorption intermediate, $[Ni(II)HCit^-MoO_2]_{ads}$. Further, Kuznetsov et al. (2005), and Manazoğlu et al. (2016) also studied the effect of citrate and ammonium ions on the reaction kinetics, and stated that an addition of unspecified amount of ammonium hydroxide (NH_4OH) to the Ni-Mo citrate increases the Faradaic efficiency (FE). Thus, it was found that the citrate ammoniacal bath is the most successful in facilitating the smooth

deposition of (Ni-Mo) alloy coatings, and the reduction of Mo is mass transport controlled process, and was made possible only in the presence of iron group metals (Podlaha 1996). However, the impact of electrolyte composition on the inherent induced co-deposition behaviour, and its effect on the product and property of alloy coatings are not yet been explored completely.

There are several reports in the literature on anticorrosion and electro-catalytic performance of electrodeposited (Ni-Mo) alloy coatings developed under different conditions of bath chemistry. Halim et al. (2012) explored the corrosion resistance of electroplated (Ni-Mo) alloy coatings, using direct current (DC) with different Mo content (11wt. % - 31wt. %) in 0.5 M aqueous NaOH medium. The experimental results showed that coatings having 15.1 wt. % Mo exhibits maximum corrosion resistance; whereas the one with 31 wt. % Mo showed poor corrosion resistance. This increased corrosion behaviour of coatings, having high Mo content was attributed to the micro-cracks on the surface, affected due to internal stresses originated from excessive hydrogen liberation during deposition. Later, Huang et al. (2015) studied the effect of plating parameters on the morphology and corrosion resistance properties of (Ni-Mo) alloy coatings, using pulsed current (PC). The coatings were developed at a constant current density of 10.0 A dm^{-2} at 30°C from alkaline citrate bath. The experimental studies revealed that coatings developed using pulsed current (PC) showed a significant increase in the Mo content in the deposit, but grains obtained were finer, crack-free with less porosity. In addition, the corrosion study carried out in 3.5% NaCl solution revealed that PC deposited coatings with 30.2 wt.% Mo content were highly corrosion resistant, indicating the fact that surface features and its Mo content bears a strong relation with pulse current parameters employed for electrodeposition. Similar conclusions were drawn from the studies carried out by Allahyarzadeh et al. (2016) on the PC electrodeposited (Ni-Mo) alloy coatings, where the films showed an increase in Mo content with increase in the pulse frequency.

Efforts have been put to understand the effect of nanocomposites on the structure and properties of electro-codeposited (Ni-Mo) alloy coatings. Rezaeiolum et al. (2018) investigated the corrosion resistance ability of monolayer and multilayer Ni-Mo and Ni-Mo-nano Al$_2$O$_3$ composite coatings, fabricated from a citrate-ammoniacal

bath using pulsed current. The coatings with different number of layers (32, 128 and 512) were electrodeposited on the low-carbon steel by 6.0 A dm^{-2} by bringing about periodic modulation of duty cycle (between 20 and 90%), at a constant frequency of 400 Hz. It was found that incorporation of Al$_2$O$_3$ nanoparticles not only improved the hardness and wear properties of bare Ni-Mo coatings, but also enhanced their corrosion protection efficacy. Further, the effect of layering on the corrosion performance of alloy coatings was evaluated using potentiodynamic polarization and electrochemical impedance techniques in 3.5% NaCl. It was found that coatings having 128 layers has the highest corrosion resistance. Thus, added nanoparticles and sub-layer formation, jointly acted as barrier for corrosion propagation in the material. Goveas et al. (2018) studied the role of mixed metal oxide nanoparticles of ZnO–SnO$_2$, ZnO–WO$_3$ and ZnO–TiO$_2$ for enhancement of the corrosion inhibiting action of Ni–Mo alloy coatings on a copper substrate.

Off late, use of magnetic field (B) effect on process of electrodeposition has been advantageously used to improve the physico-mechanical properties of metal/alloy coatings. In this direction, only handful of reports are available with respect to magneto-electrodeposition of Mo-containing Ni-alloys. Han et al. (2010) studied the influence of electromagnetic field on the deposition of (Ni-Mo-P) alloy system developed from a basic bath, having pH = 8.5, along with its effect on HER activity of water electrolysis. The micro-morphology, alloying component, crystal structure and hydrogen evolution activity of the coatings developed on the application of parallel and perpendicular magnetic field, were examined in the range of B = 0 T-1.0 T. The results showed that the surface of (Ni-Mo-P) coating obtained was smooth, fine-grained microstructure in presence of external magnetic field, whereas HER activity increased on the application of parallel magnetic field, with slight increase in Mo content. Aaboubi et al. (2015) in continuation to their work carried out in 2011(Aaboubi 2011), investigated the reaction kinetics in the presence of magnetic field on (Ni-Mo) alloys electrodeposited on a platinum, or titanium electrode by means of polarization curves and EIS measurements. The studies were carried out at B = 0 T, 0.5 T and 1.0 T. The roughness and porosity of the alloy were modified under magnetic field. Shetty and Hegde (2017) developed magneto-electrodeposited (Ni-Mo) coatings from an alkaline high concentration bath of Ni-Mo, and investigated its electro-catalytic efficacy for

water splitting.

Aaboubi and Msellak (2017) showed in their research that when a homogenous magnetic field is applied parallel to the electrode surface (perpendicular to the direction of movement of cations) in the development of ternary (Co-Ni-Mo) system, an enhancement in the mass transport rate was observed leading to grains refinement and homogeneous distribution of Co, Mo and Ni atoms in coating matrix, with increase and decrease of Co and Ni content, respectively. These findings proved that the MHD convection, affected due to induced magnetic field has increased the corrosion protection efficacy of alloy coatings by increasing both Ni and Co content of the alloy. Recently, Shetty and Hegde (2021) developed MED (Ni-Mo-Cd) alloy coatings to give better corrosion stability to ternary (Ni-Mo-Cd) alloy coatings. The inherent limitation of the bath, due to anomalous type of codeposition was thus alleviated by using magnetic field effect. It was shown that corrosion resistance property of magneto-electrodeposited alloy coatings can be improved drastically by increasing its Ni content, which is otherwise unattainable by conventional method.

Thus, from the literature it is established that magnetic fields create additional convection inside the electrochemical cell by the phenomenon, called *magnetohydrodynamic (MHD)* effect (Krause et al. 2005). Consequently, the limiting current density in the diffusion-controlled regime near the cathode can be increased, due to the localized magnetic stirring of the electrolyte. Though there are number of reports demonstrating the improved properties of electrodeposited alloy coatings for different applications using magnetic field (*B*) effect, reports on development of Ni-based alloy coatings for improved corrosion and electro-catalytic performances are very scanty. In this regard, the corrosion and electro-catalytic activity of electrodeposited Ni-based alloy coatings can be tuned beneficially by manipulation of magnetic field assisted mass transfer process towards cathode. The process and properties (in terms of composition, surface morphology and phase structure) of alloy coating can be modified by exploring the magnetic field effect. In other words, the properties of conventional electrodeposited Ni-based alloy coatings can be improved to large extent by superimposing the magnetic field (both parallel and perpendicular to the direction of movement of ions), simultaneously to the process of deposition.

2.1.2 (Ni-Fe) alloy coatings

Electrodeposited (Ni-Fe) alloys, with varied nickel content are considered to be a new class of materials due to their widespread applications, like in electronics, opto-mechanical and communication devices (like audio transformers, magnetic amplifiers, transducers, electro-valves, magnetic shields, information storage devices, printers, etc). In addition, (Ni-Fe) alloys possess low coefficient of thermal expansion (Invar, Fe-Ni36) and superior magnetic properties (Permalloy, Fe-Ni80, (Torabinejad et al. 2017, Zhou and He 2018). Thus, due to unique properties of (Ni-Fe) alloy, they can easily be synthesized by simple and inexpensive electrodeposition method. Theoretically, during electrodeposition of (Ni-Fe) alloy (including all mutual alloys of iron-group elements, like Fe, Co and Ni) follows peculiar and famous *anomalous type* of co-deposition, as envisaged by Brenner (1963). According to this during co-deposition of Ni-Fe, less noble Fe is deposited preferentially compared to more noble Ni. As a result, wt. % of less noble metal in the deposit is observed to be much higher than that in the electrolytic bath (Afshar et al. 2003). Thus, due to increased less noble metal content in the deposit, this class of *mutual alloys of Fe-group metals* show better corrosion protection efficacy to base metals by following sacrificial protection, analogous to Zn-based alloy coatings. Due to these interesting features, there are many reports on development and characterization of mutual alloys of Fe-group metals in general, and (Ni-Fe) alloy coatings in particular, in the range of electroreduction mechanism of (Ni-Fe) alloys, proposed by Dahms and Croll (1965), through Matlosz (1993) till recently by Zhou and He (2018), explained on the basis of 'poly-nuclear complexes co-deposition model'.

In addition, the role of additives and effect of incorporation of nanoparticles/ceramic particles on process of electrodeposition of (Ni-Fe) alloy coatings have been studied. How patterns and performances of alloy coatings do change with those additives, and how they are responsible for change of corrosion resistance, wear resistance and electro-catalytic properties of alloy coatings have also been reported. Harris et al. (1999) studied the effect of ethylenediamine (EDA) on the anomalous co-deposition behaviour of (Ni-Fe) in chloride bath at pH 5. It was reported that EDA adsorbs on the deposit surface, and serves as a bridge for Ni^{2+} deposition in preference to that for Fe^{2+}, which forms less stable complexes with EDA. Zech and

Landolt (2000) studied the effect of boric acid and sulfate ions on the proton discharge and water reduction in Ni-Fe plating baths through experimental and numerical simulations. Ghorbani et al. (2002) reported the combined effect of sodium citrate and glycolic acid on the electrodeposition of (Ni-Fe) coatings from chloride bath. It was found that the anomalous co-deposition behaviour, inherent of (Ni-Fe) alloy system has reduced, with decreasing Fe (less noble) content in the deposit. The quality of alloy coating was found to improve drastically, with formation of fine-grained structure lattice, affected due to addition of sodium citrate and glycolic acid, in combination.

There are many reports on use of magnetic field effect on electrodeposition of (Ni-Fe) alloy coatings for their better properties. Msellak et al. (2004) conducted a systematic investigation on the effect of magnetic field (parallel) on the co-deposition behaviour of (Ni-Fe) alloys in acid sulphate electrolytes. Experimental observations showed that under the influence of magnetic field effect, the rate of deposition of Ni^{2+} ions were inhibited further, while that of less noble metal (Fe) increased significantly. Sriraman et al. (2007) compared the corrosion behaviour of Ni-W and Ni-Fe-W alloys in 3.5% NaCl developed from high-temperature saccharin-sodium lauryl sulfate containing bath. From the corrosion study established through potentiodynamic polarization (PDP) and EIS studies, it was found that Ni-Fe-W alloys are less corrosion resistant than Ni-W alloys, eventuated by the preferential dissolution of iron from the alloy matrix. Cao et al. (2014) studied the effect of deposition temperature and applied current density on the corrosion resistance of electrodeposited (Ni–Fe) alloy coatings. They concluded that corrosion potential decreased while the deposition current density is increased. Further, it was shown that alloy coating deposited at 55°C is demonstrating the best anticorrosion performance, compared to coatings deposited at other temperatures.

Currently, the research in surface coating technology is shifted to the creation of layered structures rather than monolayer coatings in order to provide greater corrosion protection. Several research works have been published in this area, by applying different current densities during the deposition process that allows for the formation of coatings with periodic changes in composition. In fact, the different amplitude current densities are frequently employed for layered deposition (Elias and

Chitharanjan Hegde 2015, Thangaraj et al. 2009, Venkatakrishna and Chitharanjan Hegde 2010). The very advantage of multilayer deposition approach to achieve better material properties has also been explored in case of (Ni-Fe) alloy coatings. The deposit characters have been analyzed, coating configurations for best performance have been proposed and results are discussed. Torabinejad et al. (2016) developed multilayer Ni-Fe-Al_2O_3 composite coatings by means of pulse electrodeposition technique on low carbon steel. The acquired results, from PDP study demonstrated that the corrosion resistance is higher in the nanocomposite Ni-Fe-Al_2O_3 coatings compared to the bare (Ni-Fe) alloy coatings. Further, the work was extended by incorporating the Mn into the bath to develop functionally graded (FG) Ni-Fe-Mn/Al_2O_3 nanocomposite coatings (Torabinejad et al. 2017). The effect of pulse parameters, like duty cycle and frequency were used as tools to play with the microstructure, composition, microhardness, corrosion and wear behaviour of FG nanocomposite coatings. It was reported that, the change of duty cycle decreased the Mn content in the nanocomposite coatings, and change of frequency do not have any effect on the composition of composite coating. Rashmi et al. (2020) galvanostatically fabricated (Ni–Fe) nanostructured composition-modulated multilayer alloy (CMMA) coatings on steel panel and studied the effect of layering on its corrosion performance in 3.5% NaCl solution.

Many extensive works on electrodeposition and characterization of (Ni-Fe) alloy coatings have been carried out, keeping their electro-catalytic activity for alkaline water electrolysis of HER and OER in mind. The effect of bath composition and working parameters were studied for development of coatings showing best catalytic performances. In this direction, Solmaz and Kardaş (2009) reported the improvement of electro-catalytic HER activity of (Ni-Fe) alloy coatings in 1.0 M KOH, compared to their individual metal coatings. It was found that the presence of nickel with iron increases their electro-catalytic HER activity, which varies with its chemical composition. Ullal and Hegde (2014) investigated the effect of deposition current density on the electro-catalytic behaviour of electrodeposited (Ni-Fe) alloy coatings in 1.0 M KOH using CV and CP, as electrochemical tools. Recently Záchenská et al. (2022) reported the electro-catalytic efficacy of (Ni-Fe) coatings in zero-gap alkaline electrolyser developed by direct current (DC) and Pulsed DC techniques, and it was inferred that the coatings developed by DC has higher catalytic activity.

42

Thus, there are many reports in the literature on electrodeposition of Ni-M (where M = Mo and Fe) alloy coatings through different modern methods, keeping their corrosion protection behaviour and electro-catalytic activity into consideration. The highlight of the literature review pertaining to electrodeposition of (Ni-M) alloy coatings are as below:

1. The corrosion resistance of (Ni-M) alloy coatings can be increased substantially by tailoring the composition, phase structure and morphology of alloy coatings by proper manipulation of deposition conditions, like current density, temperature, pH etc.

2. The corrosion resistance of (Ni-M) alloy coatings can also be increased drastically by the superimposition of magnetic field, applied simultaneously to the process of deposition.

3. The corrosion protection efficacy of (Ni-M) alloy coatings can be increased to many folds of its magnitude by composition modulated multilayer (CMM) approach by periodic pulsing of the cathodic current, during deposition.

4. The electro-catalytic activity of (Ni-M) alloy coatings can be improved by proper manipulation of deposition conditions, and incorporation of nanomaterials into the bath, *i.e.,* through composite coating technique.

2.2 RESEARCH SCOPE AND OBJECTIVES

Having inspired by the technological importance of alloy plating, and exclusive claims of multilayer coating and magneto-electrodeposition techniques, electrodeposition of Ni-M, (where M = Mo and Fe) alloy coatings for better corrosion protection of copper is intended to achieve here. Two new baths, namely Ni-Mo and Ni-Fe will be formulated using common additives. The optimization of bath composition and operating variables will be done for development of coatings of high corrosion performance. The corrosion performance of alloy coatings will be improved further by exploring the benefit of multilayer and magneto-electrodeposition approach. The corrosion behaviour of monolayer and multilayer (Ni-M) alloy coatings will be studied, and reasons of facts responsible for enhanced corrosion protection of CMM alloy coatings will be analyzed. The effect of magnetic field, applied both parallel and perpendicular simultaneous to the process of electrodeposition will be studied, and

experimental results will be detailed in the light of magneto-convection effect. The incredible claims of electroplating, in terms of its operating variables and bath composition will be tried to exploit effectively in electro-synthesis of (Ni-Mo) and (Ni-Fe) alloys for good corrosion resistance and electro-catalytic activity. The electro-catalytic activity of these coatings for alkaline water electrolysis, in terms of their hydrogen evolution reaction (HER) and oxygen evolution reaction (OER) will be studied, and discussed. The effect of electro-codeposition of polyoxometalate (POM) into (Ni-M) alloy matrix on its electro-catalytic behaviours of both HER and OER is also planned to study here.

As conventional alloy plating is becoming insufficient to meet many of the recent technological demands, the Ni-M (where M=Mo or Fe) alloy coatings with new properties are to be tailored to cater to the needs of advanced applications. Here, the philosophy of thesis is to maximize the corrosion protection ability and electro-catalytic activity of alloy coatings from the proposed baths, namely (Ni-Mo) and (Ni-Fe) by the advent of modern electrodeposition approaches, like through MED and CMM-ED techniques.

Thus, the intended project is driven by the following objectives:
1. To optimize two electrolytic baths, namely (Ni-Mo) and (Ni-Fe) for electrodeposition of bright and corrosion resistant alloy coatings by standard Hull cell method, using glycine as additive.
2. To enhance the corrosion protection efficacy and electro-catalytic activity of binary alloy coatings using modern methods of electroplating, like magneto-electrodeposition (MED) and multilayer coatings, as tools.
3. To improve the corrosion protection efficacy of conventional monolayer (Ni-Fe) alloy coatings (deposited using direct current) by multilayer approach using modulated DC (by pulsing current in square wave pattern).
4. To optimize coating configuration of multilayer alloy coatings (in terms of composition and thickness of individual layers) for their peak performance against corrosion.

5. To increase the corrosion protection ability of monolayer (Ni-Mo) alloy coatings by exploring the phenomenon of magneto-convection. *i.e.* by superimposing magnetic field (B) simultaneously to the process of deposition.

6. To study the effect of both direction (parallel ($\parallel$) and perpendicular ($\perp$)) and intensity of B on the process and product of magneto-electrodeposition (MED), and to discuss the factors responsible for improved corrosion resistance of MED alloy coatings.

7. To study the electro-catalytic activity of (Ni-Mo) and (Ni-Fe) alloy coatings, developed under different conditions, for alkaline water electrolysis of HER and OER in 1.0 M KOH, through conventional cyclic voltammetry (CV) and chronopotentiometry (CP) methods, and to compare their performances.

8. To study the effect of incorporation of polyoxometalate (POMs) into (Ni-M) alloy matrix and its electro-catalytic behaviour, and to understand the factors responsible for it.

9. To study the effect of electro-codeposition of Ag nanoparticles in (Ni-M) alloy coating matrix towards water splitting applications of HER and OER, using cyclic CV and CP methods.

10. To compare and characterize the monolayer, multilayer and electro-codeposited composite alloy coatings by various instrumental methods, such as SEM, EDS, XRD, XPS, AFM, EIS, PDP, CV, CP etc. and to analyze the reasons responsible for their improved corrosion resistance and electro-catalytic properties.

CHAPTER 3

MATERIALS AND EXPERIMENTAL METHODOLOGY

CHAPTER 3

MATERIALS AND EXPERIMENTAL METHODOLOGY

This chapter outlines the methods adopted, and the materials used to carry out the proposed research work. The procedural aspects pertaining to optimization of baths, different methods of electrodeposition, and evaluation of different coatings for their corrosion and electro-catalytic applications are explained.

3.1 INTRODUCTION

In the thesis, two new Ni-based alloy baths, namely (Ni-Mo) and (Ni-Fe) were optimized for the development of a smooth, uniform and bright coatings of their alloys for good anti-corrosion and electro-catalytic applications. Initially, bath composition and operating parameters of two Ni-based alloy coatings were accomplished by standard Hull cell method. A sound and adherent monolayer alloy coatings were later developed from optimized baths, using direct current (DC), and were tested for their corrosion protection efficacy, and electro-catalytic activity of alkaline water electrolysis. The corrosion performance of conventional Ni-based alloy coatings were tried to improve further by magneto-electrodeposition (MED) and multilayer approach. The effect of additives on electro-catalytic behaviour of alloy coatings have been tested.

Further, the effect of the addition of highly redox-active polyoxometalates (POM) namely, 11-molybdo-1-vanadophosphoric acid (Maity 2021) and Ag nanoparticles on the electro-catalytic activity of bare (Ni-Mo) and (Ni-Fe) alloy coatings in alkaline water electrolysis were studied. The experimental results are compared and discussed, with the support of data obtained from different analytical techniques, like SEM, EDS, XRD, XPS, and AFM.

3.2 MATERIALS AND ELECTRODEPOSITION METHODS

3.2.1 Chemical reagents and materials

Laboratory Reagent (LR) grade chemicals, like nickel chloride hexahydrate ($NiCl_2 \cdot 6H_2O$), sodium molybdate dihydrate ($Na_2MoO_4 \cdot 2H_2O$), tri-sodium citrate dihydrate ($Na_3C_6H_5O_7 \cdot 2H_2O$), ammonium chloride ($NH_4Cl$), glycine ($C_2H_5NO_2$), trichloroethylene (TCE), potassium hydroxide (KOH), sodium chloride (NaCl), ammonium hydroxide (NH_4OH), hydrochloric acid (HCl), nitric acid (HNO_3) and

sulfuric acid (H_2SO_4), procured from Merck India, were used for the development of optimal (Ni-Mo) and (Ni-Fe) alloy baths. Before each deposition, cathode surface was fine polished, and bath pH was adjusted to the required value, using either HCl or NaOH, depending on the requirement. Both (Ni-Mo) and (Ni-Fe) baths are prepared using distilled water, and all electrodepositions were carried out on a copper sheet/rod of known area, and then subjected to corrosion and electro-catalytic studies in 3.5% NaCl and 1.0 M KOH medium, respectively. To study the effect of silver nanoparticles on the electro-catalytic property of (Ni-Fe) coatings, commercially available Ag nano-powder, having particles size <100 nm, was used, procured from *Sigma-Aldrich*, India.

3.2.2 Cathode surface pre-treatment

For development of monolayer, multilayer and MED Ni-based alloy coatings, copper sheets having 3.0×3.0 cm^2 active surface area was taken; and for electro-catalytic study, a copper rod with 1.0 cm^2 tip surface area, were used as cathode. Cathode surface was polished using SiC emery coated mops, followed by cleaning in trichloroethylene (TCE) solvent, under ultra-sonication for 300 s. The substrates were later degreased in a 100 g L^{-1} NaOH solution at 60°C for 600 s, as part of *alkali cleaning* to remove last trace of impurities, not cleaned by the solvent treatment. Then cleaned substrates were subjected to *water-line test* to confirm the removal of all impurities on the surface of substrate. Lastly, the substrates were acid-washed in 10 % HNO$_3$ for 30 s, followed by rinsing in distilled water, and then taken for deposition at desired current density.

3.2.3 Preparation and optimization of electrolytic baths

Optimization of electrolytic baths have been done using solution of respective metal ions, with corresponding additives by standard Hull cell method. Hull cell is a specially designed, trapezoidal miniature tank of 250 cm^3 capacity, with about 5 cm height. Hull cell is designed in such a manner that the cathode (10 cm length) can be placed inclined to the anode (5 cm length) to produce a wide range of current densities, as shown in Figure 3.1. When current is applied, the current will vary along the length of cathode, to have variety of deposits. The way in which anode and cathode (test plate) are placed in the Hull cell is shown in Figure 3.1(a). The pattern of electrical lines of force responsible for a spectrum of coatings along the length of cathode is shown in Figure 3.1(b).

50
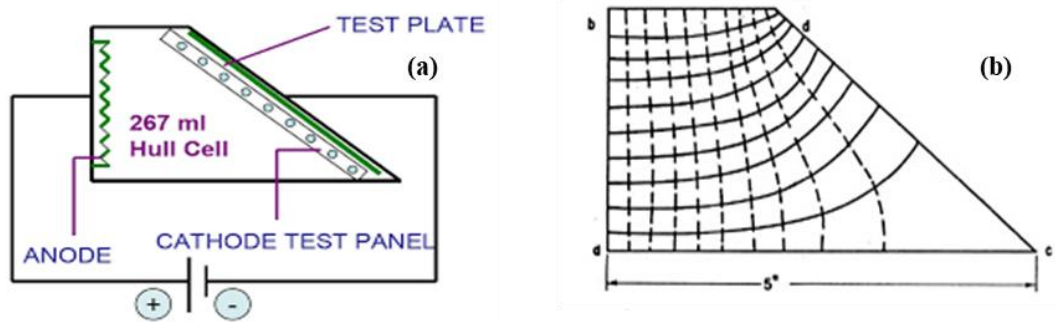
Figure 3.1- *Typical Hull cell showing: a) positioning of test plate along the cathode, and b) pattern of lines of force of electric field along the length of cathode*

Initially, bath constituents were prepared in different, but known quantities, and were stirred for homogeneity of the solution. The solution was then filtered to remove suspended impurities. The pH of the bath was adjusted with either NH_4OH or HCl, using Micro pH Meter (Systronics-362). The electrolyte was then transferred to Hull cell, and polished cathode on the inclined side of Hull cell with anode on opposite side as shown in Figure 3.1. Then, electrodeposition was allowed to take place for definite time, say 300 s, on applying definite cell current, say 1 A. After deposition on cathode, it is then removed from the cell, and then washed, rinsed with distilled water, and then dried. The cathode plates are then checked visually for a bright, uniform and sound deposition. The composition, and the current density range where visually bright and adherent (Ni-M) alloy coatings was obtained, is considered as the optimal condition of the bath, and such bath is considered as optimized, or optimal bath. The optimal current density to be used for conventional electrodeposition (where anode and cathode are placed parallel to each other) was obtained from Hull cell Ruler, shown in Figure 3.2. By knowing the cell current, and distance from high current density (HCD) side at which satisfactory deposition was obtained, the cathode current density for regular deposition was obtained using Hull cell ruler, shown in Figure 3.2.

Figure 3.2- *Hull cell ruler to find optimal current density range*

During Hull cell study, pre-treated, mechanically polished copper panels of 10.0×7.0 cm^2 area were used as cathode, and graphite as anode. The depositions are accomplished on the copper panel with an active surface area of 10.0×3.0 cm^2 by masking the remaining sides. The procedural steps followed during optimization of baths is shown typically in Figure 3.3.
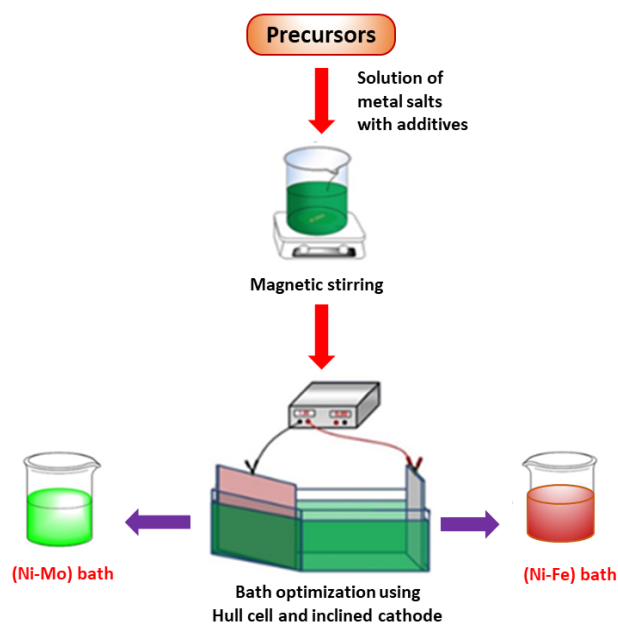
Figure 3.3- *Procedural steps followed during optimization of electrolytic baths*

3.3 DEVELOPMENT OF ALLOY COATINGS

The electrodeposition of binary alloy coatings were accomplished through different methods, and the experimental procedure used for their deposition are explained below.

3.3.1 Electrodeposition of monolayer alloy coatings

The optimized baths of (Ni-M) alloy, where M = Mo, or Fe were used for electrodeposition of respective alloy coatings on copper, through different approaches to achieve better corrosion and electro-catalytic performances. The conventional electrodeposition was carried out on a copper plate having an active surface area of 3.0×3.0 cm^2, after the process of surface cleaning. The monolayer coatings were developed at optimal current densities in a rectangular PVC cell of 250 cm^3 capacity, keeping the polished copper plate as cathode, and graphite plate (having same surface area as cathode) as anode. During regular electrodeposition, cathode and anode are kept parallel at a distance of 5 cm with provision for constant stirring of the electrolyte during

plating. The electrochemical cell employed for regular electroplating, using optimized bath is shown in Figure 3.4. DC Power Analyzer (*Keysight Technologies, N6705C, USA*) was used as the power source, for electrodeposition throughout the study. The pH of the bath was adjusted to the desired value, by proper addition of either NH_4OH or H_2SO_4, depending on the requirement, using a micro pH meter (Systronics, 362).
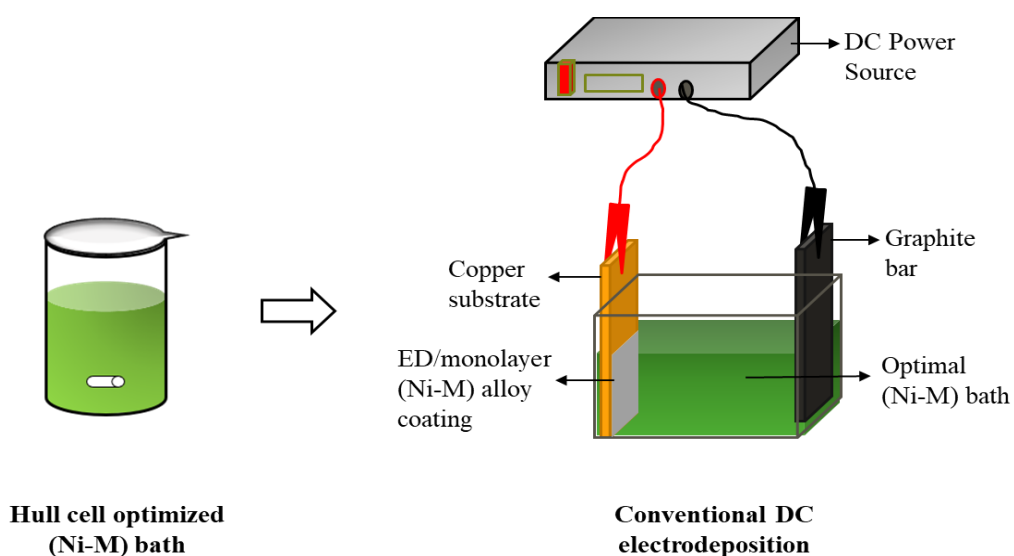
Figure 3.4- *Electrochemical cell used for conventional electroplating (monolayer) of Ni-based alloy coatings by keeping anode and cathode parallel, using optimized bath*

All coatings were carried out for the same duration (600 s), keeping temperature and pH constant, for comparison purpose. After deposition, the electro-coated substrate is removed from the electrolyte, washed, dried and then desiccated, till further analyses.

3.3.2 Magneto-electrodeposition of binary alloys

The magneto-electrodeposition (MED) of (Ni-M) alloy coatings were carried out at a particular optimal current density, using the optimized bath by super-imposing magnetic field (*B*). In other words, electrodeposition was allowed to take place under the combined effect of electric field (*E*) and magnetic field (*B*) by governing the principles of Lorentz force. The experimental setup used for magneto-electrodeposition do consists of an electrochemical cell, having cathode, anode and DC power source as described in the conventional monolayer plating process. But in magneto-electrodeposition, the electrodeposition is carried out in conjunction with an electromagnet (Polytronics, Model: EM 100), with provision to vary both direction and intensity of *B*. The magneto-electrodeposition was accomplished by keeping deposition

current density constant to see the effect of magnetic field (B), in terms of its direction (parallel and perpendicular to the direction of flow of ions in the electric field), and intensity, in tesla (T). Magneto-electrodepositions (MEDs) were carried out by varying both intensity (from 0.1T to 0.4T) and direction (parallel and perpendicular to the flow of ions), by keeping the current density constant. Experimental set-up used for magneto-electrodeposition of alloy coatings at constant current density, using electrochemical cells is shown in Figure 3.5.
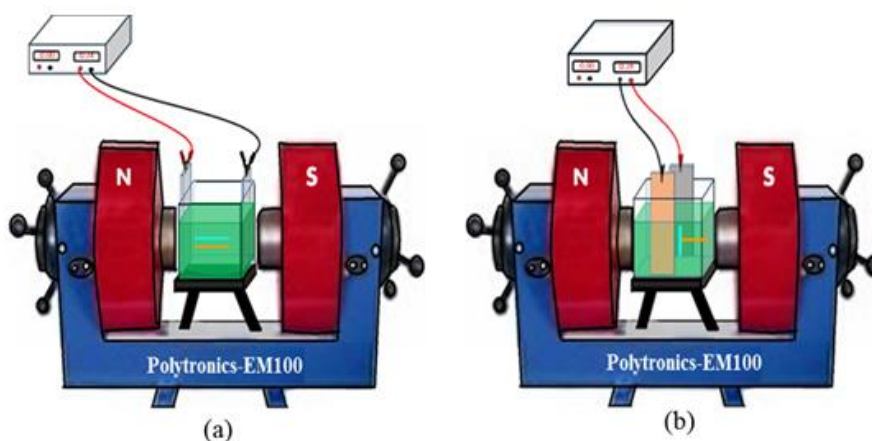
Figure 3.5- The experimental set-up used for magneto-electrodeposition of (Ni-M) alloy coatings under conditions, where the direction of electric field is: a) parallel to B, and b) perpendicular to B to the direction of flow of metal ions

It may be noted that a constant and uniform magnetic field is made to be applied on the process of electrodeposition, by keeping electrochemical cell in the space between magnetic poles. The direction of magnetic field is conveniently changed by rotating the electrochemical cell. *i.e.,* by changing the plane of cathode with respect to the direction of magnetic field, as shown in Figure 3.5. All depositions were carried out for a constant time (600s), at constant pH and temperature (303 K) for the purpose of comparison of properties and performances of alloy coatings.

3.3.3 Multilayer electrodeposition of binary alloys

Multilayer coatings of (Ni-M) alloy were electrodeposited by passing the DC in a pulsed manner between two current densities, using a DC power source (Keysight Technologies, N6705C, USA). The electrochemical cell setup used for the deposition remains same as that used for the monolayer counterpart, except the power source to generate pulsed current. In addition, alloy coatings were developed on the copper plates

having the same active surface area (3.0×3.0 cm^2) as that of the plate used in monolayer deposition. The duration of deposition was kept constant for both monolayer and multilayer alloy coatings to compare their corrosion activity. The schematic representation of the power pattern used for the development of multilayer alloy coating, in relation to conventional monolayer (monolithic) alloy coating is shown in Figure 3.6.
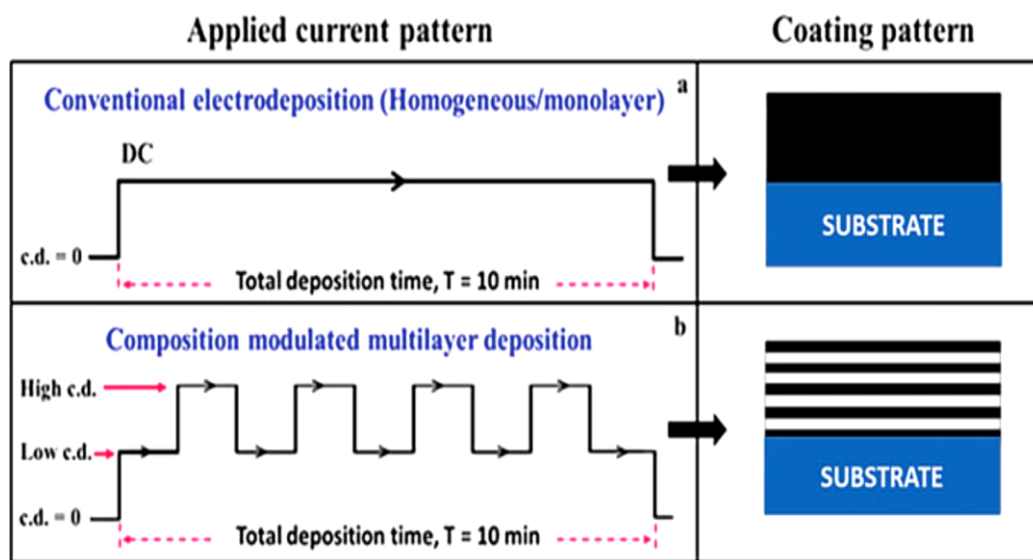
Figure 3.6 - *Schematic representation showing the current patterns (left) required for the development of a) monolayer, b) multilayer coatings. An alternate layer of alloys of different compositions may be seen in multilayer coating*

Here, it is important to note that, unlike in regular pulse plating, here cathodic current is made to pulse periodically between two preset values (lower and higher current densities). But in regular pulse plating, the current is made to reach zero value for every change pulse.

3.4 PERFORMANCE EVALUATION OF ELECTRODEPOSITED ALLOY COATINGS

The (Ni-Mo) and (Ni-Fe) alloy coatings developed through different approaches from newly proposed baths are intended for better tolerance against corrosion, and good electro-catalytic performance for water splitting applications. Therefore, the corrosion resistance and electro-catalytic activity of electrodeposited alloy coatings were evaluated by various electrochemical methods.

3.4.1 Corrosion study

Corrosion behaviour of all developed Ni-based alloy coatings was studied in a corrosion cell (of 250 cm³ capacity), having a three-electrode configuration, namely working electrode, counter electrode, and reference electrode. Here, electroplated substrate is made as working electrode (WE), saturated calomel electrode (SCE) as reference electrode (RE) and platinized platinum electrode as counter electrode (CE). The experimental set-up for the corrosion study of electrodeposited alloy coatings are shown in Figure 3.7.
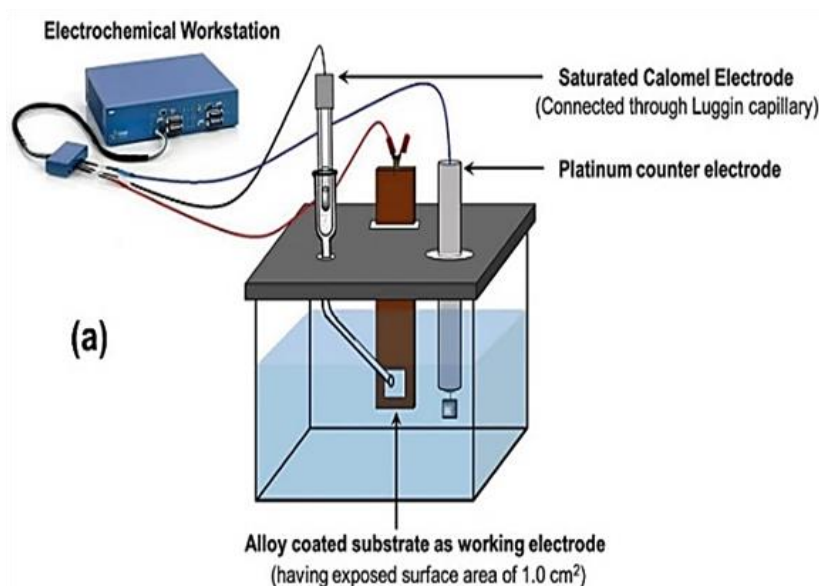
Figure 3.7- *Schematic representation of the experimental set-up used for the electrochemical measurements of (Ni-M) alloy coatings developed from various electrodeposition approaches*

All electrochemical studies were carried out by using a computer-controlled instrument potentiostat/galvanostat (VersaSTAT-3, Princeton Applied Research). The corrosion behaviour of alloy coatings (having 1.0 cm² exposed surface area) was evaluated in 3.5% NaCl at 303 K. The corrosion studies were also carried out by electrochemical impedance spectroscopy (EIS) technique followed by the potentiodynamic polarization (PDP) method. The EIS study was made in the frequency range of 10 kHz - 10 mHz by applying a small voltage perturbation of ±10.0 mV. The corresponding Nyquist plots were analyzed, and the results are discussed. The corrosion behaviour of alloy coatings was evaluated by potentiodynamic polarization method, at

a scan rate of 1.0 mV s^{-1} in a potential ramp of $\pm$ 250 mV from OCP. Based on the corrosion current (i_{corr}) obtained through Tafel extrapolation method, the corrosion rates (CR's) of all coatings were evaluated from CR Equation 1.12.

3.4.2 Electro-catalytic study

The electro-catalytic activity of alloy coatings for water splitting applications was assessed by electrodepositing it on the tip of copper rod (with exposed area 1.0 cm^2), instead of on copper plate. This is with the purpose of evaluating the electro-catalytic efficacy of alloy coating, by quantifying the amount of hydrogen and oxygen produced when they are used as an electrode in the custom-made electrolyzer. The glass set up used for electrodeposition of Ni-based alloy coatings for quantitate evaluation of the electro-catalytic activity of HER and OER, using electrolyzer is shown in Figure 3.8.
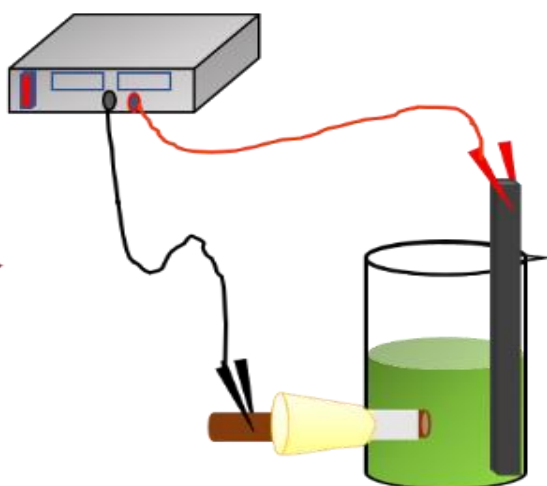
Figure 3.8- Customized experimental cell used for electrodeposition of alloy coatings on the tip of copper rod for quantitate evaluation of electro-catalytic activity of HER and OER, using electrolyzer

The electro-catalytic efficacy of Ni-based alloy coatings for HER and OER of alkaline water splitting reaction was studied in a customized tubular glass cell equipped with three electrodes (electrolyzer), in which platinized platinum is used as the counter electrode, saturated calomel electrode (SCE) as reference electrode, and alloy coated copper rod as the working electrode. A Luggin's capillary with KCl bridge was used to establish a close contact between the working electrode and reference electrode, by

minimizing the Ohmic polarization. The electro-catalytic activity of alloy coatings, in terms of its efficacy for HER (as cathode) and OER (as anode) are evaluated quantitatively by measuring the liberated H_2 and O_2 gases, using graduated burettes
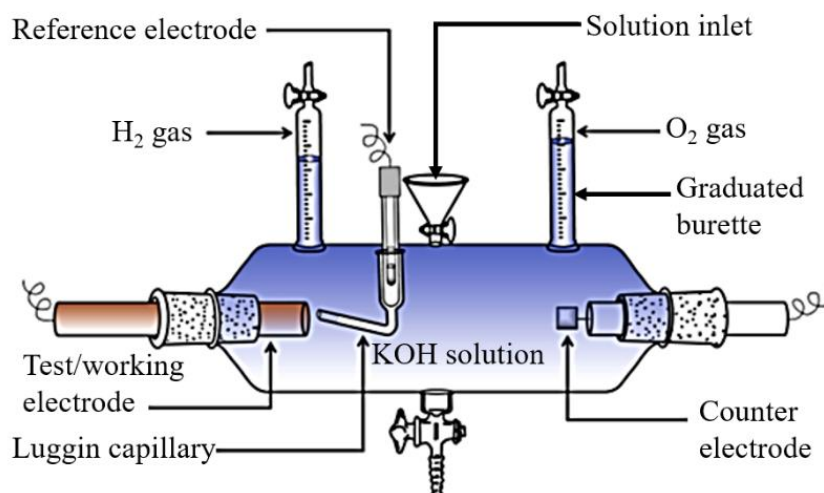
fitted on both ends of the electrolyzer as shown in Figure 3.9.

Figure 3.9- *Representational diagram showing the custom-made water electrolyzer used for quantitative assessment of H_2 and O_2 gas liberated on the surface of (Ni-M) alloy coatings*

This experimental setup enables the quantification of electro-catalytic activity of different alloy coatings (deposited at different conditions), in terms of their efficacy for HER and OER when using them as cathode and anode during water electrolysis. The electro-catalytic activity of all alloy coatings was studied by employing conventional cyclic voltammetry (CV). CV measurements were done in a potential window of 0.0 to -1.6 V for HER, and 0.0 to 0.75 V for OER, at a scan rate of 0.05 V s^{-1}. The CP analysis was done by passing a constant current of -300 mA and +300 mA for the 1800s for HER and OER, respectively. The electro-catalytic stability of (Ni-M) alloy coatings was tested by the chronopotentiometry method by monitoring the electrode reaction for 1800 s. The electro-catalytic efficiency of electrodes were evaluated quantitatively by measuring the volume of H_2 and O_2 evolved during electrolysis, by keeping other parameters constant, like 1.0 cm^2 surface area of test electrode and duration of electrolysis as 300 s.

3.5 MATERIAL CHARACTERIZATION TECHNIQUES

Electrodeposited (Ni-M) alloy, or their nanocomposite coatings were characterized using various instrumental methods. The surface morphology of the deposited coatings were characterized by Scanning Electron microscopy (SEM, Zeiss, Germany) interfaced with Energy Dispersive X-ray spectroscopy (EDS) facility (Oxford EDS). The coatings developed on the substrate with a dimension of 1.0×1.0 cm^2 were mounted directly on the sample holder using carbon tape for analysis. The crystallite phase structures of the alloy coatings and their composites were identified using X-ray diffractometer (XRD, Rigaku- miniFlex 600) by passing radiation Cu K$_\alpha$ (λ=1.54A°) at a scan rate of 2° per minute. Further, crystallite size was calculated by Scherrer's equation:

$$D = \frac{K\lambda}{\beta \, Cos\theta} \quad \text{... (3.1)}$$

Where D - crystallite size, K-the Scherrer constant, β - FWHM (Full Width at Half Maximum) and θ - Bragg's angle.

In polyoxometalate (POM) - based alloy coating, the chemical states of the elements were recorded using X-ray Photoelectron Spectroscopy (XPS, Prevac) using monochromatic Al- K$_\alpha$ radiation, by taking C1s band at binding energy (E_B) 285.2 eV as internal standard. The surface roughness of the composite coatings was measured using Atomic Force Microscopy (AFM, Innova SPM Atomic Force Microscope) by imaging the surface of alloy coatings, in tapping mode.

CHAPTER 4

CORROSION BEHAVIOUR OF ELECTRO-CODEPOSITED BINARY (Ni-Mo) ALLOY COATINGS FROM CITRATE-AMMONIACAL BATH

CHAPTER 4

CORROSION BEHAVIOUR OF ELECTRO-CODEPOSITED BINARY (Ni-Mo) ALLOY COATINGS FROM CITRATE-AMMONIACAL BATH

This chapter details the formulation of a new (Ni-Mo) citrate bath having low metal salts concentration, using standard Hull cell method. The effect of current density on structure and properties of alloy coatings have been analyzed. An optimal current density has been proposed for development of alloy coating showing the highest performance against corrosion. The change of composition of alloy coatings with current density is explained in the light of induced co-deposition, and experimental results are discussed using FESEM-EDS and XRD evidences.

4.1 INTRODUCTION

Copper is one of the oldest metals known for its good corrosion resistance property, high electrical conductivity, malleability and mechanical workability. Nevertheless, depending on the environmental conditions, pitting corrosion may occur on the copper surface in presence of oxygen and some aggressive anions such as chlorides and sulphates (Fateh et al. 2020). For many years, chromate-based inhibitors were used in the water- cooling systems to protect the bare metal surface by passivation. But owing to the adverse effect of hexavalent chromium (Yee et al. 2019) on the aquatic life, restrictions were imposed on to use it in industrial practice. Due to this reason, attention has been paid to find alternative eco-friendly inhibitors such as molybdate-based inhibitors (Emregül and Aksüt 2003; Vukasovich and Farr 1986). However, molybdate being a weak oxidizer, their inhibitory action was not found that effective as that of chromates. Hence, this shortcoming paved the way for the exploration of a new economically viable, environmentally benign and efficient deposition of reluctant molybdenum (Mo) with Fe-group element, namely Ni. Thus, electrodeposited (Ni-Mo) alloy coatings are found to be a good anti-corrosion material to protect base metals. In this direction, the present study is focussed on the optimization of a new bath of (Ni-Mo) alloy, with having low Ni and Mo contents. An optimal current density has been proposed for the development of alloy coating of highest corrosion resistance. It is also intended to understand how limitations of induced co-deposition can be used

advantageously in a low concentration bath. Experimental analyses of alloy coatings are made, and results are discussed.

4.2 RESULTS AND DISCUSSION

4.2.1 Electrodeposition of (Ni-Mo) alloy coatings

A low concentration citrate-ammoniacal bath of (Ni-Mo) alloy was selected for the present study to check the effect of nickel (Ni) and molybdenum (Mo) content on the electrode kinetics of (Ni-Mo) alloy coating. A bi-metallic electrolytic bath of (Ni-Mo), containing $NiCl_2.6H_2O$ (Ni source), $Na_2MoO_4.2H_2O$ (Mo source), $Na_3C_6H_5O_7.2H_2O$, and NH_4OH (LR grade, procured from Merck, India) are taken in desired quantities, and dissolved in double distilled water. The bath solution was magnetically stirred, and filtered before each use. From the Hull cell analysis, it was found that citrate and ammonia ions are responsible for smooth and uniform coatings of alloy coating onto the surface of substrate. Based on visual observation of Hull cell panel, concentration of electrolytes and operating parameters, like pH, current density were optimized, and is given in Table 4.1.

Table 4.1- Bath composition and plating variables of the optimized citrate-ammoniacal bath of (Ni-Mo) alloy for the development of bright coatings

Bath Ingredients	Composition (g L^{-1})	Operating variables
$NiCl_2.6H_2O$	7.0	Anode: Graphite
$Na_2MoO_4.2H_2O$	3.5	Cathode: Copper sheet
$Na_3C_6H_5O_7.2H_2O$	20.0	pH: 10.0
NH_4OH (excess)		c.d. : 1.0 A dm^{-2}- 4.0 A dm^{-2}

To understand the effect of current density on the plating characteristics, conventional electrodeposition was carried out on a pre-treated copper plate/sheet, with an exposed area of 3.0 cm^2 at different current densities ranging from 1.0 A dm^{-2}- 4.0 A dm^{-2} in a custom-made PVC cell, shown in Figure 3.4. The electrodeposition was carried out for a duration of 600 s using a DC power source (Keysight Technologies, Model: N6705C). The corrosion performance of all alloy coatings were evaluated in

3.5% NaCl solution, a common corrosion medium selected, using computer controlled Potentiostat/Galvanostat (VersaSTAT-3, Princeton Applied Research).

4.2.2 Morphological characterization

The surface morphology of electrodeposited (Ni-Mo) alloy coatings, developed at different plating current densities ($1.0 - 4.0$ A dm^{-2}) is shown by its FESEM images in Figure 4.1.
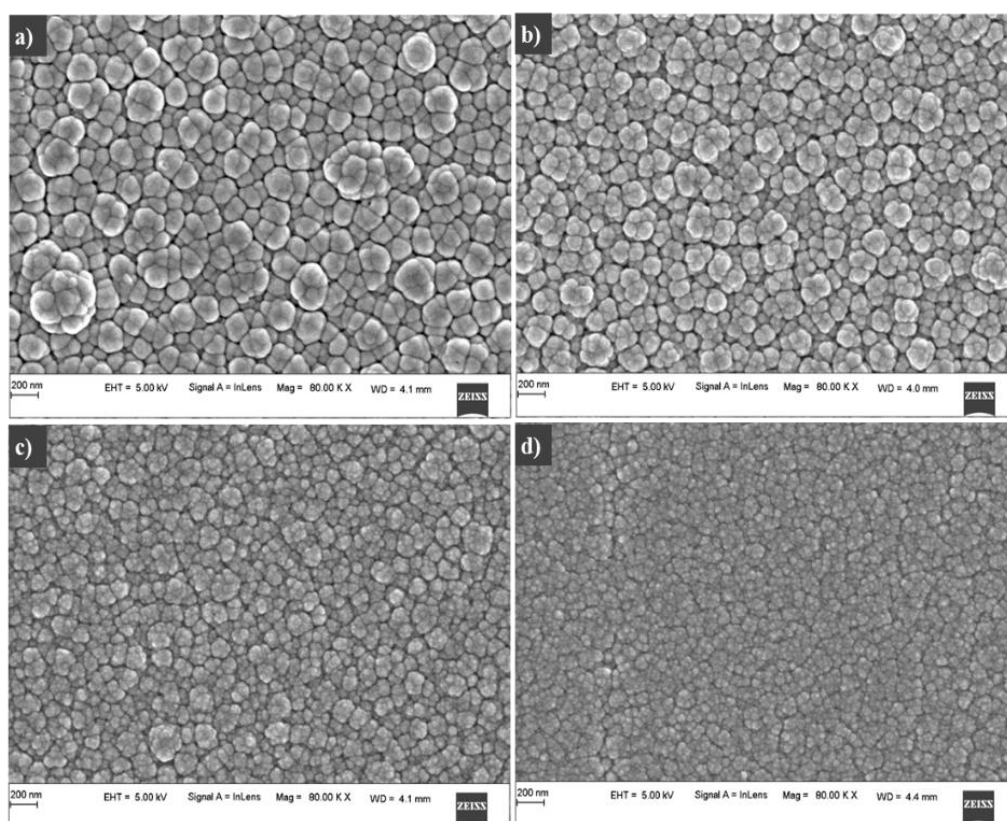
Figure 4.1- *FESEM micrographs of (Ni-Mo) coatings developed at different current densities, using optimized bath at: a) 1.0 A dm^{-2} b) 2.0 A dm^{-2} c) 3.0 A dm^{-2}, and d) 4.0 A dm^{-2}*

It may be seen that homogeneity of the coating improved drastically with increase of current density, *i.e.* from 1.0 A dm^{-2} through 4.0 A dm^{-2}. The dendritic growth of the coating was suppressed with increase of current density, resulting in the formation of a smooth coating. This may be attributed to the suppression of formation of metals hydroxide at electrical double layer (EDL) of cathode, as envisaged by Brenner (1963). According to this, as the current density is increased the concentration of H$^+$ ions around cathode decreases, due to liberation of H$_2$ gas on its surface. With

decrease of local pH, co-deposition of metal hydroxides, like $Ni(OH)_2$ is prevented, and consequently a more uniform coating, without porosity is formed. Thus, the improved homogeneity of (Ni-Mo) coatings with the growth of current density is due to increased diffusion of H^+ ions towards cathode.

4.2.3 Compositional analysis

Energy dispersive X-ray spectroscopy (EDS) is a powerful chemical microanalysis technique used in conjunction with SEM/FESEM. This enables the chemical characterization by giving elemental information of materials. In this regard, the composition of electrodeposited (Ni-Mo) coatings developed at different plating current densities were examined by EDS method, and the data obtained are reported in Table 4.2. The change of Ni and Mo content in the deposit with current density is shown graphically in Figure 4.2 (a). A representative EDS spectrum corresponding to 4.0 A dm^{-2}, signaling the presence of both Ni and Mo in the deposit is shown in Figure 4.2 (b).
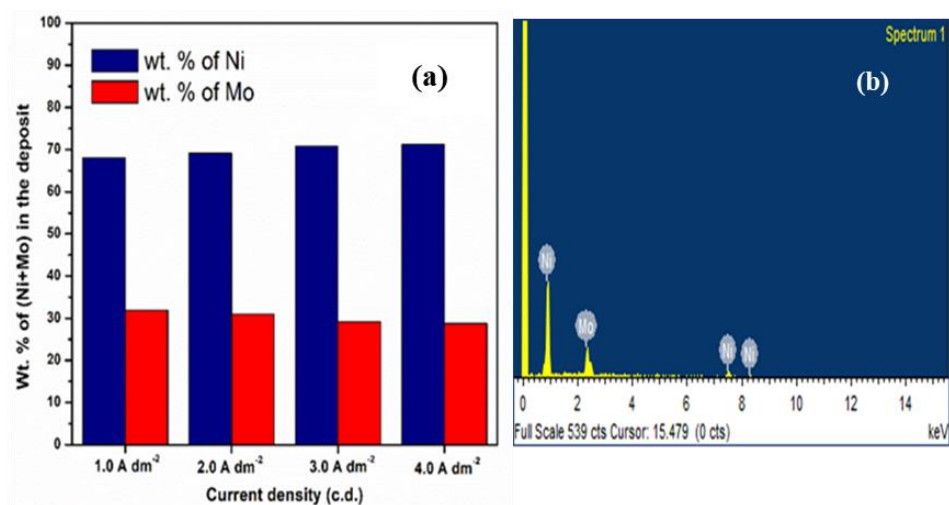
Figure 4.2- The compositional information of electrodeposited (Ni-Mo) coatings showing: a) change of wt.% of Ni and Mo in the deposit with current density, and b) representative EDS spectrum signaling the presence of both Ni and Mo in the deposit

From the composition data reported in Table 4.2, and Figure 4.2 (a), it is evident that change in the wt.% of metal contents (both Ni and Mo) in the deposit with current density is very marginal, demonstrating the characteristic feature of induced type of co-deposition (Brenner 1963). It may be recalled here that in induced co-deposition,

66

change of alloy composition with current density is very minimal and unpredictable. In addition, it may be seen in Figure 4.2 (a) that wt.% of Ni in the deposit is much higher (about 70 %), compared to its Mo content (approximately 30%). The observed high Ni content of the deposit is in compliance with the experimental work reported by Beltowska-Lehman and Indyka (2012). It was reported that change of pH of a Ni-rich citrate bath (from 8 to 11) has increased the Ni content of the alloy, by changing the kinetics of co-deposition of Ni and Mo. Hence, in the present study due to high pH (=10), the diffusing tendency of inducing metal ions (Ni^{2+}) towards cathode has increased drastically, compared to reluctant metal ions (Mo^{6+}), and is supported by the work reported by Kuznetsov et al. (2005).

Table 4.2-Corrosion parameters of electrodeposited (Ni-Mo) alloy coatings developed at different current densities

Current density (A dm^{-2})	Wt. % of Ni	Wt. % of Mo	R_s (ohms)	R_{ct} (ohms)	$-E_{corr}$ (mV vs SCE)	i_{corr} (μA cm^{-2})	CR$\times10^{-2}$ (mm y^{-1})
1.0	68.1	31.9	10.8	1344.7	496.3	20.04	16.74
2.0	69.1	30.9	10.1	1039.2	483.0	21.87	18.03
3.0	70.8	29.2	10.1	893.4	493.3	25.69	21.47
4.0	71.2	28.8	10.0	856.6	480.1	33.55	28.13

4.2.4 XRD study

The crystallite phase structure of electrodeposited (Ni-Mo) coatings obtained at varied plating current densities are revealed by X-Ray diffraction (XRD) analysis. X-ray diffractogram (Figure 4.3) showed the presence of intermetallic body-centered tetragonal MoNi$_4$ structure (Jakšić et al. 2000, Shetty et al. 2017), with five atoms in the primitive unit cell (Galanakis et al. 2001). The peaks were observed at $2\theta = 43.01°$, 50.15°, 73.76°, and 89.55° corresponding to (220), (130), (420), and (501) planes respectively, in accordance with JCPDS file number 03-065-1533. From XRD patterns seen in Figure 4.3, it may be noted that both phase structure and scattering angle of alloy coatings are remained to be the same, irrespective of the current density

at which they are electroplated. This consistency of XRD peaks for coatings of all current density may be linked to the formation of solid solution of Mo in Ni in the alloy deposit (Cullity 1978). Basically, solid solutions are one in which two metals remain in a single homogeneous phase in all proportions. However, a slight variation observed in the intensity of XRD signals, with the change of current density may be affiliated to the marginal change in the composition of alloy coatings.
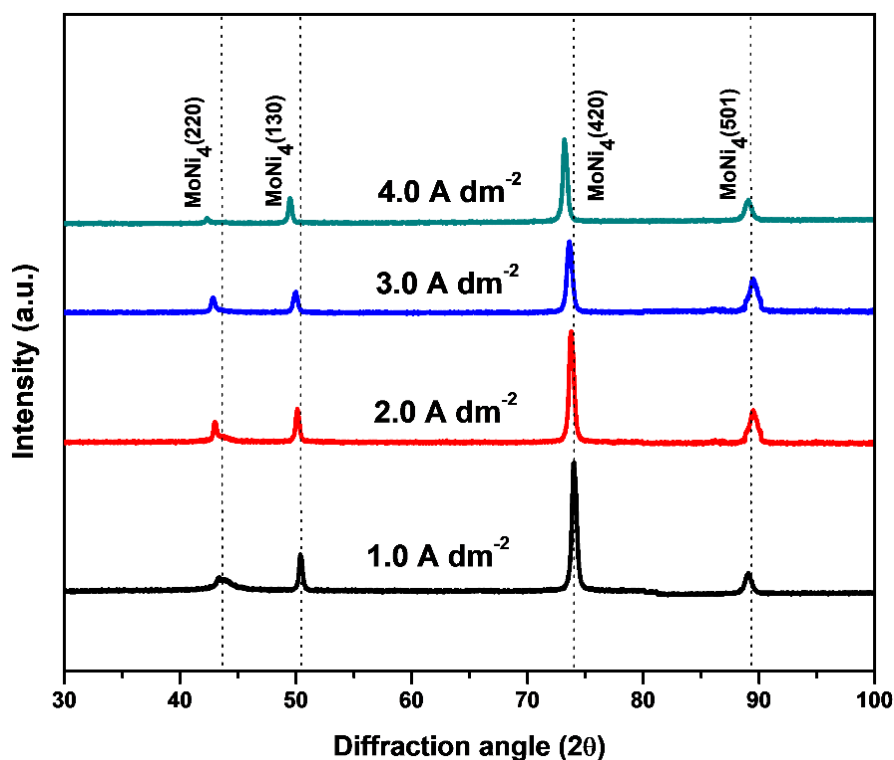
Figure 4.3- *Dependency of X-ray diffraction (XRD) peaks of (Ni-Mo) alloy coatings with deposition current density*

In addition, the observed slight shift of XRD peaks towards lower diffraction angle side (Figure 4.3) may be ascribed to the residual stress inside the crystal lattice (due to the difference in ionic radii between the Ni and Mo ion), affected during the process of deposition (Zhou et al. 2020). Further, the average crystallite size was found to be around 25 nm, calculated using Scherrer's formula (Cullity 1978).

4.2.5 Effect of current density on corrosion behaviour of (Ni-Mo) coatings

In case of induced co-deposition, the effect of plating current density on deposit character is quite vagarious, and unpredictable. There is no consistent trend in alloy composition with change of current density, and hence electrochemical behaviour is

considered to be very abnormal (Brenner 1963). Under the above background, the corrosion behaviour of visually bright and metallic (Ni-Mo) coatings obtained at varied current density (1.0 A dm^{-2}- 4.0 A dm^{-2}) were studied in 3.5% NaCl medium, by electrochemical impedance spectroscopy (EIS) and potentiodynamic polarization methods.

4.2.5.1 EIS study

The powerful and non-destructive EIS method was employed to study the corrosion behaviour of electrodeposited (Ni-Mo) alloy coatings. Here, in the EIS plot, interception of frequency response is attributed to the solution resistance (R_s), and at lower frequencies to the polarization resistance (R_p). Figure 4.4 represents the Nyquist response obtained for electrodeposited (Ni-Mo) coatings developed at different current densities.
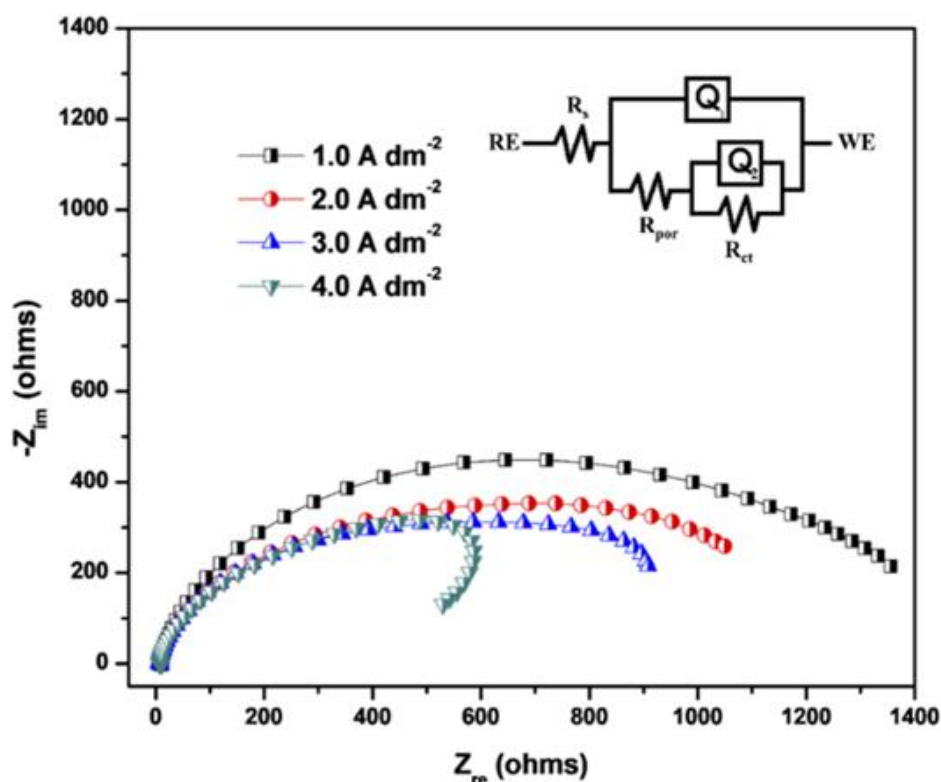
Figure. 4.4- Nyquist response of electrodeposited (Ni-Mo) alloy coatings developed at different plating current densities, from the optimal bath. In the inset is given the simulated equivalent circuit

It may be seen that all the coatings exhibit only one capacitive loop, with single incomplete semicircle. It implies that alloy coatings follow the same corrosion

mechanism with single charge transfer process, regardless of the current density at which they are deposited. Lastly, the observed high capacitive loop with large charge transfer resistance (R_{ct}) value, corresponding to (Ni-Mo) alloy coating deposited at 1.0 A dm^{-2} indicates that it is the most corrosion resistant, compared to all other coatings, and is further confirmed by equivalent circuit fitment.

In order to understand the corrosion mechanism electrochemical equivalent circuit model is simulated, using ZSimpWin circuit fitting software. The proposed equivalent circuit with best possible fitment is shown in the inset of Figure 4.4. Many circuit elements found were, solution resistance (R_s), followed by a constant phase element (CPE) that has been used as a substitute for capacitance of adsorbed coating (Q_1); and pore resistance (R_{por}) arising due to non-uniformity in coating occurred by the corrosion process followed by another constant phase element represent double layer capacitance (Q_2) arising at the delaminated coating-metal interface and the third R is ascribed to the charge transfer resistance (R_{ct}) at the electrical double layer. The numerical values of different circuit elements, R_s and R_{ct} are given in Table 4.2. From the EIS data it may be seen that the (Ni-Mo) coating developed at 1.0 A dm^{-2} exhibits highest corrosion resistance, with highest charge transfer resistance (R_{ct}=1344.7 ohms), which decreased with increase of current density. Thus, it may be summarized that the corrosion resistance property of electrodeposited (Ni-Mo) alloy coatings bear a close relation with current density employed for its deposition.

4.2.5.2 Potentiodynamic polarization study

The potentiodynamic polarization behaviour of electrodeposited (Ni-Mo) alloy coatings corresponding to different current densities have been studied, and are shown in the form of Tafel plots in Figure 4.5. The corrosion rates have been evaluated by Tafel extrapolation method, and corresponding data are reported in Table 4.2. From the corrosion rate (CR) values corresponding to different current densities (Table 4.2), it may be noted that CR values of alloy coatings increased despite of increase in its noble metal (Ni) content, with increasing current densities. This peculiarity of alloy deposition may be attributed to the low limiting current density (i_L) of Ni in the bath, due to low concentration of NiCl$_2$. 6H$_2$O in the bath (7.0 g L^{-1}). Since in simple linear diffusion, the mass transport of metal ions towards cathode surface is directly dependent

on the bulk concentration of metal ions in the electrolytic bath (Equation 1.5), a shift in the value of i_L towards lower current density was found. *i.e.* at 1.0 A dm^{-2}. As a result, the coating developed at 1.0 A dm^{-2} showed the least corrosion current density (i_{corr}), implying its maximum corrosion resistance as shown in Table 4.2.
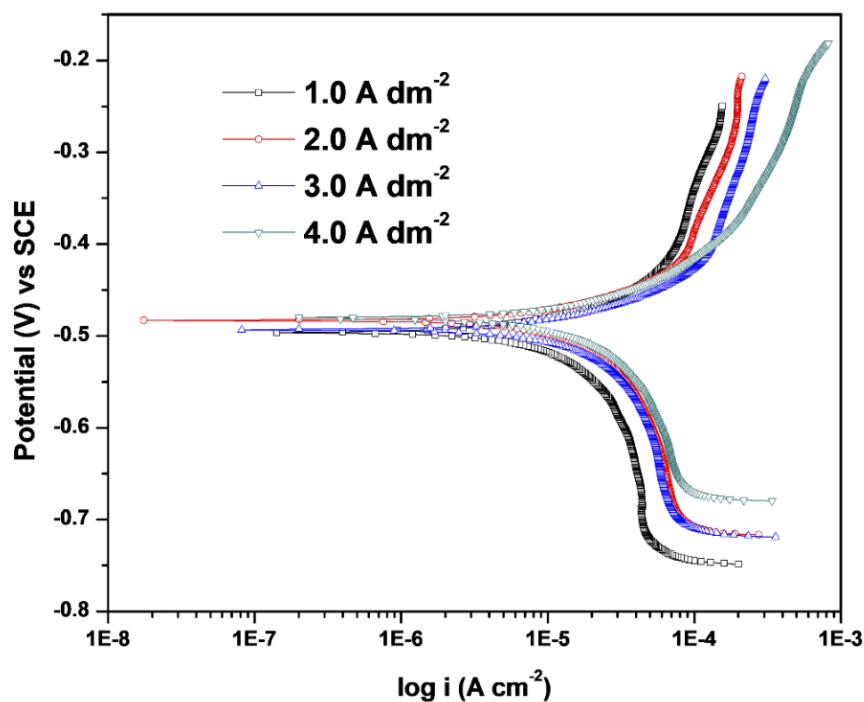
Figure. 4.5- *Potentiodynamic polarization behaviour of electrodeposited (Ni-Mo) alloy coatings corresponding to different current densities*

4.3 CONCLUSIONS

From the experimental results of investigation, following observations are made as conclusions:

1. A low concentration (both in terms of Ni and Mo), citrate-ammoniacal bath was formulated and visually bright and metallic coatings were obtained at current density range of 1.0 A dm^{-2}- 4.0 A dm^{-2}

2. Corrosion studies revealed that electrodeposited (Ni-Mo) coatings developed at 1.0 A dm^{-2} are more stable, compared to the coatings at higher current densities.

3. Composition data revealed that change in the wt.% of metal contents (both Ni and Mo) in the deposit with current density is very marginal, demonstrating the characteristic *induced type* of co-deposition.

71

4. The constancy of XRD peaks to all (Ni-Mo) coatings irrespective of the current density is attributed to the formation of solid solution of Mo in Ni, with only slight change in the composition.

5. Increased CR values of alloy coatings despite of its increased noble metal (Ni) content is attributed to low limiting current density (i_L) of Ni prevailing in the bath, due to low concentration of its metal salt.

CHAPTER 5

DEVELOPMENT OF HIGH CORROSION RESISTANT (Ni-Mo) ALLOY COATINGS: EFFECT OF MAGNETOCONVECTION

CHAPTER 5

DEVELOPMENT OF HIGH CORROSION RESISTANT (Ni-Mo) ALLOY COATINGS: EFFECT OF MAGNETOCONVECTION

This chapter is devoted to explore the benefit of magnetic field (B) effect on process of electrodeposition of (Ni-Mo) alloy coatings to increase its corrosion protection efficacy. The less corrosion performance of (Ni-Mo) alloy coatings of newly proposed bath, limited by its low limiting current density (i_L) due to low concentration of metal salts was attempted to improve further by taking the advantage of magneto-convection. Magneto-electrodeposited (MED) (Ni-Mo) alloy coatings developed under conditions of parallel and perpendicular B (applied simultaneously to the process of deposition) was found to be, respectively five and eight times more corrosion resistant than its conventionally electrodeposited (ED) alloy coatings, developed from the same bath for same duration. Properties of MED alloy coatings have been analyzed by FESEM, EDS and XRD studies. The reasons responsible for improved corrosion resistance of MED coatings were explained through B controlled diffusion of more noble Ni^{+2} ions, and results are discussed.

5.1 INTRODUCTION

In electroplating, mass transport of metal ions towards cathode is the most important factor responsible for the composition and phase structure of electrodeposited coatings. Basically, mass transport resistance results from the depletion of the electroactive species at the cathode surface due to low concentration of metal ions in the bulk of electrolyte. Therefore, by taking the mass transfer process as tool, it is possible to bring a marked change in the composition, and hence performance of (Ni-Mo) alloy coatings. In this aspect, the present study is focussed on the production of high corrosion resistant (Ni-Mo) by taking the benefit of phenomenon, called *magneto-convection*, by electroplating under the effect of external magnetic field (*B*). There are numerous studies concerning possible effects of static magnetic fields on the process of electrodeposition, and several potential interaction mechanisms have also been proposed (Ngo Boum and Alemany 1999). In addition, the influence of an imposed *B* on the electrochemical process is reviewed by Fahidy (1983), and applications of magnetoelectrolysis has been explained by Tacken and Janssen (1995) in their most

cited publications. Thus, from the literature it is well established fact that induced magnetic fields create an additional convection inside the electrochemical cell by imparting magnetohydrodynamic (MHD) effect, inside the bath (Krause et al. 2005). Thus, combined effects of electric/magnetic fields on electrolyte properties, influence the mass transport, electrode kinetics and the quality of electroplated metals. Moreover, it is stated in the literature that magnetic field effect is relatively strongest when mass transport is the controlling mode, *i.e.*, in the neighbourhood of the limiting current plateau. Taking this as the incentive, the magnetic field has been used as tool to improve the corrosion resistance behaviour of (Ni-Mo) alloy coatings, from newly formulated low concentration bath (Chapter - 4), by proper manipulation of limiting current density (i_L) and intensity of magnetic field (B). By using advent of magneto-convection, the low i_L of Ni (the main limitation of the bath due to low concentration of Ni salt) was tried to increase by inducing magnetically the flow patterns of Ni^{+2} ions towards cathode through artificial convection of magnetohydrodynamic (MHD) effect. Magneto-electrodeposition was carried out by superimposing the magnetic field (B), in conjunction with the regular deposition of metal ions, as metal atoms. Thus using the mass transfer process as tool, the present chapter focuses on the effect of magneto-convection on the anticorrosion performance of (Ni-Mo) alloy coatings. The potential possibility of improving the mass transport process of electrolytic cell, magnetic field (B) effect (in both direction and intensity) has been experimented to improve the pattern and properties of alloy coating. The benefit of magnetic field effect has been tried to explore to the fullest of its possibility to increase the corrosion resistance behaviour of (Ni-Mo) alloy coatings from a low concentration bath. The effect of B on surface morphology, composition and phase structure of alloy coatings have also been detailed here.

5.2 EXPERIMENTAL

The magneto-electrodeposition was carried out using the (Ni-Mo) low concentration bath (Table 4.1), but under different conditions of induced B (parallel and perpendicular to the direction of lines of electric field, depending on the requirement). A electromagnet (Polytronics, Model: EM 100, India), shown in Figure 3.5 was used as the source of magnetic field in present study. The magneto-electrodeposition was

accomplished on polished copper substrate under both conditions of *B* (applied parallel and perpendicular to the direction of movement of metal ions), by keeping the electrolytic cell in the uniform magnetic field located between poles of electromagnet, as shown in Figure 3.5. All depositions were made for 600 seconds similar to that of conventional electrodeposited (ED) (Ni-Mo) alloy coatings, for the purpose of comparison. The magneto-electrodeposited alloy coatings were developed at different intensity of *B* (from 0.1- 0.4 T (tesla), both parallel and perpendicular at optimal current density (1. 0 A dm^{-2}, arrived on the basis of the least corrosion rate observed among different current densities from 1.0 to 4.0 A dm^{-2}), using the proposed bath shown in Table 4.1. The corrosion performances of all coatings were evaluated in 3.5% NaCl at 298 K by electrochemical AC and DC methods (VersaSTAT-3, Princeton Applied Research) in a three-electrode cell, using MED coatings as test electrode (TE), platinized platinum electrode as counter electrode (CE), and saturated calomel electrode (SCE) as reference electrode. The corrosion rates (CR's) of all coatings were evaluated by Tafel extrapolation method. Electrodeposited (Ni-Mo) alloy coatings are represented conveniently, as ED (Ni-Mo). Magneto-electrodeposited (Ni-Mo) coatings are represented, respectively as MED‖ $(Ni-Mo)_x$ and MED $\perp$ $(Ni-Mo)_x$ for parallel (‖) and perpendicular ($\perp$) *B* applied. Here, 'x' stands for intensity of *B* at which magneto-electrodeposition is carried out. In addition, electrodeposited (Ni-Mo) alloy coatings are conveniently abbreviated as ED(Ni-Mo).

5.3 RESULTS AND DISCUSSION

The electrodeposition in the presence of magnetic field (*B*), called magneto electrodeposition of (Ni-Mo) alloy were carried out using optimized bath (Table 4.1) under conditions of both parallel (‖), and perpendicular ($\perp$) *B*, and experimental observations are described below.

5.3.1 Effect of parallel *B*
5.3.1.1 FESEM study

It is well known that the induction of *B,* during electroplating can uniquely alter the surface microstructure of electrodeposited coatings (Fahidy 1983, Tacken and Janssen 1995). In this regard, the FESEM micrographs of MED‖ (Ni-Mo) alloy coatings developed at different *B* intensity, are shown in Figure 5.1. It may be seen that *B* applied

during the deposition influenced the morphology of coatings to a large extent. The regular columnar dendritic structure of ED (Ni-Mo) alloy coating, shown in Figure 5.1(a) was found to be slightly suppressed to get a relatively smooth surface on superimposition of B at MED|| (Ni-Mo)$_{0.4\ T}$ as may be seen in Figure 5.1 (d). As dendritic structure is generally connected with the diffusion-control processes, relatively more homogeneous structure of MED|| (Ni-Mo)$_{0.4\ T}$ alloy coating was obtained under mixed-control process. *i.e.*, under control of both electric field and magnetic field. Thus, it may be inferred that B-induced limiting current density (i_L) of Ni bears a close relationship with smoothness and corrosion resistance of MED|| (Ni-Mo) alloy coatings, which increased with intensity of B.
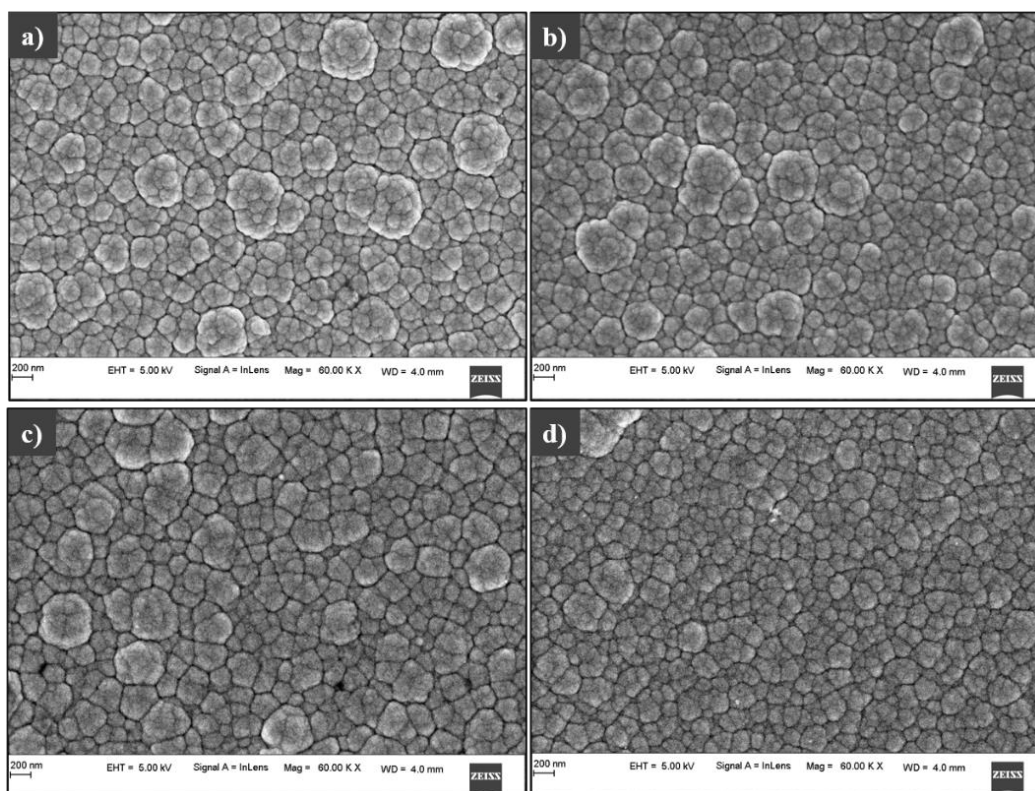
Figure 5.1- *The surface morphology* of *MED|| (Ni-Mo) alloy coatings, under different conditions of applied B*

5.3.1.2 XRD study

To understand, if there is any influence of B on the phase composition and deposit structure, XRD investigations were carried out. Figure 5.2 shows the XRD patterns of MED|| (Ni-Mo) alloy coatings, corresponding to B = 0.1 T, 0.2 T, 0.3 T and 0.4 T. It

78

may be noted that almost same XRD patterns (having almost same diffraction angle (2θ), and peak intensity) were demonstrated by all coatings of parallel configurations, regardless of the intensity of *B*. The characteristic diffraction peaks of all MED || coatings, observed at around $2\theta = 44°$, 50°, 74° and 89° are corresponding to $MoNi_4(220)$, $MoNi_4(130)$, $MoNi_4(420)$ and $MoNi_4(501)$ planes, respectively [from JCPDS database].
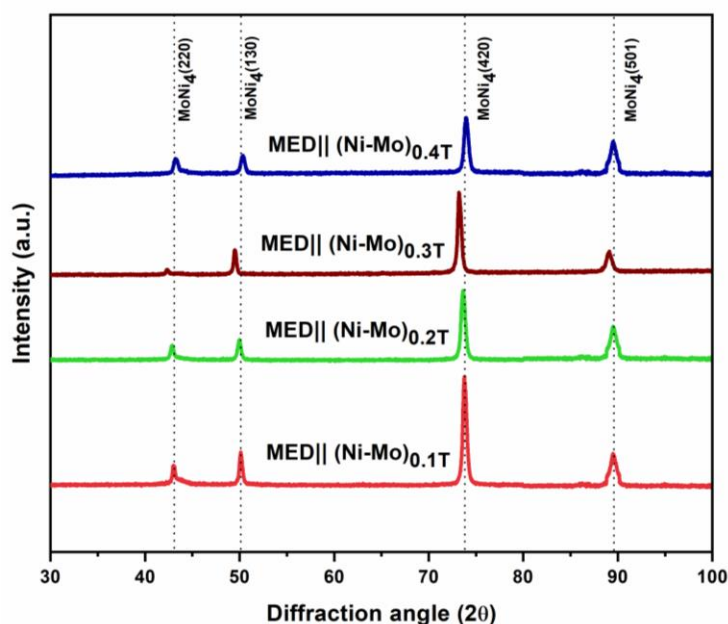
Figure 5.2- *X-ray diffraction spectra of MED|| (Ni-Mo) alloy coatings deposited under different intensities of B from the optimal bath*

Though there are many reports in the literature showing a significant change in the phase structure and crystallinity of MED alloy coatings with change of both direction and intensity of *B*, compared to its ED alloy coatings (Rao et al. 2013), in the present study no such changes are demonstrated in terms of both intensity and (2θ) of XRD patterns, as may be seen in Figure 5.2. The same XRD peaks (having almost same 2θ values) of all MED coatings of parallel configurations indicates that early nucleation and preferred orientation of the crystal planes is specific of the deposition current density (at 1.0 A dm^{-2}), and not with the intensity of *B*. In other words, electro-crystallization of MED|| (Ni-Mo) alloy coatings is controlled by magnetic field induced mass transfer process, and not by current driven charge transfer process. Further, a slight shift of XRD peaks towards lower angle side of 2θ was observed (Figure 5.2), which increased with intensity of *B*. It may be attributed to residual stress inside the

crystal lattice due to H_2 evolution, or due to the difference in ionic radii between the main element and the dopant ion, affected during process of deposition (Cullity 1978).

5.3.1.3 Compositional study

Further, the composition data of MED‖ (Ni-Mo) alloy coatings corresponding to different intensities of *B,* obtained from EDS analysis are tabulated in Table 5.1. As per Equation (1.6) it may be noted that as the lines of electric field (*i*) and *B* are parallel, the second term of Lorentz force (F_L) equation reduces to zero. Accordingly, it was expected that Ni content of all MED‖ (Ni-Mo) alloy coatings should have been independent of the effect of *B*. But from composition data reported in Table 5.1, it may be seen that Ni content of MED‖ (Ni-Mo) alloy coatings changed substantially with induction of *B*. Moreover, it was found to be increased progressively with magnitude of intensity of *B*. This increase of Ni with intensity of *B* may be attributed to the paramagnetic concentration gradient force, arising from paramagnetic Ni^{+2} ions of electrolyte (Koza et al. 2010, Odenbach 1994). Waskaas and Kharkats (2001) proposed that the interaction of paramagnetic ions with *B* is magnetoconvective in nature, and it causes an additional transfer of all components of the solution, including H^+ ions which is generated in the vicinity of the electrode surface. Therefore, an increase in the Ni content of (Ni-Mo) alloy with superimposition of ‖ *B* is attributed to magnetoconvection phenomenon, which includes the paramagnetic gradient force of Ni^{+2} ions (Fahidy 1983). Figure 5.3 shows a pictorial representation of the hydrodynamic flow near electrode during development of alloy coatings under natural convention (Figure 5.3 (a)) and under different conditions of applied *B* (Figures 5.3 (b) and 5.3(c)). When paramagnetic Ni^{+2} ions interact with applied *B*, an additional driving force is created inside the bath, which is responsible to reduce the thickness of cathode diffusion layer from δ_{ED} to $\delta_{MED‖}$, as shown in Figure 5.3 (b). This force has the same direction as the gradient of Ni^{+2} ions, allows the redistribution of velocities in the diffusion layer. Thus, an additional convective transport of all the components of the bath makes the thickness of EDL to be reduced, and consequently to increase the i_L of Ni.
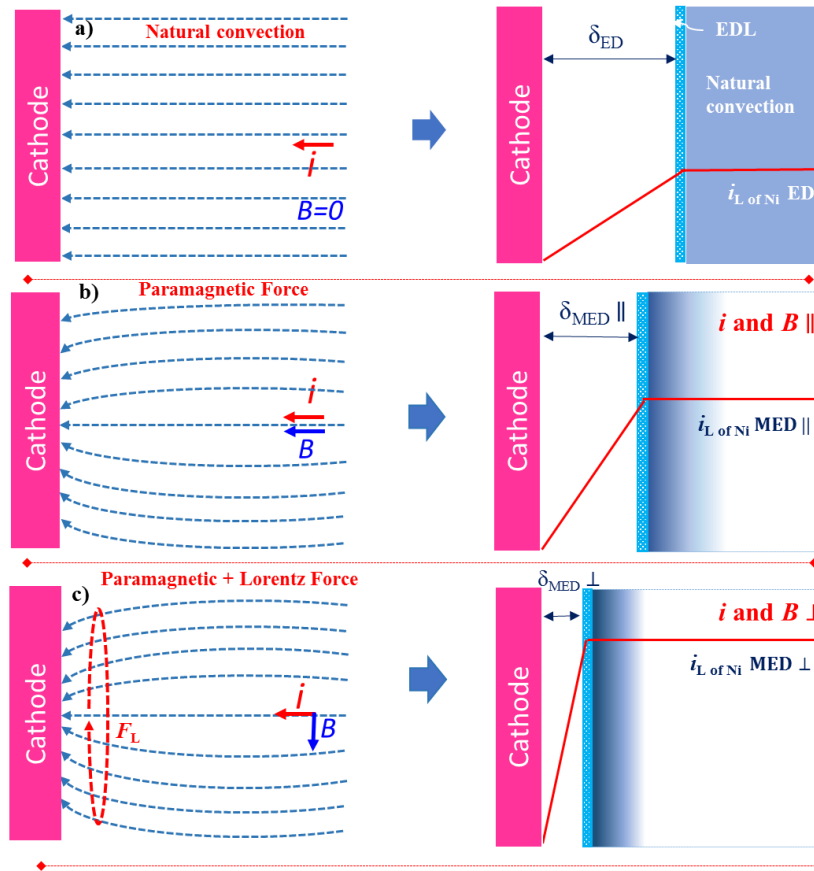
Figure 5.3- *Representative diagram showing the hydrodynamic flow near electrode during electrodeposition of alloy coatings under different conditions: a) B-free electrodeposition in a uniform electric field (i), b) electric field is || to the induced B, and c) electric field is ⊥ to the induced B. The change of i_L of Ni, responsible for change of its content in the deposit due to change in convection effect is shown on the right*

However, the degree of paramagnetic field gradient is based on the magnetic susceptibility (μ_0) of the ions, and it is a measure of the extent to which ions become magnetized when it is placed in an external B. Several experimental study of magnetoelectrolysis revealed that B effect increases with increase of both magnetic flux density, and magnetic susceptibility of the solution (Fahidy 1983). Therefore, progressive increase of Ni content in the deposit with intensity of || B may be ascribed to the increased convective transport of Ni^{+2} ions towards cathode, affected due to increased paramagnetic gradient field created inside the bath.

5.3.1.4 Corrosion study

Corrosion performances of MED‖ (Ni-Mo) alloy coatings deposited at different intensity of *B* were studied by potentiodynamic polarization and electrochemical impedance spectroscopy (EIS) methods, and are detailed below.

i) Potentiodynamic polarization study

Potentiodynamic polarization behaviour of MED‖ (Ni-Mo) alloy coatings, developed at different intensity of *B* are shown in Figure 5.4. The CR's of MED‖ (Ni-Mo) alloy coatings were evaluated by Tafel extrapolation method, and corresponding data are reported in Table 5.1.
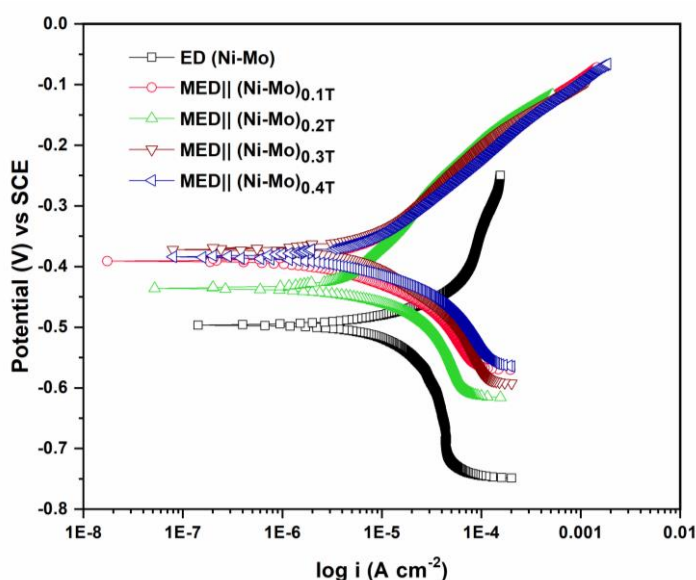
Figure 5.4- *Potentiodynamic polarization behaviour of MED‖ (Ni-Mo) alloy coatings at different intensity of B, in relation to ED (Ni-Mo) alloy deposited from same bath*

It may be seen that CR's of MED‖ (Ni-Mo) alloy coatings are substantially less, compared to ED (Ni-Mo) alloy coating deposited from the same bath at 1.0 A dm^{-2}, followed by a gradual increase in the wt.% of Ni in the deposit with the intensity of *B* as reported in Table 5.1. It confirms the fact that magnetic field effect is proportional to the gradient in the magnetic susceptibility of Ni^{+2} ions, and hence Ni content of the deposit. In addition, E_{corr} values were found to be shifted towards noble side (Figure 5.4) alongside the decrease i_{corr} values (Table 5.1) reveals the fact that increase of corrosion protection efficacy of MED‖ (Ni-Mo) coatings with intensity of *B* is resulted due to increase of its Ni content.

Table 5.1- Change of composition and corrosion rates of MED (Ni-Mo) alloy coatings under different conditions of applied magnetic field (B). Corrosion data of conventionally electrodeposited (Ni-Mo) alloy coating, denoted as ED(Ni-Mo), deposited from the same bath is also shown for comparison purpose

Coating configuration	wt. % of Ni	wt. % of Mo	R_s (ohms)	R_{ct} (ohms)	$-E_{corr}$ (mV vs SCE)	i_{corr} ($\mu A\ cm^{-2}$)	$CR \times 10^{-2}$ ($mm\ y^{-1}$)
ED (Ni-Mo)	68.1	31.9	10.8	1344.7	496.3	20.0	16.7
Magneto-electrodeposition							
Under parallel B							
MED‖ (Ni- Mo)$_{0.1T}$	69.3	30.7	15.4	1373.2	387.8	18.7	15.5
MED‖ (Ni- Mo)$_{0.2T}$	70.6	29.4	12.1	1612.0	435.8	16.2	13.6
MED‖ (Ni- Mo)$_{0.3T}$	71.1	28.9	14.6	1455.2	371.9	9.4	7.9
MED‖ (Ni- Mo)$_{0.4T}$	73.1	26.9	13.8	2213.8	399.3	3.9	3.4
Under perpendicular B							
MED$\perp$ (Ni- Mo)$_{0.1T}$	71.7	28.3	12.55	1539.3	383.1	14.1	11.9
MED$\perp$ (Ni- Mo)$_{0.2T}$	75.3	24.7	11.90	2046.7	353.2	8.2	7.1
MED$\perp$ (Ni-Mo)$_{0.3T}$	77.9	22.1	12.64	3024.0	327.9	2.5	2.2
MED$\perp$ (Ni- Mo)$_{0.4T}$	73.4	26.6	12.88	1531.4	373.3	9.9	8.5

ii) EIS study

The impedance response of MED‖ (Ni-Mo) alloy coatings corresponding to different intensities of B, in relation to ED (Ni-Mo) coating obtained on drawing real part of the impedance (Z_{re}) against the imaginary part ($-Z_{im}$) is shown in Figure 5.5. It may be noted that all coatings exhibited incomplete depressed semicircle, with constant increase in the value of charge transfer resistance (R_{ct}) with the intensity of B,

demonstrating that corrosion resistivity of MED coatings increases with intensity of *B*. In other words, the axial radius of the semicircle is found to be increased with intensity of *B*, indicating that induced *B* has increased the Ni content, and hence corrosion resistance of MED∥ (Ni-Mo) alloy coatings progressively. It is supported by the data, reported in Table 5.1.
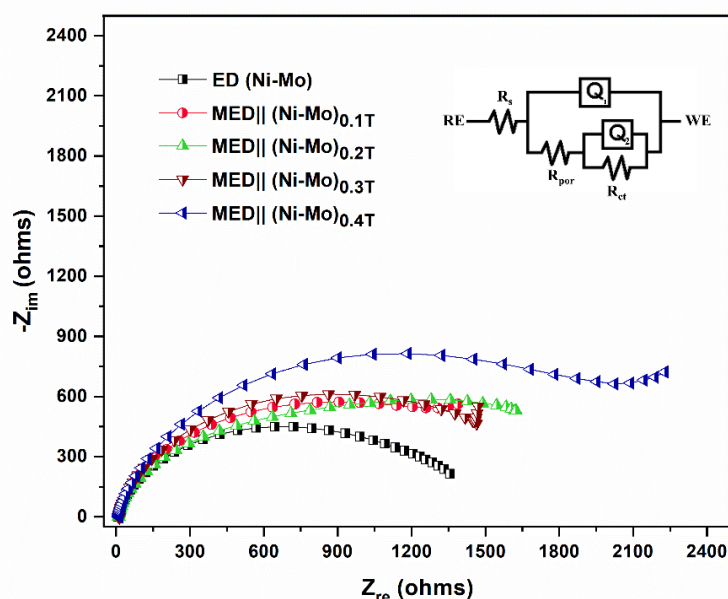
Figure 5.5- *Electrochemical impedance response of MED (Ni-Mo) alloy coatings deposited under different conditions of induced B (∥), in relation to ED coating deposited from the same bath*

5.3.2 Effect of perpendicular *B*

5.3.2.1 FESEM study

The FESEM images of MED⊥ (Ni-Mo) coatings developed at different magnetic flux densities, *i.e. B* = 0.1 T, 0.2 T, 0.3 T, and 0.4 T is shown in Figure 5.6. A significant change in the surface microstructure along with increase in wt.% of more noble Ni in the alloy deposit was found as the intensity of ⊥ *B* is changed from 0.1 T to 0.4 T. This change of surface morphology with intensity of *B* may be explained as follows: It is well known that during electrodeposition, it is quite natural that co-evolution of hydrogen leads to the formation of H_2 bubbles on the cathode surface, and this phenomenon can change the properties of deposits. The H_2 formed during the process of electrodeposition may sometimes deteriorate the properties of electroplated metals/alloys. Similarly, during MED⊥ (Ni-Mo) alloy deposition, the induced *B*

increased the mass transport rate of H^+ ions to the cathode surface to form H_2 bubbles. But, the presence of B also accelerates desorption of H_2 bubbles, due to Lorentz force acting radially on the surface of cathode. This results in the formation of more homogeneous deposits, at lower limits of intensity of B as shown in Figure 5.6 (a) to Figure 5.6 (c). As Ni is having low hydrogen overvoltage, excessive H_2 is evolved on the surface of the coatings at higher limits of B, Hence, MED$\perp$ (Ni-Mo) alloy coating, corresponding to 0.4T becomes more porous as shown in Figure 5.6 (d).
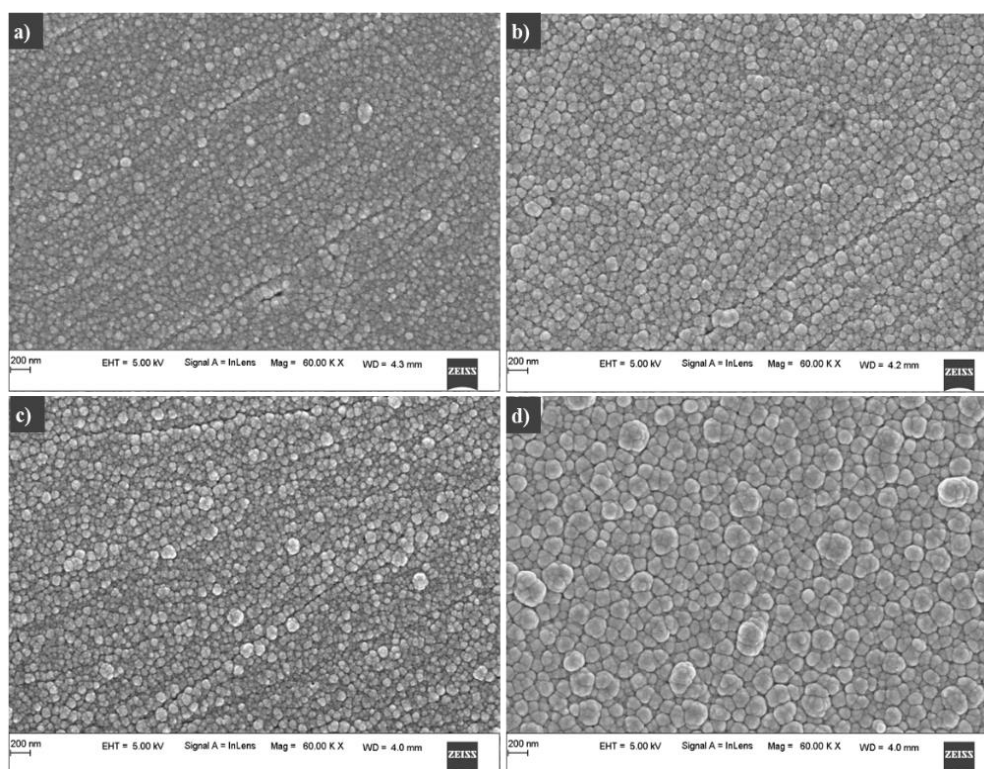
Figure 5.6- *FESEM images of MED ⊥ (Ni-Mo) alloy coatings deposited at different intensity of B (perpendicular), deposited from the optimal bath: (a) 0.1 T, (b) 0.2 T, (c) 0.3 T and (d) 0.4 T*

The smaller grain size of MED $\perp$ (Ni-Mo) alloy coatings may be explained in terms of enhanced mass transfer of Ni^{+2} ions in the close vicinity of the electrode, due to increased convection, which makes the obtained grains smaller and similar in size (Kołodziejczyk et al. 2018). Actually, during electrodeposition of MED $\perp$ (Ni-Mo) alloy coatings, the second term of Lorentz force (F_L) Equation (1.6) comes into play, which keeps the charged species (metal ions) in whirl-pool motion as discussed in Section 1.5.2 (Figure 1.4). The macroscopic stirring, affected due to Lorentz force

induced convection creates microscopic minute vortexes, called micro-MHD effect. Thus, it may be summarized that better uniformity of MED coatings (both parallel and perpendicular) is due to sharply localized spots of high current density on the surface of cathode, affected due to micro-MHD effect.

5.3.2.2 XRD study

The change in the crystal structure of (Ni-Mo) alloy coatings due to induced magnetic field (B) was studied by X-ray diffraction (XRD) analysis. Figure 5.7 shows the XRD patterns of MED$\perp$(Ni-Mo) alloy coatings, deposited under the effect of different intensities of B i.e., B = 0.1 T- 0.4 T, in comparison with the one, without the effect of magnetic field (B = 0 T).
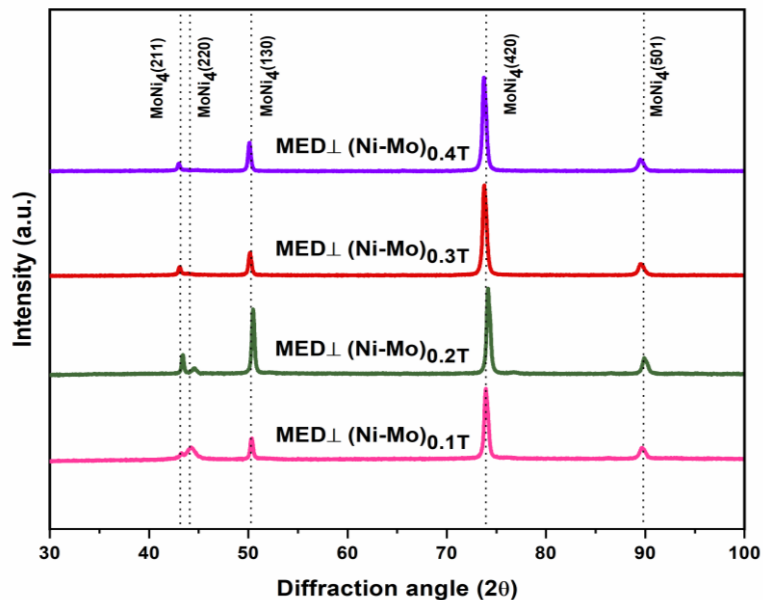
Figure 5.7- *X-ray diffraction spectra of MED $\perp$ (Ni-Mo) alloy coatings deposited under different intensities of B from the optimal bath*

It may be noted that even under the influence of perpendicular B, there is no significant change in the XRD patterns, except an increase of intensity of peak with strength of B, as may be seen in Figure 5.7. The XRD patterns clearly indicate that prominent peak corresponding to MoNi$_4$ reflection is the characteristic of (Ni-Mo) alloy coatings of all configurations (Jakšić et al. 2000). However, increase in the intensity of peaks with B may be attributed to the increase in the wt.% of Ni in the deposit, affected due to MHD effect. In addition, one small additional peak corresponding to MoNi$_4$(211)

plane was observed in all MED $\perp$ (Ni-Mo) alloy coatings, different from that of $\parallel$ configuration, as may be seen in Figure 5.7. This signature peak of (211) plane may be the characteristic of MED $\perp$ (Ni-Mo) coatings.

5.3.2.3 Compositional study

The compositional change of MED $\perp$ (Ni-Mo) coatings, deposited at different intensity of *B* (perpendicular) have also been made, and is reported in Table 5.1. It may be seen that wt. % of Ni in the deposit is increased drastically with intensity of *B*. In addition, effect of *B* on Ni content of the alloy is more pronounced in the case of perpendicular *B*, compared to parallel field. It may be attributed to the increased mass transport of metal ions towards cathode, affected due to micro-MHD effect as discussed in Section 5.3.1.3.

5.3.2.4 Corrosion study

The corrosion behaviours of MED $\perp$ (Ni-Mo) coatings, deposited at different intensity of *B* (from 0.1 T to 0.4 T) were studied, and corresponding Nyquist and Tafel responses are shown in Figure 5.8. From the nature capacitive loops of MED $\perp$ (Ni-Mo) coatings, shown in Figure 5.8(a) it may be inferred that their CR's decreased with intensity of *B*, and it is minimum for MED $\perp$ (Ni-Mo)$_{0.3T}$ (due to its maximum R_{ct} value).
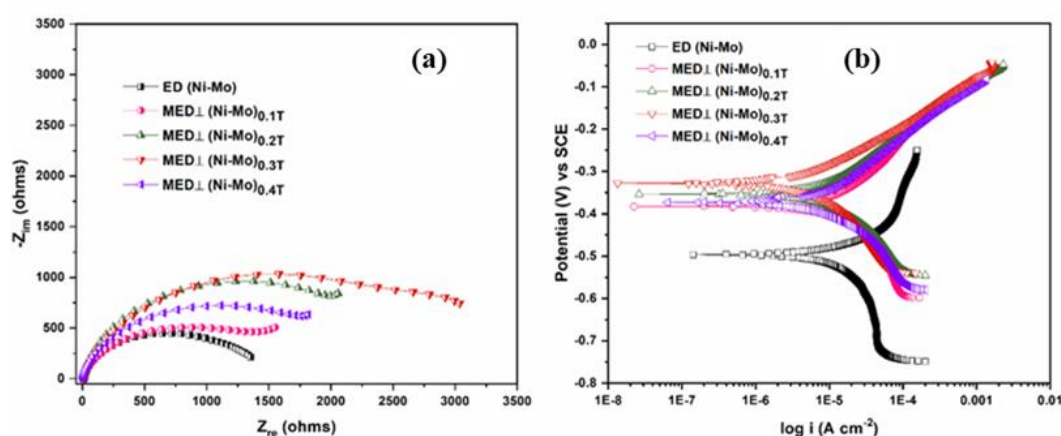
Figure 5.8- Corrosion response of MED $\perp$ (Ni-Mo) coatings, deposited at different intensity of B (from 0.1 T to 0.4 T): a) Impedance plots, and b) Tafel plots for coatings deposited from the same bath, at same current density and for same duration

In EIS study, electrochemical processes associated with the electrolyte/interface and redox reactions can be simulated/computed as an electric circuit (equivalent

circuit), involving electrical components (resistors, capacitors, inductors). Such equivalent circuit is very useful to understand and evaluate the individual components of the EIS system. Resistance of solution (R_s), double layer capacitance at the surface of the electrode (C_{dl}), charge transfer resistance (R_{ct}) etc. In this regard, based on the EIS data obtained, a best fitting electrochemical equivalent circuit corresponding to MED $\perp$ (Ni-Mo)$_{0.3\ T}$ has been simulated, and is shown in Figure 5.9.
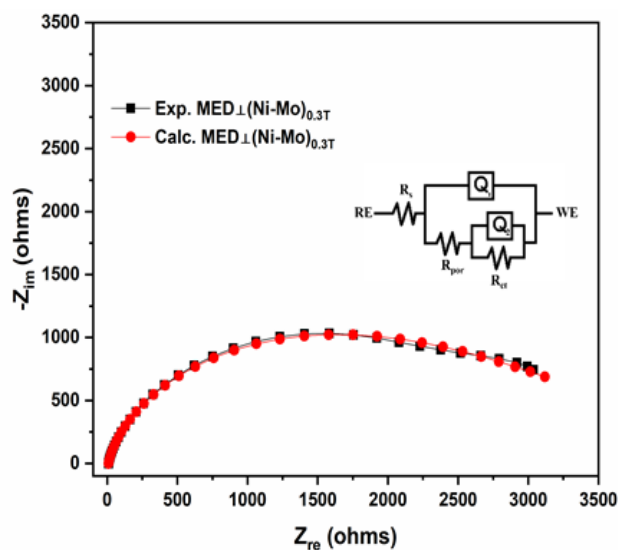
Figure 5.9- *Electrochemical equivalent circuit fitment corresponding to MED $\perp$ (Ni-Mo)$_{0.3T}$ alloy coating showing the highest corrosion protection efficacy*

In addition, the nature of Tafel plots, shown in Figure 5.8(b) endorse the fact that corrosion resistance of MED(Ni-Mo) alloy coatings increased with intensity of *B*, and it is maximum in case of MED $\perp$ (Ni-Mo)$_{0.3T}$. Thus, from both EIS and Tafel studies, MED $\perp$ (Ni-Mo)$_{0.3T}$ alloy coatings showed a drastic increase in corrosion resistance (CR=2.2×10^{-2} mm y^{-1}), compared to conventional ED(Ni-Mo) alloy coating (CR=16.2×10^{-2} mm y^{-1}), Hence, this coating configuration is considered as optimal configuration for best performance of the coatings, deposited from this particular bath. This increase of corrosion resistance property of MED $\perp$ (Ni-Mo)$_{0.3T}$ coating is attributable to the combined effect of Lorentz force, which is maximum when the magnetic field is perpendicular to the process of electrodeposition, as discussed in the previous section. Further, it is important to note that corrosion resistance of MED $\perp$ (Ni-Mo) coating was found to be decreased at 0.4T (Figure 5.8 and Table 5.1). This is due to the excessive H$_2$ evolution, due to Lorentz force induced magneto-hydrodynamic

(MHD) effect. This situation is corresponding to the formation of more porous coating, with decreased Ni content, and is evident from Figure 5.6 (d), and Table 5.1.

5.3.3 Effect of *B* on Ni content of the alloy

The very objective of using the advantage of magnetoconvection in electrodeposition is to increase the Ni content, and hence corrosion resistivity of (Ni-Mo) alloy coatings. Hence, the change of Ni in the deposit in MED (Ni-Mo) alloy coatings, with the strength of *B* (in both ∥ and ⊥ configuration) is shown in Figure 5.10.
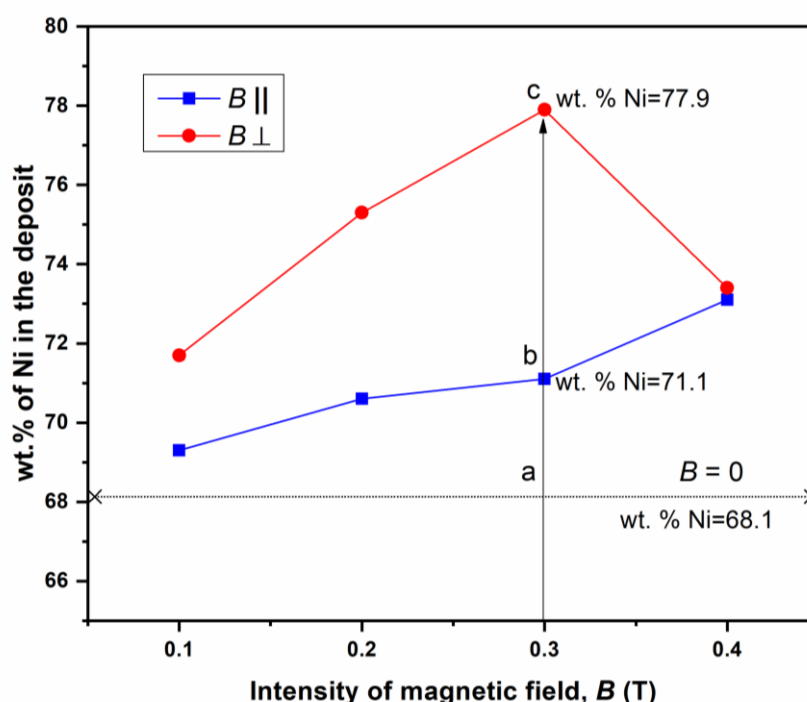
Figure 5.10- *Change of Ni content in the deposit with intensity of B, under parallel and perpendicular conditions. Horizontal line corresponds to the Ni content of ED (Ni-Mo) alloy coating, deposited at optimal condition, where B = 0 T*

It may be noted that Ni content of MED∥ (Ni-Mo) alloy coatings, increased linearly with intensity of *B*. It indicates that the magnetoconvection effect, responsible for diffusion of Ni^{+2} ions increased with the amplitude of *B*. Further, the surface roughness of MED∥ (Ni-Mo) alloy coatings was found to be decreased due to increased nucleation process on the cathode surface. Thus, under parallel configuration, the increase of Ni in the deposit is attributed to the paramagnetic field gradient of Ni^{+2} ions (present in the bath), which increased with the strength of *B*.

But in case of MED $\perp$ (Ni-Mo) alloy coatings, the Ni content of the alloy increased sharply with the intensity of *B*, up to 0.3T and then started decreasing, as shown in Figure 5.10. This sharp increase of Ni with *B* is attributed to the combined effect of paramagnetic and Lorentz force induced micro-MHD effect. The increase of Ni in the MED $\perp$ (Ni-Mo) alloy coatings up to *B* = 0.3T indicates that its composition and properties can be modified up to that intensity of *B*, with its beneficial effect of large-scale convection. However, the decrease of Ni at higher limits of *B*, *i.e.,* at *B* = 0.4 T suggests that *B* has reached its limiting value, beyond which the effect of *B* has no effect to increase the Ni content of the alloy coating.

It may be noted that under optimal conditions, Ni content of MED‖ (Ni-Mo) alloy coatings increased to 73.1 wt.% from 68.1 wt.%, corresponding to ED (Ni-Mo) alloy coating. But in case of MED $\perp$ (Ni-Mo) alloy coating, it increased to 77.9 wt.%, compared to its conventional ED and MED‖ (Ni-Mo) alloy coatings, as shown by the line *abc* in Figure 5.10. Hence, it may be summarized that the corrosion resistance of (Ni-Mo) alloy deposits increased with the intensity of *B* in both ‖ and $\perp$ configuration, depending on the Ni content. The effect is more pronounced in the case of *B* due to combined effect of both paramagnetic field gradient and Lorentz force induced micro-MHD effect. It is important to note that an early reaching of optimal limiting *B* intensity (*B* = 0.3T) in the case of perpendicular field, compared to parallel field (*B* = 0.4T) is affiliated to the combined effect of paramagnetic field and Lorentz force.

5.3.4 Comparison of ED and MED (Ni-Mo) alloy coatings

As corrosion performance of alloy coatings largely depends on their surface morphology and phase structures, the comparison of XRD peak patterns and surface microstructure of ED (Ni-Mo), MED‖ (Ni-Mo)$_{0.4T}$ and MED $\perp$ (Ni-Mo)$_{0.3T}$ alloy coatings (all corresponds to optimal conditions) were made, and are shown in Figure 5.11. It is well known that the texture of electrodeposited alloy coatings depends on the current density and the hydrogen evolution reaction. As discussed earlier, coatings deposited at optimal current density of 1.0 A dm^{-2} showed a significant change in the surface morphology, when electroplated under the effect of *B,* as shown in Figures 5.1 and 5.5.
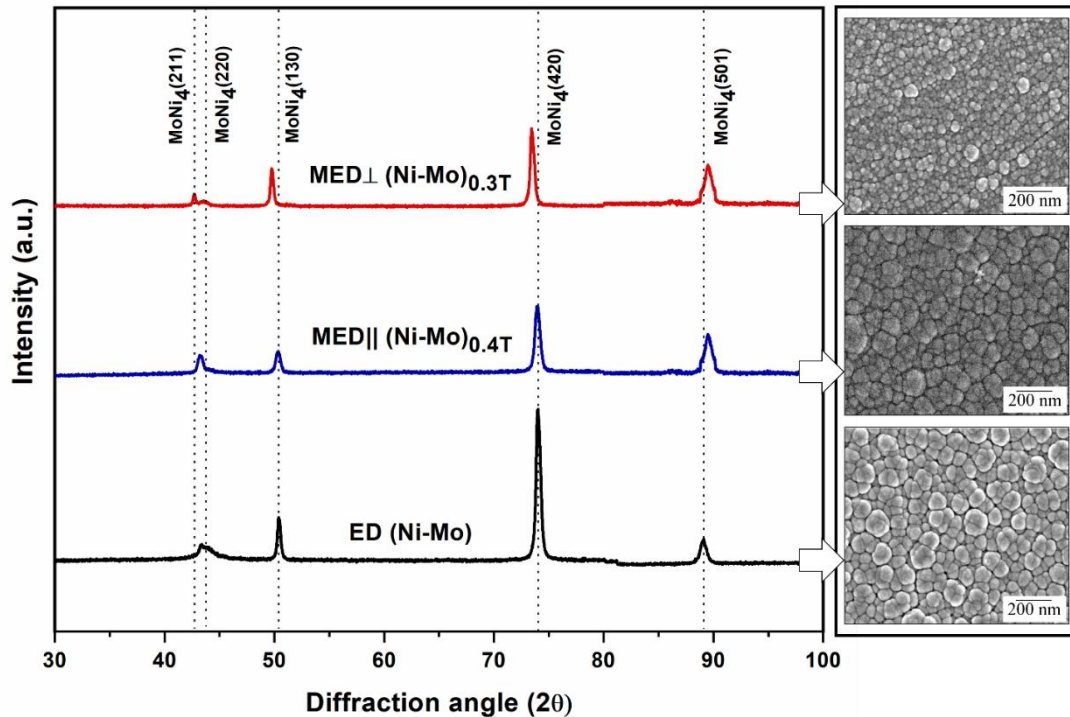
Figure 5.11 *- Phase structures and surface microstructure of ED (Ni-Mo) alloy coatings, in comparison with MED (Ni-Mo) alloy coatings of parallel and perpendicular configuration (all under optimal conditions), deposited from same bath*

In addition, all peaks corresponding to $MoNi_4(220)$, $MoNi_4(130)$, $MoNi_4(420)$ and $MoNi_4(341)$ planes of ED Ni-Mo alloy coatings were found even in MED coatings of both ∥ and ⊥ configurations as shown in Figure 5.11. However, an additional small peak corresponding to $MoNi_4$ (211) plane was found in case of only MED ⊥ (Ni-Mo) coatings, and this is attributed to the effect of micro-MHD phenomenon, governed by Lorentz force. The constancy of XRD peaks (except small shifts) of ED (Ni-Mo), MED∥ (Ni-Mo)$_{0.4T}$ and MED ⊥ (Ni-Mo)$_{0.3T}$ alloy coatings is due to the fact that *B* induced (Ni-Mo) alloy deposition is purely a diffusion controlled process, and has no effect on the reaction kinetics (Cullity 1978, Ganesh et al. 2005, Rao et al. 2013). Except for compositions (hence CR's), surface morphology of MED (Ni-Mo) alloy coatings were found not to vary much with direction and intensity of *B*. It may be ascribed to the limiting magnetic field effect on the process of deposition, rather than the electric field (which as low as 1.0 A dm^{-2}). From the surface morphology of (Ni-Mo) alloy coatings, shown on the right of Figure 5.11, confirms that the growth of the globular dendritic

growth of electrodeposit is considerably suppressed with the induction of *B,* with de-sorption of H$_2$. The dendritic growth is further suppressed with the growing intensity of *B*, up to *B* = 0.3T. Hence, MED $\perp$ (Ni-Mo) $_{0.3T}$ is found to be more uniform and highest corrosion resistant, compared to all other coatings. Hence, MED $\perp$ (Ni-Mo)$_{0.3T}$ coating is considered as the optimal configuration for best performance against corrosion.

5.3.5 Comparison of corrosion behaviours

The corrosion protection efficacy of ED (Ni-Mo), MED|| (Ni-Mo) $_{0.4T,}$ and MED $\perp$ (Ni-Mo)$_{0.3T}$ alloy coatings showing the least CR (all under optimal conditions) are shown in Figure 5.12.
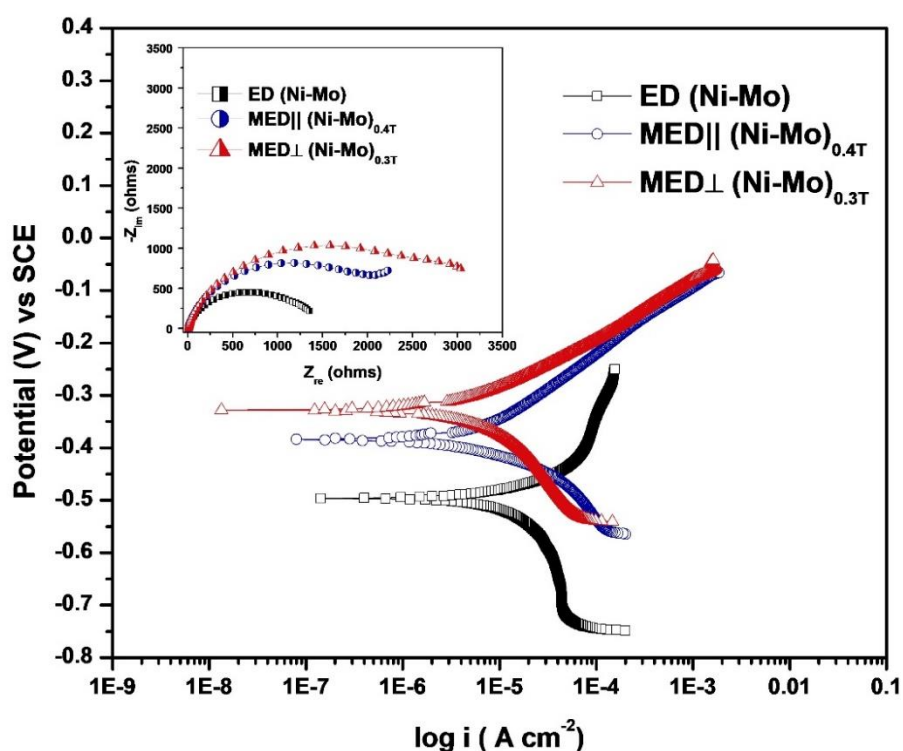
Figure 5.12 - *Comparison of Tafel behaviours of MED (Ni-Mo) alloy coatings deposited under conditions of induced B (both || and $\perp$) in relation to ED (Ni-Mo) coating deposited from the same bath (all corresponds to optimal condition)*

The potentiodynamic polarization curves of (Ni-Mo) alloy coatings distinctly demonstrate that MED $\perp$ (Ni-Mo)$_{0.3T}$ alloy coating is the most corrosion resistant, compared to other coatings. The highest corrosion stability of MED $\perp$ (Ni-Mo)$_{0.3T}$ alloy coatings is evident from its both i_{corr} and E_{corr} values. The relative response of their EIS

plots are also shown in the inset of Figure 5.12. Thus, from the polarization behaviour and corrosion data it may be summarized that ED (Ni-Mo) alloy coating, having 68.1 wt.% Ni showed CR = 16.7×10^{-2} mm y^{-1}, MED coatings having configuration MED|| (Ni-Mo)$_{0.4\ T}$ and MED $\perp$ (Ni-Mo)$_{0.3T}$ having, respectively 73.1 wt. % and 77.9 wt. % Ni showed CR's = 3.4×10^{-2} mm y^{-1} and 2.2×10^{-2} mm y^{-1}, respectively. Therefore it may be concluded that MED (Ni-Mo) alloy coatings, developed under both || and $\perp B$, are respectively about 5 times and 8 times more corrosion resistant than electrodeposited (ED) alloy coatings, developed from the same at same current density (1.0 A dm^{-2}).

5.4 CONCLUSIONS

*The inherent limitation of low concentration bath in developing the (Ni-Mo) alloy coatings of high corrosion resistance is successfully resolved using advantageously the phenomenon of magneto-convection, and the following observations were made as conclusion*s:

1. High corrosion resistant (Ni-Mo) alloy coatings can be developed from a low concentration bath by proper manipulation of i_L of metal ions, using *magneto-convection effect* as tool.

2. The low limiting current density (i_L) of Ni, linked to the low concentration bath of (Ni-Mo) bath is successfully alleviated using the magnetic field effect, to improve the corrosion resistance property of its alloy coating.

3. The i_L of Ni in low concentration bath was increased by proper manipulation of flow patterns of Ni^{+2} ions towards cathode through artificial convection of magnetohydrodynamic (MHD) effect, by superimposing *B* parallel and perpendicular to the direction of electric field.

4. Increase of Ni content of the deposit with the intensity of *B,* under both || and $\perp$ configuration, is ascribed to the increased convective transport of Ni^{+2} ions towards cathode, affected due to increasing strength of induced *B*.

5. The corrosion study demonstrated that magneto-electrodeposited (Ni-Mo) alloy coatings, developed under both || and $\perp B$, represented as MED|| (Ni-Mo) and MED $\perp$ (Ni-Mo) are, respectively about 5 times and 8 times more corrosion resistant than electrodeposited (ED) alloy coatings, developed from the same bath.

6. High corrosion resistivity of MED $\perp$ (Ni-Mo) coatings, compared to MED$\parallel$ (Ni-Mo) coatings is attributed to magnetoconvective effect, contributed from both paramagnetic and micro-MHD origin.

7. The properties of (Ni-Mo) alloy coatings, such as surface morphology, composition and phase structures, responsible for better corrosion resistance of alloy coatings were found to be controlled mainly by the intensity of B used during deposition, supported by FESEM, EDS and XRD study, respectively.

CHAPTER 6

ELECTROCHEMICAL WATER ELECTROLYSIS USING ELECTRO-DEPOSITED (Ni-Mo) COATINGS FROM LOW CONCENTRATION BATH

CHAPTER 6

ELECTROCHEMICAL WATER ELECTROLYSIS USING ELECTRO-DEPOSITED (Ni-Mo) COATINGS FROM LOW CONCENTRATION BATH

This chapter discusses the electro-catalytic activity of (Ni-Mo) alloy coatings deposited from the newly optimized bath towards alkaline water splitting applications in 1.0 M KOH. Electro-catalytic efficacy for hydrogen evolution reaction (HER) and oxygen evolution reaction (OER) were studied by cyclic voltammetry (CV) and chrono-potentiometry (CP) techniques. An inverse dependency of electro-catalytic activity of HER and OER of alloy coatings were found with their low and high deposition current densities, and it was attributed to their composition based redox activity. The surface features, structural and compositional change of alloy coatings, responsible for better electro-catalytic activity were examined using field emission scanning electron microscopy (FESEM), X-ray diffraction (XRD) and Energy dispersive X-ray spectroscopy (EDS) techniques.

6.1 INTRODUCTION

Here, an attempt has been made to evaluate the electro-catalytic performance of (Ni-Mo) alloy coatings deposited from optimized bath, proposed in Chapter 4. It is also intended to study the effect of reduced metal salt concentrations on the overall performance of alloy coatings. The electro-catalytic efficacy of (Ni-Mo) alloy coatings for both hydrogen evolution reaction (HER) and oxygen evolution reaction (OER) in alkaline water electrolysis were studied. The electro-catalytic kinetic parameters of alloy coatings were evaluated by means of cyclic voltammetry (CV) and chronopotentiometric (CP) study, and the experimental results are compared with those obtained from its high concentration bath, having same constituents. The experimental results are discussed in the line of information derived from different analytical techniques, such as FESEM, EDS, and XRD studies.

6.2 EXPERIMENTAL

A low concentration bath of (Ni-Mo) alloy has been formulated (Table 4.1), by dissolving small quantities of metal salts of Ni and Mo. *i.e.* only 7.0 g L^{-1} and 3.5 g L^{-1}, respectively. Small quantity of metal salts were deliberately taken to

understand the effect of (Ni) and molybdenum (Mo) content on the electrode kinetics of electrodeposited (Ni-Mo) alloy coatings. The current density range and operating variables required to develop (Ni-Mo) alloy coatings are described in Chapter 4. The compositional and topographical study of (Ni-Mo) alloy coatings were carried out by developing them on polished copper plates (3.0 cm^2), using an electrochemical cell, shown in Figure 3.4. To enable the electro-catalytic study of (Ni-Mo) alloy coatings, they are developed on the cross-sectional side of the copper rod (1.0 cm^2), using custom-made cell as shown in Figure 3.8. Further, electro-catalytic study of electrodeposited alloy coatings were carried out in a three-electrode custom-made electrolyser, shown in Figure 3.9. The electrolyzer is fitted with graduated burettes at both ends as shown in, for quantitative measurement of hydrogen (H_2) and oxygen (O_2) gases evolved during the electrolysis. The electrodeposition of all (Ni-Mo) alloy coatings were accomplished using DC power source (Keysight Technologies, Model: N6705C) for fixed length of time (600 s), in order to correlate the coating characteristics and their performances.

6.3 RESULTS AND DISCUSSION

6.3.1 Morphological and compositional analysis

Surface morphology is one of the key factors that determine the heterogeneous electro-catalytic ability of an electrode material. Generally, electrode kinetics greatly depends on the number of active sites on the surface, which favours the rate of evolution of H_2/O_2 gases (Elias et al. 2015). The morphological change of (Ni-Mo) alloy coatings with their deposition current density is shown by its FESEM images in Figure 4.1. It may be seen that the homogeneity of alloy coatings improved drastically with increase of plating current density. This change of surface homogeneity may be attributed to the suppression of formation of metal hydroxides at the electrical double layer (EDL) region, due to excessive diffusion of H^+ ions towards cathode (Brenner 1963). With the decrease of local pH, co-deposition of metal hydroxides, like $Ni(OH)_2$ is prevented, consequently a more uniform coating, without porous structures is formed. The improved homogeneity of (Ni-Mo) coatings with the growth of current density is due to increased diffusion of H^+ ions towards cathode. The composition data of (Ni-Mo) alloy coatings, corresponding to different current densities obtained from EDS study is recalled here, and is reported in Table 6.1. It clearly indicates that wt. % of Ni in the

deposit has increased only slightly with plating current density, as the characteristic feature of induced type co-deposition, followed in binary alloy coatings of metals from Fe-group and transition group.

Table 6.1- EDS composition data obtained for electrodeposited (Ni-Mo) alloy coatings developed at varied plating current densities, from the optimized bath

Plating current density (A dm^{-2})	Wt.% of Ni in the deposit	Wt. % of Mo in the deposit
1.0	68.1	31.9
2.0	69.1	30.9
3.0	70.8	29.2
4.0	71.2	28.8

From the composition data reported in Table 6.1, it is evident that the wt. % of nickel in the deposit is much higher (in the range of 70%), in relation to Mo content (approximately 30%). Generally, the electro-catalytic capacities of (Ni-Mo) coating for HER is more favoured at its lower Mo content, and is supported by current density findings of Hu and Weng (2000). Hence, it may be inferred that electro-catalytic efficacy of (Ni-Mo) alloy coating bears a close relation with its metal contents, governed by its deposition current density, and pH employed for its deposition.

6.3.2 XRD study

It is well known fact that apart from active sites available on the electrode surface, there are other factors which can contribute greatly to the electro-catalytic activity of electrode materials. Therefore, to understand the effect of phase structures on electro-catalytic performance of electrodeposited (Ni-Mo) coatings, the XRD patterns corresponding to different current densities, reported in Section 4.1.4 may be recalled. From the XRD peak analysis, it was found that all peaks correspond to the formation of single-phase homogeneous intermetallic compound, MoNi$_4$ irrespective of the current densities at which they are deposited. Based on density functional theory (DFT), it was proposed by Zhou et al. (2020) that in alkaline medium, MoNi$_4$ possess lowest energy barrier for activation (0.32 eV), which greatly facilitates water dissociation by

producing adsorbed hydrogen species, leading to better HER activity. This is in agreement with our findings, that electrodeposited (Ni-Mo) coatings from the proposed bath showed a better tendency for H_2 generation (approximately 10.5 cm^3), compared to O_2 production (approximately 6.5 cm^3), at all plating current density's.

6.3.3 Evaluation of electro-catalytic activity

Water electrolysis is considered to be the most promising technology for sustainable energy conversion, and production of high-purity hydrogen and oxygen for fuel cells and various industrial applications. In this regard, electrochemical water splitting technologies through alkaline water electrolysis generally consist of two coupled half reactions: the hydrogen evolution reaction (HER) and the oxygen evolution reaction (OER). Accordingly, electro-catalytic behaviours of metal/metal-based electrode materials can be assessed to their effectiveness, for water splitting applications (Sapountzi et al. 2017). In this respect, cyclic voltammetry (CV) and chrono-potentiometry (CP) techniques provide a better insight into their electrode kinetics, in terms of different electro-catalytic kinetic parameters. Hence, electrodeposited (Ni-Mo) alloy coatings from the proposed low concentration bath (Table 4.1), deposited at different current densities have been studied for their electro-catalytic efficacies of water splitting in 1.0 M KOH medium, using an electrolyzer (Figure 3.9). The experimental results of their electro-catalytic activity for HER and OER are reported here.

6.3.3.1 Electro-catalytic activity for HER

a) Cyclic voltammetry study

Cyclic voltammetry (CV) study is a very useful tool to understand the thermodynamics of redox processes, kinetics of heterogeneous electron-transfer reactions, and coupled chemical reactions involving the adsorption process (Shetty et al. 2017). The cyclic voltammograms for HER performance of (Ni-Mo) coatings, electrodeposited at varied current densities were recorded (between 0.0 V and -1.6 V at a scan rate of 0.05 V s^{-1}) and is shown in Figure 6.1.
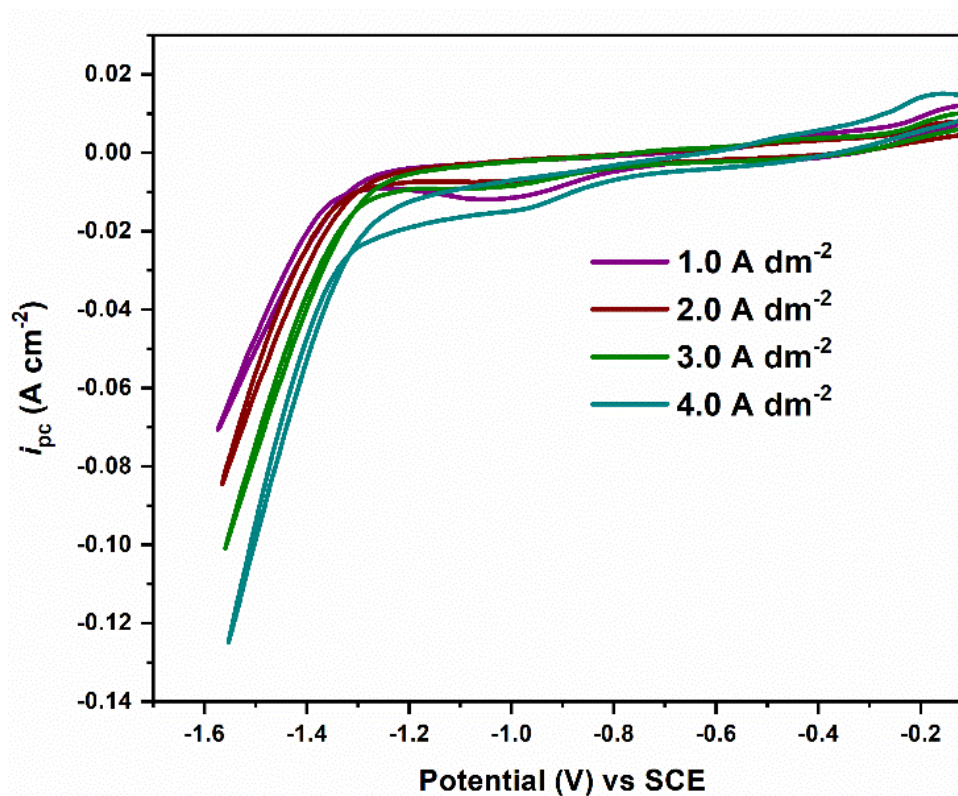
Figure 6.1- *Cyclic voltammograms of (Ni-Mo) alloy coatings developed at varied current densities, showing a constant increase of i_{pc} value with deposition current density*

In an electrochemical redox reaction, cathode peak current density (i_{pc}) is an index of its tendency to undergo reduction reaction. Hence, the observed different i_{pc} values corresponding to (Ni-Mo) alloy coatings of different current densities are a measure of their capability to bring about the HER on their surface. Hence, from both composition data (Table 6.1) and nature of CV curves, it may be inferred that electro-catalytic efficiency of (Ni-Mo) alloy coatings increased with deposition current density, and hence their Ni content, and it is maximum at 4.0 A dm^{-2}. Thus, it may be summarized that (Ni-Mo) alloy coating deposited at 4.0 A dm^{-2} is best electrode material for HER with highest i_{pc} value (-0.124 A cm^{-2}) and least onset potential (-1.18 V), compared to all other coatings. The electro-catalytic kinetic parameters for HER, corresponding to different plating current density is given in Table 6.2. Further, it may be seen that the onset potential for HER of (Ni-Mo) alloy coatings has decreased with increase in their Ni content.

Table 6.2- Electro-catalytic kinetic parameters for HER activity of (Ni-Mo) coatings electrodeposited at varied current densities from optimized bath

Plating current density (A dm^{-2})	Cathodic peak current density i_{pc} (A cm^{-2})	Onset potential for HER (V) vs SCE	Volume of H$_2$ evolved for 300 s (cm^3)
1.0	0.070	-1.25	9.4
2.0	0.082	-1.23	10.0
3.0	0.100	-1.20	10.7
4.0	0.124	-1.18	11.5

This improved electro-catalytic behaviour of (Ni-Mo) alloy coatings may be attributed to the synergetic effect of Mo (transition group metal) and Ni (Fe-group metal) as reported by Herraiz-Cardona et al. (2011). It has been mentioned that improved electro-catalytic efficacy for HER is reasoned by two factors. One is due to increase of noble metal (Ni) content in the deposit, and other one is due to the fact that in alkaline medium (KOH) being more corrosive for reluctant Mo, their phases were easily leached out from the metal matrix of the alloy coatings. As a result, more number of active sites of Ni (electro-catalytically active metal) has formed on the electrode surface (Kutyła et al. 2019).

b) Chronopotentiometry study

Chronopotentiometry (CP) technique is another useful approach to assess the electrochemical stability and activity of electrode materials. The quantitative measurement of H$_2$ gas liberated during water reduction is the direct means of evaluating the catalytic response of alloy coatings. Accordingly, the CP study of electrodeposited (Ni-Mo) coatings for HER were studied by applying a constant current of -0.3 A for a period of 1800 s. The volume of H$_2$ generated was recorded for the first 300 s and is given in Table 6.2. The chronopotentiograms of (Ni-Mo) coatings, referring to different current densities are shown in Figure 6.2. The volume of H$_2$ evolved during electrolysis is shown as bar charts, in the inset.
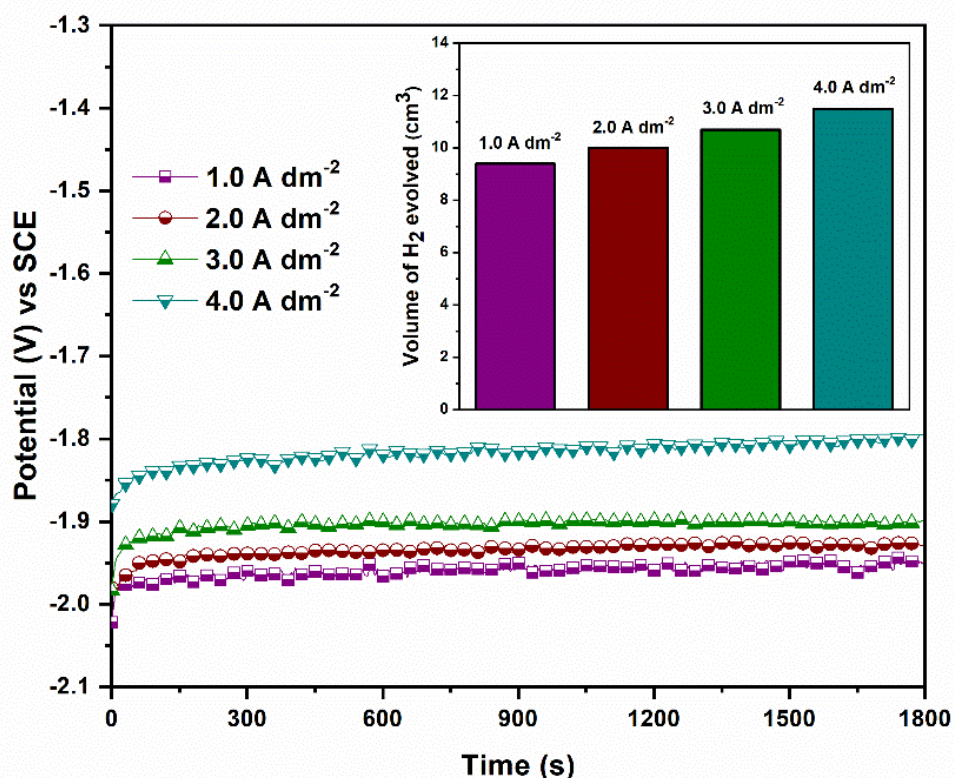
Figure 6.2- *Chronopotentiograms of (Ni-Mo) coatings developed at varied plating current densities, and the volume of H_2 gas evolved is shown as bar charts (in the inset)*

In CP study, when the current is passed between the counter electrode (CE) and test electrode (TE), the potential change is very rapid, as charge builds up at the electrode-electrolyte (E-E) interface. This proceeds until a steady-state potential is attained at which the electrolysis on electrode surface commences (Herraiz-Cardona et al. 2011). Almost same trend was observed in all (Ni-Mo) alloy coatings as shown in Figure 6.2. The horizontal part of each chrono-potentiograms (Figure 6.2) indicates that at particular constant potential, a steady state equilibrium is established between the H^+ ions and H_2 gas liberating on the electrode during water splitting (Ullal and Hegde 2014). Thus from potential vs. time response of the (Ni-Mo) electrode materials, it can be deduced that (Ni-Mo) coatings corresponding to 4.0 A dm^{-2} attained the state of equilibrium for HER at much lower negative potential than other coatings. In other words, this particular (Ni-Mo) alloy coating is electro-catalytically more active for HER, than other coatings.

The experiment was repeated for 20 cycles to obtain stable voltammograms. The current density at which a stable state equilibrium for H_2 evolution is reached, and is termed as cathodic peak current density (i_{pc}). This corresponds to a state of equilibrium between the rate of adsorption and desorption of hydrogen on the surface of cathode. Thus, i_{pc} and onset potential values of (Ni-Mo) coatings corresponding to different current densities were determined as a measure of their electro-catalytic efficacy for HER, through their CV curves, shown in Figure 6.1.

6.3.3.2 Electro-catalytic activity for OER

a) Cyclic voltammetry study

During water splitting, the hydrogen evolution reaction (HER) takes place at cathode, and the oxygen evolution reaction (OER) takes place at anode (Khan et al. 2018). Accordingly, (Ni-Mo) alloy coatings deposited at varied plating current densities was made as anode, and tested for their capability to bring about OER on their surface in the same KOH medium. Same experimental procedure, as discussed in the previous section was used for OER study. CV studies were conducted in a potential ramp of 0.0 V to 0.75 V at a scan rate of 0.05 V s^{-1} (same scan rate was used as in HER study). The CV response recorded for OER on the surface of different (Ni-Mo) coatings is given in Figure 6.3.
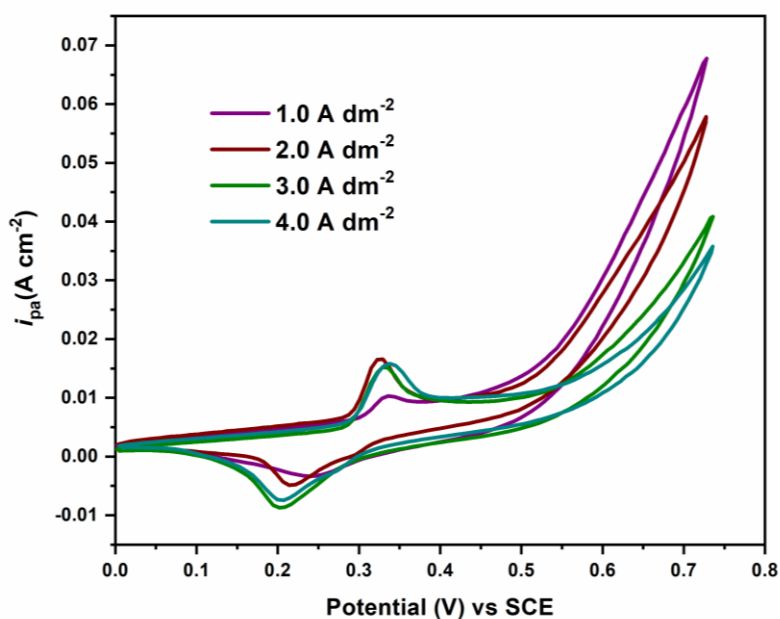
Figure 6.3- *CV response of (Ni-Mo) coatings developed at varied current densities showing a steady increase of i$_{pa}$ with deposition current density*

Accordingly, values of anodic peak current density (i_{pa}), and onset potentials for OER of all (Ni-Mo) coatings are listed in Table 6.3. From the nature of CV curves, one can figure out that (Ni-Mo) alloy corresponding to 1.0 Adm^{-2} shows its highest efficacy for OER compared to all other coatings. The value of kinetic data reveals that (Ni-Mo) coatings electrodeposited at 1.0 A dm^{-2} exhibited the maximum i_{pa} value, with the least onset potential (0.59 V). The value of these kinetic parameters clearly indicates that (Ni-Mo) coating developed at 1.0 A dm^{-2} is the most suitable electrode material for good OER activity.

Table 6.3- Electro-catalytic kinetic parameters for OER on (Ni-Mo) coatings developed at different current densities

Plating current density (A dm^{-2})	Anodic peak current density i_{pa} (A cm^{-2})	Onset potential for OER (V) vs SCE	Volume of O_2 evolved for 300 s (cm^3)
1.0	0.067	0.50	6.8
2.0	0.057	0.53	6.6
3.0	0.040	0.57	6.2
4.0	0.035	0.59	6.0

b) Chronopotentiometry study

Figure 6.4 shows the chronopotentiograms obtained for OER performance of different (Ni-Mo) coatings. For OER assessment, a current pulse of +0.3 A was applied for a fixed period of 1800 s and the volume of O_2 gas evolved was noted, as done for HER study. A stable chronopotentiogram was obtained after a definite time, and it was corresponding to the state of equilibrium associated with newly forming O_2 bubbles, and bubbles escaping from the surface coatings (Kim et al. 2012). From chronopotentiogram response of (Ni-Mo) coatings (Figure 6.4), one can figure out that coating at 1.0 A dm^{-2}, having high wt.% of Mo is more active towards OER, compared to the coatings at higher current densities. This high electro-catalytic behavior of (Ni-Mo) coating having high wt.% of Mo towards OER is attributed to the oxophilic nature of Mo (Hasan et al. 2019).
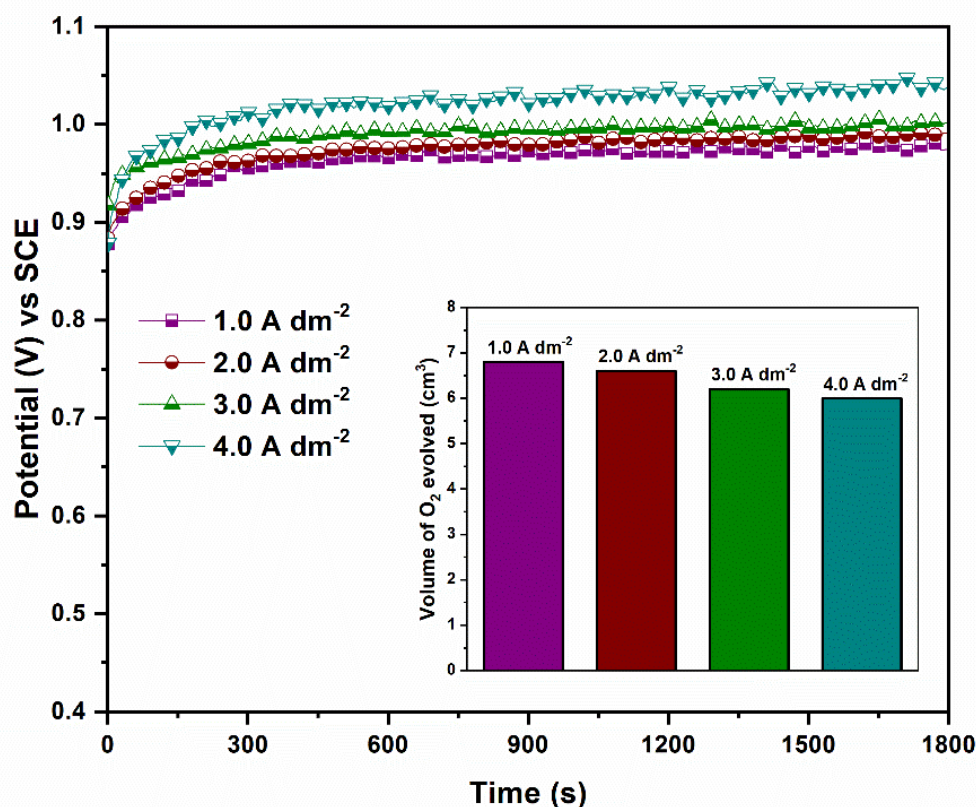
Figure 6.4- *Chronopotentiograms of different electrodeposited (Ni-Mo) coatings, with the volume of O₂ evolved shown by bar chart in the inset*

Higher wt.% Mo is found to be responsible for the formation of MoO_4^{2-} making it more favorable for OER than $Ni(OH)_2$ and NiOOH (Platatorres et al. 2007). It may be noted that the change of volume of O_2 gas produced is negligible when the plating current density is changed, as may be seen in Figure 6.4. This could be due to the oxophilic nature of Mo, where Mo is believed to undergo electrochemical dissolution in alkaline medium (Lützenkirchen-Hecht and Frahm 2001). This electrochemical leaching of Mo reduces the electrochemical stability of (Ni-Mo) coatings, having more wt.% of Mo in their alloy matrix. Thus from the electro-catalytic study of (Ni-Mo) coatings for water electrolysis of both HER and OER, it may be inferred that electrodeposited (Ni-Mo) coatings show a strong dependency on the plating current density for HER performance compared to OER. The compositional and morphological features of alloy coatings favoring the HER has an opposite effect on the OER, and vice versa, depending on the current density at which they are deposited.

106

6.3.4 Inverse dependency of electro-catalytic efficacy of HER and OER with composition

The electro-catalytic activity of (Ni-Mo) alloy coatings for both HER and OER, deposited at different current densities are summarized in Tables 6.2 and 6.3. From the data, it may be noted that as the deposition current density is increased (or as Ni content of the deposit increased), the electro-catalytic efficacy of (Ni-Mo) alloy coatings for HER (cathodic process) increased; whereas for OER (anodic process), it decreased. This inverse dependency of electro-catalytic efficacy of HER and OER with Ni content of alloy coatings may be accredited to the redox behavior of alloy coatings, having different composition. It may be explained in terms of the tendency of the electrons to transmit between working electrodes (test electrodes) and counter electrode.
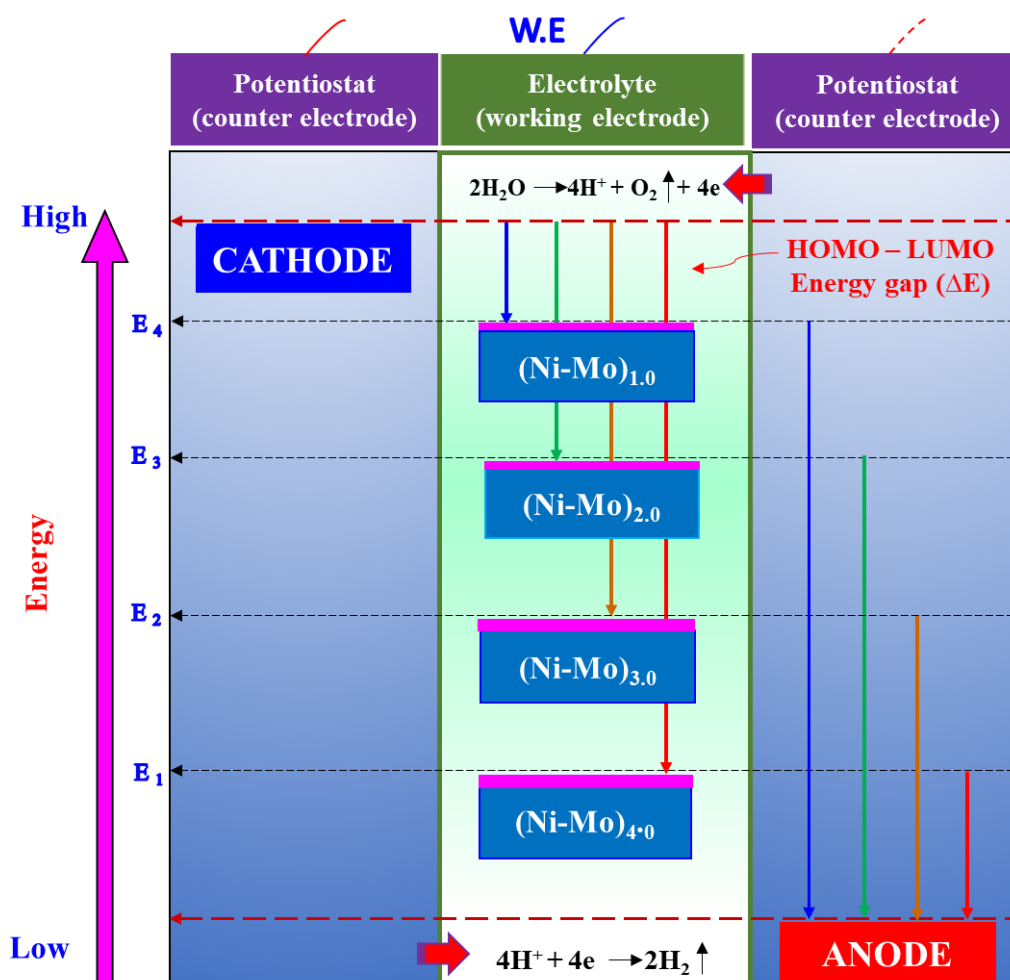
Figure 6.5- Representational diagram showing inverse dependency of (Ni-Mo) alloy coating, deposited at different current densities for HER and OER in alkaline water electrolysis

It is to recall here that in the electrochemical study, working electrode is an electrical conductor, and by means of an external power source (potentiostat), voltage can be applied to it to modulate the energy of the electrons in the electrode. Hence, the driving force of a particular reaction can be controlled, and the ease with which thermodynamic and kinetic parameters can be measured (Elgrishi et al. 2018). In the backdrop of the above principle, a conceptual diagram showing the efficacy of (Ni-Mo) alloy coatings, having different Ni content towards HER and OER during alkaline water electrolysis is given in Figure 6.5.

It may be noted that during alkaline water electrolysis, H_2 and O_2 gases are liberated on working electrode (Ni-Mo) alloy coatings having different compositions, when relatively negative and positive potentials are applied, respectively through the potentiostat. When electrons in the (Ni-Mo) alloy coatings are at higher energy than the Lowest Unoccupied Molecular Orbital (LUMO) of the electrolyte constituent (H^+), electron from the electrode is transferred to electrolyte constituent to release H_2. Similarly, when electrons in the (Ni-Mo) alloy coating is at lower energy than the Highest Occupied Molecular Orbital (HOMO) of electrolyte constituent (OH^-), electron from the electrolyte constituent is transferred to electrode to release O_2. Thus, depending on the Ni content of the alloy (depending on the deposition current density), Ni-Mo alloy coatings can assume different electrode potential values (E_1, E_2, E_3 and E_4) along the energy axis (depending on the Ni content), as shown in Figure 6.5, and hence different energy gap (ΔE) between HOMO-LUMO. Therefore, transferring of electrons takes place from HOMO to LUMO to favor either HER or OER, depending on its composition. If the efficacy of (Ni-Mo) alloy coating, deposited at a particular current density, say at 1.0 A dm^{-2} (having the least Ni content) is less favourable for HER (due to low energy gap ΔE), and more favourable for OER (due to large energy gap ΔE), as shown in Figure 6.5. But (Ni-Mo) alloy coating, deposited at 4.0 A dm^{-2} (having highest Ni content) is less favourable for OER (and more favourable for HER), as may be seen in Figure 6.5. Thus, it may be summarized that a mutually opposite electro-catalytic activity of (Ni-Mo) alloy coatings towards HER and OER, which changes with deposition current density is attributed to the change in composition of the alloy, in terms of their Ni and Mo content. In other words, the driving force of electrochemical reaction of water splitting of both HER and OER of (Ni-Mo) alloy coating is a function

of energy difference between working electrode and counter electrode, and show mutually opposite trends.

6.3.5 Dependency of electro-catalytic behaviour on concentration of baths

The electro-catalytic capability of (Ni-Mo) alloy coatings electrodeposited from the present bath is compared with that of already reported high concentration bath, by Shetty et al. (2017). The experimental results revealed that concentrations of metal salts hardly affect the electro-catalytic performances of alloy coatings. It was found that even when salts' concentrations are reduced by several folds (7.0 g L^{-1} $NiCl_2$ against 18.0 g L^{-1} $NiSO_4$, 3.5 g L^{-1} $Na_2MoO_4.2H_2O$ against 48.0 g L^{-1} and 20.0 g L^{-1} $Na_3C_6H_5O_7. 2H_2O$ against 105 g L^{-1}), electro-catalytic performances remained almost the same. It is evident from the volumes of H_2 and O_2 evolved under identical conditions, shown in Table 6.4. Moreover, no significant change in Ni and Mo content of the alloy coatings was found with the change of bath's plating current densities, and bath concentrations as shown in Table 6.4.

Table 6.4- Comparison of composition and efficacy for HER and OER of (Ni-Mo) coatings electrodeposited from the proposed bath in relation to the reported bath[*]

Plating c. d. (A dm^{-2})	wt.% of Ni		wt.% of Mo		Volume of H_2 evolved (cm^3)		Volume of O_2 evolved (cm^3)	
	P	R	P	R	P	R	P	R
1.0	68.1	61.7	31.9	38.3	9.4	12.0	6.8	8.1
2.0	69.1	64.3	30.9	35.7	10.0	11.5	6.6	8.7
3.0	70.8	65.6	29.2	34.4	10.7	10.8	6.2	9.5
4.0	71.2	66.8	28.8	33.2	11.5	10.2	6.0	10.3

*P - Present work and R - Reported work (Shetty et al. 2017)

Hence, it can be inferred that electro-catalytic efficacy of (Ni-Mo) alloy coatings for HER and OER has a direct relation with only the composition of alloy, rather than concentration of the bath. Thus, it may be concluded that electro-catalytic property of alloy coatings following induced type of co-deposition cannot be increased just by increasing metal content in the bath.

6.4 CONCLUSIONS

Based on the experimental study on electro-catalytic characterization of (Ni-Mo) alloy coatings from a low concentration bath, following conclusions are drawn:

1. Electrodeposited (Ni-Mo) coatings were found to exhibit good electro-catalytic response, on par with those developed from its high concentration bath.

2. The experimental results demonstrated that (Ni-Mo) coatings, developed at 1.0 A dm^{-2} and 4.0 A dm^{-2} are good electrode materials for OER and HER, respectively, confirmed by CV and CP techniques.

3. The ED (Ni-Mo) coatings, favoring cathodic HER has an opposite effect on the anodic OER, and vice-versa, due to strong dependency of electro-catalytic properties on their compositions.

4. The high electro-catalytic activity for HER of (Ni-Mo) coatings deposited at high plating current density, compared to OER may be attributed to the change of their composition and surface features, evidenced by FESEM, EDS and XRD studies.

5. The formation of MoNi$_4$ phase structure is more favourable to HER activity of the electrode than OER, evidenced by XRD peak analysis.

6. Mutually opposite electro-catalytic activity of (Ni-Mo) alloy coatings towards HER and OER with deposition current density is attributed to the difference in the energy gap between HOMO - LUMO states of electrode materials, depending on their composition, in terms of their Ni and Mo content.

7. Less dependency of electro-catalytic response of (Ni-Mo) alloy coatings with concentration of the electrolyte used is due to the inherent induced type of co-deposition, where the change of alloy composition with plating variables are very small.

CHAPTER 7

DEVELOPMENT OF POLYOXOMETALATE (POM) BASED (Ni-Mo) ALLOY COATINGS AS BIFUNCTIONAL ELECTRODE MATERIAL FOR WATER SPLITTING APPLICATIONS

CHAPTER 7

DEVELOPMENT OF POLYOXOMETALATE (POM) BASED (Ni-Mo) ALLOY COATINGS AS BIFUNCTIONAL ELECTRODE MATERIAL FOR WATER SPLITTING APPLICATIONS

This chapter presents the experimental results of investigation on the effect of addition of redox-active polyoxometalates (POM) into the optimized (Ni-Mo) bath. A drastic improvement in the electro-catalytic efficacy of POM-modified (Ni-Mo) alloy coatings was found for both HER and OER of alkaline water electrolysis. The limitation of conventional (Ni-Mo) alloy electro catalyst, i.e., showing good electro-catalytic performance for either HER or OER, but not for both is alleviated by adding a known quantity of POM into the bath. Improved electro-catalytic activities were attributed to the increased surface roughness, porosity and reactive site due to the incorporation of POM into the (Ni-Mo) lattice structure supported by FESEM, EDS, AFM and XPS studies.

7.1 INTRODUCTION

The electro-catalytic study of (Ni-Mo) alloy detailed in Chapter 6 revealed that (Ni-Mo) coatings exhibiting highest HER activity is least active for OER, and vice versa (depending on the current density and, hence the composition). Due to this limitation, they need to be used either as cathode for HER, or an anode for OER (depending on the requirement), but not as both. In this connection, the present study is focussed on improvement of both HER and OER activity by the inclusion of highly redox-active polyoxometalates into the (Ni-Mo) alloy matrix, *via* simple electrodeposition technique.

Polyoxometalates (POMs for convenience) are a new class of compounds that are a combination of oxygen and early transition metals (e.g., M = V, Nb, Ta, Mo, W), at their highest oxidation states. They may also contain a variety of heteroatoms (e.g., X = P, As, Si, Ge) (Ammam 2013). POMs are remarkable in several respects, including the multitude of their properties based on their sizes, shapes, charge densities, and reversible redox potentials, or their enormous diversity in structures. Due to this, POM-based solid-state materials fascinate synthetic chemists and thus have been explored in recent years as a promising precursor in the field of energy applications

(Fernandes et al. 2018, Liu et al. 2017, Ullah et al. 2021, Vannathan et al. 2020). Besides, POM's readily deposit on the electrode surface via 'self-assembly' process (Liu et al. 2017) and show high tolerance towards their contact environment, without itself undergoing any structural degradation, thereby making them efficient 'mediators' for catalysis (Gao et al. 2019, Ullah et al. 2021, Zhang et al. 2009), energy storage devices (Li et al. 2018, Vannathan et al. 2020) and as anti-corrosive agents (Al-Dawsari 2019, Katsoulis 1998). Consequently, POMs are considered as ideal candidates for designing electrocatalysts by tuning their chemical properties by choosing proper constituting elements as they have an ability to undergo reversible multivalence reductions/oxidations, leading to the formation of mixed-valence species, which brings about favourable electro-catalytic properties with regard to several electrochemical processes (Keita and Nadjo 2007). However, till date, there are only few reports on polyoxometalate-based materials used in alkaline water splitting reactions (Luo et al. 2017, Zhang et al. 2019). In this direction, the most versatile and fascinating redox behaviour of POMs was tried to explore to enhance the electro-catalytic efficacy of (Ni-Mo) alloy coatings by the addition of POM in varied concentrations into the optimized (Ni-Mo) citrate-ammoniacal bath. The effect of addition of POM on both HER and OER properties were analyzed in relation to the bare-(Ni-Mo) deposit, electrodeposited from the same bath. POM doped (Ni-Mo) deposits are conveniently represented in this study as [POM(Ni-Mo)]. The experimental results of [POM(Ni-Mo)] alloy coatings were compared with that of bare-(Ni-Mo) alloy and the results are discussed.

7.2 EXPERIMENTAL

7.2.1 Electrodeposition of [POM (Ni-Mo)] alloy coatings

The POM-based (Ni-Mo) bath was prepared by adding a known quantity of POM into the optimized low concentration (Ni-Mo) bath (Table 4.1). In the present study Keggin type 11-molybdo-1-vanadophosphoric acid ($H_4[PVMo_{11}O_{40}].32H_2O$) was used, as the source of POM. It was prepared following the procedure as reported by Akba et al. (1997). The crystals of POM were dissolved in the bath first, and then the solution was homogenized by stirring overnight using a magnetic stirrer. It is filtered and dried, and then used as electrolyte for electrodeposition. The representational set-up used for the preparation of POM(Ni-Mo) bath is shown in Figure 7.1 (a).

For compositional and morphological characterization, [POM(Ni-Mo)] alloy coatings deposition was carried on polished copper plates (having 3.0 cm^2 active surface area); and for electro-catalytic study, they are deposited on the polished copper tip having 1.0 cm^2 cross-sectional surface area, shown schematically in Figure 7.1 (b). Similar to bare (Ni-Mo) coatings, [POM(Ni-Mo)] alloy coatings were electrodeposited under constant agitation using DC power source (Keysight Technologies, Model N6705C) for 600 s, using graphite bar of same exposed area, as anode. To see the effect of composition-activity relationships of [POM(Ni-Mo)] alloy coatings, POMs are added in two concentrations. *i.e.,* 1.0 g L^{-1} and 2.0 g L^{-1}. Further addition of POM content into the bath, *i.e.* 3.0 g L^{-1} ended up with adverse effect on the nature of electrodeposit. The (Ni-Mo) alloy coatings corresponding to 1.0 g L^{-1} and 2.0 g L^{-1}, are represented conveniently as [POM(Ni-Mo)]$_{1.0}$ and [POM(Ni-Mo)]$_{2.0}$, respectively.
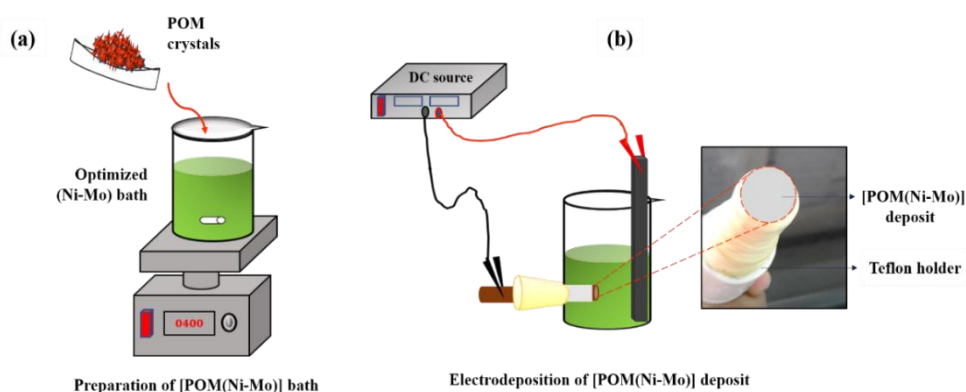
Figure 7.1- *Representational set-up used for: a) preparation of POM-based (Ni-Mo) bath, and b) used for electrodeposition of [POM(Ni-Mo)] deposits onto the tip of copper rod for electro-catalytic study*

7.2.2 Electro-catalytic performance study

POM doped (Ni-Mo) coatings, abbreviated as [POM(Ni-Mo)] were electrodeposited galvanostatically on copper substrate, using optimized low concentration (Ni-Mo) bath (Table 4.1). Accordingly, [POM(Ni-Mo)]$_{1.0}$ and [POM(Ni-Mo)]$_{2.0}$ coatings were deposited by selecting optimal current density of 4.0 A dm^{-2}. The electrodeposited coatings were rinsed with double distilled water, air-dried, and then subjected to electro-catalytic study using the custom-made electrolyzer, in Figure 3.8. The electro-catalytic studies of POM (Ni-Mo) coatings were carried out in the same line as that for

bare-(Ni-Mo) alloy coatings using a VersaSTAT-3 Potentiostat/Galvanostat (Princeton Applied Research, USA).

7.3 RESULTS AND DISCUSSION

7.3.1 Material characterization

7.3.1.1 FESEM-EDS study

It is desirable that stable and efficient electrocatalysts need to possess abundant active sites for the adsorption and desorption process, alongside the excellent electrical conductivity for fast transfer of electrons, and a robust nanostructure (Zhang et al. 2019). In this regard, to understand the change of topographical features of electrodeposited POM-based alloy coatings, they were examined under Field Emission Scanning Electron Microscope (FESEM). The FESEM micrographs of different coatings and their Energy Dispersion X-ray Spectrum (EDS) are shown in Figure 7.2.
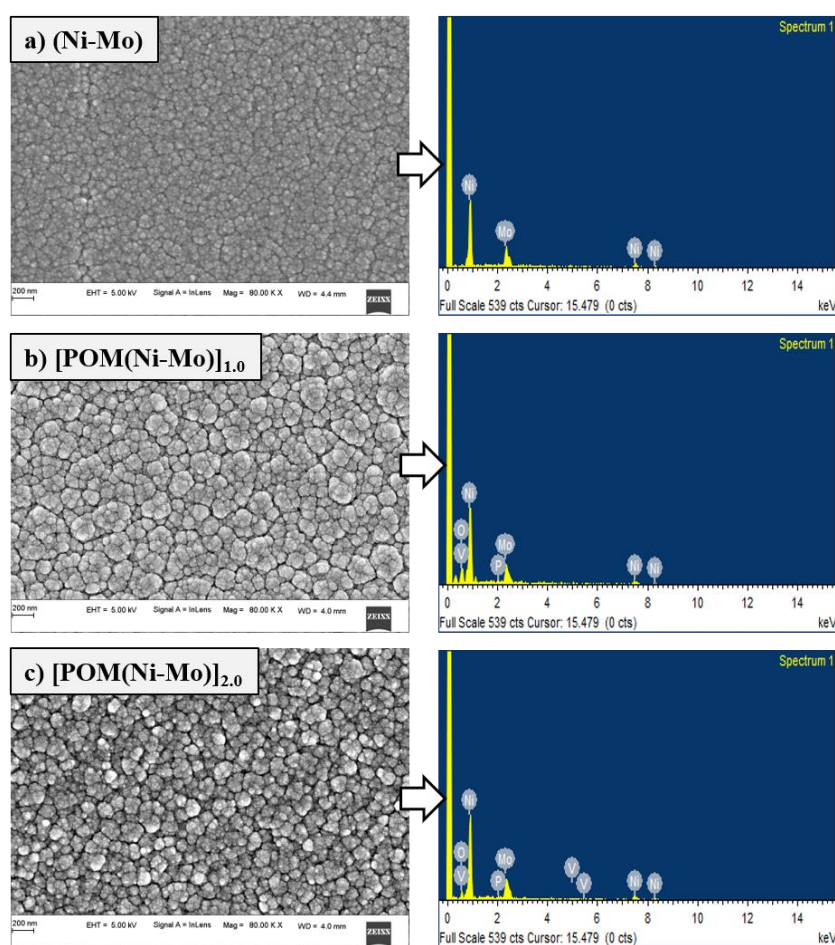
Figure 7.2 - FESEM microstructure of different alloy coatings: a) (Ni-Mo), b) [POM(Ni-Mo)]$_{1.0}$, and c) [POM(Ni-Mo)]$_{2.0}$, and their EDS signals on the right showing the incorporation of V, O and P

116

From the FESEM image, it may be noted that the surface homogeneity of (Ni-Mo) alloy coating has changed drastically due to addition of POM. A significant change in the surface roughness was found in [POM(Ni-Mo)]$_{1.0}$ and [POM(Ni-Mo)]$_{2.0}$ coatings (Figure 7.2(b) and 7.2(c)), compared to (Ni-Mo) alloy coating (Figure 7.2(a)). Further, it may be noted that the size of granules responsible for surface roughness has decreased with increase of POM content, leading to the formation of coarse granular microstructures, and is evident from the micrograph of [POM(Ni-Mo)]$_{1.0}$ and [POM(Ni-Mo)]$_{2.0}$. This change may be due to the fact that when POM is administered into the alloy matrix, it enhanced the stage of nucleation process and thereby altered the kinetics of electrodeposition. Thus, it may be summarized that addition of POM increased drastically the surface roughness of the alloy coating, required for an efficient electrocatalyst. EDS analysis of the electrodeposited specimens was done at various regions, presenting the effective atomic concentration of different metals, and oxygen species on top surface layers. EDS data, reported in Table 7.1 reveals the presence of Ni, Mo, V, P, and oxygen in the POM-doped alloy coating. It may also be noted that addition of POM resulted in decrease of both Ni and Mo content of the deposit alloy, and extent of decreasing is increased with POM content. This supports that added POM, responsible for improved electro-catalytic activity is doped into the alloy matrix.

Table 7.1- Composition data of [POM(Ni-Mo)]$_{1.0}$ and [POM(Ni-Mo)]$_{2.0}$ alloy coatings, in relation to (Ni-Mo) alloy deposited from optimized bath at 4.0 A dm^{-2}

Coating configuration	Wt. % Ni	Wt.% Mo	Wt.% P	Wt.% V	Wt.% O
(Ni-Mo)	71.20	28.80	-	-	-
[POM(Ni-Mo)]$_{1.0}$	68.75	20.18	0.07	0.95	10.05
[POM(Ni-Mo)]$_{2.0}$	58.60	17.59	0.12	1.83	21.86

7.3.1.2 XRD study

Crystallographic characterization of electrodeposited POM-based alloy coatings were undertaken using XRD techniques. Figure 7.3 shows the XRD patterns of (Ni-Mo), [POM(Ni-Mo)]$_{1.0}$ and [POM(Ni-Mo)]$_{2.0}$ alloy coatings. The XRD pattern of POM,

$H_4[PVMo_{11}O_{40}].32H_2O$ (Reference JCPDS Card No.: 00-045-0611) (Vannathan et al. 2020), used in the present study is given in inset of Figure 7.3.
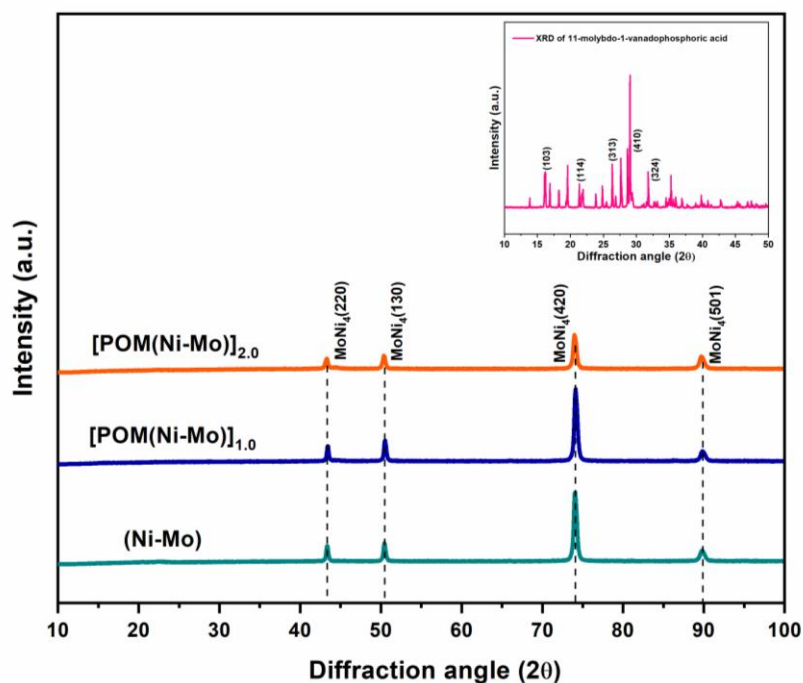
Figure 7.3- *Comparison of XRD signals obtained for (Ni-Mo), [POM(Ni-Mo)]$_{1.0}$, and [POM(Ni-Mo)]$_{2.0}$ alloy coatings with reference XRD pattern of pure POM (inset)*

As may be seen in Figure 7.3, all XRD signals predominantly showed the diffraction peaks around 43.2°, 50.6°, 74.08° and 89.8° corresponding to tetragonal $MoNi_4$(220), $MoNi_4$(130), $MoNi_4$(420) and $MoNi_4$(501) planes, respectively [JCPDS Card no.: 03-065-1533], depicting the formation of single-phase solid solution of Mo in Ni with no/slight change in scattering angle(2θ). However, there were no apparent peaks corresponding to POM reflected in the XRD pattern of either [POM(Ni-Mo)]$_{1.0}$ or [POM(Ni-Mo)]$_{2.0}$ alloy coatings, shown in Figure 7.3. This could be due to lower reflection peaks of pure POM (as shown in the inset). The observed diminution of peak intensity with increase of POM content may be linked to decrease of Ni (from 71.2 % to 58.6 %) and Mo content (from 28.80 % to 17.59 %), respectively due to addition of POM (Table 7.1). Further, the average crystallite size, calculated using Scherrer formula (Cullity 1978) was found to increase from 24 nm to 31 nm, for POM-based alloy coatings, indicating their structure change due to incorporation of POM.

7.3.1.3 XPS study

In induced type of co-deposition of (Ni-Mo) alloy, the individual metal content in the deposit is quite vagarious and unpredictable (Brenner 1963); and discharge of Ni (II) and Mo(VI) complex ions and hydrogen evolution occur on the cathode at the same time (Shetty et al. 2018). In this direction, surface-sensitive technique, like X-ray photoelectron spectroscopy (XPS) analysis of electrodeposited alloy coatings was carried out to investigate the chemical states of the elements, and are shown in Figures 7.4 and 7.5. Figure 7.4 displays the wide scan XPS spectra of (Ni-Mo) and [POM(Ni-Mo)]$_{2.0}$ alloy coatings, and survey spectrum of (Ni-Mo) alloy coating is shown in Figure 7.5 (a). The deconvoluted elemental peaks corresponding to different binding energies are confirming the presence of Ni, Mo, C and O in the deposit (Ni 2p, Mo 3d, C 1s and O 1s). The presence of C 1s peak may be due to carbon surface contamination and trace solvent residue (Gao et al. 2017), and O 1s peak is possibly due to molybdenum oxide which may co-exist in the deposit (Chassaing et al. 2004). XPS survey spectra of [POM(Ni-Mo)]$_{2.0}$ alloy deposit shown in Figure 7.5 (b) clearly show the presence of V, P and O in the deposit (V 2p, P 2p and O 1s alongside Ni 2p, Mo 3d and C 1s). Thus, XPS study endorses the incorporation of POM into the alloy matrix of (Ni-Mo), affected due to electro-codeposition.
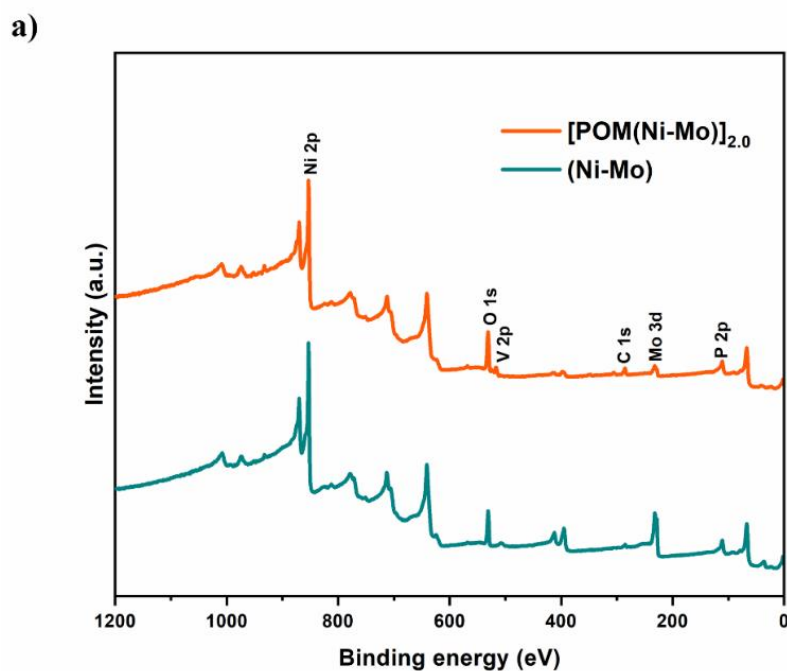
Figure 7.4- *XPS wide scan spectra of (Ni-Mo) and [POM(Ni-Mo)]$_{2.0}$ alloy coatings*
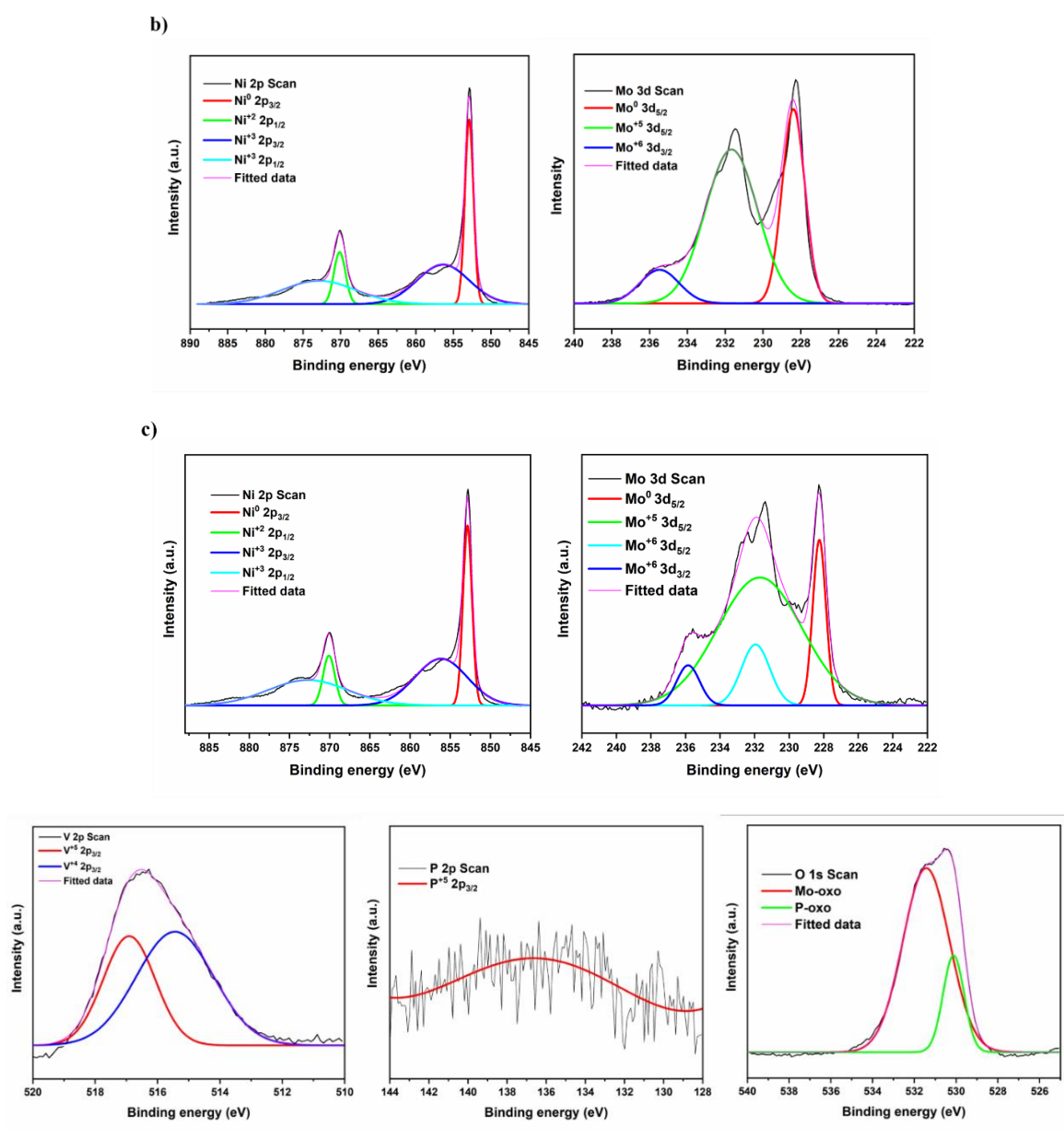
Figure 7.5- *a) Deconvoluted XPS survey spectra of Ni 2p and Mo 3d elemental peaks in (Ni-Mo) coatings, and b) Deconvoluted XPS survey spectra of [POM(Ni-Mo)]₂.₀ alloy coating showing elemental peaks corresponding to Ni 2p, Mo 3d, V 2p, P 2p, and O 1s*

High resolution XPS spectra presented in Figure 7.5 (a) and (b), show respective deconvoluted elemental photopeaks obtained for (Ni-Mo) and [POM(Ni-Mo)]$_{2.0}$ alloy coatings. In Figure 7.5 (a), the deconvoluted Ni 2p spectra show the binding energies (E_B) for Ni^0 2p$_{3/2}$, E_B=852.9 eV), Ni^{+3} 2p$_{3/2}$ (E_B =856.7), Ni^{+2} 2p$_{1/2}$ (E_B =869.9) and Ni^{+3} 2p$_{1/2}$ (E_B=873.5 eV). Similarly for Mo, deconvoluted 3d peaks corresponding to Mo^0 3d$_{5/2}$, E_B =228.3 eV), Mo^{+6} 3d$_{3/2}$ (E_B =235.5 eV) and Mo^{+5} 3d$_{5/2}$ (E_B =231.8 eV) are

120

observed (Abhilash et al. 2022, Shetty et al. 2018). The presence of metallic Ni and Mo peaks in the spectra confirms the presence of basic metals of (Ni-Mo) alloy coating. In Figure 5.4(c), Ni 2p scan show deconvoluted Ni^0 $2p_{3/2}$ (E_B =852.8 eV), Ni^{+3} $2p_{3/2}$ (E_B =856.1 eV), Ni^{+2} $2p_{1/2}$ (E_B =870.2 eV) and Ni^{+3} $2p_{1/2}$ (E_B =873.7 eV) peaks (similar to that of bare (Ni-Mo) alloy coating) and for Mo, 3d peaks corresponding to Mo^{+6} $3d_{5/2}$ (E_B =232.1 eV) , Mo^{+6} $3d_{3/2}$ (E_B=235.9 eV) and Mo^{+5} $3d_{5/2}$ (E_B=231.7 eV) , in addition to metallic Mo^0 $3d_{5/2}$ (E_B=228.3 eV), are observed. These Mo^{+6} ion peaks are found to be from the Keggin Mo species linked to P. Similarly, deconvoluted V 2p peaks correspond to V^{+5} $2p_{3/2}$ (E_B =517 eV) and V^{+4} $2p_{3/2}$ (E_B =515.8 eV) photopeaks, relatable to the vanadium present in the Keggin POM. Further, a P^{+5} $2p_{3/2}$ peak around 135eV shows the presence of Keggin PO_4 and deconvoluted O 1s shows the presence of two photopeaks with binding energies 531.4 eV and 530.1 eV which could be attributed to the oxygen atoms of Keggin anion bonded to Mo and P, respectively when both are present in the same compound (Maity et al. 2021, Jing et al. 2015; Wang et al. 2009). Thus detailed XPS study confirms the inclusion of POM, responsible for improved redox activity in the electrodeposited (Ni-Mo) alloy matrix.

7.3.1.4 AFM study

AFM is a powerful technique used for taking the topographical image of any surface. In this technique a sharp probe is made to scan mechanically across the surface, and the motion of probe is captured with a computer. The probe's motion is then used to create a three-dimensional image of the surface. Accordingly, AFM image of bare-(Ni-Mo) and [POM(Ni-Mo)]$_{2.0}$ alloy coatings, taken in (10µm × 10µm) area is shown in Figure 7.6. The surface roughness parameters, such as average roughness (R_a) and root mean square roughness (R_q) values obtained are tabulated in Table 7.2.

Table 7.2 - The surface roughness data of (Ni-Mo), [POM(Ni-Mo)]$_{2.0}$ alloy coatings obtained at constant current density of 4.0 A dm^{-2}

Coating configuration	R_a(nm)	R_q(nm)
(Ni-Mo)	18.0	13.6
[POM(Ni-Mo)]$_{2.0}$	43.9	35.4
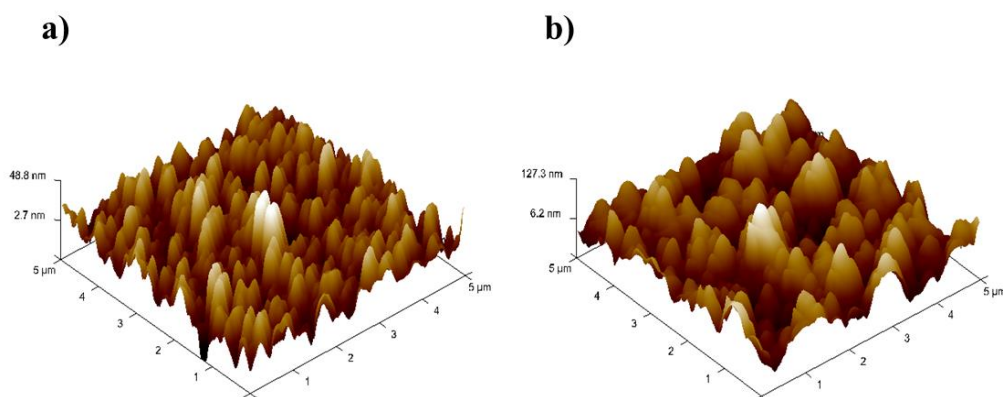
Figure 7.6- *AFM images featuring the surface roughness of: a) bare-(Ni-Mo) alloy,*
and b) [POM(Ni-Mo)]$_{2.0}$ alloy coatings developed at 4.0 A dm^{-2} from optimized bath

It may be seen that on addition of POM, the surface roughness of alloy has
increased substantially, compared to bare-(Ni-Mo) alloy coatings. Moreover, from the
experimental data of AFM study, it is evident that average roughness (R_a) of bare-(Ni-Mo) coating has increased from 18.0 nm to 43.9 nm, due to incorporation of POM into
the alloy matrix.

7.3.2 Electro-catalytic HER and OER studies

7.3.2.1 Electro-catalytic HER study

Cyclic voltammetry (CV) technique was employed to understand HER activity for
[POM(Ni-Mo)] alloy coatings in a potential range of 0.0 V to -1.6 V at a potential scan
rate of 0.05 V s^{-1}, for 20 cycles. For the first 10 cycles, there was a shift in peak cathodic
current density (i_{pc}) values, which at later stage started retracing the path of the previous
cycle. This is the stage corresponding to the state of equilibrium between the adsorption
of H atom and detachment of H$_2$ gas from the cathode surface. Figure 7.7 (a) shows CV
plot of HER's of [POM(Ni-Mo)] alloy coatings, under different concentrations of
POM, *i.e.* [POM(Ni-Mo)]$_{1.0}$ and [POM(Ni-Mo)]$_{2.0}$, in comparison with that of bare-(Ni-Mo) alloy coating. The corresponding electro-catalytic parameters are listed in
Table 7.3.
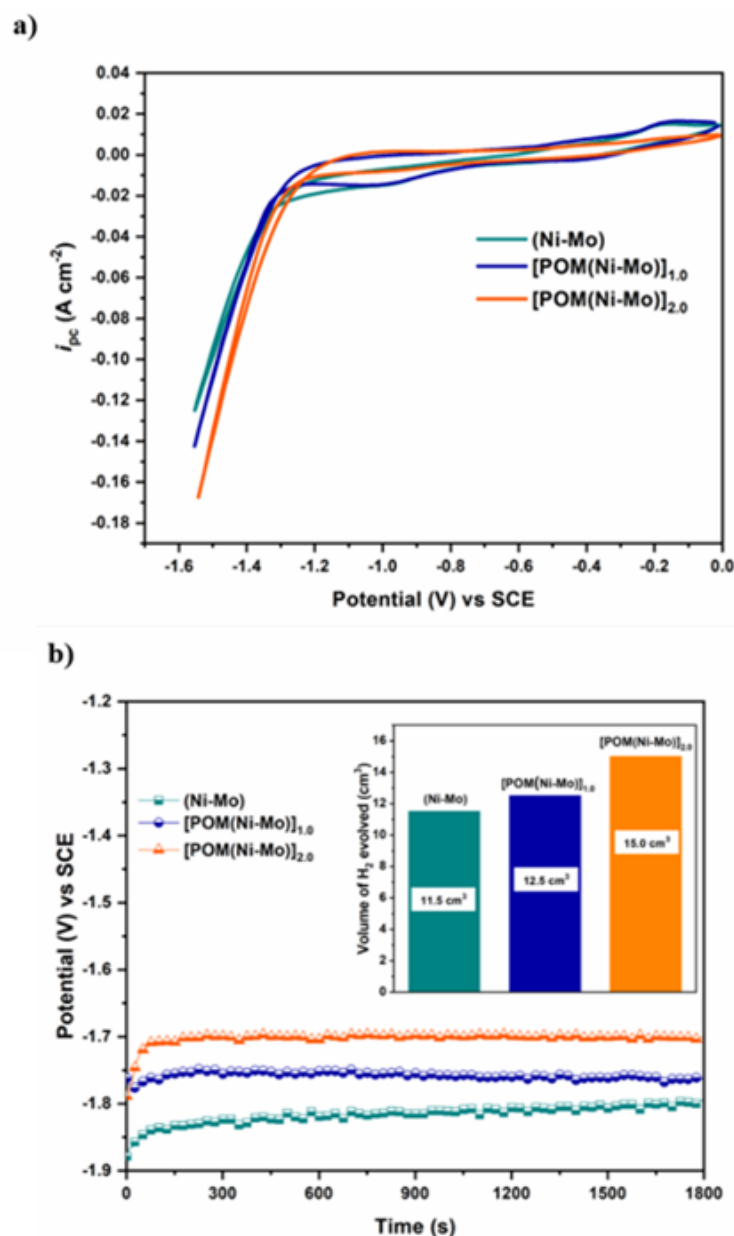
Figure 7.7- *Electro-catalytic behaviour of [POM(Ni-Mo)] alloy coatings for HER in relation to that of bare-(Ni-Mo) alloy: a) CV curves, and b) CP responses (volume of H₂ liberated are shown in the inset)*

From the value of i_{pc} and onset potential for HER, it may be confirmed that the electro-codeposition of POM into the bare-(Ni-Mo) alloy matrix has increased its electro-catalytic activity, which increased with POM content in the deposit. However, further increase of POM into the alloy matrix found to have an adverse effect on its electro-catalytic efficacy (not shown in this study).

Table 7.3- Electro-catalytic performance of POM-based (Ni-Mo) alloy coating as cathode (HER) and anode (OER) during alkaline water electrolysis in relation to its bare-(Ni-Mo) alloy coating

Coating configuration	*Electro-catalytic parameters of HER*				*Electro-catalytic parameters of OER*		
	i_{pc} (A cm^{-2})	Onset potential for HER (V) vs SCE	Volume of H_2 evolved for 300 s (cm^3)		i_{pa} (A cm^{-2})	Onset potential for OER (V) vs SCE	Volume of O_2 evolved for 300 s (cm^3)
Ni-Mo	0.124	-1.18	**11.5**		0.035	0.59	**6.0**
[POM(Ni-Mo)]₁.₀	0.141	-1.12	**12.5**		0.135	0.46	**9.3**
[POM(Ni-Mo)]₂.₀	0.179	-1.04	**15.0**		0.175	0.45	**11.6**

The CP study of alloy coatings carried out at constant current of -300 mA for a time interval of 1800 s is shown in Figure 7.7 (b). Here, it may be seen that [POM(Ni-Mo)]$_{2.0}$ coatings show better HER performance by liberating 15.0 cm^3 of H_2 gas for the initial 300 s, compared to all other coatings. Thus from the nature of CP curves, shown in Figure 7.7 (b), it may be confirmed that [POM(Ni-Mo)]$_{2.0}$ alloy is more stable, confirmed by its rapid attainment of more positive potential value compared to all other coatings. Thus, it may be summarized that [POM(Ni-Mo)]$_{2.0}$ alloy coating showed maximum electro-catalytic activity of HER with liberation of 15.0 cm^3 of H_2, affected due to changed surface structure.

7.3.2.2 Electro-catalytic OER study

The OER activity of **[POM(Ni-Mo)]** alloy coatings were also tested, by using them as anode. The CV and CP study was carried out in the same way as conducted for HER activity in the potential window of 0.0 V to 0.75 V at a scan rate of 0.05 V s^{-1}. The CV patterns of [POM(Ni-Mo)]$_{1.0}$ and [POM(Ni-Mo)]$_{2.0}$ alloy was shown in Figure 7.8 (a), in relation to (Ni-Mo) alloy coating, deposited under same condition of current density.
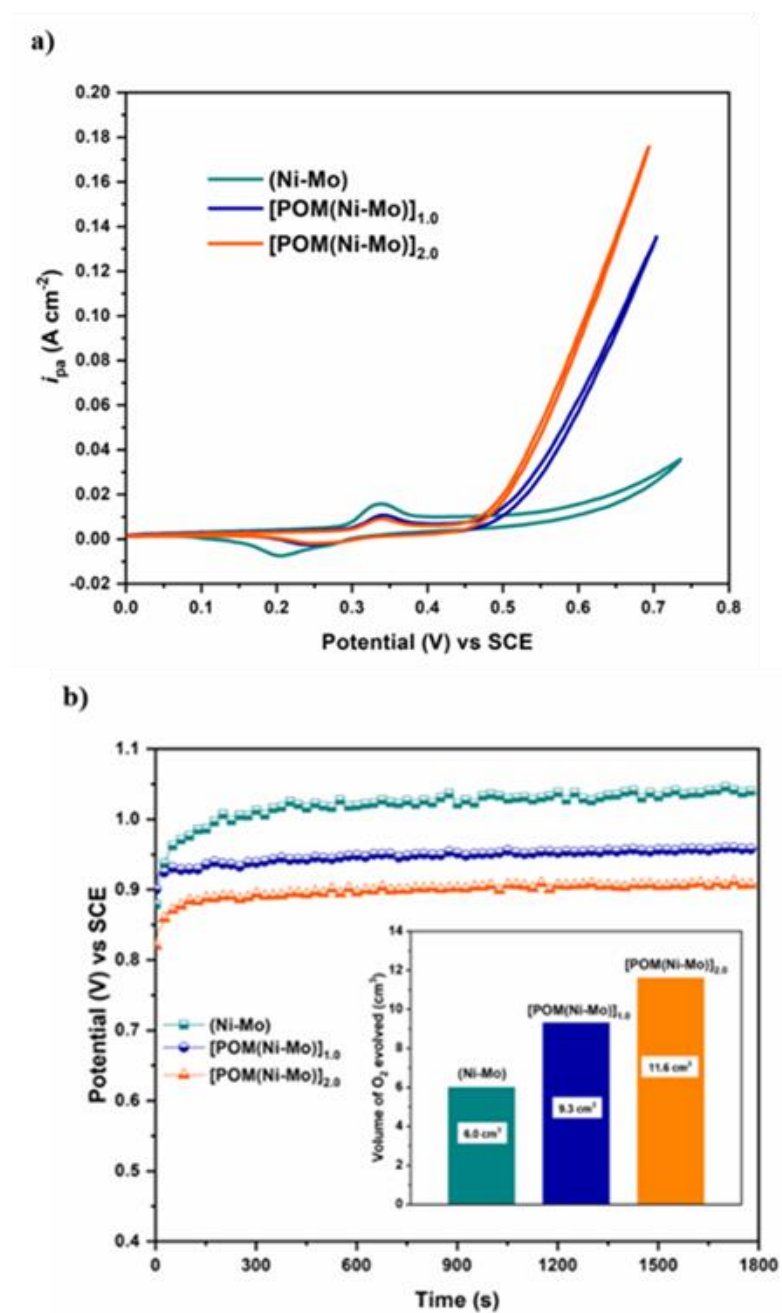
Figure 7.8- *Electro-catalytic performance of [POM(Ni-Mo)] alloy coating for OER, in comparison to (Ni-Mo) alloy coating: a) CV curves, and b) CP responses (volume of O₂ liberated are shown in the inset)*

The values of electro-catalytic kinetic parameters, like peak anodic current density (i_{pa}) recorded for OER on different coatings are reported in Table 7.3. From the nature of CV curves in Figure 7.8 (a) and the value of i_{pa}, it may be inferred that addition of POM increased drastically the electro-catalytic activity of bare-(Ni-Mo) alloy

coating. Here, in Figure 7.8 (a) also it may be seen [POM(Ni-Mo)]$_{2.0}$ alloy coatings exhibit maximum i_{pa} value, alongside the least onset potential (0.45 V). From CP measurements shown in Figure 7.8 (b), it is observed that [POM(Ni-Mo)]$_{2.0}$ attained stability at lower potential in comparison to other coatings. Moreover, it showed a significant increase in the volume of O$_2$ gas evolved (11.6 cm^3), compared to bare-(Ni-Mo) alloy coatings (6.0 cm^3). From these findings, it may be summarized that [POM(Ni-Mo)]$_{2.0}$ alloy coating showed maximum OER activity as well, when it was used as anode in alkaline water splitting.

7.3.3 Comparison of electro-catalytic efficacy of bare-(Ni-Mo) and [POM(Ni-Mo)] alloy coatings

The volume of H$_2$ and O$_2$ gas liberated, as a measure of electro-catalytic activity of (Ni-Mo), [POM(Ni-Mo)]$_{1.0}$ and [POM(Ni-Mo)]$_{2.0}$ alloy coatings for overall water splitting is shown in Figure 7.9. From the volume of H$_2$ and O$_2$ gas liberated, it may be inferred that electro-catalytic behaviour of bare-(Ni-Mo) alloy coating increased drastically on incorporation of POM into the alloy matrix. In addition, from the volume of H$_2$ and O$_2$ gas liberated, it may be inferred that [POM(Ni-Mo)]$_{2.0}$ alloy coating is electro-catalytically more active (for both HER and OER), compared to bare-(Ni-Mo) alloy coating. *i.e.* the volume of H$_2$ and O$_2$ gas increased from 11.5 cm^3 and 6.0 cm^3 to 15.0 cm^3 and 11.6 cm^3, respectively. It is important to note that the addition of POM has increased the kinetics of sluggish OER better, compared to HER which is evident from the (i_{pa}) value, reported in Table 7.3. The observed increase of electro-catalytic activity of POM-modified (Ni-Mo) alloy coating, compared to bare-(Ni-Mo) alloy is attributable to the inherent property of the added POM as envisaged by Du et al. (2020). This is to recall that basically POMs are a class of well-defined early transition metal-oxo clusters, with excellent reversible redox activity. By the virtue of which, they can behave as ideal catalysts for both oxidation and reduction processes during electrolysis, and they can behave as a good source/sink of electron. *i.e.,* with good proton and electron reservoir ability. As a result, they can transmit electrons and protons between electrodes and reactants of electrolyte easily during electrolysis. Thus, this good redox activity of added POM is responsible for bifunctional behaviour of [POM(Ni-Mo)] alloy coating to favour both HER and OER.
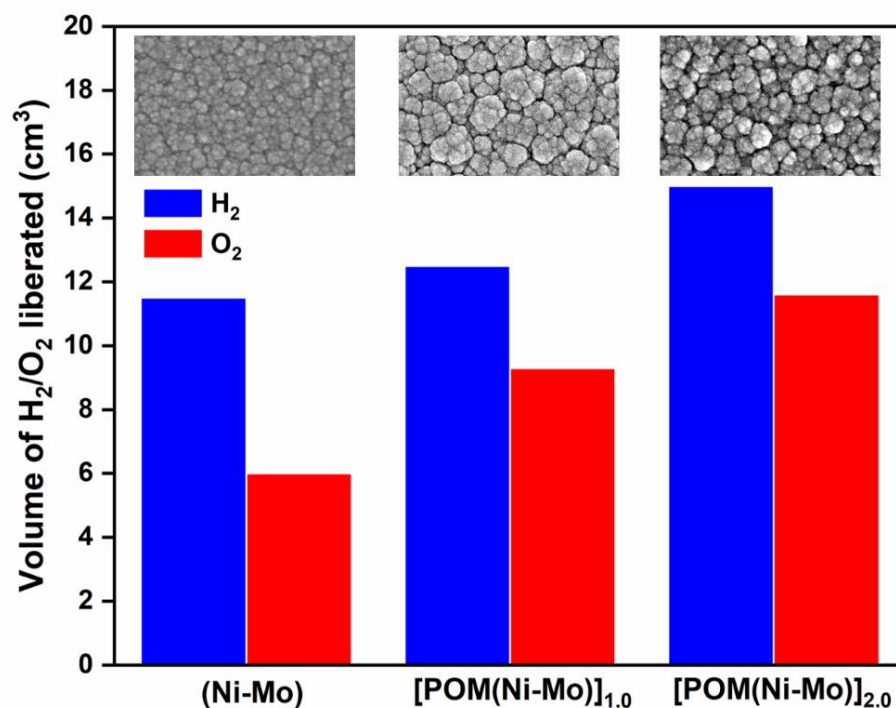
Figure 7.9- Comparison of electro-catalytic activity of bare-(Ni-Mo) and [POM(Ni-Mo)] alloy coatings (deposited at 4.0 A dm^{-2}) in terms of volume of H$_2$ and O$_2$ gas liberated at cathode and anode. Above are shown the surface feature of coatings responsible for their bifunctional electro-catalytic activity

Therefore, better electro-catalytic activity of POM- incorporated (Ni-Mo) alloy coatings for both HER and OER, compared to bare-(Ni-Mo) alloy coatings is attributable to enhance the electrical conductivity, good redox property and changed electronic structures, affected due to addition of POM (Gautam et al. 2021). A significant change in the surface feature of alloy coating was found due to inclusion of POM as may be seen in the inset of Figure 7.9. Increased porosity, in terms of electroactive sites and electrochemically active surface area, are responsible for its better activity of both HER and OER. Further, inclusion of a greater number of redox-active surface centers, affected due to POM addition (signaled as EDS and XPS peaks in Figure 7.2 and 7.5, respectively), are found to be responsible for its better catalytic activity. Thus, it may be summarized that observed bifunctional electro-catalytic property of POM(Ni-Mo)]$_{2.0}$ deposit is attributed by the increased surface-active spots, and changed electrochemical processes, affected due to addition of POM.

7.4 CONCLUSIONS

Based on the electro-catalytic study of POM-incorporated (Ni-Mo) alloy coatings from a low concentration bath of (Ni-Mo), following observations are made as conclusions:

1. The cost-effective polyoxometalate (POM) modified (Ni-Mo) alloy coatings have been developed successfully from its low concentration bath by simple electrodeposition method, and their electro-catalytic behavior in alkaline water electrolysis have been studied.

2. The electro-catalytic study revealed that the addition of POM into the growing (Ni-Mo) alloy matrix improved the efficiency of alkaline water electrolysis for both HER and OER, simultaneously.

3. [POM(Ni-Mo)]$_{2.0}$ alloy coating (optimal) was found to be most active and stable for both HER and OER compared to its bare-(Ni-Mo) alloy coatings, validated by CV and CP studies.

4. Drastic improvement in electro-catalytic efficacy of POM-modified (Ni-Mo) alloy coatings is accredited to increased surface roughness, porosity and reactive sites, due to the incorporation of POM into the bare-(Ni-Mo) alloy lattice structure, supported by FESEM, EDS, AFM and XPS study.

5. The unique reversible redox activity of POMs are responsible for effective electro-catalytic behavior of [POM(Ni-Mo)] alloy coating for both HER and OER, simultaneously during water electrolysis, and is affected due to easy transmission of electrons and protons between electrodes and reactants.

6. The limitation of conventional (Ni-Mo) alloy electrocatalyst, *i.e.* showing good electro-catalytic performance for either HER or OER, but not for both is alleviated by adding a known quantity of POM into the bath.

7. Lastly, experimental results demonstrated the possibility of POM - incorporation strategy for development of cost-effective bifunctional catalysts through electrodeposition for water electrolysis applications.

CHAPTER 8

ELECTROCHEMICAL SYNTHESIS OF ANTICORROSIVE (Ni-Fe) MULTILAYERED COATINGS FROM CITRATE-GLYCINE BATH

CHAPTER 8

ELECTROCHEMICAL SYNTHESIS OF ANTICORROSIVE (Ni-Fe) MULTILAYERED COATINGS FROM CITRATE-GLYCINE BATH

Here, the advantage of electroplating linked to cathodic current density has been exploited for development of (Ni-Fe) alloy coatings of high corrosion resistance. After optimization of a new alkaline citrate bath of (Ni-Fe) alloy, using glycine as the additive, multilayer (Ni-Fe) alloy coatings of better corrosion protection have been developed by periodic pulsing of current densities between two values, during the process of deposition. The multilayer (Ni-Fe) alloy coatings of different configurations, in both composition and thickness were developed by proper modulation of amplitude and duration of current pulse, respectively. The deposition conditions were optimized for best performance of alloy coatings against corrosion. Our experimental study revealed that under optimal condition, multilayer (Ni-Fe) coating having (Ni-Fe)$_{1.0/3.0/120}$ configuration is almost ten times more corrosion resistant than its monolayer counterpart, deposited from same bath for same duration. The reason for improved corrosion performance of multilayer alloy coating was explained in the light of effect of more number of interfaces, affected due to layers of alloys having alternatively different composition, confirmed by SEM, EDS, and XRD study. The mechanism of corrosion, in relation to its monolayer coating is shown schematically, and results are discussed.

8.1 EXPERIMENTAL

8.1.1 Electrodeposition of monolayer (Ni-Fe) alloy coatings

Generally in aqueous electrolyte, Fe has a natural tendency to precipitate as its hydroxide at lower pH than Ni (Brenner 1963). This causes a detrimental effect on the plating rate, and leading to the formation of burnt deposit at higher pH range. However, (Ni-Fe) alloy coatings developed using glycine in conjunction with citrate ions, in the bath pH = 8.0 allowed the formation of visually bright and adherent coatings. This significant change in the nature of electro-coatings is attributable to the presence of glycine in the bath, which exists in its Zwitter-ionic form, $(NH_2CH_2COO)^{\pm}$, thus acts as a buffer and prevents the precipitation of metal hydroxides in the bath (Kovalska et al. 2019).

Keeping the above facts in mind, a new electrolytic bath, consisting of known quantities of nickel chloride ($NiCl_2.6H_2O$), ferrous chloride ($FeCl_2.4H_2O$), tri-sodium citrate ($Na_3C_6H_5O_7.2H_2O$), and glycine ($C_2H_5NO_2$) was prepared by dissolving them in known volume of distilled water. The optimal condition (in both bath constituents and operating parameters) required for the development of smooth, uniform, bright and metallic coatings of (Ni-Fe) alloy over wide range of current density was identified by standard Hull cell method, described elsewhere (Kanani 2004). From Hull cell study, it was found that the citrate and glycine contribute synergistically for the improving the uniformity and brightness of alloy coating onto to the surface of substrate. Thus, based on the visual observation of coating characteristics, developed on Hull cell panel bath ingredients and operating variables, like current density range, pH and temperature were identified. This Hull cell optimization procedure enables to get a smooth and uniform coating on the surface of entire cathode (over a range of current density), when anode and cathode are kept parallel to each other, as followed in conventional electrodeposition using direct current (DC). Thus, bath constituents and operating variables arrived, to get smooth, bright and uniform coating of (Ni-Fe) alloy over a range of current density is shown in Table 8.1.

Table 8.1- Bath composition and plating variables of optimized alkaline citrate-glycine bath of (Ni-Fe) alloy, used for electrodeposition of both monolayer and multilayer (Ni-Fe) alloy coatings

Bath Ingredients	Composition (g L^{-1})	Operating variables
$NiCl_2.6H_2O$	25.0	Anode: Graphite bar
$FeCl_2.4H_2O$	5.0	Cathode: Copper sheet
$Na_3C_6H_5O_7.2H_2O$	70.0	pH: 8.0
$C_2H_5NO_2$	20.0	Current density range: 1.0 A dm^{-2}-6.0 A dm^{-2}

After bath optimization, monolayer (Ni-Fe) alloy coatings were deposited on polished copper substrate using optimized bath (Table 8.1) at varied current density, by passing direct current (DC) for 600 s. After electrodeposition, alloy coatings were

washed with distilled water, dried and then evaluated for their corrosion performances. Corrosion behaviour of all alloy coatings were studied by electrochemical AC and DC methods, in 3.5% NaCl solution for comparison purpose.

8.1.2 Optimization of cyclic cathode current densities (CCCD's)

The basic principle of *multilayer* coating is that improvement in the performance of multilayer metal/alloy coating is possible only when gradation in the composition of alternate layers and number of intervening layers are more. *i.e.* more the difference in the composition of alternate layers, and more the number of alternate layers better will be the performance of multilayer coatings. Taking the above incentives of multilayer coating, the optimization of composition individual layers have been made by depositing the alloy in different sets of cyclic cathode current densities (CCCD's). Here, electrodeposition is allowed to take place in layered fashion by cycling the cathode current densities between two known values using pulsed DC power source (Keysight Technologies, Model: N6705C). Due to alternatively changing cathode current densities, coatings with alternate layers having two different alloy compositions are produced. The development of multilayer coating due to effect of periodic change of square wave current pulses of DC is shown schematically in Figure 3.6, in comparison with its monolayer coatings. The multilayer (Ni-Fe) alloy coatings are deposited at different sets of CCCD's (chosen arbitrarily), deposition was confined to produce 10 layers. *i.e.* 10 layers of alternatively changing composition, and their corrosion rates were evaluated by Tafel's method. Among different sets of CCCD's tried, multilayer coating (having 10 layers) showing the lowest corrosion rate (CR) was considered as optimal CCCD's, and it was taken as the optimal CCCD for further layering. This procedure allowed to optimize the composition of alloy layers for better demarcation between layers.

8.1.3 Development of multi-layered (Ni-Fe) alloy coatings

Multi-layered (Ni-Fe) alloy coatings were electrodeposited from optimized (Ni-Fe) bath by periodic pulsing of the current between the optimized cyclic cathode current densities. The total plating time was maintained same as that for monolayer deposition, *i.e.* 600s. Thus multi-layered (Ni-Fe) alloy coatings having 10, 60, 120, 300 and 600 layers (within the limitation of power source used) were developed to examine the

effect of increasing the number of layers on their corrosion behaviour. For convenience, all monolayer (Ni-Fe) alloy coating deposited at a particular current density 'x' is represented as $(Ni-Fe)_x$; and multi-layered (Ni-Fe) coatings having layers of alloys of different compositions are represented as $(Ni-Fe)_{1.0/4.0/n}$ (where 1.0 and 4.0 indicate the CCCD's and 'n' the number of layers formed during total plating time).

8.2 RESULTS AND DISCUSSION

8.2.1 SEM-EDS study

Current density (current density) plays a prominent role on structure, composition and properties of coatings of mutual alloys of Fe-group metals (Ni, Co, Fe and Mn). Hence, the surface morphology of monolayer (Ni-Fe) coatings developed at different plating current densities (1.0 - 6.0 A dm^{-2}) were subjected to SEM-EDS analysis. Figure 8.1 shows the SEM micrographs of monolayer (Ni-Fe) alloy coatings developed at varied current densities from optimized citrate-glycine bath, given in Table 8.1.
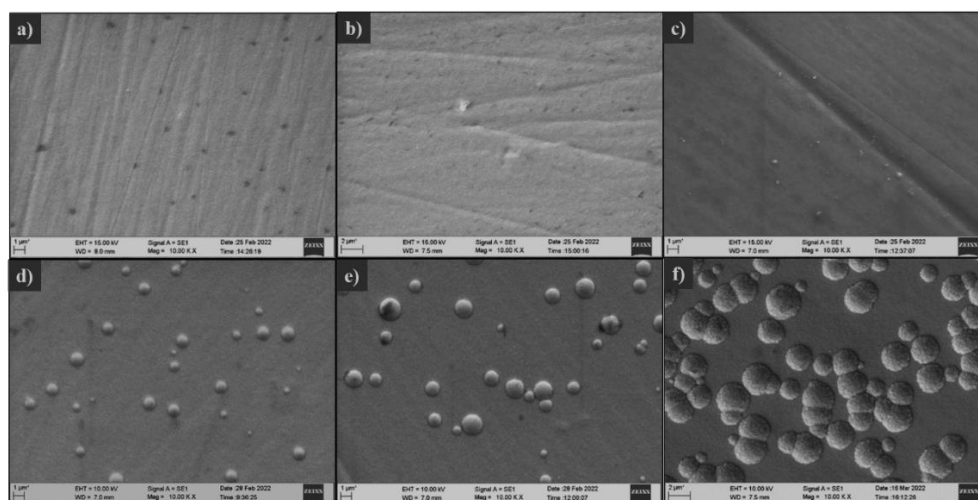
Figure 8.1- Surface micrographs of monolayer (Ni-Fe) coatings developed from alkaline citrate-glycine bath at: a) 1.0 A dm^{-2}, b) 2.0 A dm^{-2}, c) 3.0 A dm^{-2}, d) 4.0 A dm^{-2}, e) 5.0 A dm^{-2} and f) 6.0 A dm^{-2}

In Figure 8.1, it may be seen that homogeneity of the coating decreased with increase of the current density, *i.e.* from 1.0 A dm^{-2} through 6.0 A dm^{-2}. At low current density (Figure 8.1 a & b), the deposit was found to be rough and porous, and towards high current densities globules started forming on the surface. It may be due to entrapped H_2 in the deposit, formed due to excessive liberation of H_2 during deposition, which

increased to its maximum at 6.0 A dm^{-2}, as may be seen in Figure 8.1(f). Further to know the change of composition of monolayer alloy coatings with deposition current density, EDS study of (Ni-Fe) alloy coatings have been carried out. The composition of binary (Ni-Fe) alloy coatings (in terms of their Fe and Ni content), developed at different current density are shown graphically in Figure 8.2, and data are reported in Table 8.2. It may be seen that at lower current densities (1.0 A dm^{-2} and 2.0 A dm^{-2}), wt.% of less noble Fe in the deposit is much higher (66.0 % and 62.0 %) than in the bath (16.7 %), which is shown by a horizontal line in Figure 8.2.
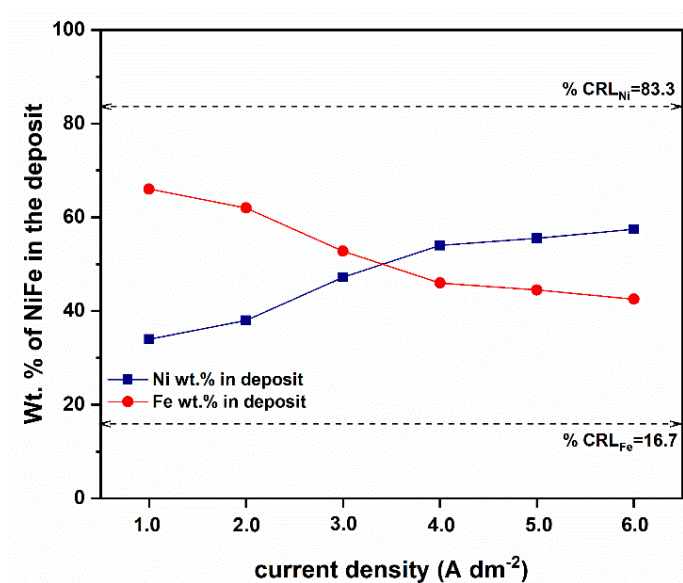
Figure 8.2- *Graphical representation showing change of Fe and Ni content in (Ni-Fe) deposit with deposition current density. Ni and Fe content in the bath is shown by perforated horizontal line based on the composition of the bath*

It is a clear situation of anomalous type of co-deposition. But on increasing current density it was found to be decreased, making the Ni content increase. This observed increase of noble metal (Ni) content, with increase of current density indicates that co-deposition of (Ni-Fe) alloy tends to change from anomalous to normal type. At lower limits of current density, (Ni-Fe) alloy system follows peculiar anomalous type of co-deposition. *i.e.,* less noble Fe deposits preferentially than nobler Ni. At higher limits of current density, it tends to approach normal type of codeposition. *i.e.*, nobler Ni deposits preferentially than less noble Fe, evident from the plot of change of metals contents in the deposit with increasing plating current density, shown in Figure 8.2.

This observation may be ascribed by the fact that co-deposition of mutual alloys of Fe-group metals follow both anomalous and normal type of codeposition depending on the alkalinity of bath, as envisaged by Brenner (1963). This trend was witnessed in various electroplating baths (Torabinejad 2016), and was explained on the basis of Fe deposition mechanism. Horkans (1979) in his studies suggested that reduction of Ni^{2+} is activation controlled, whereas that of Fe^{2+} is diffusion controlled. An increase in current density leads to the increase in cathodic over-potential, thereby making the process an activation controlled, causing an increase in Ni content (or decrease Fe content) in the alloy deposit. However, from Figure 8.2, and data in Table 8.2, it may be noted that even though the wt. % of Ni in the coatings increased with plating current density, at no current density the wt. % of Ni in the deposit reached that in the bath (83.3%). This observation clearly indicates that the bath follows the anomalous type of co-deposition in the entire range of current density studied here. However, change of current density is sufficient enough to bring change in the surface feature and composition of alloy coatings, required for compositional gradation in multilayer coating alloy coatings (Rashmi et al. 2020).

8.2.2 XRD study

The crystallite phase structure of monolayer (Ni-Fe) coatings obtained at varied plating current densities were determined through X-Ray diffraction (XRD) analysis. Figure 8.3 shows the X-ray diffractogram obtained for developed (Ni-Fe) coatings. It may be seen that XRD signals showed the presence of Ni (111) (200) and (220) (2θ = 43.8°, 50.02° and 73.9°) fcc phases, alongside peaks of pure Fe, *i.e.* bcc Fe (220) (2θ= 65.8°), and fcc Fe (220) (2θ=73.7°) and (311) (2θ= 89.5°) phases, arrived by verifying with representative JCPDS data files (00-047-1417 and 03-065-4150). It may also be noted that the bcc Fe (200) phase observed at 1.0 A dm^{-2} diminishes, with increased deposition current density This is quite relatable to our compositional data (Table 8.2) *i.e.* a decrease in wt.% of Fe, or increase of wt.% of Ni in the alloy deposit takes place with increase of current density. Thus, XRD study evidences that Ni content of (Ni-Fe) alloy increased with current density, in compliance of reported work (Ullal and Hegde 2014).
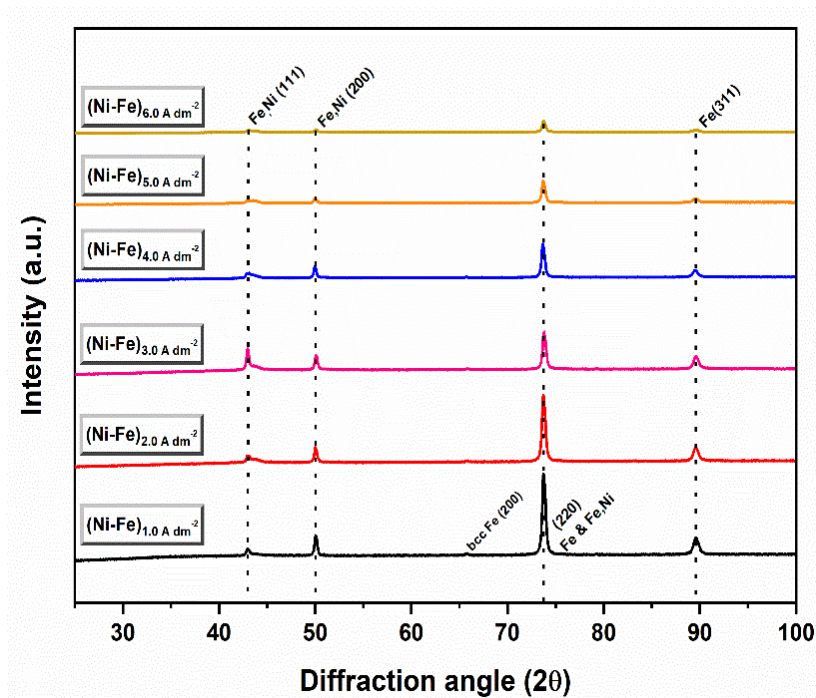
Figure 8.3- *X-ray diffraction (XRD) spectra of monolayer (Ni-Fe) alloy coatings electrodeposited at varied current density from the optimized citrate-glycine bath*

8.2.3 Effect of current density on corrosion performance

The corrosion behaviour of (Ni-Fe) alloy coatings, deposited at varied current density (1.0 A dm^{-2}-6.0 A dm^{-2}) from optimized bath were studied, using electrochemical impedance spectroscopy (EIS) and potentiodynamic polarization methods.

8.2.3.1 EIS study

A powerful and non-destructive EIS method was employed to study the corrosion behaviour of monolayer (Ni-Fe) coatings. The Nyquist responses of monolayer (Ni-Fe) alloy coatings, developed at different current densities are shown in Figure 8.4. From the plot of -Z_{im} against Z_{re}, it may be seen that all coatings exhibit only one capacitive loop, or single incomplete semicircle irrespective of the current density at which they are deposited. This implies that same corrosion mechanism is followed in all coatings, with a single charge transfer process involved. The capacitive loop corresponding to (Ni-Fe) alloy coating obtained at 4.0 Adm^{-2} showing the highest charge transfer resistance (R_{ct}) indicates that it is the most corrosion resistant, compared to all other coatings. Hence, corrosion resistance property of monolayer (Ni-Fe) alloy coatings bears a close relation with deposition current density.
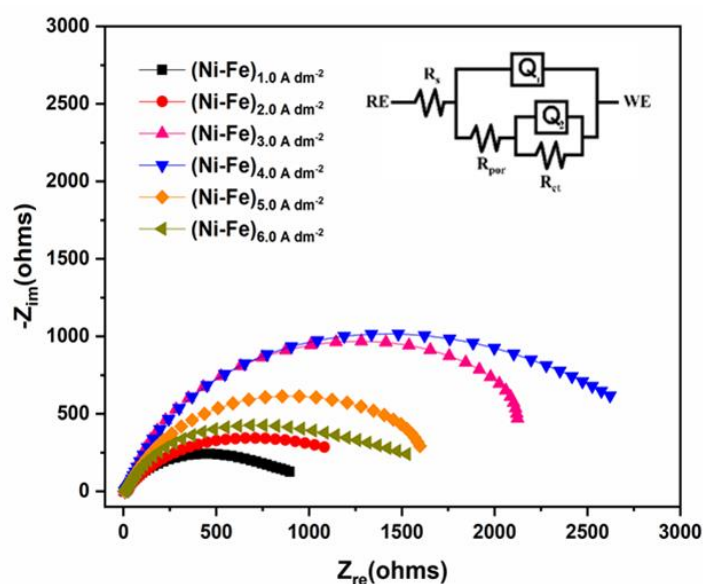
Figure 8.4- *Nyquist response obtained for monolayer (Ni-Fe) alloy coatings developed at different plating current densities, deposited from the optimized citrate-glycine bath*

8.2.3.2 Potentiodynamic polarization study

To deduce the corrosion rate (CR) values corresponding to each monolayer (Ni-Fe) alloy coatings, developed at different current densties their potentiodynamic polarization study have been made. The Tafel responses of all monolayer (Ni-Fe) alloy coatings are shown in Figure 8.5. The corrosion data of alloy coatings corresponding to different current densties are reported in Table 8.2.
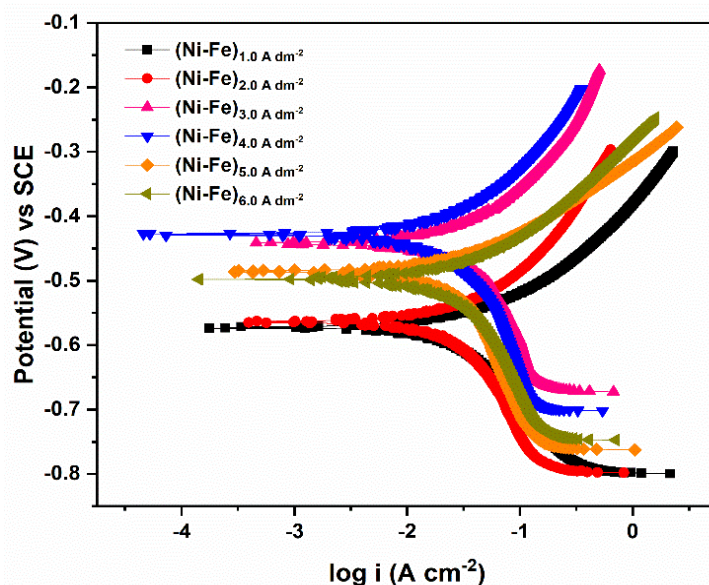
Figure 8.5- *Tafel response of monolayer (Ni-Fe) alloy coatings developed at different current densities, deposited from citrate-glycine alkaline bath*

138

Table 8.2- Corrosion data of monolayer (Ni-Fe) alloy coatings deposited at different current densities from the optimized bath

Current density (A dm^{-2})	Wt.% Fe	Wt. % Ni	R_s (ohms)	R_{ct} (ohms)	$-E_{corr}$ (V) vs SCE	i_{corr} (µA cm^{-2})	CR × 10^{-2} (mm y^{-1})
1.0	66.0	44.0	6.7	888.6	0.573	31.8	36.1
2.0	62.0	38.0	6.4	1076.5	0.564	29.2	33.0
3.0	52.8	47.2	6.4	2117.5	0.440	23.6	23.6
4.0	**46.0**	**54.0**	**6.4**	**2615.3**	**0.427**	**16.1**	**17.9**
5.0	44.5	55.5	6.7	1590.7	0.486	23.2	25.9
6.0	42.5	57.5	6.9	1519.5	0.498	25.5	28.4

Corrosion rate data reported in Table 8.2, reveals that monolayer (Ni-Fe) alloy coating developed at 4.0 A dm^{-2} is more corrosion resistant (with least CR = 17.9 × 10^{-2} mm y^{-1}), compared to all other coatings. This is in compliance with the observed results in EIS study. The least corrosion rate of monolayer (Ni-Fe) alloy coating, deposited at 4.0 A dm^{-2} may be attributed to its increased noble metal (Ni), where corrosion is inhibited due to the formation of NiO layer in the corrosive environment (Moniruzzaman and Islam 2013). However, the observed increase of CR at very high current densities (at 5.0 and 6.0 A dm^{-2}), despite of increased Ni content (as seen in Table 8.2) is attributed to the formation of high degree of adatoms, which may be explained as: At high current density, mass transport of ions and evolution of hydrogen predominates causing fast depletion of H$^+$ ions in the vicinity of the cathode. As a result, the diffusion of metal ions may be speeded up, and adatoms may not reach the most favourable positions, leading to the formation of less ordered deposits with macroscale features (Brenner 1963, Moniruzzaman and Islam 2013). Consequently, corrosion protection efficacy of (Ni-Fe) alloy coatings, deposited at highest current density decreased, despite of their high Ni content.

8.2.4 Optimization of CCCD configuration

To improve the corrosion protection efficacy of monolayer (Ni-Fe) alloy coatings, deposited at optimal current density of 4.0 Adm^{-2} (CR= 17.9 × 10^{-2} mm y^{-1}) through multilayer approach, the most important requirement is the right selection of individual layers, in terms of their composition which is dictated by deposition current density. Hence, keeping number of layers as 10 (arbitrarily chosen), multilayer coatings of (Ni-Fe) were developed through different sets of cyclic cathode current densities (CCCD's), and their corrosion performances were evaluated, and are reported in Table 8.3. It may be noted that among many sets of CCCD's tried, the least CR was observed in case of (Ni-Fe)$_{1.0/4.0/10}$ configuration. This indicates that coating with alternate layers having compositions, corresponding to 1.0 A dm^{-2} and 4.0 A dm^{-2} is most suitable for further layering, to get the best performance against corrosion. Hence, this set of CCCD was selected for development of coatings, having more number of layers for best performance against corrosion. Accordingly, the power source was set to switch between these two plating current densities (1.0 A dm^{-2} and 4.0 A dm^{-2}), and the effect of layering on corrosion protection efficacy of multi-layered (Ni-Fe) coatings were investigated.

Table 8.3- Corrosion parameters of 10-layered (Ni-Fe) alloy coatings of different compositions, deposited at different current densities from the optimal bath

Coating configuration	-E_{corr} (V) vs SCE	i_{corr} (μA cm^{-2})	CR × 10^{-2} (mm y^{-1})
(Ni-Fe)$_{4.0 \text{ A dm}^{-2}}$	0.427	16.1	17.9
(Ni-Fe)$_{1.0/4.0/10}$	0.308	7.2	8.1
(Ni-Fe)$_{2.0/5.0/10}$	0.399	11.3	12.7
(Ni-Fe)$_{3.0/6.0/10}$	0.438	12.2	13.6
(Ni-Fe)$_{1.0/5.0/10}$	0.359	9.3	10.4
(Ni-Fe)$_{2.0/6.0/10}$	0.418	12.6	14.1

8.2.5 Corrosion study of multi-layered (Ni-Fe) alloy coatings

By taking 1.0 A dm^{-2} and 4.0 A dm^{-2} as CCCD's, multi-layered (Ni-Fe) alloy coatings have been developed with different degree of layering, and their corrosion stability have been studied by electrochemical impedance spectroscopy (EIS) and potentiodynamic polarization methods, and experimental results are reported below.

8.2.5.1 EIS study

The Nyquist plots corresponding to multi-layered (Ni-Fe) coatings having different number of layers, developed on taking 1.0 A dm^{-2} and 4.0 A dm^{-2} as CCCD's are shown in Figure 8.6. EIS response clearly shows that the value of charge transfer resistance (R_{ct}) increased progressively with number of layers up to 120 layers, and then decreased (Table 8.4). The decreased diameter of capacitive loop corresponding to (Ni-Fe)$_{1.0/4.0/300}$ and (Ni-Fe)$_{1.0/4.0/600}$ indicates that corrosion protection of multi-layered (Ni-Fe) alloy coating decreases at high degree of layering. Thus from the nature of capacitive loop corresponding to (Ni-Fe)$_{1.0/4.0/120}$ coatings, it may be inferred that it is the most corrosion resistant compared to all other coatings. The electrochemical equivalent circuit showing the possible electrical components responsible for best corrosion protection is given in the inset of Figure 8.6.
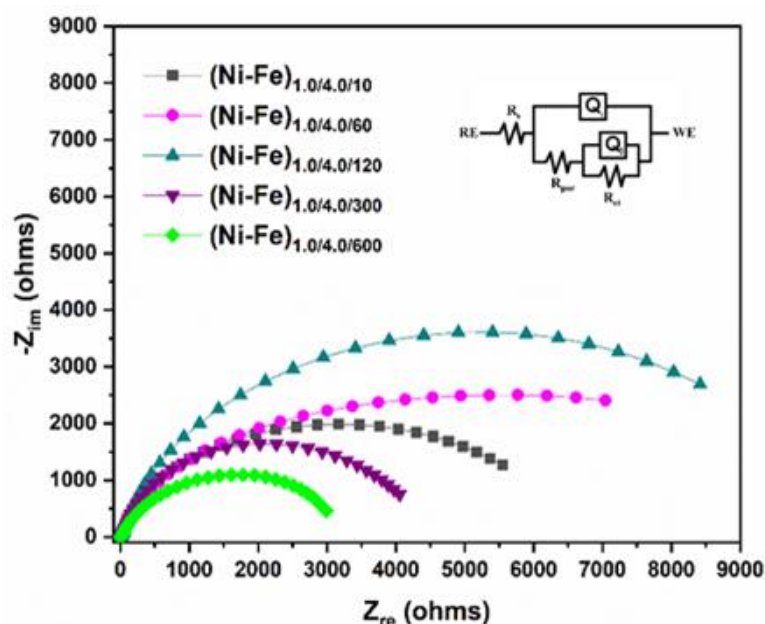
Figure 8.6- *Nyquist responses corresponding to multi-layered (Ni-Fe) coatings having different number of layers, developed on taking 1.0 A dm^{-2} and 4.0 A dm^{-2} as CCCD's*

8.2.5.2 Potentiodynamic polarization study

Potentiodynamic polarization behaviour of multi-layered $(Ni-Fe)_{1.0/4.0}$ coatings with different degree of layering is shown in Figure 8.7. The corrosion rate (CR) values evaluated by Tafel extrapolation method is given in Table 8.4, with other data. It may be noted that as the number of layers increased, time taken to deposit each layer has decreased.
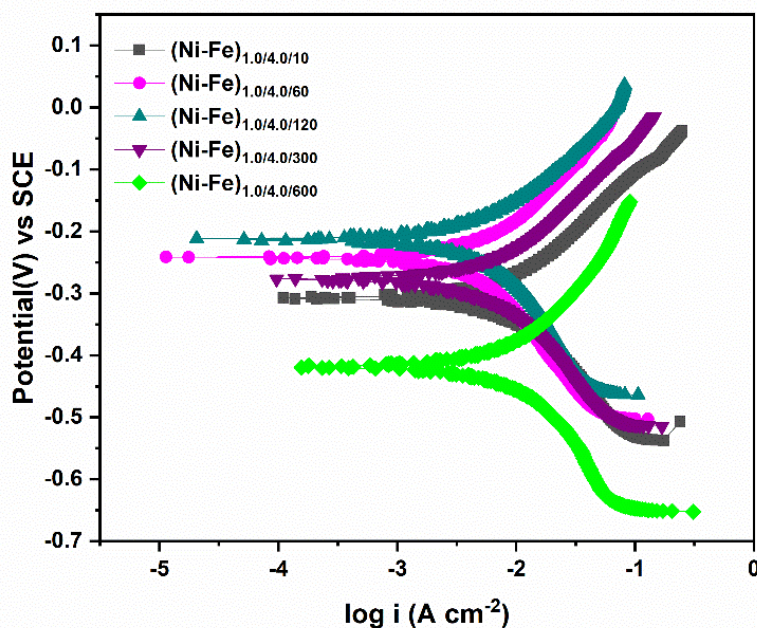
Figure 8.7 - *Tafel responses corresponding to multi-layered (Ni-Fe) coatings having different number of layers, developed on taking 1.0 A dm^-2 and 4.0 A dm^-2 as CCCD's*

Thus from the corrosion rate data (Table 8.4), it may be noted that corrosion resistance of multi-layered (Ni-Fe) coatings increased with number of layers up to 120 (CR= 1.7×10^{-2} mm y^{-1}), and then increased at higher number of layers. Hence, (Ni-Fe)$_{1.0/4.0/120}$ coating is considered as the optimal configuration for best performance against corrosion.

Table 8.4- Corrosion parameters of multi-layered (Ni-Fe)$_{1.0/4.0}$ coatings with different extent of layering

Coating configuration	Time for each layer (s)	R_s (ohms)	R_{ct} (ohms)	$-E_{corr}$ (V) vs SCE	i_{corr} (μA cm^{-2})	CR $\times$ 10^{-2} (mm y^{-1})
(Ni-Fe)$_{1.0/4.0/10}$	60	6.2	5543.4	0.308	7.2	8.1
(Ni-Fe)$_{1.0/4.0/60}$	10	6.0	7038.9	0.241	4.9	5.5
(Ni-Fe)$_{1.0/4.0/120}$	**5**	**6.4**	**8411.4**	**0.211**	**1.5**	**1.7**
(Ni-Fe)$_{1.0/4.0/300}$	2	6.6	4050.1	0.277	5.7	6.4
(Ni-Fe)$_{1.0/4.0/600}$	1	6.7	2984.2	0.418	11.5	12.8

8.2.6 Comparison of monolayer and multi-layered (Ni-Fe) alloy coatings

The comparison of corrosion protection performance of monolayer and multi-layered (Ni-Fe) alloy coatings are made here. The potentiodynamic polarization behaviour corresponding to (Ni-Fe)$_{1.0/4.0/120}$ alloy coating is shown in relation to that of monolayer (Ni- Fe)$_{1.0\ Adm^{-2}}$ and (Ni-Fe)$_{4.0\ Adm^{-2}}$ alloy coatings in Figure 8.8. Impedance responses of (Ni-Fe)$_{1.0/4.0/120}$ alloy coating, and monolayer coatings corresponding to (Ni- Fe)$_{1.0Adm^{-2}}$ and (Ni-Fe)$_{4.0\ Adm^{-2}}$ configurations, shown in the inset also validate the improved corrosion resistance of multilayer coating, compared to its monolayer counterpart.
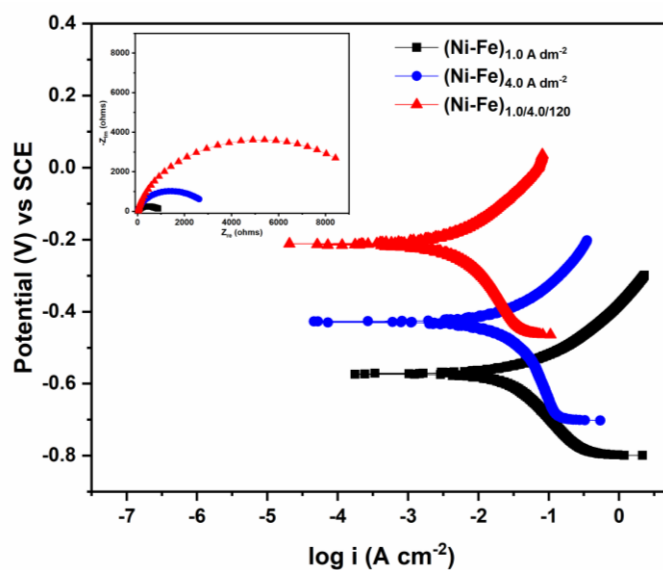
Figure 8.8- *Comparison of corrosion behaviours of multi-layer (Ni-Fe)$_{1.0/4.0/120}$ with its monolayer counterparts, ((Ni-Fe)$_{1.0\ Adm^{-2}}$ and (Ni-Fe)$_{4.0\ Adm^{-2}}$, deposited from same bath*

The corrosion parameters of multi-layered $(Ni-Fe)_{1.0/4.0/120}$ alloy, monolayer $(Ni-Fe)_{1.0 \, Adm^{-2}}$ and monolayer $(Ni-Fe)_{4.0 \, Adm^{-2}}$ are reported in Table 8.5. From the corrosion data, it may be inferred that multi-layered $(Ni-Fe)_{1.0/4.0/120}$ coatings show about 10 times better corrosion resistance than its monolayer counterpart at 4.0 Adm^{-2}, deposited from same bath for same duration.

Table 8.5- Comparison of corrosion data of multi-layered (Ni-Fe) alloy coating in relation to its monolayer counterparts (at 1.0 A dm^{-2} and 4.0 A dm^{-2})

Coating configuration	$-E_{corr}$ (V) vs SCE	i_{corr} ($\mu A \, cm^{-2}$)	$CR \times 10^{-2}$ (mm y^{-1})
$(Ni-Fe)_{1.0 \, A \, dm^{-2}}$	0.573	31.8	36.1
$(Ni-Fe)_{4.0 \, A \, dm^{-2}}$	0.427	16.1	17.9
$(Ni-Fe)_{1.0/4.0/120}$	0.211	1.5	**1.7**

The improved corrosion resistance of multilayer alloy coating, compared to its monolayer counter parts may be explained as follows: From the SEM-EDS study discussed in Figure 8.1 and Table 8.2), it was observed that monolayer (Ni-Fe) alloy coatings developed at 1.0 A dm^{-2} showed the presence of pores along with highest wt. % of Fe (66.0) in the deposit; whereas the coatings developed at 4.0 A dm^{-2} did not show any porous structure, and in addition showed decreased in wt.% of Fe (46.0). As a result, due to layering, the defects of one layer is masked or controlled by the second layer, eventually leading to delay in the corrosion attack. The increase in anticorrosion performance of multi-layered (Ni-Fe) coating with number of layers up to certain numbers (here up to 120 layers) is due to the increase in the number of interfaces formed due to layering. Formation of layered coating has been confirmed by acid test, done by adding drop of HNO_3 (dilute) just to dissolve the coatings partially. Examining the corroded part under SEM, gives structural features of alloy coatings. Here, Figure 8.9 displays the SEM images obtained for electrodeposited monolayer and multi-layered alloy coatings, after acid etching. It may be seen that on acid etching, the monolayer (Ni-Fe) coating, shown in Figure 8.9 (a) breached very easily leading to exposure to the substrate; whereas in multi-layer $(Ni-Fe)_{1.0/4.0/20}$ coating, shown in Figure 8.9(b),

breaching of coating has taken place layer by layer, resulting in delayed exposure of the substrate.
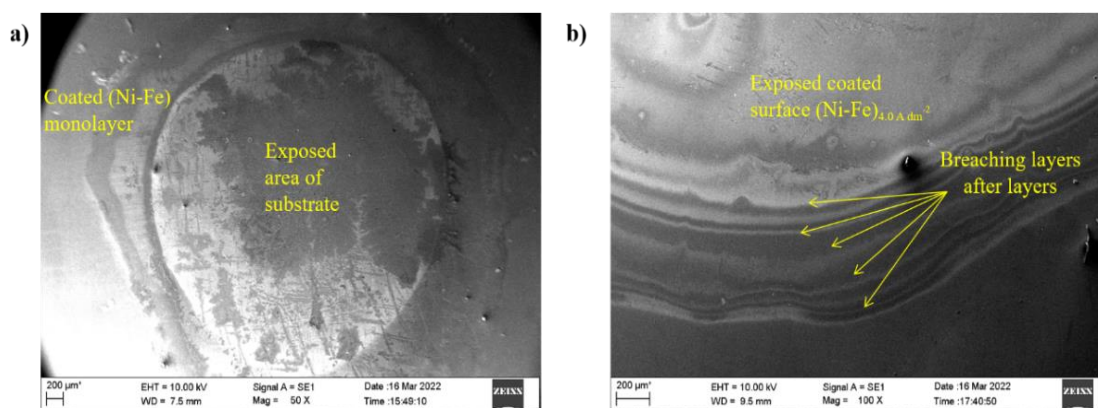
Figure 8.9- *SEM micrographs a) monolayer(Ni-Fe), and b) multillayered (Ni-Fe)$_{1.0/4.0/20}$ coatings after acid test*

8.2.7 Corrosion mechanism in multi-layered (Ni-Fe) alloy coating

The reason for improved corrosion performance of multi-layered (Ni-Fe) alloy coating may be explained in the light of effect of more number of interfaces, affected due to layers of alloys having alternatively different composition. This may be explained through a schematic representation, shown in Figure 8.10. In case of monolayer alloy coatings, the coating being homogeneous, corrosion occurs continuously, and electrolyte (corrosion medium) reaches the substrate very quickly, as shown in Figure 8.10 (a).
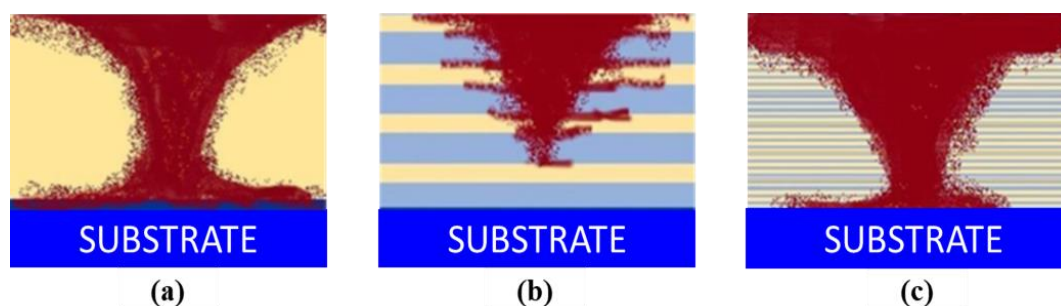
Figure 8.10- *Representative diagram showing the corrosion mechanism in (Ni-Fe) alloy coatings, deposited under different conditions: (a) direct attack of the substrate in monolayer coating, (b) delayed corrosion due to layered structure of coating, and (c) direct attack of coating due to diffused layers*

145

Whereas, in the case of multi-layered coatings developed under optimal condition the electrolyte spreads both laterally and vertically, due to the presence of well-defined phase boundaries between layers (Elias et al. 2016), shown in Figure 8.10 (b). Consequently, substrate will get exposed to the corrosion medium only after the destruction of all layers and hence corrosion occurs slowly compared to monolayer coating.

However, multilayer coatings deposited under condition of rapid pulsing of DC, *i.e.,* coatings with more than 120 layers, layers are so thin that diffusion of individual layers takes place as shown in Figure 8.10 (c), This situation make the multi-layered coating to turn into a monolayer one, without any additional protection against corrosion. This is supported by the observed high CR value of multi-layered (Ni-Fe)$_{1.0/4.0}$ alloy coatings, developed at 300 and 600 layers (Table 8.4). At high degree of layering, modulation in composition is not likely to take place. Therefore, decrease of CR at a higher degree of layering may be attributed to the lesser relaxation time for redistribution of metal ions (Fe^{2+} and Ni^{2+}) at the diffusion layer during the deposition and eventually, multi-layered (Ni-Fe) coatings above 300 layers tend to behave like monolayer, showing less corrosion resistance compared to (Ni-Fe) $_{1.0/4.0/120}$. Therefore, it is important to note that discrete phase boundary between layers affected due to pulsing of current during deposition, is responsible for improved anticorrosion property of multi-layered (Ni-Fe) coatings. Hence, the compositional gradation of layers one over the other is responsible for delayed corrosion of multilayer alloy coatings, supported by work reported by Raveendran and Hegde (2021).

8.3 CONCLUSIONS

In an effort to improve the corrosion resistance of monolayer (Ni-Fe) alloy coatings from newly formulated bath by composition graded multi-layer approach, following conclusions are arrived:

1. A new alkaline citrate-glycine (Ni-Fe) bath was formulated to get smooth, bright and uniform coatings (Ni-Fe) alloy over a wide range of current density (1.0 A dm^{-2}- 6.0 A dm^{-2}), using Hull cell method.

2. The bath followed anomalous type of co-deposition (with more wt. % of less noble Fe in the deposit than in the bath) in the entire range of current density studied.

3. Corrosion resistance of monolayer (Ni-Fe) alloy coatings obtained by conventional electrodeposition using DC has improved drastically by multilayer approach, using pulsed DC.

4. Multilayered (Ni-Fe) alloy coatings have been developed by periodic modulation of current density. The composition and thickness of alternate layers were controlled by proper modulation of current densities (pulse amplitude) and duration of pulse (time), respectively.

5. The corrosion stability of multilayered (Ni-Fe) alloy coatings were found to be increased with degree of layering up to one level; and then decreased due to diffusion of layers. In other words, multilayer coating turns into monolayer.

6. Under optimal condition, multilayered (Ni-Fe) alloy coating, having $(Ni\text{-}Fe)_{1.0/4.0/120}$ configuration is found to about 10 times more corrosion resistant than its monolayer counterpart.

7. The improved corrosion performance of multilayered (Ni-Fe) alloy coatings were attributed to the increased number of interfaces, affected due to formation of layers of alloys having low and high Ni content (affected due to pulsing of current density during deposition), confirmed by SEM analysis.

CHAPTER 9

ELECTRO-CATALYTIC STUDY OF (Ni-Fe) ALLOY COATINGS AND EFFECT OF ADDITION OF Ag NANOPARTICLES INTO THE BATH

CHAPTER 9

ELECTRO-CATALYTIC STUDY OF (Ni-Fe) ALLOY COATINGS AND EFFECT OF ADDITION OF Ag NANOPARTICLES INTO THE BATH

This chapter is devoted to study the electro-catalytic behaviour of monolayer electrodeposited (Ni-Fe) alloy coatings for alkaline water splitting applications. The (Ni-Fe) alloy coatings at different current densities, deposited from the optimized bath were used as electrode material for hydrogen evolution reaction (HER) and oxygen evolution reaction (OER). The electro-catalytic performance of alloy coatings were evaluated in 1.0 M KOH medium through cyclic voltammetry (CV) and chrono-potentiometry (CP) study. The factors responsible for changed electro-catalytic activity of (Ni-Fe) alloy coatings, developed at different current densities were explained in terms of their changed surface features, composition and phase structure, analyzed through SEM, AFM, EDS and XRD techniques. The effect of addition of Ag nanoparticles into bath on electro-catalytic activity of HER was tested. A significant improvement in the electro-catalytic activity of HER was found, affiliated to the incorporation Ag nanoparticles in (Ni-Fe) alloy matrix. The deposition conditions for best electro-catalytic activity of both (Ni-Fe) and (Ni-Fe)Ag composite coatings were proposed, and results are discussed.

9.1 INTRODUCTION

Ni-based alloys have gained much scientific attention due to their potential use as effective catalysts for water splitting of both OER and HER in alkaline solutions. Various Ni-Fe based compounds, like (Ni-Fe) alloys, Ni-Fe oxides and hydroxides, or Ni-Fe materials with non-metallic elements (S, N, P etc.) have been investigated (Ge et al. 2020, Gong and Dai 2015). However, an increase of the catalytic surface area can upgrade the electro-catalytic activity of the material (Khan et al. 2018), which can be achieved either by synthesizing material with nanostructured morphology, or by the inclusion of nanoparticles ((Záchenská et al. 2022). In this regard, the present study attempts to see the electro-catalytic activity of electrodeposited (Ni-Fe) alloy coatings developed from the proposed citrate-glycine (Ni-Fe) bath (Chapter -8), and influence of Ag nanoparticles on its HER activity. This chapter unfolds in two parts, the first part details the effect of current density (as function of the alloy composition) on electro-

catalytic efficacy of monolayer (Ni-Fe) alloy coatings towards electro-splitting of water for both hydrogen evolution reaction (HER) and oxygen evolution reaction (OER); and the second part explains the effect of addition of Ag nanoparticles into the bath on electro-catalytic potential of bare-(Ni-Fe) alloy coating. The electro-catalytic kinetic parameters of alloy coatings were evaluated by means of cyclic voltammetry (CV) and chronopotentiometric (CP) study, and the experimental results of the same were discussed in the line of information derived from different analytical methods, such as Scanning Electron Microscopy (SEM), Energy Dispersive X-Ray Spectroscopy (EDS), X-ray Diffraction (XRD) and Atomic Force Microscopy (AFM) analyses. The effect of Ag-nanoparticles on electro-catalytic HER performance has been studied, and experimental results are discussed.

9.2 EXPERIMENTAL

9.2.1 Development of (Ni-Fe) coatings

(Ni-Fe) alloy coatings were electrodeposited from the proposed alkaline citrate-glycine bath, reported in Chapter 8. Composition and plating conditions of the optimized bath is given in Table 8.1. For electro-catalytic study, electrodeposition of (Ni-Fe) alloy coatings have been carried out, from the optimized bath on the pre-treated copper tip having 1.0 cm^2 cross-sectional surface area in a custom-made electrolytic cell, shown in Figure 3.8. This mode of electrodeposition allows the electroplated (Ni-Fe) alloy coating to use as anode/cathode, depending on the requirement in the electrolyzer, shown in Figure 3.9. It may be seen that the electrolyzer is provided with two graduated burettes at the ends of the electrolyzer, to enable the quantification of hydrogen (H$_2$) and oxygen (O$_2$) gases evolved during the electro-splitting of water.

Electrodeposition of (Ni-Fe) alloy coatings have been accomplished on copper tip at 2.0 A dm^{-2}, 4.0 A dm^{-2} and 6.0 A dm^{-2}. These current densities are chosen to represent the range of current density at which bright and uniform coating was obtained. For compositional and surface characterization, (Ni-Fe) alloy coatings were developed on polished copper plates (3.0 cm^2). The electro-catalytic performance of the alloy coatings were evaluated by depositing them on pre-polished copper tip for length of 600 s, using constant current power source (Keysight Technologies, Model: N6705C).

152

9.2.2 Development of (Ni-Fe)Ag composite coatings

The effect of addition of Ag nanoparticles on the electro-catalytic efficacy of bare-(Ni-Fe) alloy coatings was tried to study by adding Ag nanoparticles, in known quantities into the bath. The experimental results showing the effect of deposition current density on the electro-catalytic performance of (Ni-Fe) alloy coating revealed that (Ni-Fe) alloy corresponding to 6.0 A dm^{-2} was showing the maximum efficacy for HER. Based on the above fact, it was tried to increase the efficacy of (Ni-Fe) alloy coatings for HER by adding Ag-nanoparticles in different quantities. This is done by dispersing Ag nano-powder (having particle size <100 nm, procured from Sigma-Aldrich) into the optimal (Ni-Fe) bath, in three different quantities, *i.e.* 0.5 g L^{-1}, 1.0 g L^{-1} and 2.0 g L^{-1}. The solution was kept overnight, under ultrasonic agitation. The electro-deposition of (Ni-Fe)Ag composite coatings were made on copper tip, as bare (Ni-Fe) alloy coatings at current density of 6.0 Adm^{-2}. For convenience, (Ni-Fe)Ag composite coatings were represented as (Ni-Fe)Ag $_x$, where 'x' stands for the amount of Ag nanoparticles added into the bath.

9.3 RESULTS AND DISCUSSION

9.3.1 Evaluation of electro-catalytic activity of (Ni-Fe) coatings

The electro-catalytic activity of (Ni-Fe) alloy coatings, from the optimized bath (Table 8.1) electrodeposited at different current densities were subjected to electro-catalytic study by using them as cathode and anode for evaluating their efficacy for hydrogen evolution reaction (HER) and oxygen evolution reaction (OER), respectively in 1.0 M KOH solution. Experimental observations are recorded as below.

9.3.1.1 Electro-catalytic activity for HER

i) Cyclic Voltammetry study

The cyclic voltammograms of (Ni-Fe) alloy coatings, corresponding to different plating current densities are shown in Figure 9.1. From CV curves, cathodic peak current density (i_{pc}) and the onset potential (the measure of the catalytic tendency for HER of the cathode material, here (Ni-Fe) deposit) were obtained and are reported in Table 9.1. The nature of CV curves clearly indicates that electro-catalytic efficiency of (Ni-Fe) alloy coatings increased with increase in deposition current density (Figure 9.1).
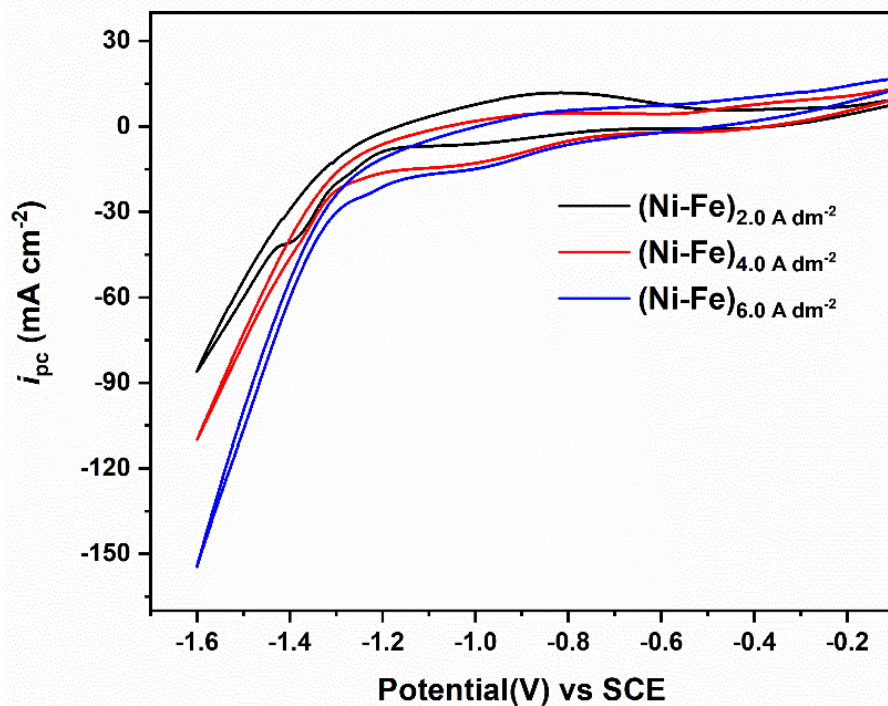
Figure 9.1- *CV response of (Ni-Fe) alloy coatings electrodeposited at varied current densities showing constant increase in the value of i$_{pc}$ with plating current density*

It may be recalled here that in CV study, cathodic peak current density (i_{pc}) is the index of capability of the electrode material to bring about HER on its surface. Basically, this situation is corresponding to a state of equilibrium between the rates of adsorption and desorption of hydrogen on the surface of cathode. The change in the value of i_{pc} with deposition current density is shown in Table 9.1.

Table 9.1- Electro-catalytic kinetic parameters of HER on (Ni-Fe) alloy coatings corresponding to different current densities

Coating configuration	wt.% of Ni	wt. % of Fe	Cathodic peak current density i_{pc} (mA cm^{-2})	Onset potential for HER (V) vs SCE	Volume of H$_2$ (cm^3)
(Ni-Fe)$_{2.0 \text{ A dm}^{-2}}$	33.9	66.1	-85.32	-1.27	7.9
(Ni-Fe)$_{4.0 \text{ A dm}^{-2}}$	54.1	45.9	-109.15	-1.25	8.8
(Ni-Fe)$_{6.0 \text{ A dm}^{-2}}$	57.5	42.5	-154.4	-1.24	9.4

From the composition data shown in Table 9.1, it may be seen that the onset potential for H_2 evolution (HER) decreased with the increase of deposition current density (or also with Ni content of the deposit), and it is maximum at 6.0 A dm^{-2}. Moreover, highest i_{pc} value (-0.154 mA cm^{-2}) corresponding to 6.0 A dm^{-2} indicates that (Ni-Fe)$_{6.0\ A\ dm^{-2}}$ coating is more favorable for HER. Thus, it may be concluded that (Ni-Fe)$_{6.0\ A\ dm^{-2}}$ alloy coatings deposited at 6.0 Adm^{-2} is good electrode material for HER, evident from the values of highest i_{pc}, and lowest onset potential of HER.

ii) *Chronopotentiometry study*

CP study of electrodeposited (Ni-Fe) coatings for HER were made by applying a constant current of -300 mA for a period of 1800 s and the volume of H_2 generated was recorded for the first 300 s, is given in Table 9.1. The chronopotentiograms of (Ni-Fe) alloy coatings, referring to different current densities are shown in Figure 9.2. The volume of H_2 evolved during electrolysis is also shown as bar charts in the inset of Figure 9.2.
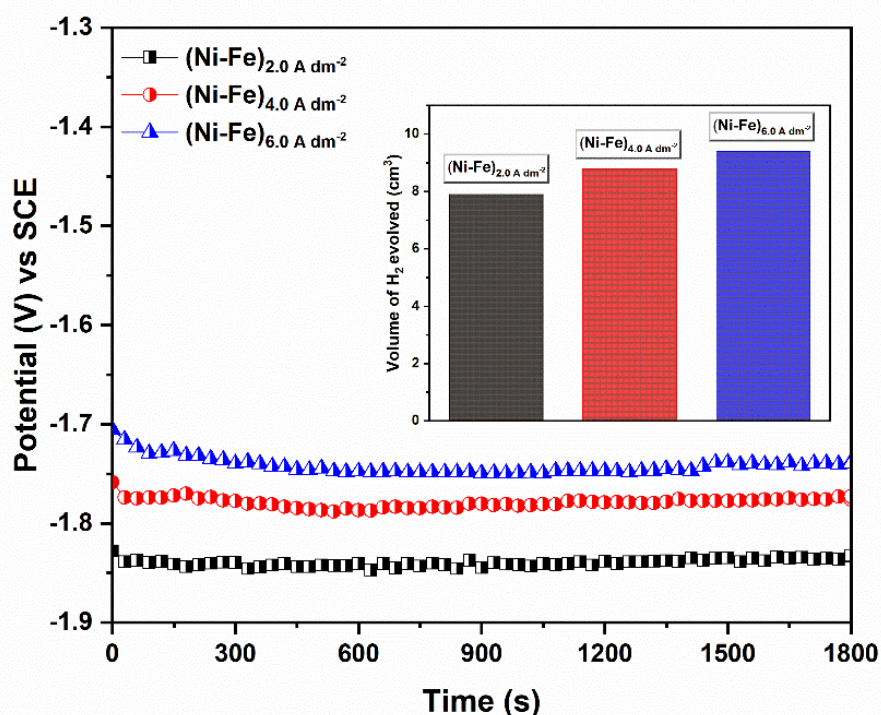
Figure 9.2- *Chronopotentiograms of (Ni-Fe) alloy coatings developed at varied plating current densities. The volume of H_2 gas evolved during electrolysis are shown by bar charts (in the inset)*

155

In Figure 9.2, the horizontal part of each chronopotentiogram indicates that at a particular potential, a steady state equilibrium is established between the H^+ ions and H_2 gas liberated, during water splitting (Ullal and Hegde 2014). Thus, from potential vs. time response of the (Ni-Fe) electrode materials, it can be deduced that (Ni-Fe) alloy coatings corresponding to 6.0 A dm^{-2} attained a state of equilibrium for HER much earlier, than other coatings. In other words, (Ni-Fe)$_{6.0\ A\ dm^{-2}}$ alloy coating is electro-catalytically more active for HER, than other coatings, it is supported by the highest volume of H_2 gas (9.4 cm^3) liberated during electrolysis.

9.3.1.2 Electro-catalytic activity for OER

i) Cyclic voltammetry study

(Ni-Fe) alloy coatings deposited at varied plating current densities were made as anode, and tested for their capability to bring about OER on their surface. Same experimental procedure, as discussed in the previous section was used for OER study here. CV studies were conducted in a potential ramp of 0.0 V to 0.75 V at a scan rate of 0.05 V s^{-1}. The CV response recorded for OER, on to the surface of different (Ni-Fe) alloy coatings are shown in Figure 9.3.
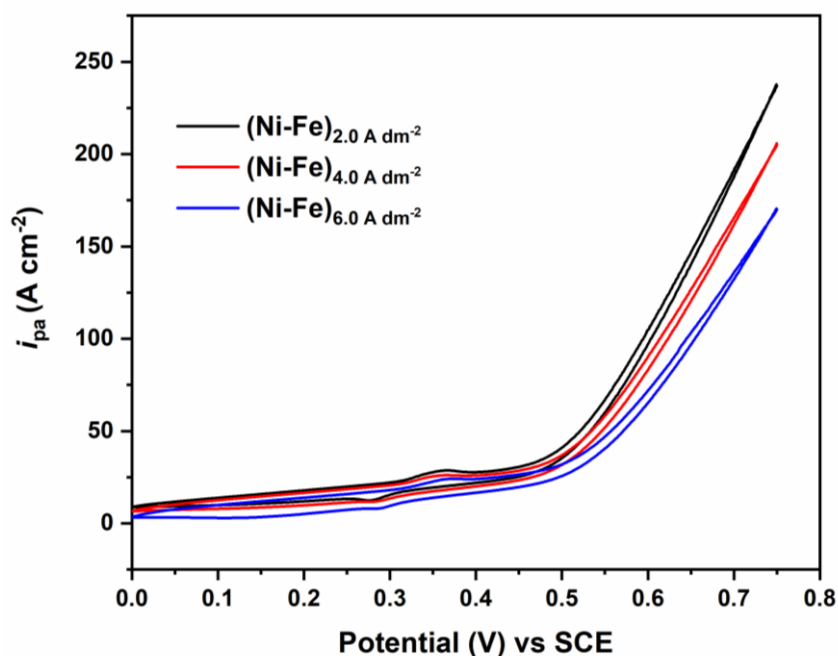
Figure 9.3- *CV response of (Ni-Fe) alloy coatings developed at varied current densities, showing increase of anodic peak current density (i_{pa}) with current density*

The value of anodic peak current density (i_{pa}), and onset potentials for OER, of all (Ni-Fe) coatings are listed in Table 9.2. The value of kinetic data reveals that (Ni-Fe) coatings electrodeposited at 2.0 A dm^{-2}, represented as (Ni-Fe)$_{2.0 \text{ A dm}^{-2}}$ exhibited the maximum anodic peak current density (i_{pa}) value, alongside the least onset potential (0.46 V). Thus it may be summarized that (Ni-Fe)$_{2.0 \text{ A dm}^{-2}}$ coating is electro-catalytically more active for OER, than other coatings, it is supported by the highest volume of O$_2$ gas (6.4 cm^3) liberated during electrolysis.
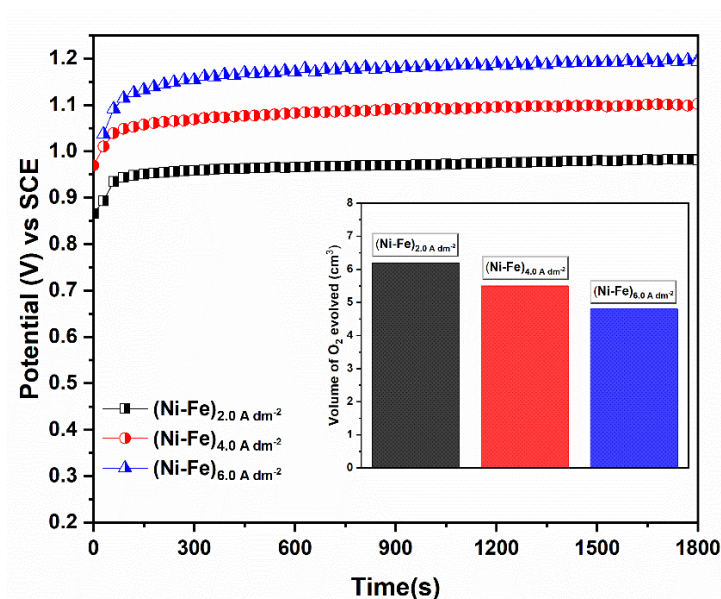
***Figure 9.4**-Chronopotentiograms of electrodeposited (Ni-Fe) alloy coatings at different current densities from the same bath. The volume of O₂ evolved during electrolysis is shown in the inset as bar charts*

ii) Chronopotentiometry study

Figure 9.4 depicts the chronopotentiograms obtained for OER performance of different (Ni-Fe) coatings. For assessment of OER, a current pulse of +300 mA was applied for a fixed period of 1800 s, and the volume of O$_2$ gas evolved was noted, as done in HER study. The stability of chronopotentiogram was attained after some time, on attainment of state of equilibrium associated with newly forming O$_2$ bubbles, and the bubbles escaping from the surface coatings (Kim et al. 2012). From chronopotentiogram response, shown in Figure 9.4 one can figure out that (Ni-Fe) alloy coated at 2.0 A dm^{-2}, represented as (Ni-Fe)$_{2.0 \text{ A dm}^{-2}}$ is more active towards OER, compared to coatings, deposited at high current densities.

Table 9.2- Electro-catalytic kinetic parameters for OER on (Ni-Fe) alloy coatings, corresponding to different current densities

Coating configuration	wt.% of Ni	wt. % of Fe	Anodic peak current density i_{pa} (mA cm^{-2})	Onset potential for OER (V) vs SCE	Volume of O$_2$ (cm^3)
(Ni-Fe)$_{2.0 \text{ A dm}^{-2}}$	33.9	66.1	237.56	0.46	6.2
(Ni-Fe)$_{4.0 \text{ A dm}^{-2}}$	45.9	54.1	204.71	0.48	5.5
(Ni-Fe)$_{6.0 \text{ A dm}^{-2}}$	57.5	42.5	174.57	0.49	4.8

From composition data (Table 9.2), it may be noted that the Ni content of (Ni-Fe)$_{2.0 \text{ A dm}^{-2}}$ coating having the highest efficacy for OER is the least, compared to all other coatings.

9.3.2 Surface characterization of (Ni-Fe) coatings

The morphological and compositional change of (Ni-Fe) alloy coatings, with deposition current density is shown in Figure 9.5, and Table 9.1, respectively. In Figure 9.5, it may be seen as deposition current density is increased, from 2.0 A dm^{-2} to 6.0 A dm^{-2}, a drastic change in the surface morphology of (Ni-Fe) alloy coatings was found. In other words, the homogeneity of alloy coatings decreased with the increase of plating current density, as shown in Figure 9.5. Moreover, from the compositional data obtained from EDS study, it is evident that wt.% of Ni in the deposit has increased with current density (Table 9.1), as the characteristic feature of mutual alloy of iron group metals.
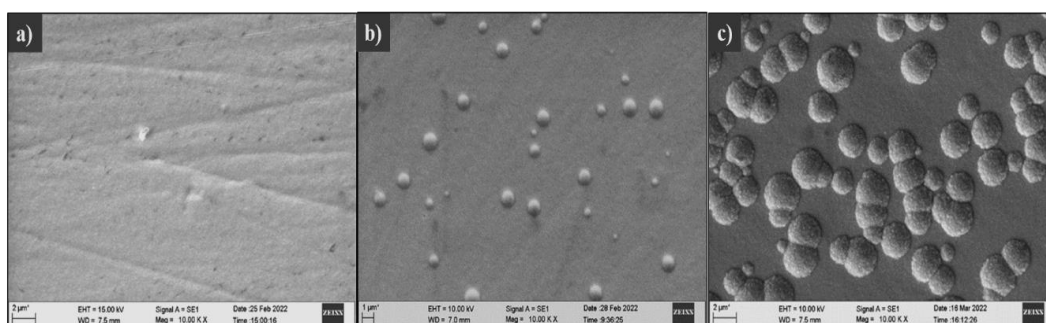
Figure 9.5- SEM micrographs of (Ni-Fe) coatings developed at: a) 2.0 A dm^{-2}, b) 4.0 dm^{-2}, and c) 6.0 A dm^{-2} from the optimal bath

Further, the effect of phase structures on the electro-catalytic performance of alloy coatings was tried to interpret with respect to their XRD peaks. The XRD reflections of (Ni-Fe) alloy coatings of different current densities are presented in Figure 9.6. From XRD peak analysis it was found that the intense peaks correspond to taenite Fe, Ni (111) (200) and (220) ($2\theta = 43.8°$, $50.02°$ and $73.9°$) fcc phases alongside peak of pure Fe fcc (311) ($2\theta= 89.5°$) phase, arrived by comparing those with representative JCPDS data files (00-047-1417 and 03-065-4150). Thus, based on the observed facts, it may be inferred that electro-catalytic capacities of (Ni-Fe) alloy coatings bear a close relation with their individual metal contents, depending on the current density employed for their deposition.
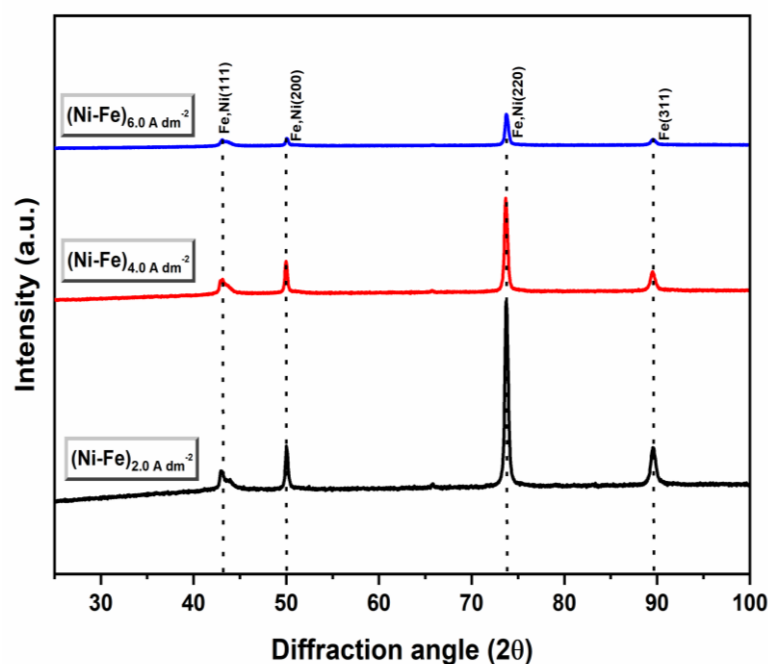
Figure 9.6- *XRD signals corresponding to (Ni-Fe) alloy coatings deposited at different current densities from the optimal bath*

9.3.3 Inverse dependency of electro-catalytic efficacy of HER and OER with Ni and Fe content of alloy coatings

The electro-catalytic activity of (Ni-Fe) alloy coatings for both HER and OER, corresponding to different deposition current densities are summarized in Table 9.3. The corresponding peak current densities, and volumes of H_2 and O_2 liberated are reported. From the data, it may be noted that as deposition current density increased (in

other words, as Ni content of the deposit increased), the electro-catalytic efficacy of (Ni-Fe) alloy coatings for HER increased, whereas for OER it decreased.

Table 9. 3- Change of catalytic activity of (Ni-Fe) alloy coatings for HER and OER with change of composition of alloy

current density (A dm^{-2})	Wt. % of Ni in the deposit	HER			OER	
		Cathodic peak current density i_{pc} (mA cm^{-2})	Volume of H$_2$ evolved for 300 s (cm^3)		Anodic peak current density i_{pa} (mA cm^{-2})	Volume of O$_2$ evolved for 300 s (cm^3)
2.0	38	-85.32	7.9		237.56	6.2
4.0	54	-109.15	8.8		204.71	5.5
6.0	58	-154.4	9.4		174.57	4.8

This inverse dependency of electro-catalytic efficacy of HER and OER with Ni content of alloy may be accredited to redox behavior of the electrodeposited alloy coatings. It may be recalled that in the electrochemical study, working electrode is an electrical conductor, and by means of an external power source (potentiostat), voltage can be applied to the electrode to modulate the energy of the electrons in the electrode. Hence, driving force of a particular reaction can be controlled, and the ease with which thermodynamic and kinetic parameters can be measured (Elgrishi et al. 2018). In the backdrop of above principle, a conceptual diagram showing the efficacy of (Ni-Fe) alloy coatings, having different wt. % of Ni content towards HER and OER during alkaline water electrolysis is given in Figure 9.7. It may be noted that during alkaline water electrolysis, H$_2$ and O$_2$ gases are liberated on working electrode, *i.e.* (Ni-Fe) alloy coatings, when relatively negative/positive potentials are applied respectively, through the potentiostat. When electrons in the (Ni-Fe) alloy coatings are at a higher energy than the Lowest Unoccupied Molecular Orbital (LUMO) of the electrolyte constituent (H$^+$), electron from the electrode is transferred to electrolyte constituent to release H$_2$.

Similarly, when electrons in the (Ni-Fe) alloy coating is at lower energy than the Highest Occupied Molecular Orbital (HOMO) of electrolyte constituent (OH$^-$), electron from the electrolyte constituent is transferred to electrode to release O$_2$. Thus, depending on the Ni content, (Ni-Fe) alloy can assume different electrode potential value as shown in Figure 9.7, and hence different energy gap (ΔE) between HOMO-

LUMO. Therefore, transferring of electrons takes place from HOMO to LUMO to favor either HER or OER, depending on its composition.
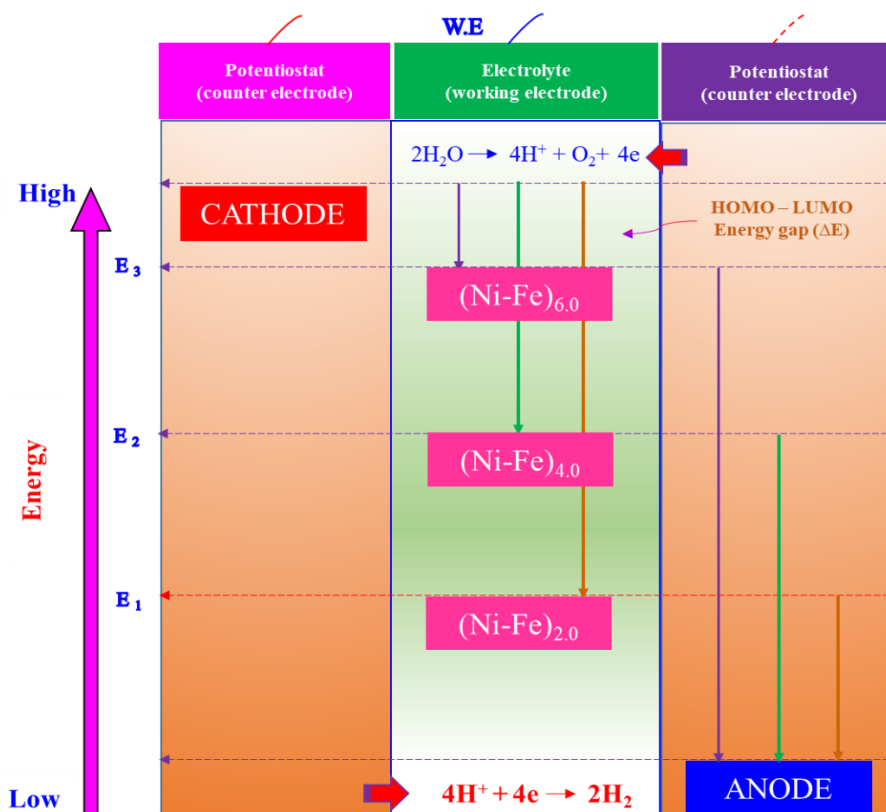
Figure 9.7- *Conceptual diagram showing the efficacy of (Ni-Fe) alloy coating, deposited at different current densities for HER and OER during alkaline water electrolysis. Transferring of electrons may be seen from HOMO to LUMO to favour either HER or OER on the surface of (Ni-Fe) alloy coatings, depending on the composition of alloy*

It is important to note that the Ni content of alloy coatings dictates its electrode potential value. Therefore, $(Ni-Fe)_{6.0\,A\,dm^{-2}}$ coating being having high electrode potential value due to its high Ni content, it shows better tendency for HER, compared to other coatings. Similarly, $(Ni-Fe)_{2.0\,A\,dm^{-2}}$ coating being having the least electrode potential value due to its low Ni content, it shows better tendency for HER, compared to other coatings. Thus, electrodeposited (Ni-Fe) alloy coatings showing highest efficacy for HER (higher ΔE value) is showing least efficacy for OER, and vice versa as shown by energy diagram in Figure 9.7.

9.3.4 Effect of addition of Ag-nanoparticles

From the electro-catalytic study of electrodeposited (Ni-Fe) coatings, it was found that (Ni-Fe)$_{6.0 \text{ A dm}^{-2}}$ shows its best performance for HER, compared to all other coatings. In this direction, HER performance of (Ni-Fe)$_{6.0 \text{ A dm}^{-2}}$ alloy coating was tried to improvise further by adding known quantity of Ag-nanoparticles into the bath. (Ni-Fe)Ag composite coatings by adding 0.5 g L^{-1}, 1.0 g L^{-1} and 2.0 g L^{-1} of Ag nanoparticles, and their electro-catalytic performances were evaluated in 1.0 M KOH.

9.3.4.1 Evaluation of HER activity of (Ni-Fe)Ag composite coatings

i) Cyclic voltammetry

Cyclic voltammetry technique was employed to understand HER activity for (Ni-Fe)Ag composite coatings in a potential range of 0.0 V to -1.6 V at a potential scan rate of 0.05 V s^{-1} for 20 cycles. For the first 10 cycles, there was a shift in i_{pc} values, which at later stage retraced the path of previous cycle. Figure 9.8 represents the CV plots of (Ni-Fe)Ag composite coatings, with different quantities of Ag-nanoparticles, with that of bare-(Ni-Fe) alloy coating. The electro-catalytic parameters corresponding to HER were tabulated in Table 9.4.
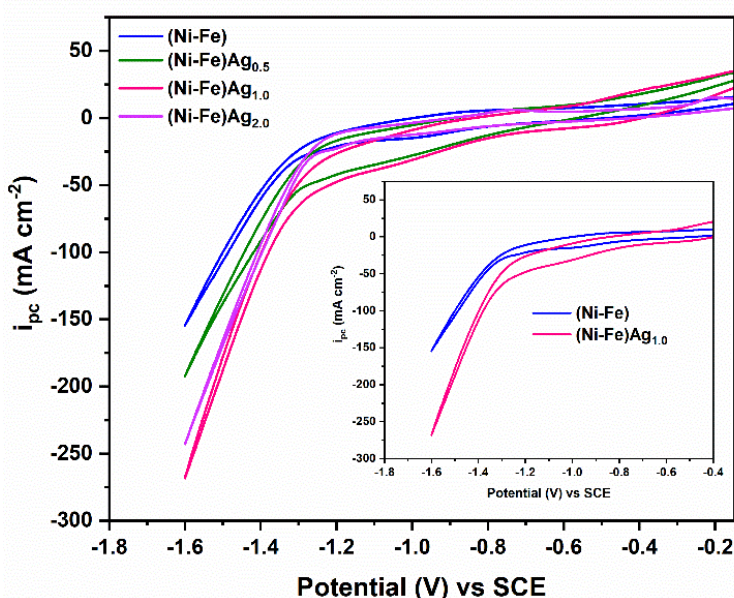
Figure 9.8- *CV responses for HER activity of (Ni-Fe) and (Ni-Fe)Ag composite coatings having varied concentrations of Ag-nanoparticles, electrodeposited at 6.0 A dm^{-2}. In the inset is given CV response of alloy coatings corresponding to optimal (Ni-Fe)Ag$_{1.0}$ composite coating.*

162

Among Ag-nanoparticles added coatings, it may be seen that $(Ni-Fe)Ag_{1.0}$ composite coatings shows the highest i_{pc} and lowest onset potential values as shown in Figure 9.8. To examine the electro-catalytic stability of composite alloy coatings, their CP study have been made by applying a constant current of -300 mA for time interval of 1800 s, and nature of their chronopotentiograms are shown in Figure 9.9. It may be seen that $(Ni-Fe)Ag_{1.0}$ coatings showed highest performance of HER, by liberating 14.0 cm^3 of H_2 gas in initial 300 s, compared to other coatings.
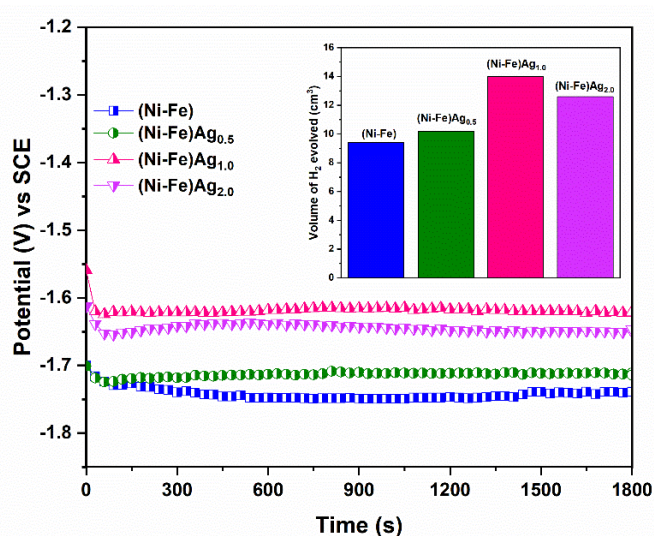
Figure 9.9- *CP responses of (Ni-Fe)Ag composite coatings for HER showing their electro-catalytic stability, and volume of H_2 gas liberated (in the inset) with varied amount of Ag nanoparticles, in relation to that of (Ni-Fe) alloy coatings. All are deposited at 6.0 A dm^{-2}.*

Table 9.4- Electro-catalytic HER parameters obtained for bare (Ni-Fe) and (Ni-Fe)Ag composite coatings developed at 6.0 A dm^{-2}

Coating configuration	Cathodic peak current density i_{pc} (mA cm^{-2})	Onset potential for HER (V) vs SCE	Volume of H_2 evolved (cm^3)
(Ni-Fe)	-154.40	-1.24	9.4
$(Ni-Fe)Ag_{0.5}$	-192.31	-1.22	10.2
$(Ni-Fe)Ag_{1.0}$	-268.28	-1.19	14.0
$(Ni-Fe)Ag_{2.0}$	-237.46	-1.20	12.6

The value of cathodic peak current density (i_{pc}), and onset potentials for HER of all (Ni-Fe) Ag composite coatings are reported in Table 9.4, with the volume of H_2 gas evolved during initial 300 s. Thus from electro-catalytic study of (Ni-Fe)Ag composite coatings, (Ni-Fe)Ag$_{1.0}$ alloy coating is electro-catalytically more active for HER, than other coatings, it is supported by the highest volume of H_2 gas (12.6 cm^3) liberated during electrolysis, compared to bare (Ni-Fe) alloy deposited at same current density.

9.3.5 Morphological characterization of (Ni-Fe)Ag composite coatings
9.3.5.1 SEM-EDS study

Figure 9.10 represents the SEM micrographs obtained for (Ni-Fe)Ag composite coatings with different amounts of Ag nanoparticles added, into the optimal bath. It is evident, from Figure 9.10 that Ag nanoparticles are embedded in the (Ni-Fe) alloy matrix homogeneously. It may also be noted that the adsorption of Ag nanoparticles onto the (Ni-Fe) deposit resulted in the formation of micro-cracks at higher amount of Ag particles as may be seen in Figure 9.10 (c).
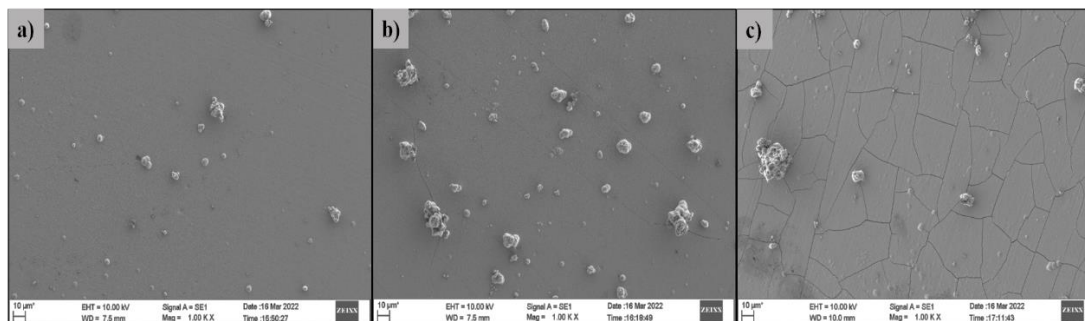
Figure 9.10- *SEM micrographs of a) (Ni-Fe)Ag$_{0.5}$, b) (Ni-Fe)Ag$_{1.0}$ and c) (Ni-Fe)Ag$_{2.0}$ composite coatings deposited at 6.0 Adm^{-2} from the same optimal bath*

Further, from the EDS analysis of (Ni-Fe)Ag composite coatings, it was found that metals content of composite coating have changed due to addition of Ag nanoparticles into the bath. Change of metals content in the composite coatings with different amount of Ag nanoparticles is shown in Table 9.5. From the composition data, it may be seen that increment in nano-Ag particles in the bath resulted in the variation in the wt.% of Fe and Ni composition in the deposit. The presence of wt. % of Ag confirms the incorporation of nano Ag onto the substrate along with alloy deposit.

Importantly, the addition of only 1.0 g L^{-1} of Ag nano-particles into the bath is good enough to bring improvement on the electro-catalytic activity of HER.

Table 9.5- Change in the wt. % of Fe, Ni and Ag in (Ni-Fe)Ag composite coatings with varied amount of Ag nanoparticles, developed at 6.0 A dm^{-2}

Coating configuration	Wt.% of Fe	Wt. % of Ni	Wt. % of Ag	Volume of H$_2$ evolved (cm^3)
(Ni-Fe)	42.5	57.5	-	9.4
(Ni-Fe)Ag$_{0.5}$	40.6	58.7	0.7	10.2
(Ni-Fe)Ag$_{1.0}$	41.8	56.9	1.3	14.0
(Ni-Fe)Ag$_{2.0}$	43.3	53.9	2.8	12.6

9.3.5.2 XRD study

Crystallographic study of (Ni-Fe)Ag composite coatings have been made in relation to that bare-(Ni-Fe) alloy coatings, and is shown in Figure 9.11. From the nature of XRD reflections, it may be seen a peak corresponding to Ag (200) (JCPDS Card No. 00-004-0783) was identified for (Ni-Fe)Ag composite coatings alongside other intense peaks corresponding to taenite Fe,Ni phases, as discussed in Chapter 8.
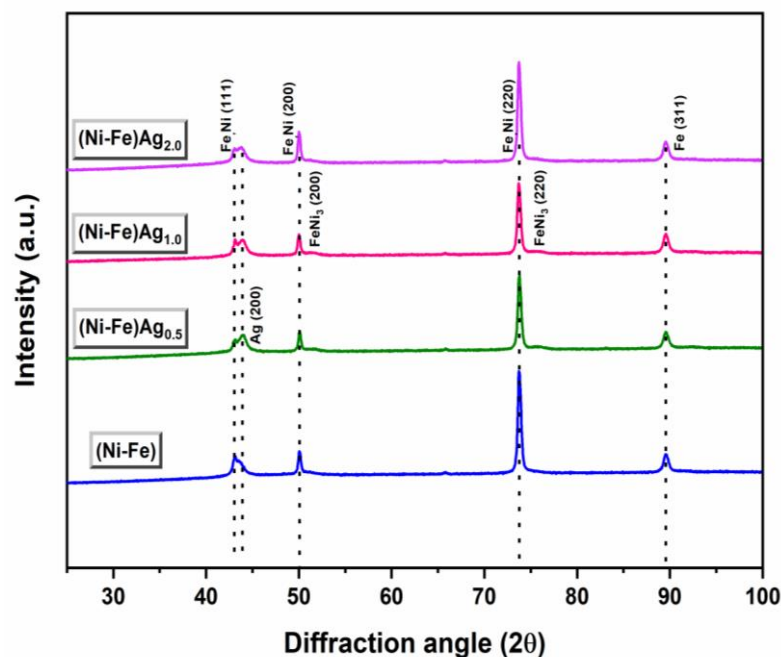
Figure 9.11- *Comparison of XRD signals obtained for bare (Ni-Fe) and (Ni-Fe)Ag composite coatings developed at 6.0 A dm^{-2}*

In addition, two less intense peaks appeared at diffraction angle, $2\theta = 51.6°$ and 75.7° corresponding to intermetallic fcc FeNi$_3$ (200) and (220) phases (JCPDS Card No. 38-0419) for (Ni-Fe)Ag composite coatings.

9.3.5.3 AFM Study

Surface roughness is considered to be an important parameter that influences HER of electrode materials. Accordingly, Atomic Force Microscopy (AFM) analysis was carried out for bare (Ni-Fe) and (Ni-Fe)Ag$_{1.0}$ composite coatings to get valuable information about the surface properties, particularly surface average roughness. Figures 9.12 (a) and 9.12 (b), gives the AFM images for bare (Ni-Fe) and (Ni-Fe)Ag$_{1.0}$ composite coatings deposited at 6.0 A dm^{-2}, respectively. The surface roughness data, revealed that average surface roughness of bare-(Ni-Fe) alloy coating is increased from 4.62 nm to 17.13 nm due to addition of 1.0 g L^{-1} Ag nanoparticles into the bath. Thus, substantial improvement in the electro-catalytic efficacy of (Ni-Fe)Ag$_{1.0}$ composite coatings for HER, compared to bare (Ni-Fe) alloy coatings may be due to increased active sites and surface roughness of alloy coatings.
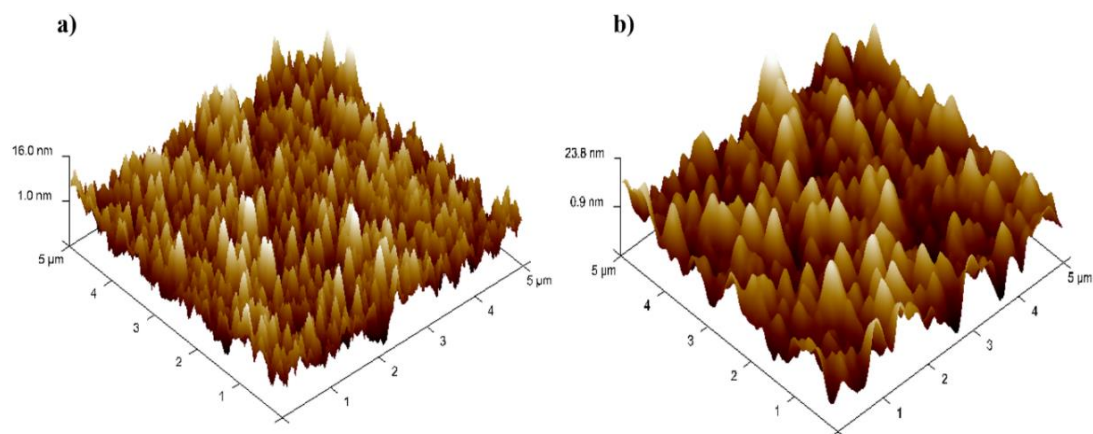
Figure 9.12- AFM images of bare (Ni-Fe) and (Ni-Fe)Ag$_{1.0}$ composite coatings developed at 6.0 A dm^{-2}, deposited from the optimal bath

9.4 CONCLUSIONS

Based on the experimental study on electro-catalytic characterization of (Ni-Fe) and (Ni-Fe)Ag composite coatings from optimized (Ni-Fe) bath following conclusions are drawn:

1. Electrodeposited (Ni-Fe) alloy coatings can be used as an active electrode material, as both cathode and anode for alkaline water splitting applications.

2. Experimental results demonstrated that electro-catalytic activity of (Ni-Fe) alloy coating for both HER and OER is highly dependent on deposition current density, and hence the composition of alloy.

3. (Ni-Fe) alloy coatings, developed at 6.0 A dm^{-2} and 2.0 A dm^{-2} are good electrode materials for HER and OER, respectively, confirmed by CV and CP techniques.

4. The mutually opposite electro-catalytic activity of (Ni-Fe) alloy coatings towards HER and OER, which changes with deposition current densities is attributed to the changed composition of alloy, in terms of their Ni and Fe content.

5. Experimental study demonstrated that electro-catalytic efficacy of (Ni-Fe) alloy coatings can be increased drastically by incorporation of Ag nanoparticles into the alloy matrix.

6. The increased electro-catalytic activity of (Ni-Fe)Ag composite coatings is affiliated to the increased surface roughness, composition and phase structure of the deposit, due to the inclusion of Ag nanoparticles in the alloy matrix, evidenced by SEM, AFM, EDS, XRD, CV and CP studies.

CHAPTER 10

SUMMARY AND CONCLUSIONS

CHAPTER 10

SUMMARY AND CONCLUSIONS

This chapter summarizes the overall research outcome and significant conclusions driven from the working chapters, based on the experimental results of investigation carried out on corrosion resistance and electro-catalytic activity of (Ni-Mo) and (Ni-Fe) alloy coatings developed through both conventional and modern methods of electrodeposition, with a note on the scope for future work at the end.

10.1 THESIS LAYOUT

Off late, the subject of alloy plating is growing in both evolutionary and revolutionary ways, and it is due to the vastness of possible alloy combinations, and their practical applications. Motivated by the above facts, two new Ni-based alloy baths have been formulated for developing more corrosion resistant and electro-catalytically active alloy coatings. Optimization of bath compositions and operating variables have been done using Hull cell method. The current densities have been optimized for development of coatings showing best performance against corrosion, and good electro-catalytic activity of electro-splitting of water (as cathode and anode). The corrosion resistance and electro-catalytic activities of conventional monolayer alloy coatings, developed using direct current were tried to improve further, through modern methods of electroplating, namely magneto-electrodeposition and multilayer deposition. The flow chart of the research work carried out in the titled thesis is presented in Figure 10.1.
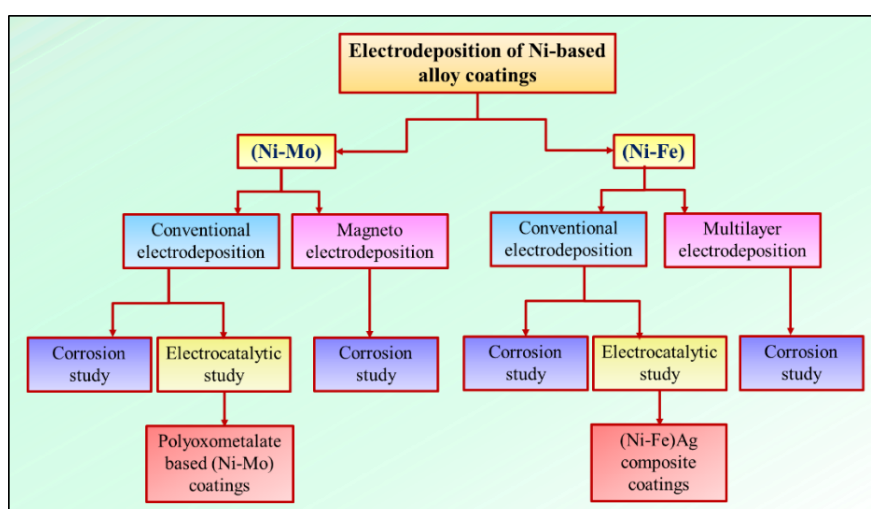
Figure 10.1- *Flow chart of the research work presented in the thesis*

10.2 EXPERIMENTAL FRAMEWORK

10.2.1 Optimization of (Ni-Mo) and (Ni-Fe) alloy baths

The optimal conditions necessary to obtain a quality (Ni-Mo) and (Ni-Fe) alloy coatings on substrate have been formulated by standard Hull cell method (Kanani 2004). The bath composition and deposition parameters of baths reached, based on the formation of their bright, uniform and metallic coatings are given in Table 10.1.

Table 10.1-Composition and deposition parameters of (Ni-Mo) and (Ni-Fe) alloy baths used for electrodeposition and characterization of different alloy coatings

Bath Constituents	(Ni-Mo) bath (g L^{-1})	(Ni-Fe) bath (g L^{-1})
Nickel chloride hexahydrate	7.0	25.0
Sodium molybdate dihydrate	3.5	-
Ferrous chloride tetrahydrate	-	5.0
Trisodium citrate dihydrate	20.0	70.0
Glycine	-	20.0
Ammonium hydroxide	Excess	-
Deposition parameters		
Bath pH	10.0	8.0
c.d. range	1.0- 4.0 Adm^{-2}	1.0-6.0 Adm^{-2}
Temperature	303K	
Anode	Graphite bar	
Cathode (substrate)	Copper sheet/rod	
Deposition time	600 s	

10.2.2 Different methods of electrodeposition of alloy coatings

The corrosion and electro-catalytic performances of (Ni-Mo) and (Ni-Fe) alloy coatings have been further improved by different methods, namely magneto-electrodeposition and multilayer. Different electrodeposition approaches adopted to develop coatings of high performances (in terms of corrosion and electro-catalytic activity) is shown schematically in Figure 10.2.
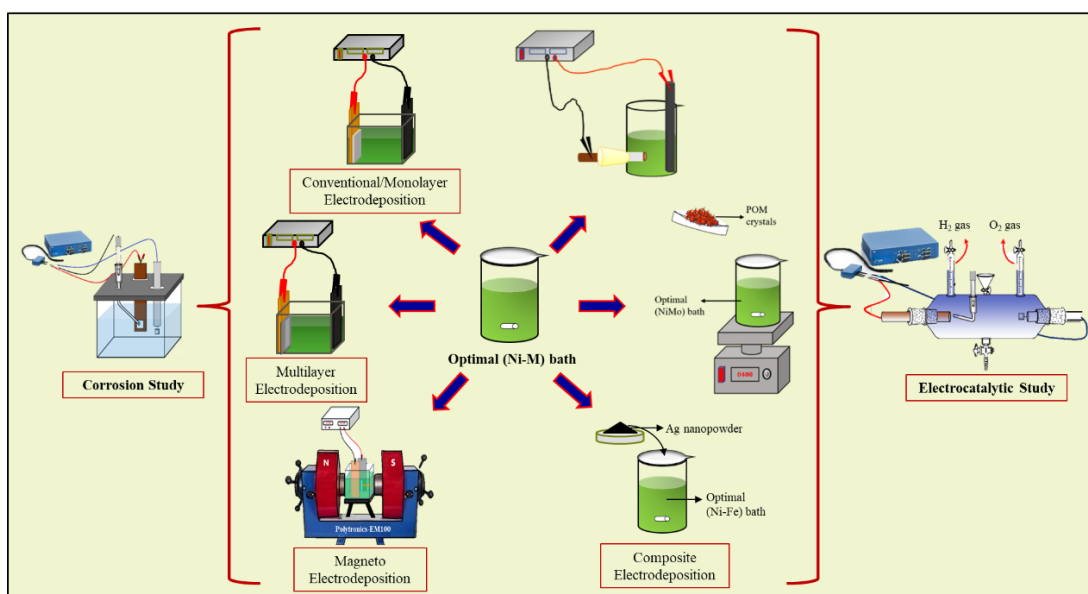
Figure 10.2- *Schematic diagram showing different methods of electrodeposition to achieve better performances alloy coatings (both corrosion and electro-catalytic activity) using same optimized bath*

10.2.2.1 Conventional electrodeposition

In the thesis, (Ni-Mo) and (Ni-Fe) alloy baths were optimized, and their monolayer (conventional) alloy coating have been accomplished using direct current (DC), and their corrosion behaviors were studied. Monolayer alloy coatings of (Ni-Mo) and (Ni-Fe) alloy was carried out at different current densities, and optimal current density for deposition of their coatings, showing best performance against corrosion was identified. The electro-catalytic activity of alloy coatings were studied by depositing them on the tip of copper rod ($1.0 \, cm^2$ area), to enable it to use in the electrolyzer, as shown in Figure 10.2.

10.2.2.2 Magneto-electrodeposition and multilayer electrodeposition

To improve the corrosion resistance property of conventional monolayer alloy coatings, deposited using DC was tried to improve further by magneto-electrodeposition (MED) and multilayer methods. The advent of magnetic field effect on electrodeposition of (Ni-Mo) alloy coatings was tried by superimposing magnetic field *B*, parallel to the process of deposition by keeping the current density as constant (optimal). The magneto-electrodeposited (MED) (Ni-Mo) alloy coating was carried out at different intensities of *B*, applied both parallel and perpendicular to the direction of flow of ions.

Further, the corrosion resistance behaviour of (Ni-Fe) alloy system was tried to enhance by multilayer approach. Multilayer (Ni-Fe) alloy coatings of different configurations, having alternatively different alloy composition and thickness were developed by setting up the power source to switch between two cathode current density values. This approach was found to increase the corrosion resistance only up to a certain number of layers, and thereafter no improvement in its corrosion resistance was found.

10.3 SIGNIFICANT FINDINGS

10.3.1 Corrosion study of electrodeposited alloy coatings

The thesis presents two new Ni-based alkaline baths, namely (Ni-Mo) and (Ni-Fe), optimized for the development of the most corrosion protective alloy coatings in 3.5% NaCl medium. The alloy coatings were developed initially at varied current density (arrived from Hull cell method) using direct current (DC) and tested for their corrosion protection efficacy. The current density at which conventional monolayer (Ni-Mo) and (Ni-Fe) coatings showed highest corrosion protection was considered as the optimal current density. Taking that optimal current density as the deposition current density, corrosion protection efficacy of monolayer (Ni-Mo) and (Ni-Fe) alloy coatings were tried to improve further by superimposition of external magnetic field (B), and multilayer methods to develop MED (Ni-Mo) and multilayered (Ni-Fe) coatings respectively. The corrosion rates (CR's) were evaluated by Tafel extrapolation method. A significant improvement in the corrosion resistance of MED coatings was found (under both parallel and perpendicular B). It was attributed to the increased Ni content of the alloy, due to magneto-convection effect. Further, MED (Ni-Mo) alloy coatings, developed under perpendicular B was found to show superior properties, compared to that under parallel B. The increased corrosion stability of MED coatings were attributed to the maximum MHD effect due to the additional effect of Lorentz force.

Then, composition modulated multilayer electrodeposited (CMM-ED), simply multilayered (Ni-Fe) alloy coatings of different configurations (having different number of layers, with alternatively different alloy composition) were developed by setting up the power source to switch between two cathode current density values. The corrosion resistance behaviour of multilayer (Ni-Fe) alloy coating was found to be improved with the increase in number of layers, and then started decreasing. Hence, an

optimal configuration was identified for best performance of (Ni-Fe) alloy coating, against corrosion.

A comparative account of bath pH, current density, coating configuration and corrosion rates of (Ni-Mo) and (Ni-Fe) alloy coatings are summarized in Table 10.2. It may be seen that MED (Ni-Mo) with coating configuration MED$_\perp$ (Ni- Mo)$_{0.3T}$ and CMM-ED (Ni-Fe) alloy coatings with (Ni-Fe)$_{1.0/4.0/120}$ configuration was found to be 8 times and 10 times more corrosion resistant than their respective conventional monolayer counterparts.

Table 10.2- Comparative account of CR's of (Ni-Mo) and (Ni-Fe) alloy coatings developed from different electrodeposition techniques

Alloy coating	(Ni-Mo)	MED (Ni-Mo)	(Ni-Fe)	Multilayer (Ni-Fe)
Bath pH	10.0		8.0	
Coating configuration	1.0 A dm^{-2}	MED$_\perp$ (Ni- Mo)$_{0.3T}$	4.0 A dm^{-2}	(Ni-Fe)$_{1.0/4.0/120}$
i$_{corr}$ (μA cm^{-2})	20.0	2.5	16.1	1.5
CR ×10^{-2} (mm y^{-1}) (in 3.5% NaCl)	16.7	2.2	17.9	1.7

To summarize, with objective of developing a better corrosion resistant Ni-based alloy coatings from two baths, namely (Ni-Mo) and (Ni-Fe), using different modern methods of electrodeposition, like magneto-electrodeposition and multilayer method, a good degree of success was achieved. The corrosion performance of all coatings, deposited for same duration (600 s) were evaluated in common corrosion medium. It was concluded that corrosion performance of monolayer coatings of both alloys can be improved to many folds better by both multilayer and MED approaches, as evidenced by their CR values. Thus from corrosion study, it was found that CR's of monolayer Ni-based alloy coatings (developed by conventional method using DC) can be decreased to many folds of their magnitude by following modern methods of

electrodeposition, namely magneto-electrodeposition (MED) and multilayer methods. It is evident from the plot of CR vs. different alloy coatings, shown in Figure 10.3.
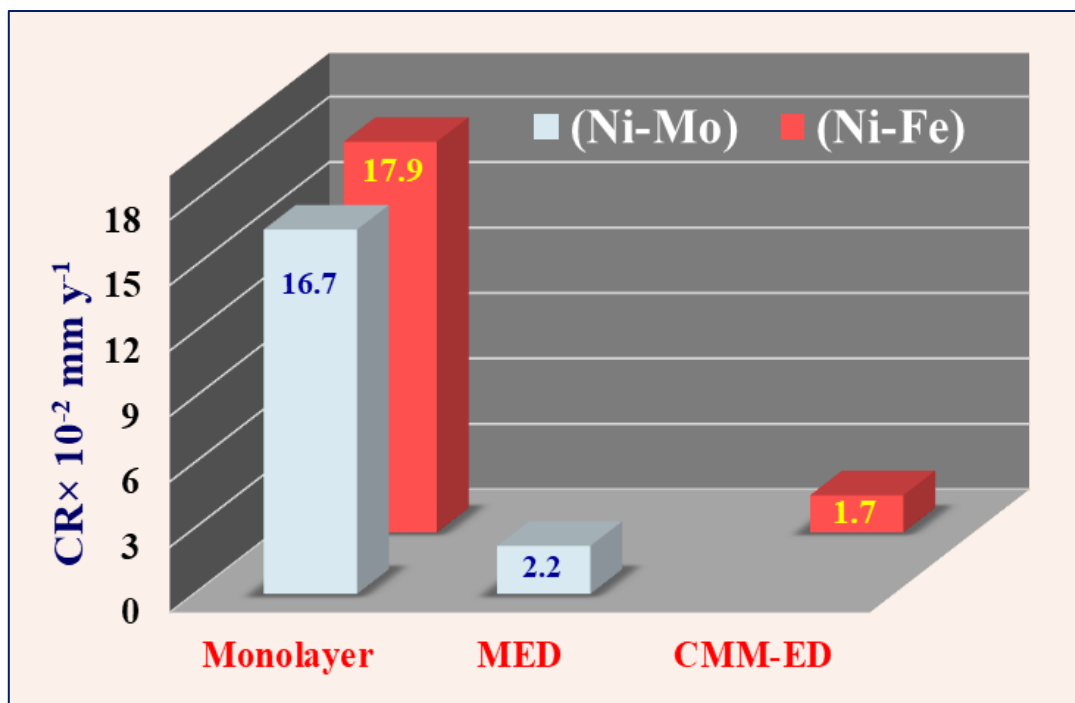
Figure 10.3- Histogram showing the CR's of (Ni-Mo), (Ni-Fe) and MED (Ni-Mo) and multilayered (Ni-Fe) alloy coatings studied in 3.5% NaCl medium (all at optimal condition)

10.3.2 Electro-catalytic performance of alloy coatings

Electro-catalytic study of electrodeposited (Ni-Mo) and (Ni-Fe) alloy, and their composite coatings developed from the proposed optimal baths were studied. The electro-catalytic efficacy of alloy coatings were studied for electro-splitting of water, by using them as cathode (for HER) and anode (for OER) in 1.0 M KOH medium. Electro-catalytic potential, in terms of both HER and OER were quantitatively assessed by measuring the amount of H_2 and O_2 evolved by the downward displacement of electrolyte from the graduated burette fitted to the custom-made alkaline water electrolyzer. CV and CP methods were used to evaluate the electro-catalytic parameters and stability of the electrode material (ED alloy coatings) respectively. The experimental conditions used for electro-catalytic study of different coatings are shown in Table 10.3. To begin with (Ni-Mo) and (Ni-Fe) alloy coatings deposited at different current densities. The effect of metal contents on the electro-catalytic performances, in

terms of HER and OER, have been studied. It was observed that the alloy coatings with higher wt. % of Ni in the deposit (obtained at higher current density) showed better activity for HER, compared to OER. Further, the effect of additives *i.e.*, polyoxometalates (POM) in (Ni-Mo) bath, and Ag nanoparticles in (Ni-Fe) bath in varied concentrations on their electro-catalytic efficacy have been tested.

Table 10.3- Experimental conditions employed for the electro-catalytic study of (Ni-Mo), (Ni-Fe), POM(Ni-Mo) and (Ni-Fe)Ag composite coatings

Operating parameters	*Working conditions*
Working electrode	(Ni-Mo), (Ni-Fe), POM(Ni-Mo), (Ni-Fe)Ag coatings
Reference electrode	Saturated calomel electrode
Counter electrode	Platinized platinum
Medium	1.0 M KOH
Potential range for CV(HER)	0.0 to -1.6V
Potential range for CV(OER)	0.0 to 0.75V
Scan rate for CV study	0.05 V s^{-1}
Time chosen HER and OER study	300 s
Applied constant current for CP analysis during HER activity	-300 mA
Applied constant current for CP analysis during OER activity	+300 mA
Duration of CP study	1800 s

The electro-catalytic activity of (Ni-Mo)/Ni-Fe) alloy and their composite coatings were evaluated for alkaline water splitting applications, by taking 1.0 M KOH as the electrolyte, and alloy coatings as electrodes. *i.e.* as cathode for HER and anode for OER.

177

Table 10.4- Volume of H₂ and O₂ evolved, as a measure of their electro-catalytic activity on the surface of different alloy coatings during alkaline water electrolysis

Coating configuration	Optimal c.d. for HER (A dm^{-2})	Volume of H$_2$ evolved in 300 s (cm^3)	Optimal c.d for OER (A dm^{-2})	Volume of O$_2$ evolved in 300 s (cm^3)
(Ni-Mo)	4.0	11.5	1.0	6.8
(Ni-Fe)	6.0	9.4	2.0	6.2
POM(Ni-Mo)	4.0	15.0	4.0	11.6
(Ni-Fe)Ag	6.0	14.0	-	-

Electro-catalytic efficacy for hydrogen evolution reaction (HER) and oxygen evolution reaction (OER) were studied by cyclic voltammetry (CV) and chrono-potentiometry (CP) techniques. The experimental results of electro-catalytic study, such as peak current density of both HER and OER (i_{pc} and i_{pa}) and the volume of H$_2$ and O$_2$ liberated during electrolysis is summarized in Table 10.4. The electro-catalytic performance of conventionally electrodeposited (Ni-Mo), (Ni-Fe), POM(Ni-Mo) and (Ni-Fe)Ag composite coatings are shown diagrammatically in Figure 10.4.
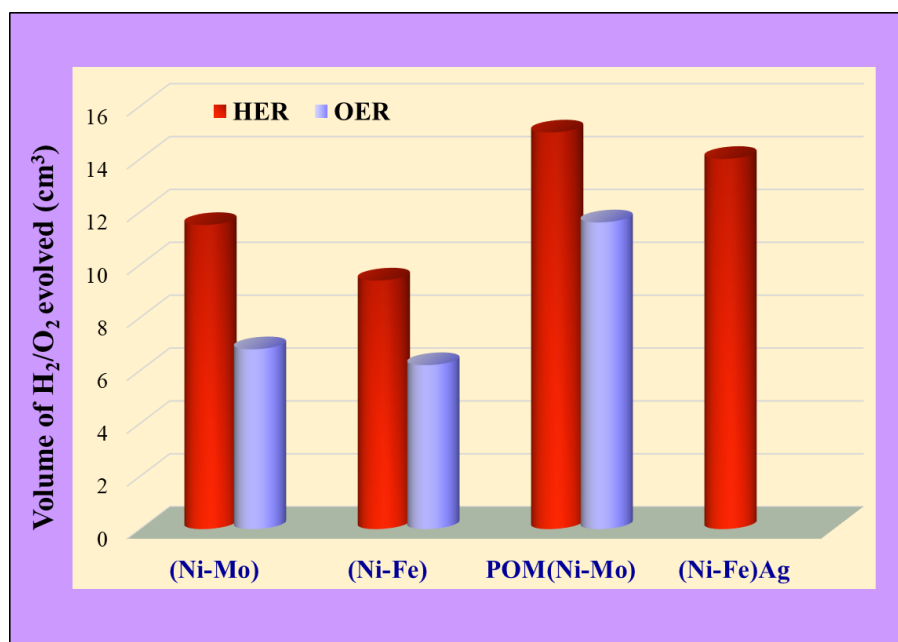
Figure 10.4-Relative electro-catalytic performance of conventionally electrodeposited (Ni-Mo), (Ni-Fe), POM(Ni-Mo) and (Ni-Fe)Ag composite coatings obtained at their optimal coating configurations

From the overall experimental investigation, it was found that POM based (Ni-Mo) coatings having [POM(Ni-Mo)]$_{2.0}$ configuration performed exceptionally good, not only in terms of HER (15.0 cm^3) but also contributed significantly towards OER (11.6 cm^3) in comparison to all other alloy coatings used in our study. This bifunctional activity of POM incorporated (Ni-Mo) alloy coatings was attributed to the effect of addition of highly redox-active transition-metal oxo POM clusters into the alloy matrix of (Ni-Mo), evidenced by CV, CP, FESEM-EDS, XRD, XPS and AFM studies. Thus, POM based (Ni-Mo) coatings are considered to be good bifunctional electrode material for alkaline water electrolysis.

10.4 CONCLUSIONS

Based on the experimental results of investigation carried out on electrodeposition of (Ni-Mo) and (Ni-Fe) alloy coatings from newly optimized baths, through different methods of electrodeposition, and in the pursuit of achieving electrodeposits of higher efficiency of corrosion protection, and better electro-catalytic efficacy for water electro-splitting, the following conclusions are drawn:

1. Two new alkaline baths of low concentrations have been proposed for development of (Ni-Mo) and (Ni-Fe) alloy coatings on copper substrate, and plating conditions were optimized using standard Hull cell method.

2. The corrosion protection efficacy and electro-catalytic activity of alloy coatings from the proposed baths have been increased drastically through magneto-electrodeposition (MED) and multilayer coating approach.

3. The developed (Ni-Mo) and (Ni-Fe) alloy baths were found to follow induced and anomalous types of co-deposition, respectively over the entire range of current density studied.

4. The corrosion performance of conventionally electrodeposited (Ni-Mo) alloy coatings was improved about 5 times and 8 times through MED technique, by superimposing magnetic field *B* parallel and perpendicular, respectively during deposition.

5. The effect of perpendicular *B* is more pronounced, than parallel field due to increased magneto-convection contributed by combined paramagnetic force and Lorentz force, leading to an increase in the mass transport process at cathode layer.

6. The corrosion resistance property of monolayer (Ni-Fe) alloy coating developed using alkaline citrate-glycine bath was increased substantially about 10 times with composition modulated multilayer electrodeposition technique.

7. Electrochemical corrosion study demonstrated that the multilayer (Ni-Fe) alloy coatings with 120 layers, represented as $(Ni\text{-}Fe)_{1.0/4.0/120}$ showed the least CR $(1.7 \times 10^{-2}$ mm $y^{-1})$ compared to its monolayer counterpart, developed from same bath for same duration.

8. From the electro-catalytic study of electrodeposited (Ni-Mo), (Ni-Fe), POM(Ni-Mo) and (Ni-Fe)Ag composite coatings, it was found that POM(Ni-Mo) coating, having $[POM(Ni\text{-}Mo)]_{2.0}$ configuration is more efficient bifunctional electrode material for alkaline water electrolysis of both HER and OER, owing to the presence of highly redox active polyoxometalate clusters.

9. The experimental results of different electrodeposited (Ni-Mo) and (Ni-Fe) alloy, and their composite coatings showed that their corrosion stability and electro-catalytic efficacy bears a strong dependency on their properties, like composition, structure and surface morphology, supported by SEM-EDS, XRD, AFM and XPS analyses.

10. Lastly, it is generalized that the corrosion protection ability of binary alloy coatings can be improved to many folds of its magnitude by exploring the benefit of magneto-electrodeposition and composition modulated multilayer electrodeposition (CMM-ED) technique, even from baths of low concentration.

10.5 SCOPE FOR FUTURE WORK

- To study the role of polyoxometalates in respect of anticorrosion and electro-catalytic performances, using advanced simulation techniques such as Density Functional Theory (DFT) studies.

- To use other non-noble metals/polyoxometalates in Ni-based alloy coatings to achieve higher corrosion resistance and electro-catalytic activity.

- To incorporate other additives or alloying elements (to form ternary alloy) for further improvement of coating characteristics, by multilayer or magneto-electrodeposition approaches.

- To explore the effect of doping of other nanoparticles in the alloy matrix for improved electro-catalytic activity of both HER and OER.

REFERENCES

Aaboubi, O. (2011). "Hydrogen evolution activity of Ni-Mo coating electrodeposited under magnetic field control." *Int. J. Hydrog. Energy.,* 36 (8), 4702-4709.

Aaboubi, O. and Msellak, K. (2017). "Magnetic field effects on the electrodeposition of CoNiMo alloys." *App. Surf. Sci.,* 396, 375-383.

Aaboubi, O., Omar, A. Y. A., Franczak, A. and Msellak, K. (2015). "Investigation of the electrodeposition kinetics of Ni-Mo alloys in the presence of magnetic field." *J. Electroanal. Chem.,* 737, 226-234.

Abhilash, S., Sumi, V. S., Sarika, S., Deepa, J. P., Sreekala, C. O. and Rijith, S. (2022). "Development and characterization of NiMoP alloy coating for electrocatalytic hydrogen evolution reaction in alkaline media." *Fuel*, 318, 123598.

Afshar, A., Dolati, A. G. and Ghorbani, M. (2003). "Electrochemical characterization of the Ni–Fe alloy electrodeposition from chloride–citrate–glycolic acid solutions." *Mat. Chem. Phys.*, 77(2), 352–358.

Ahmad, Y. H., Mohamed, A. M. A., Golden. T.D. and D'Souza N. (2014). "Electrodeposition of nanocrystalline Ni-Mo alloys from alkaline glycinate solutions." *Int. J. Electrochem. Sci.,* 9 (11), 6438-6450.

Akba, O., Güzel, F., Yurdakoc, K., Gümgüm, B. and Tez, Z. (1997). "Preparation and characterization of polyoxometallates of molybdenum, tungsten and their salts." *Synthesis and reactivity in inorganic and metal-organic chemistry*, 27(9), 1399–1415.

Al-Dawsari, A., Turkustani, A. M. and Bannani, F. (2019). "Acid-resistant corrosion protection polyoxometalate ionic liquids as anticorrosion coatings." *J. Mater. Environ. Sci.*, 10(11), 1135-1151.

Alemu, H. and Jüttner, K. (1988). "Characterization of the electrocatalytic properties of amorphous metals for oxygen and hydrogen evolution by impedance measurements." *Electrochim. Acta*, 33(8), 1101–1109.

Allahyarzadeh, M. H., Ashrafi, A., Golgoon, A. and Roozbehani, B. (2016). "Effect of pulse plating parameters on the structure and properties of electrodeposited NiMo films." *Mater. Chem. Phys.*, 175, 215–222.

Ammam, M. (2013). "Polyoxometalates: formation, structures, principal properties, main deposition methods and application in sensing." *J. Mater. Chem. A*, 1(21), 6291.

Bard, A. J. and Faulkner, L.R. (2004). *Electrochemical methods: fundamentals and applications*. John Wiley & Sons, New York.

Beltowska-Lehman, E. and Indyka, P. (2012). "Kinetics of Ni–Mo electrodeposition from Ni-rich citrate baths." *Thin Solid Films*, 520(6), 2046–2051.

Bhat, R. S. and Hegde, A. C. (2012). "Electrodeposition of cyclic multilayer Zn-Co films using square current pulses and investigations on their corrosion behaviors." *JMMCE*, 11(09), 896–903.

Bockris, J. O., Reddy, A. K. N. and Aldeco, M. G. (2002). *Modern electrochemistry second edition fundamentals of electrodics.* Kluwer Academic Publishers, New York, 1285.

Brenner, A. (1963). *Electrodeposition of alloys: principles and practice*. Vol. 1 & 2. Academic Press, New York.

Brooman, E. W. (2004). "Wear behavior of environmentally acceptable alternatives to chromium coatings: nickel-based candidates." *Met. Finish.*, 102(9), 75–82.

Busch, M., Wodrich, M. D. and Corminboeuf, C. (2015). "Linear scaling relationships and volcano plots in homogeneous catalysis – Revisiting the Suzuki reaction." *Chem. Sci.* 6, 6754–6761.

Cao, Y., Wei, G. Y., Ge, H. L. and Meng, X. F. (2014). "Study on preparation of NiFe films by galvanostatic electrodeposition." *Surf. Eng.*, 30(2), 97–101.

Cesiulis, H., Tsyntsaru, N., Ramanavicius, A. and Ragoisha, G. (2016). "The study of thin films by electrochemical impedance spectroscopy." *Nanostructures and thin films for multifunctional applications*, NanoScience and Technology, I. Tiginyanu, P. Topala, and V. Ursaki, eds., Springer International Publishing, Cham, 3–42.

Chassaing, E., Portail, N., Levy, A. and Wang, G. (2004). "Characterisation of electrodeposited nanocrystalline Ni-Mo alloys." *J. Appl. Electrochem.*, 34(11), 1085–1091.

Cullity, B. D. (1978). *Elements of X-ray diffraction*. Addison-Wesley Publishing Company.

Dahms, H. and Croll, I. M. (1965). "The anomalous codeposition of iron-nickel alloys." *J. Electrochem. Soc.*, 112(8), 771.

Du, J., Lang, Z.-L., Ma, Y.-Y., Tan, H.-Q., Liu, B.-L., Wang, Y.-H., Kang, Z.-H. and Li, Y.-G. (2020). "Polyoxometalate-based electron transfer modulation for efficient electrocatalytic carbon dioxide reduction." *Chem. Sci.*, 11(11), 3007–3015.

Elgrishi, N., Rountree, K. J., McCarthy, B. D., Rountree, E. S., Eisenhart, T. T., and Dempsey, J. L. (2018). "A practical beginner's guide to cyclic voltammetry." *J. Chem. Educ.*, 95(2), 197–206.

Elias, L. and Chitharanjan Hegde, A. (2015). "Electrodeposition of laminar coatings of Ni–W alloy and their corrosion behaviour." *Surf. Coat. Technol.*, 283, 61–69.

Elias, L. and Hegde, A. C. (2016). "Synthesis and characterization of Ni-P-Ag composite coating as efficient electrocatalyst for alkaline hydrogen evolution reaction." *Electrochim. Acta*, 219, 377–385.

Elias, L., Scott, K. and Hegde, A. C. (2015). "Electrolytic synthesis and characterization of electrocatalytic Ni-W alloy." *J. Mater. Eng. Perform*, 24(11), 4182–4191.

Eliaz, N. and Gileadi, E. (2008). "Induced codeposition of alloys of tungsten, molybdenum and rhenium with transition metals." *Modern aspects of electrochemistry*, C. G. Vayenas, R. E. White, and M. E. Gamboa-Aldeco, eds., New York, NY: Springer, 191–301.

Emregül, K. C. and Aksüt, A. A. (2003). "The effect of sodium molybdate on the pitting corrosion of aluminum." *Corr. Sci.*, 45(11), 2415–2433.

Fahidy, T. Z. (2001). "Characteristics of surfaces produced via magnetoelectrolytic deposition." *Prog. Surf. Sci.,* 68(4), 155-188.

Fahidy, T. Z. (2002). "The effect of magnetic fields on electrochemical processes." *Modern aspects of electrochemistry*, B. E. Conway, J. O. Bockris, and R. E. White, eds., Boston: Kluwer Academic Publishers, 333–354.

Fahidy, T.Z. (1983). "Magnetoelectrolysis." *J. Appl. Electrochem.*, 13(5), 553–563.

Fateh, A., Aliofkhazraei, M. and Rezvanian, A. R. (2020). "Review of corrosive environments for copper and its corrosion inhibitors." *Arab. J. Chem.*, 13(1), 481–544.

Fernandes, D. M., Araújo, M. P., Haider, A., Mougharbel, A. S., Fernandes, A. J. S., Kortz, U. and Freire, C. (2018). "Polyoxometalate-graphene electrocatalysts for the hydrogen evolution reaction." *ChemElectroChem*, 5(2), 273–283.

Fontana, M.G. (2005). *Corrosion engineering*. Tata McGraw Hill Education Private Limited, New Delhi.

Fukushima, H., Akiyama, T., Akagi, S. and Higashi, K. (1979). "Role of iron-group metals in the induced codeposition of molybdenum from aqueous solution." *Trans. Jpn. Inst. Met*, 20(7), 358–364.

Gadag, R.V. and Shetty, A.N. (2006). *Engineering chemistry*. NITK International.

Galanakis, I., Oppeneer, P. M., Ravindran, P., Nordström, L., James, P., Alouani, M., Dreysse, H. and Eriksson, O. (2001). "Sign reversal of the orbital moment via ligand states." *Phys. Rev. B*, 63(17), 172405.

Ganesh, V., Vijayaraghavan, D. and Lakshminarayanan, V. (2005). "Fine grain growth of nickel electrodeposit: effect of applied magnetic field during deposition." *Appl. Surf. Sci.*, 240(1–4), 286–295.

Gao, D., Trentin, I., Schwiedrzik, L., González, L. and Streb, C. (2019). "The reactivity and stability of polyoxometalate water oxidation electrocatalysts." *Molecules*, 25(1), 157.

Gao, M. Y., Yang, C., Zhang, Q. B., Zeng, J. R., Li, X. T., Hua, Y. X., Xu, C. Y. and Dong, P. (2017). "Facile electrochemical preparation of self-supported porous Ni–Mo alloy microsphere films as efficient bifunctional electrocatalysts for water splitting." *J. Mater. Chem. A*, 5(12), 5797–5805.

Gautam, J., Liu, Y., Gu, J., Ma, Z., Zha, J., Dahal, B., Zhang, L., Chishti, A. N., Ni, L., Diao, G. and Wei, Y. (2021). "Fabrication of polyoxometalate anchored zinc cobalt sulfide nanowires as a remarkable bifunctional electrocatalyst for overall water splitting." *Adv. Funct. Mater.,* 31(46), 2106147.

Ge, Z., Fu, B., Zhao, J., Li, X., Ma, B. and Chen, Y. (2020). "A review of the electrocatalysts on hydrogen evolution reaction with an emphasis on Fe, Co and Ni-based phosphides." *J. Mater. Sci.*, 55(29), 14081–14104.

Ghorbani, M., Dolati, A. G., and Afshar, A. (2002). "Electrodeposition of Ni–Fe alloys in the presence of complexing agents." *Russ. J. Electrochem.*, 38(11), 1173–1177.

Gong, M. and Dai, H. (2015). "A mini review of NiFe-based materials as highly active oxygen evolution reaction electrocatalysts." *Nano Res.*, 8(1), 23–39.

Goveas, J. J., Shetty, S., Mascarenhas, N. P., Hegde, A. C. and Gonsalves, R. A. (2018). "Corrosion inhibiting action of Ni–Mo alloy coatings in the presence of mixed metal oxide nanocomposites." *New J. Chem.,* 1-7.

Halim, J., Abdel-Karim, R., El-Raghy, S., Nabil, M. and Waheed, A. (2012). "Electrodeposition and characterization of nanocrystalline Ni-Mo catalysts for hydrogen production." *J. Nanomater.*, e845673.

Han, Q., Cui, S., Pu, N., Chen, J., Liu, K. and Wei, X. (2010). "A study on pulse plating amorphous Ni-Mo Alloy used as HER Cathode in Alkaline Medium." *Int. J. Hydrog. Energy,* 35 (11), 51945-5201.

Harris, T. M., Wilson, J. L. St. C. and Bleakley, M. (1999). "Effect of ethylenediamine on the electrodeposition of Ni-Fe Alloys." *J. Electrochem. Soc.*, 146(4), 1461–1464.

Hasan, S. N., Xu, M. and Asselin, E. (2019). "Electrodeposition of metallic molybdenum and its alloys – a review." *Can. Metall. Q.*, 58(1), 1–18.

Herraiz-Cardona, I., Ortega, E., Antón, J. G. and Pérez-Herranz, V. (2011). "Assessment of the roughness factor effect and the intrinsic catalytic activity for hydrogen evolution reaction on Ni-based electrodeposits." *Int. J. Hydrog. Energy*, 36(16), 9428–9438.

Horkans, J. (1979). "On the role of buffers and anions in NiFe electrodeposition." *J. Electrochem. Soc.* 126 (11), 1861–1867.

Hu, C.-C. and Weng, C.-Y. (2000). "Hydrogen evolving activity on nickel-molybdenum deposits using experimental strategies." *J. Appl. Electrochem.*, 30(4), 499–506.

Huang, P.-C., Hou, K.-H. and Wang, G.-L. (2015). "Corrosion resistance of the Ni-Mo alloy coatings related to coating's electroplating parameters." *Int. J. Electrochem. Sci.,*10, 4972-4984.

Jakšić, J. M., Vojnović, M. V. and Krstajić, N. V. (2000). "Kinetic analysis of hydrogen evolution at Ni–Mo alloy electrodes." *Electrochim. Acta*, 45(25–26), 4151–4158.

Jing, F., Katryniok, B., Bordes-Richard, E., Dumeignil, F. and Paul, S. (2015). "Structural evolution under reaction conditions of supported $(NH_4)_3HPMo_{11}VO_{40}$ catalysts for the selective oxidation of isobutane." *Catalysts*, 5(1), 460–477.

Kanani, N. (2004). *Electroplating: Basic principles, processes and practice*. Elsevier, U.K.

Katsoulis, D. E. (1998). "A survey of applications of polyoxometalates." *Chem. Rev.*, 98(1), 359–388.

Keita, B. and Nadjo, L. (2007). "Polyoxometalate-based homogeneous catalysis of electrode reactions: Recent achievements." *J. Mol. Catal. A: Chemical*, 262(1–2), 190–215.

Khan, M.A., Zhao, H., Zou, W., Chen, Z., Cao, W., Fang, J., Xu, J., Zhang, L. and Zhang, J. (2018). "Recent progresses in electrocatalysts for water electrolysis." *Electrochem. Energy Rev.*, 1, 483–530.

Kim, K. H., Zheng, J. Y., Shin, W. and Kang, Y. S. (2012). "Preparation of dendritic NiFe films by electrodeposition for oxygen evolution." *RSC Adv.*, 2(11), 4759.

Kołodziejczyk K., Miękoś, E., Zieliński, M., Jaksender, M., Szczukocki, D., Czarny, K. and Krawczyk B. (2018). "Influence of constant magnetic field on electrodeposition of metals, alloys, conductive polymers, and organic reactions." *J. Solid State Electrochem.* 1-19.

Kovalska, N., Pfaffeneder-Kmen, M., Tsyntsaru, N., Mann, R., Henrikas Cesiulis, Hansal, W. and Kautek, W. (2019). "The role of glycine in the iron-phosphorous alloy electrodeposition." *Electrochim. Acta*, 309, 450–459.

Koza, J. A., Mogi, I., Tschulik, K., Uhlemann, M., Mickel, C., Gebert, A. and Schultz, L. (2010). "Electrocrystallisation of metallic films under the influence of an external homogeneous magnetic field -Early stages of the layer growth." *Electrochim. Acta*, 55, 6533–6541.

Krause A, Uhlemann M, Gebert A. and Schultz, L. (2005). "The effect of magnetic fields on the electrodeposition of Co and Cu. *Proceedings of the 15th Riga and 6th PAMIR Conference on Fundamental and Applied MHD Magnetoelectrolysis.* 131-134.

Kubisztal, J., Budniok, A. and Lasia, A. (2007). "Study of the hydrogen evolution reaction on nickel-based composite coatings containing molybdenum powder." *Int. J. Hydrog. Energy*, 32(9), 1211–1218.

Kutyła, D., Kołczyk-Siedlecka, K., Kwiecińska, A., Skibińska, K., Kowalik, R. and Żabiński, P. (2019). "Preparation and characterization of electrodeposited Ni-Ru alloys: morphological and catalytic study." *J. Solid State Electrochem.*, 23(11), 3089–3097.

Kuznetsov, V. V., Pavlov, M. R., Chepeleva, S. A. and Kudryavtsev, V. N. (2005). "Effect of concentration of ammonia and citrate ions on the kinetics of cathodic reactions during electrodeposition of a nickel-molybdenum alloy." *Russ. J. Electrochem.*, 41(1), 75–81.

Li, Q., Zhang, L., Dai, J., Tang, H., Li, Q., Xue, H. and Pang, H. (2018). "Polyoxometalate-based materials for advanced electrochemical energy conversion and storage." *Chem. Eng. J.*, 351, 441–461.

Li, Y., Bao, X., Chen, D., Wang, Z., Dewangan, N., Li, M., Xu, Z., Wang, J., Kawi, S. and Zhong, Q. (2019). "A minireview on Nickel-based heterogeneous electrocatalysts for water splitting." *ChemCatChem*, 11(24), 5913–5928.

Lima-Neto, P. de, Correia, A. N., Vaz, G. L. and Casciano, P. N. S. (2010). "Morphological, structural, microhardness and corrosion characterisations of electrodeposited Ni-Mo and Cr coatings." *J. Braz. Chem. Soc.*, 21(10), 1968–1976.

Liu, W., Wang, X.-L. and Lan, Y.-Q. (2017). "Polyoxometalates assemblies and their electrochemical applications." *Polyoxometalate-based assemblies and functional materials*, *structure and bonding*, Y.-F. Song, ed., Springer International Publishing, Cham. 89–119.

Luo, W., Hu, J., Diao, H., Schwarz, B., Streb, C. and Song, Y.-F. (2017). "Robust polyoxometalate/nickel foam composite electrodes for sustained electrochemical oxygen evolution at high pH." *Angew. Chem. Int. Ed.*, 56(18), 4941–4944.

Lützenkirchen-Hecht, D., and Frahm, R. (2001). "Corrosion of Mo in KOH: Time Resolved XAFS Investigations." *J. Phys. Chem. B*, 105(41), 9988–9993.

Maity, S., Vannathan, A. A., Kella, T., Shee, D. and Mal, S.S. (2021). "Electrochemical performance of activated carbon-supported vanadomolybdates electrodes for energy conversion." *Cer. Int.*, 47, 27132–27141.

Manazoğlu, M., Hapçı, G. and Orhan, G. (2016). "Effect of electrolysis parameters of Ni–Mo alloy on the electrocatalytic activity for hydrogen evaluation and their stability in alkali medium." *J. Appl. Electrochem.*, 46(2), 191–204.

Matlosz, M. (1993). "Competitive adsorption effects in the electrodeposition of iron-nickel alloys." *J. Electrochem. Soc.*, 140(8), 2272–2279.

Matsumoto, Y. and Sato, E. (1986). "Electrocatalytic properties of transition metal oxides for oxygen evolution reaction." *Mat. Chem. Phys.*, 14(5), 397–426.

Melo, R. L., Casciano, P. N. S., Correia, A. N. and Lima-Neto, P. de. (2012). "Characterisation of electrodeposited and heat-treated Ni−Mo−P coatings." *J. Braz. Chem. Soc.*, 23(2), 328–334.

Milan, M. and Nedeljko, V. (1998). *"Electrocatalytic and hydridic theory for hydrogen electrode reactions and prediction of synergetic catalysts in the light of Fermi dynamics and structural bonding factors."* *Hydrogen power: Theoretical and engineering solutions.* T.O. Saetre, ed., Springer, Dordrecht, 103-118.

Moniruzzaman, Md. and Islam, Md. A. (2013). "Effects of bath composition and current density on the electrodeposition of Fe-Ni alloy on copper substrate and the property of deposited alloy." *Bangladesh J. Sci. Ind. Res.*, 47(4), 379–386.

Monzon L. M. and Coey, J.M.D. (2014). "Magnetic fields in electrochemistry: The Lorentz force. A mini-review." *Electrochem. Comm.,* 42, 38-41.

Mousavi, R., Bahrololoom, M. E., Deflorian, F. and Ecco, L. (2016). "Improvement of corrosion resistance of Ni Mo alloy coatings: effect of heat treatment." *Appl. Surf. Sci.*, 364, 9–14.

Msellak, K., Chopart, J.-P., Jbara, O., Aaboubi, O. and Amblard, J. (2004). "Magnetic field effects on Ni–Fe alloys codeposition." *J. Magn. Magn. Mater.*, 281(2–3), 295–304.

Ngo Boum, G. B. and Alemany, A. (1999). "Numerical simulations of electrochemical mass transfer in electromagnetically forced channel flows." *Electrochim. Acta*, 44(11), 1749–1760.

Odenbach, S. (1994). "Convection driven by forced diffusion in magnetic fluids." *Phys. Fluids*, 6(7), 2535–2539.

Ooka, H., Huang, J. and Exner, K. S. (2021). "The Sabatier principle in electrocatalysis: Basics, limitations, and extensions." *Front. Energy Res.,* 9, 654460.

Parthasaradhy, N. V. (1988). *Practical electroplating handbook*, Prentice-Hall Incl. Pub., New Jersey.

Paunovic, M. and Schlesinger, M. (2006). *Fundamentals of electrochemical deposition*, second edition. John Wiley & Sons, New Jersey.

Platatorres, M., Torreshuerta, A., Dominguezcrespo, M., Arceestrada, E., and Ramirezrodriguez, C. (2007). "Electrochemical performance of crystalline Ni–Co–Mo–Fe electrodes obtained by mechanical alloying on the oxygen evolution reaction." *Int. J. Hydrog. Energy*, 32(17), 4142–4152.

Podlaha, E. J. (1996). "Induced Codeposition." *J. Electrochem. Soc.*, 143(3), 885.

Podlaha, E. J. and Landolt, D. (1997). "Induced codeposition: III. Molybdenum alloys with nickel, cobalt, and iron." *J. Electrochem. Soc.*, 144(5), 1672–1680.

Prakash, J. B. S., Venugopal, R., Shivakumaraiah and Iyengar, P. (2011). *Chemistry for engineering students*. Lakshmi Mudranalaya, Bangalore.

Prioteasa, P., Anicai, L. and Visan, T. (2010). "Synthesis and corrosion characterization of electrodeposited Ni-Mo alloys obtained from aqueous solutions." *U. P. B. Sci. Bull. Series B,* 72(4), 11-24.

Raj, I. A. (1993). "Nickel-based, binary-composite electrocatalysts for the cathodes in the energy-efficient industrial production of hydrogen from alkaline-water electrolytic cells." *J. Mater. Sci.*, 28(16), 4375–4382.

Rao, V. R., Bangera, K. V. and Hegde, A. C. (2013). "Magnetically induced electrodeposition of Zn–Ni alloy coatings and their corrosion behaviors." *J. Magn. Magn. Mater.*, 345, 48–54.

Rashmi, D., Pavithra, G. P., Praveen, B. M. and Devapal, D. (2020). "Development of nanocrystalline multilayer Ni–Fe alloy coatings: characterization and its corrosion behaviour at elevated temperature." *Bull. Mater. Sci.*, 43(1), 131.

Raveendran, M. N., and Hegde, A. C. (2021). "Electrodeposition of multilayer NiW alloy coating for improved anticorrosion performance." *Bull. Mater. Sci.*, 44(2), 84.

Ray, A. (2015). "Electrodeposition of thin films for low-cost solar cells." *Electroplating of nanostructures*, M. Aliofkhazraei, ed., InTech, 145-174.

Revie, R. W. and Uhlig, H.H. (2008). *Corrosion and corrosion control*: *An introduction to corrosion science and engineering*. A. John Wiley & Sons, New Jersey.

Rezaeiolum, A., Aliofkhazraei, M., Karimzadeh, A., Rouhaghdam, A. S. and Miresmaeili, R. (2018). "Electrodeposition of Ni–Mo and Ni–Mo-(nano Al_2O_3) multilayer coatings." *Surf. Eng.*, 34(6), 423–432.

Ribeiro, D. V. and Abrantes, J. C. C. (2016). "Application of electrochemical impedance spectroscopy (EIS) to monitor the corrosion of reinforced concrete: A new approach." *Constr. Build. Mater.*, 111, 98–104.

Sanches, L. S., Domingues, S. H., Carubelli, A. and Mascaro, L. H. (2003). "Electrodeposition of Ni-Mo and Fe-Mo alloys from sulfate-citrate acid solutions." *J. Braz. Chem. Soc.*, 14(4), 556–563.

Santos, D. M. F. and Sequeira, C. A. C. (2013). "Hydrogen production by alkaline water electrolysis." *Quim. Nova,* 36(8)*,* 1176-1193.

Sapountzi, F. M., Gracia, J. M., Westrate, C. J., Fredriksson, H. O. and Niemantsverdriet, J. W. (2017). "Electrocatalysts for the generation of hydrogen, oxygen and synthesis gas." *Prog. Energy Combust. Sci.,* 58, 1-35.

Shetty, A.R, and Hegde, A.C. (2021). "Magnetoelectrodeposition of Ni-Mo-Cd alloy coating for improved corrosion resistance." *Chem. Data Collect.*, 32, 100639.

Shetty, S. S., Sadiq, M. M. J., Bhat, D. K. and Hegde, A. C. (2017). "Electrodeposition and characterization of Ni-Mo alloy as an electrocatalyst for alkaline water electrolysis." *J. Electroanal. Chem.,* 796*,* 57-65.

Shetty, S., Sadiq, M. M. J., Bhat, D. K. and Hegde, A. C. (2018). "Electrodeposition of Ni–Mo–rGO composite electrodes for efficient hydrogen production in an alkaline medium." *New J. Chem.*, 42(6), 4661–4669.

Solmaz, R. and Kardaş, G. (2009). "Electrochemical deposition and characterization of NiFe coatings as electrocatalytic materials for alkaline water electrolysis." *Electrochim. Acta*, 54(14), 3726–3734.

Souza, A. K. P., Moraes Cruz, C. A. de, Marques, G. C., Castro, L. S. O. de and Bezerra, T. B. (2019). "A compact current conveyor CMOS potentiostat circuit for electrochemical sensors." *4th Int. Symp. on Instrumentation Systems, Circuits and Transducers (INSCIT)*, São Paulo, Brazil, 1–6.

Sriraman, K. R., Ganesh Sundara Raman, S. and Seshadri, S. K. (2007). "Corrosion behaviour of electrodeposited nanocrystalline Ni–W and Ni–Fe–W alloys." *Mater. Sci. Eng.: A*, 460–461, 39–45.

Stansbury, E. E. and Buchanan, R. A. (2000). *Fundamentals of electrochemical corrosion*. Materials Park, OH: ASM International.

Subramania, A., Sathiya Priya, A. R. and Muralidharan, V. S. (2007). "Electrocatalytic cobalt–molybdenum alloy deposits." *Int. J. Hydrog. Energy*, Int. Conf. on Materials for Hydrogen Energy: Solar Hydrogen (ICMHE 2004), 32(14), 2843–2847.

Tacken, R.A. and Janssen, L.J.J. (1995). "Applications of magnetoelectrolysis." *J. Appl. Electrochem.*, 25(1), 1–5.

Thangaraj, V., Eliaz, N. and Hegde, A. C. (2009). "Corrosion behavior of composition modulated multilayer Zn–Co electrodeposits produced using a single-bath technique." *J. Appl. Electrochem.*, 39(3), 339.

Torabinejad, V., Aliofkhazraei, M., Assareh, S., Allahyarzadeh, M. H. and Rouhaghdam, A. S. (2017). "Electrodeposition of Ni-Fe alloys, composites, and nano coatings–A review." *J. Alloys Compd.*, 691, 841–859.

Torabinejad, V., Aliofkhazraei, M., Rouhaghdam, A. S. and Allahyarzadeh, M. H. (2017). "Electrodeposition of Ni–Fe–Mn/Al$_2$O$_3$ functionally graded nanocomposite coatings." *Surf. Eng.*, 33(2), 122–130.

Torabinejad, V., Rouhaghdam, A. S., Aliofkhazraei, M. and Allahyarzadeh, M. H. (2016). "Electrodeposition of Ni–Fe and Ni–Fe-(nano Al$_2$O$_3$) multilayer coatings." *J. Alloys Compd.*, 657, 526–536.

Ullah, I., Munir, A., Haider, A., Ullah, N. and Hussain, I. (2021). "Supported polyoxometalates as emerging nanohybrid materials for photochemical and photoelectrochemical water splitting." *Nanophotonics*, 10(6), 1595–1620.

Ullal, Y. and Hegde, A. C. (2014). "Electrodeposition and electro-catalytic study of nanocrystalline Ni–Fe alloy." *Int. J. Hydrog. Energy*, 39(20), 10485–10492.

Vannathan, A. A., Maity, S., Kella, T., Shee, D., Das, P. P. and Mal, S. S. (2020). "In situ vanadophosphomolybdate impregnated into conducting polypyrrole for supercapacitor." *Electrochim. Acta*, 364, 137286.

Venkatakrishna, K. and Chitharanjan Hegde, A. (2010). "Electrolytic preparation of cyclic multilayer Zn–Ni alloy coating using switching cathode current densities." *J. Appl. Electrochem.*, 40(11), 2051–2059.

Vukasovich, M. S. and Farr, J. P. G. (1986). "Molybdate in corrosion inhibition—A review." *Polyhedron*, Proceedings of the Climax Fifth International Conference, 5(1), 551–559.

Wang, T., Jin, R., Wu, X., Zheng, J., Li, X. and Ostrikov, K. (2018). "A highly efficient Ni–Mo bimetallic hydrogen evolution catalyst derived from a molybdate incorporated Ni-MOF." *J. Mater. Chem. A*, 6(19), 9228–9235.

Wang, Z., Ma, Y., Zhang, R., Xu, D., Fu, H. and Yao, J. (2009). "Fabrication of self-assembled ultrathin photochromic films containing mixed-addenda polyoxometalates $H_5[PMo_{10}V_2O_{40}]$ and 1,10-decanediamine." *J. Solid State Chem.*, 182(4), 983–988.

Waskaas, M. and Kharkats, Y. I. (2001). "Effect of magnetic fields on convection in solutions containing paramagnetic ions." *J. Electroanal. Chem.*, 502(1–2), 51–57.

Yang, L. (2008). *Techniques for corrosion monitoring*, Elsevier, USA.

Yee, J. C., Kee, K. E., Hassan, S., Nor, M. F. M. and Ismail, M. C. (2019). "Corrosion inhibition of molybdate and nitrite for carbon steel corrosion in process cooling water." *J. Eng. Sci. Technol.,* 14 (4), 2431-2444.

Yuan, X. -Z. R., Song, C., Wang, H. and Zhang, J. (2009). "Electrochemical impedance spectroscopy in PEM fuel cells: fundamentals and applications, Springer Science & Business Media, Germany.

Záchenská, J., Jorík, V., Vančo, Ľ., Mičušík, M. and Zemanová, M. (2022). "Ni–Fe cathode catalyst in zero-gap alkaline water electrolysis." *Electrocatalysis*.

Zech, N. and Landolt, D. (2000). "The influence of boric acid and sulfate ions on the hydrogen formation in Ni-Fe plating electrolytes." *Electrochim. Acta*, 45(21), 3461–3471.

Zhang, L., Ding, X., Cong, M., Wang, Y. and Zhang, X. (2019). "Self-adaptive amorphous $Co_2P@Co_2P$/Co-polyoxometalate/nickel foam as an effective electrode for electrocatalytic water splitting in alkaline electrolyte." *Int. J. Hydrog. Energy*, 44(18), 9203–9209.

Zhang, Q., Cao, C., Xu, T., Sun, M., Zhang, J., Wang, Y., and Wan, H. (2009). "NiO–polyoxometalate nanocomposites as efficient catalysts for the oxidative dehydrogenation of propane and isobutane." *Chem. Commun.*, (17), 2376.

Zhou, Q. and He, F. (2018). "Insight into the mechanism of the Fe-Ni alloys co-deposition from poly-nuclear complexes." *J. Electrochem. Soc.*, 165(14), D681–D686.

Zhou, Y., Lin, T., Luo, X., Yan, Z., Wu, J., Wang, J. and Shen, Y. (2020). "Mechanistic study on nickel-molybdenum based electrocatalysts for the hydrogen evolution reaction." *J. Catal.*, 388, 122–129.

RESEARCH PAPER PUBLICATIONS

1. Gonsalves C. N. and Hegde A. C. (2021). "Electrochemical water electrolysis using electrodeposited (NiMo) coatings from a low concentration bath." *Chem. Data Collect,* 100697.

2. Gonsalves C. N. and Hegde A. C. (2021). "Development of high corrosion resistant Ni-Mo coatings from a low-concentration bath: effect of magnetoconvection." *Mater. Sci. Technol.,* 37, 1187-1198.

3. Gonsalves C. N., Vannathan A. A., Mal S. S. and Hegde A. C. and Hegde A. C. "Development of polyoxometalate (POM) based (Ni-Mo) alloy coatings for bifunctional electrode applications in alkaline water splitting." *New J. Chem.* (Under review)

PAPERS PRESENTED AT THE CONFERENCES

1. Gonsalves C. N., Raveendran. M. N. and Hegde A.C. (2018). "Corrosion behavior of electrodeposited Cu-Ni alloy in alkaline medium." 37th Annual National Conference of Indian Council of Chemists, held at NITK, Surathkal on December 12-14, 2018.

2. Gonsalves C. N. and Hegde A. C. (2019). "Enhanced corrosion protection of magnetoelectrodeposited Ni-Mo alloy coatings." Twelfth International Symposium on Advances in Electrochemical Science and Technology (iSAEST-12) held at Chennai, on January 8-10, 2019.

3. Gonsalves C. N. and Hegde A. C. (2020). "Effect of addition of ceric sulphate on corrosion behavior of Ni-Mo alloy coatings." International Conference on Electrochemistry in Industry, Health and Environment (EIHE- 2020), held at BARC, Anushakthinagar, Mumbai, January 21-25, 2020.

4. Gonsalves C. N., Sneha, I. M. and Hegde A. C. (2021). "Effect of pH on process of electro-crystallization of Ni-Cd alloy coatings and their anticorrosion performance." National Symposium on Electrochemical Science and Technology 2020 (NSEST-2020), held via online mode at IISc, Bengaluru on January 21 - 22, 2021.

5. Gonsalves C. N. Vannathan A. A., Mal S. S. and Hegde A.C. (2021). "Electrodeposition of polyoxometalate reinforced Ni-Mo alloy coatings and their electrocatalytic behaviour", 27th International Conference of International Academy

of Physical Sciences (CONIAPS XXVII) on Recent Advances in Catalysis Science & Engineering (RACSE), held at National Institute of Technology Jamshedpur, on October 26-28, 2021.

BIO-DATA

Personal Information:

Name	: Cindrella Nishmitha Gonsalves
Father's name	: Clifford Gonsalves
Gender	: Female
Nationality	: Indian
Date of birth	: 12-07-1992
Marital Status	: Single
Religion	: Christian
Permanent Address	: Johnson Traders
	N.H. 66, Tallur, Kundapura Tq.
	Udupi, Karnataka.
Pin Code	: 576230
Contact No. (Mob)	: +919739421994
Email-id	: cinishmitha@gmail.com

Educational Qualification:

Qualification	Year of Passing	Board/University/Institute	Marks (%)
M.Sc Chemistry	2015	St. Agnes Centre for PG Studies and Research (Autonomous) Mangaluru	75.54
B.Sc (B.Z.C.)	2013	St. Agnes College (Autonomous) Mangaluru	87.70
P.U.C./Plus Two (P.C.M.B.)	2010	Milagres P.U. College Kallianpur, Udupi	75.00
S.S.L.C.	2008	Holy Rosary English Medium School Kundapura, Udupi	89.12

Academic Achievements:

- Secured *First Rank* in B.Sc (B.Z.C.) from St. Agnes College (Autonomous), Mangaluru.

- Awarded the *"Best All-Round Runner-up Science Student"* of St. Agnes College (Autonomous), Mangaluru, for the year 2012-13.

Work Experience:

i) **Assistant Professor (2016-2017)**, St. Agnes College (Autonomous), Centre for Post Graduate Studies and Research, Mangaluru

ii) **Lecturer (Part-time, 2015-2016)**, Saraswathi Vidyalaya P.U. College, Gangolli, Kundapura

Area of Research: *Electroplating,* specifically on *Ni-based alloy electroplating and its application in corrosion mitigation and water splitting activity*.

Research Experience (2017-2022):

- Skillful in developing alloy coatings using advanced methods of electrodeposition like magnetoelectrodeposition and multilayer electrodeposition

- Hands-on experience in using electrochemical workstations VersaSTAT-3, Biologic-SP 150 and Gill AC

- Good in material characterization techniques like Electrochemical Impedance Spectroscopy, Cyclic Voltammetry, XRD, Scanning Electron Microscopy

- Assisted students in completing M.Sc. and Summer Internship projects on Electroplating

Research Publications in Peer-reviewed Journals/Conference Proceedings: 03

Papers presented at Conferences: National-02; International-03

Awards and Recognition:

i) *Best Paper Award*- 'Effect of pH on process of electro-crystallization of Ni-Cd alloy coatings and their anticorrosion performance." *National Symposium*, NSEST-2020, organized by IISc, Bengaluru via online mode on January 21-22, 2021.

ii) *Best Virtual Presentation (Second position)*- 'Electrodeposition of polyoxometalate reinforced Ni-Mo alloy coatings and their electrocatalytic behaviour', *International Conference*, CONIAPS XXVII on Recent Advances in Catalysis Science & Engineering (RACSE), organized by NIT Jamshedpur, via online mode on October 26-28, 2021.

Place: Surathkal

Date: 20-07-2022   **CINDRELLA N. GONSALVES**